Resource Allocation for Full-Duplex Multiple-Antenna Communication Systems

Von der Fakultät für Elektrotechnik und Informationstechnik
der Rheinisch-Westfälischen Technischen Hochschule Aachen
zur Erlangung des akademischen Grades eines Doktors
der Ingenieurwissenschaften genehmigte Dissertation

vorgelegt von

Master of Science
Seyed Omid Taghizadeh Motlagh

aus Tehran

Berichter: Universitätsprofessor Dr. rer. nat. Rudolf Mathar
Universitätsprofessor Dr. -Ing. Slawomir Stanczak

Tag der mündlichen Prüfung: 14. June 2018

Diese Dissertation ist auf den Internetseiten
der Hochschulbibliothek online verfügbar.

Preface

This thesis was written during my time as a research assistant at the Institute for Theoretical Information Technology at RWTH Aachen University.

I would like to thank Univ.-Prof. Dr. rer. nat. Rudolf Mathar for giving me the opportunity to work on my dissertation and to be a part of his research team. I also would like to thank him for his continuous support and for being an excellent example of a fair and practical leadership.

Many thanks to Univ.-Prof. Dr.-Ing. Slawomir Stanczak for providing constructive comments, and taking the effort to act as a referee for my thesis.

I would like to express my deepest gratitude to all my present and former colleagues at the Institute for Theoretical Information Technology at RWTH Aachen University, for the friendly and positive research atmosphere I have enjoyed over the last four years. A special thank you goes to Dr.-Ing. Gholamreza Alirezaei for his always-open door whenever I had a question. I have learned so much from our long discussions on a wide range of topics. Also, I would like to thank my colleagues M.Sc. Halil Alper Tokel, M.Sc. Ehsan Zandi, M.Sc. Tianyu Yang, M.Sc. Vimal Radhakrishnan, and M.Sc. Alireza Zamani for proof-reading parts of my thesis.

I am grateful to all of my teachers and professors who have promoted my interest in research over the span of my education. In particular, I would like to thank Prof. Dr.-Ing. Martin Haardt for his extremely informative lectures on mobile communications and array signal processing and Prof. Dr. Esfandiar Mehrshahi for his conceptual lecture on engineering mathematics, which shaped the foundation of my current understanding of wireless communication systems. Moreover, I would like to thank Dr. Ali Cagatay Cirik, for our constructive discussions on the area of signal processing for full-duplex wireless systems, which have inspired my research in many ways.

Finally, I would like to thank my parents, Nahid Doroudi and Bahman Taghizadeh, for their unconditional love, support and positive encouragements throughout my life. I am forever grateful for the significant time of their special and valuable lives dedicated to introduce me to the world of math and logic, without which my current path of research would not have been possible.

This thesis is dedicated to the memory of my beloved grandmother, Manijeh Moallemi. I can still hear her prayers for me to become an honest educated man, upholding to her unique moral principles of good-heartedness and forgiveness. I am forever grateful and empowered by her love.

Aachen, December 2017

Seyed Omid
Taghizadeh Motlagh

Contents

Preface **iii**

1 Introduction **1**
1.1 Scope . . . 1
1.2 Related Works . . . 2
1.2.1 FD transceiver realization: self-interference (SI) cancellation . . . 2
1.2.2 Applications of FD transceivers . . . 5
1.3 Thesis Outline and Contributions . . . 10
1.4 Mathematical Notations and Conventions . . . 11
1.4.1 Sets . . . 11
1.4.2 Matrix and vector operations . . . 12
1.4.3 Statistical notations . . . 12

2 Full-Duplex Bidirectional MIMO OFDM Communications **13**
2.1 Overview . . . 13
2.1.1 Related works on FD multi-carrier systems . . . 14
2.1.2 Chapter outline and contributions . . . 14
2.2 System Model . . . 16
2.2.1 Limited dynamic range in an FD OFDM system . . . 17
2.2.2 Remarks . . . 20
2.3 Linear Transceiver Design for Multi-Carrier Communications . . . 20
2.3.1 Weighted MSE minimization via Alternating QCP (AltQCP) . . . 20
2.3.2 Weighted MMSE (WMMSE) design for sum rate maximization . . . 22
2.4 Robust Design with Imperfect CSI . . . 23
2.4.1 Norm-bounded CSI error . . . 24
2.4.2 Alternating SDP (AltSDP) for worst-case MSE minimization . . . 25
2.4.3 WMMSE for sum rate maximization . . . 28
2.5 Discussions . . . 29
2.5.1 Worst case CSI error . . . 29
2.5.2 Computational complexity . . . 30
2.6 Simulation Results . . . 31
2.6.1 Algorithm analysis . . . 32
2.6.2 Performance comparison . . . 34
2.7 Conclusion . . . 36

3 Linear Transceiver Optimization for Full-Duplex Relaying under Hardware Impairments 39
3.1 Overview . . . 39
3.1.1 Chapter outline and contributions . . . 40
3.2 System Model . . . 41
3.2.1 Source-to-relay communication . . . 41
3.2.2 Distortion signal statistics . . . 42
3.2.3 Relay-to-destination communication . . . 43
3.2.4 Distortion loop . . . 43
3.2.5 Remarks . . . 43
3.3 Performance Analysis of MIMO AF-FD Relaying with Hardware Impairments . . . 45
3.3.1 Optimization problem . . . 46
3.4 Gradient Projection for SDNR maximization . . . 47
3.4.1 Iterative update for relay amplification . . . 47
3.4.2 Iterative update for source Tx power . . . 49
3.4.3 Iterative update for destination Rx filter . . . 49
3.4.4 Convergence . . . 50
3.5 An Intuitive Approach: Distortion-Aware Multi-Stage Rank-1 Relay Amplification (MuStR1) . . . 50
3.5.1 Transmit filter . . . 51
3.5.2 Receive filter . . . 52
3.5.3 Relay amplification . . . 52
3.5.4 Design of destination Rx filter . . . 54
3.5.5 Alternating enhancement of MuStR1 (AltMuStR1) . . . 54
3.5.6 Convergence . . . 55
3.6 FD Decode-and-Forward Relaying Under Residual Self-Interference . . . 55
3.6.1 DF relaying . . . 56
3.7 Simulation Results . . . 59
3.7.1 Algorithm analysis . . . 60
3.7.2 Performance comparison . . . 61
3.8 Conclusion . . . 64

4 Secrecy Energy Efficiency of an FD MIMOME Wiretap Channel: Does FD Jamming Reduce the Energy-Cost of a Secure Bit? 67
4.1 Scope . . . 67
4.1.1 Chapter outline and contributions . . . 68
4.2 System Model . . . 69
4.2.1 Signal model . . . 70
4.2.2 Distortion signal statistics . . . 71
4.2.3 Power consumption model . . . 71
4.2.4 Secrecy energy efficiency . . . 72
4.2.5 Remarks . . . 73

4.3 Secrecy Energy Efficiency Maximization . . . 73
4.3.1 SUIAP algorithm . . . 74
4.3.2 Convergence . . . 75
4.3.3 Initialization . . . 75
4.3.4 Computational complexity . . . 75
4.4 Secure Bidirectional Communication: Joint Full-Duplex Operation at Alice and Bob . . . 76
4.4.1 Extended SUIAP for bidirectional-SEE maximization . . . 78
4.5 Secrecy Energy Efficiency Maximization with Statistical CSI . . . 78
4.5.1 Successive selection and statistical lower bound maximization . . . 79
4.6 Simulation Results . . . 84
4.6.1 Algorithm analysis . . . 85
4.6.2 Performance comparison . . . 86
4.7 Conclusion . . . 91

5 Full-Duplex Cellular Networking: A Minimum-Cost Wireless Backhauling Approach 93
5.1 Overview . . . 93
5.1.1 An overview on FD wireless radio access . . . 93
5.1.2 FD wireless backhaul network planning . . . 94
5.1.3 Related works . . . 96
5.1.4 Chapter outline and contributions . . . 96
5.2 System Model . . . 97
5.2.1 Acquisition of network information . . . 98
5.2.2 Wireless link throughput . . . 101
5.2.3 Role of planning . . . 101
5.3 Minimum Cost Network Planning and Optimization . . . 102
5.3.1 Decision variables . . . 102
5.3.2 Network cost model . . . 103
5.3.3 Constraints . . . 104
5.3.4 Network planning: an MILP model . . . 106
5.3.5 Network re-tuning: an SIA model . . . 109
5.4 Simulation Results . . . 111
5.5 Conclusion . . . 114

6 Conclusion 117
6.1 Summary . . . 117
6.2 Outlook . . . 119

7 Appendix 121
7.1 Proof to Lemma 2.2.1 . . . 121
7.2 Proof to the Lemma 3.4.1 . . . 121
7.3 Equivalent Relay Transmit Distortion Channel Expression (3.35) . . . 122
7.4 Derivation of (3.42)-(3.43) and the Coefficients (3.44)-(3.48) . . . 123

7.5 Proof to Lemma 4.5.2 . . . 124
7.5.1 Proof of tightness: . . . 124
7.5.2 Proof of equal directional derivative: . . . 124

List of Acronyms **127**

List of the Used Symbols **131**

Bibliography **139**

1 Introduction

Full-duplex (FD) transceivers are known for their capability to transmit and receive at the same time and frequency, hence showing the potential to enhance various aspects of wireless communication systems, e.g., latency, security, and spectral efficiency [1]. Such potentials are interesting, considering the growing demand for low-latency and high data-rate services, calling for energy and spectral efficient wireless solutions. Nevertheless, FD transceivers suffer from the inherent SI from their own transmitter, due to the co-channel transmission and reception. In theory, since the transceiver is aware of its own transmitted signal, it can estimate and subtract the received SI. However, this process is challenging in practice, since the strong SI signal saturates the receiver front-end, e.g., low noise amplifier (LNA), analog-to-digital converter (ADC), and degrades the desired received signal. As a result, for a successful realization of an FD transceiver, the SI signal must be attenuated at the radio frequency (RF) domain, prior to saturating the limited dynamic range of the receiver chain. In this regard, specialized self-interference cancellation (SIC) techniques have been developed in the recent years, employing a combination of various analog and digital signal processing. The proposed SIC in [2] has obtained an adequate level of isolation between transmit (Tx) and receive (Rx) directions to facilitate an FD communication, complying with WiFi 802.11.ac standard. Such results have motivated multiple recent studies on the potential gains, and the promising use-cases for the application of the FD transceivers in future wireless communication systems.

1.1 Scope

The work presented in this dissertation provides novel insights and design frameworks for the gainful application of FD transceivers into the wireless communication systems, from the aspects of radio resource allocation and optimization. On one hand, the simultaneous transmission and reception at the same channel appears as a promising communication paradigm with the potential to obtain a higher level of spectral efficiency and security. On the other hand, the co-existence of multiple transmissions at the same channel appears as a potential threat to the performance of wireless systems, if the impact of the additional interference paths are not properly controlled. This calls for smart resource and interference management schemes, in order to avoid the negative impacts of the additional interference. In this thesis, optimized allocation of the fundamental communication resources, i.e., power, spectrum, antenna and radio

front ends, have been studied for different promising scenarios regarding the application of FD nodes. In each case an optimization framework is provided and the achievable gains, associated with the application of FD capability, are evaluated.

In the following, a summary on the available related works is provided in the context of implementation and design of the FD wireless communication systems.

1.2 Related Works

We can divide the available related studies on FD wireless systems into two main categories. The first category includes studies on the realization and implementation of an FD transceiver, addressing the main historic question: *if and how the strong SI signal, resulting from the co-channel transmission in an FD transceiver, can be adequately suppressed?*. The second category, includes studies on the application of FD transceivers, addressing the question: *where, how, and how much gain can be obtained via the application of FD capability to the wireless communication systems?*. The answer to the first question revisits multiple fundamental aspects in the design of wireless transceivers, whereas the second question requires reconsideration of the traditional system design and resource allocation, with the goal of integrating the new paradigm into different communication scenarios.

1.2.1 FD transceiver realization: SI cancellation

As previously mentioned, due to the proximity of the transmit and receive front ends, the SI signal is distinctly stronger than the desired received signal, thereby saturating the limited dynamic range of the receiver chain elements. As a result, a successful SI cancellation scheme must include measures to attenuate the SI signal prior to it saturates the receiver chain. Considering the fact that the SI signal is initially the known transmit signal from the same transceiver, hence, the SI cancellation may include measures taken at different signal domains: the baseband signal domain at the transmit and receive chains, as well as the RF signal domain at the transmitter or at the receiver. As a result, the available implementations of SIC offer different approaches for attenuating the SI signal at the aforementioned domains as briefly summarized in the following, see Fig.1.1 .

Passive attenuation

The passive SI attenuation is obtained as the natural attenuation of the propagated SI signal from the transmit antenna to the receiver side. The works in [3–5] have obtained promising levels of passive isolation by employing separated set of antennas for transmission and reception, relying on directional isolation, cross polarization, as well

as the addition of RF absorbing materials. In [6] it is observed that $60-70$ dB of passive isolation can be obtained by exploiting antenna directivity in an FD relaying scenario, with opposite directions for signal transmission and reception. In [5] it is observed that more than 70 dB of attenuation can be obtained at an anechoic chamber environment with a very low reflection floor, when both cross-polarization and absorptive shielding are applied together. However, the same study concludes that the isolation quality degrades rapidly in the presence of the reflective paths, hence requiring a combined passive and active cancellation strategy for most practical environments. For the devices using a shared antenna for transmission and reception, passive isolation is obtained via 3-port RF-circulator. Thanks to the anisotropic property, RF circulator are capable of providing around 15 dB of isolation among Tx and Rx, however, falling short in comparison to the reported attenuation via physical antenna separation. Nevertheless, they are used as a part of the SI cancellation for the devices with relatively small form factors, e.g., [2, 7, 8].

Active RF cancellation

The reported isolation obtained via passive cancellation methods is not sufficient for most practical scenarios. Hence, active cancellation appears as an inevitable part of a successful SIC strategy. In general, active RF cancellation includes an active reconstruction and subtraction of the SI signal at the RF domain, which has to take place prior to the SI signal reaching the sensitive receiver chain elements. In the following, we briefly explain the main approaches for the implementation of an active RF cancellation, i.e., antenna cancellation and injection approaches.

Antenna cancellation Antenna cancellation includes the utilization of an auxiliary transmit antenna, with the intention of actively nullifying the SI signal at the location of the receive antenna. This can be done, e.g., by employing an 180-degree analog phase shifter on a duplicate secondary transmission, or by placing the secondary Tx antenna at the distance $d + \frac{\lambda}{2}$ to the Rx antenna, d being the distance between the primary transmit and receive antennas, and λ being the wavelength corresponding to the used carrier frequency. The idea of antenna cancellation has been presented in [9–11] as the first SIC strategy to demonstrate the feasibility of FD wireless communications. The auxiliary transmission in [9] achieves 20 dB of attenuation at the center frequency of 2.4 GHz, for an optimal placement of the antennas. However, the obtained cancellation is valid for the narrow bandwidth of 5 MHz, since the phase difference generated as a result of the fixed distance frequency dependent. Consequently, the works in [12,13] have obtained overall cancellation of 45 dB over the extended bandwidth of 10 MHz, replacing the distance-based design with an RF analog phase shifter. Moreover, the latter work has generalized the proposed antenna cancellation scheme for an FD multiple-input multiple-output (MIMO) transceiver.

Signal injection The signal injection approach is based on the reconstruction and subtraction of an auxiliary SI RF signal. However, in contrast to the antenna cancellation which relies on on-the-air auxiliary transmissions, the injection approaches rely on the direct injection of the reconstructed SI signal, i.e., with no auxiliary transmissions. This results in a more accurate control over the auxiliary signal, however, requires a more complex RF circuitry, particularly as the number of transmit and receive chains increase. Two separate implementations can be recognized for the injection approaches, summarized in the following.

Auxiliary reconstruction In [14], and later in [8, 15–17], active SIC schemes are proposed where an auxiliary transmit chain is utilized to reconstruct the estimate of the SI signal at the RF domain. The constructed RF signal is then subtracted from the received signal, immediately after the Rx antenna. The implementation in [17] has obtained around 85 dB of total cancellation, over the bandwidth of 20 MHz. Due to the dedication of a complete transmit chain, the constructed SI can be shaped by controlling the baseband signal of the auxiliary chain, via digital processing. This increases the capability of this method to adapt to the multi-path reflections, as well as improving the SIC performance over a larger bandwidth. However, the usage of an additional chain leads to the additional transmit distortions, which is the drawback of this approach. The works in [18–21] have introduced additional digital signal processing measure with the goal of reducing the impact of RF impairments, e.g., I/Q imbalance [20, 21], and phase noise [18, 19].

Direct injection As mentioned, the utilization of a separate Tx chain for reconstructing the RF SI signal leads to the additional hardware distortions from the auxiliary chain. In contrast, the direct injection methods generate the estimate of the SI signal at the RF domain, by directly feeding the up-converted signal at the Tx chain to an attenuator and phase shifter unit. This design, i.e., [10], uses a balanced-unbalanced (Balun) transformer to invert a copy of the transmitted signal and adjust its delay and attenuation using programmable attenuators and delay lines, obtaining around 45 dB of cancellation over the 40 MHz bandwidth. However, this design is sensitive to the accurate tuning of the delay lines. A similar approach is also presented in [22,23], where digitally-controlled hybrid transformers are used to generate the inverted version of the SI signal. The works in [2,7] have presented the idea of fixed and uniformly distributed delay lines, implemented as connection links with different lengths on a printed circuit board (PCB), where the attenuation at each line is digitally controlled. It is observed that in comparison to [10], the application of fixed delay lines results in a significant improvement, where 110 dB of overall cancellation is obtained in [2], complying with WiFi 802.11.ac requirements. The extensions in [24, 25] present an all-analog SIC, utilizing a clustered tap with digitally controllable attenuators and a blind digital tuning approach. It is observed that the clustered delay approach is capable of enhancing the

frequency response of the SIC, obtaining $70-80$ dB of analog cancellation over the 100 MHz bandwidth.

Digital domain cancellation

Once the SI signal is attenuated via the combination of passive and active RF methods to comply with the dynamic range of the receive chain elements, it can be then down-converted, together with the desired received signal, and further processed at the receiver. While the analog and passive cancelers perform well for the attenuation of the dominant SI paths, e.g., a line-of-sight (LOS) or short-distance reflections, receiver digital processing is best suited to resolve the residual reflective paths which contain less power but are less stationary, e.g., due to mobility. Moreover, the digital processing at the Tx side can be employed to reduce the resulting SI power, via Tx beamforming. The works in [26–28] have considered a limit on the SI power, as a constraint for Tx beamforming, thereby protecting the receiver chains from saturation. However, the practical impact of such consideration has not been verified via experiments. For the transceivers with a large transmit antenna arrays, i.e., massive multiple-input multiple-output (mMIMO), the application of analog cancelers becomes costly due to the increased number of chains. In this regard, it is shown in [29] that transmit beamforming can act as an essential part of SIC. In fact, 50 dB of cancellation is reported in the latter work via a combination of passive isolation and transmit beamforming, employing a 72-antenna array system. In the receiver side, the application of digital processing is a common measure for almost all of the available SIC techniques. The remaining parts of the SI signal at the receiver baseband shall be processed and further reduced, exploiting the remaining spatial and temporal dependencies. In [2, 30, 31], it is observed that the impact of non-linear signal distortions, resulting from the non-linearity at Tx and Rx chains, can be reduced by employing a non-linear signal processing at the receiver, outperforming the linear models. The employed digital processing in [2] has obtained 15 dB of additional cancellation via non-linear signal processing, leading to 50 dB overall cancellation in the digital domain.

1.2.2 Applications of FD transceivers

The coexistence of transmission and reception at the same channel has been considered as a potentially gainful paradigm for various aspects of wireless systems. In the following, we review the main scenarios for which the application of FD capability is motivating, see Fig. 1.2.

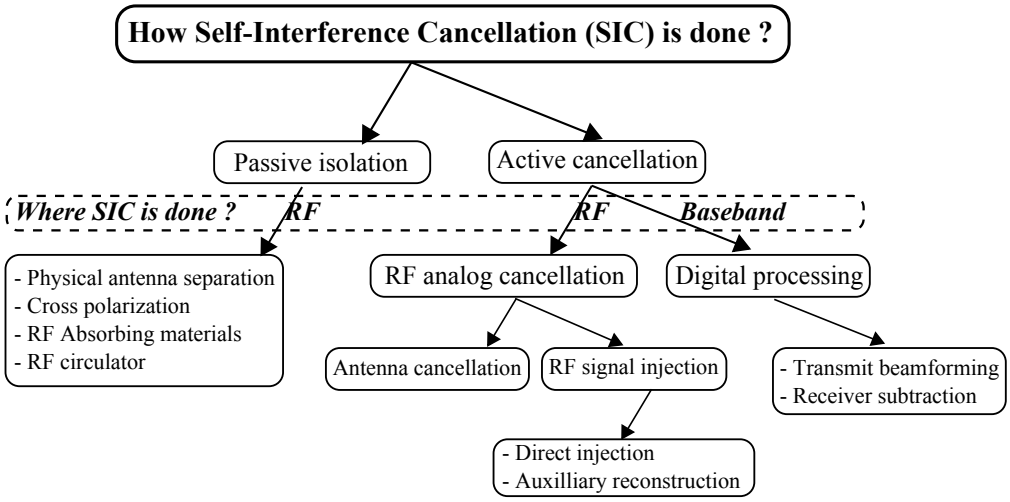

Figure 1.1: An overview on the main approaches for SIC.

FD bidirectional communications

In a bidirectional communication, a single or multiple pairs of nodes perform a two-way communication. At each communicating pair, the transmission and reception is traditionally separated over orthogonal channel resources, e.g., via time division duplexing (TDD) or frequency division duplexing (FDD). When nodes are enabled with FD capability, the opposite communication directions can be facilitated on the same channel resource, thereby improving the spectral efficiency. However, such systems suffer from the interference from other communicating nodes, in case of multi-pair communication, as well as the residual self-interference (RSI) which remains from the implemented SIC process. In [32] the achievable rates of a two-node FD bidirectional communication is studied under the impact of RSI, where nodes are equipped with multiple antennas. It is observed that an FD system outperforms its HD counterpart, in terms of the achievable rate, if the RSI is sufficiently small and reaches the theoretical two-fold gain for a perfect SIC. The problem of sum rate maximization has been also revisited in [27, 28, 33–36] offering diverse modeling and design frameworks. The consideration of energy efficiency under known rate requirements has been considered in [37–39]. The coexistence of an in-band bidirectional system with an underlay primary network, has been studied in [40, 41], considering a minimum mean-squared error (MMSE) design. The extension of the basic setup in [32] into a multi-pair bidirectional setup is studied in [38, 40, 42, 43].

FD cellular networking

Application of FD capability at a basestation (BS) node, is shown to be gainful in the context of wireless cellular communication networks in three distinct ways. Firstly, An

FD BS is capable of serving uplink (UL) and downlink (DL) users at the same channel, hence, showing potential for a higher spectral efficiency in the access network. Secondly, an FD BS may transmit jamming signals to the potentially illegitimate receivers, while receiving information from the UL. This leads to a higher information security in the physical layer. And third, FD capability enables an in-band wireless backhauling, where the received UL information can be relayed to the core network at the same operating channel. In the following, we focus on the first application, where the second and the third scenarios are explained in more details in the subsequent parts.

The initial works [44–46] have presented an FD cellular communication system, where an FD BS is simultaneously communicating with multiple UL and DL users, showing superior performance compared to the system with an HD BS. However, the impact of RSI, or the co-channel interference (CCI) among the UL and DL users, appearing as a result of co-channel transmission and reception, are neglected. In [44,47], it is discussed that the co-existence of the several traditionally separated transmission and receptions on the same channel leads to the emergence of the additional interference paths, which are not negligible for the resulting system performance. Consequently, various design methodologies have been proposed for a single cell FD cellular system [48–51], where the impact of the RSI, as well as the CCI are effectively controlled by the means of beamforming and power adjustment at a multiple antenna FD BS, and HD users. The works in [52,53] have proposed a channel allocation scheme for an FD multi-user setup, where the impact of CCI is controlled via smart channel assignment. The coexistence possibility of an unlicensed FD cellular system with a primary network is studied in [51] by protecting the primary system via interference power constraints. In [43, 54] an FD BS is considered, where in addition to the UL and DL users the BS is responsible for wirelessly transferring energy to the nodes relying on external energy sources. The extension of the studied single-cell setup to a multi cell, multi user setup has been given in [55–57], considering sum rate, and total energy consumption as design objectives.

FD relaying

A relay node is responsible for receiving and forwarding information from an information source to a destination, thereby potentially enhancing coverage and end-to-end capacity when a direct connection is weak. However, the operation of the source-to-relay, and the relay-to-destination links are traditionally separated via a TDD or an FDD scheme, in order to avoid self-interference. In contrast, an FD relay is capable of receiving information from a source, while simultaneously forwarding the information to the destination, thereby reducing the end to end latency and preserving the spectral efficiency. Different possibilities for reducing the loop interference in an FD relaying system is discussed in [58], leveraging from the separation of the transmit and receive spatial directions, as well as digital processing. The problems regarding relay resource allocation and power adjustment for the systems with single or multiple single-antenna

FD relays with amplify and forward (AF) process are studied in [59–64], and then extended for multiple-antenna setups in [65–77]. Studies on the FD relays with decode and forward (DF) process are given in [78–82]. In [83–85] the application of FD relays are considered where the relay node is equipped with a massive antenna array, thereby facilitating the relay transceiver with directive beams with the goal of a better SIC, as well as higher spectral and energy efficiency. In [86–88] an FD relaying setup is considered where the relay relies on the wireless energy reception to perform the relaying task. A secure information relaying is proposed in [86, 89, 90], where the FD relay benefits from the simultaneous information reception and transmission, as well as transmitting jamming signal to the potential eavesdroppers. In [91–95], the idea of FD in-band relaying is applied on an FD BS, where the UL information is relayed to the core network at the same channel, hence, providing a spectral efficient wireless backhaul link with reduced latency. The energy efficiency of the FD relaying systems is also studied in [96, 97].

FD and physical layer (PHY) security

Due to their broadcast nature, wireless systems are prone to interception by unauthorized receivers, i.e., eavesdroppers, hence compromising the confidentiality of the communicated data. Currently, information security is provided by the means of cryptographic approaches at the higher layers of the communication protocol stack, relying on the distribution of secret keys. However, such approaches are prone to attack due to the increasing computational capability of the receivers, as well as the challenges in the distribution and management of secret keys. In contrast, PHY security exploits the physical characteristics of the communication and the wiretap channels, with the intention that the communicated information is not received by the eavesdropper, hence obtaining perfect secrecy. In this regard, the application of FD nodes is promising, since they are capable of transmitting an artificial noise (AN) while receiving the useful information, thereby degrading the decoding capability of the eavesdropper. In [98–100] the application of FD transceivers is studied in the presence of eavesdropper nodes, however, assuming a perfect SIC. The works in [48, 48, 101, 102] have then considered the impact of RSI, where the FD transceiver is equipped with multiple antennas. It is observed that the joint consideration of FD jamming capability, together with multiple antenna beamforming, results in an effective jamming gain when channel state information (CSI) can be obtained for the channel to the eavesdropper. An unfortunate scenario where FD capability is employed by an eavesdropper is studied in [103], where the illegitimate receiver actively degrades the desired communication link via FD jamming. The work in [103] studies the optimization of PHY security on a bidirectional communication system where both nodes are capable of FD operation. In the latter case, the FD capability is utilized for both jamming, as well as simultaneous information transmission and reception. The consideration of PHY security in an FD-enabled cellular system is addressed in [48, 48, 101], where an FD basestation provides a secure communication simultaneously for UL and DL users. In [104, 105], PHY security in an FD-relaying system is studied, where an FD relay performs instantaneous and secure

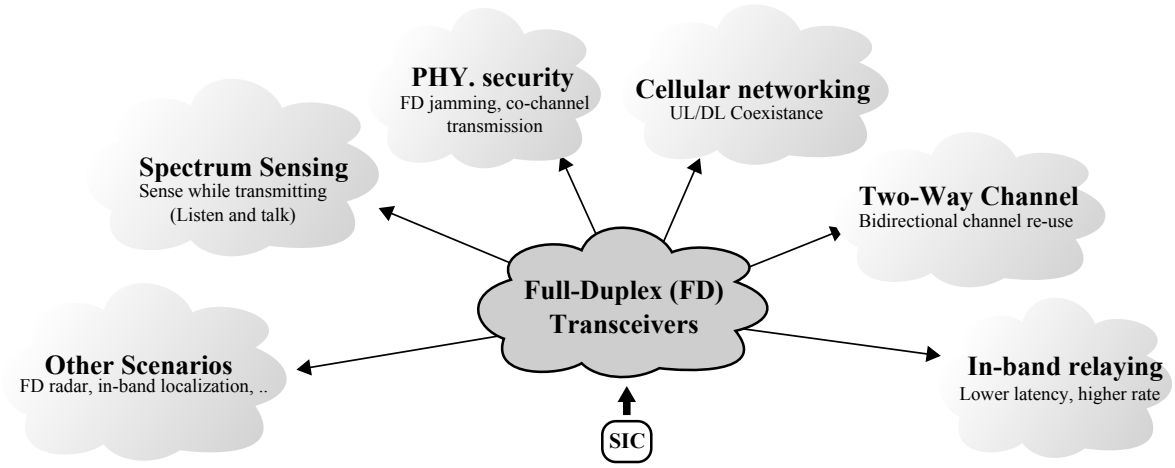

Figure 1.2: An overview on the applications of FD radios.

information forwarding, simultaneously with transmitting artificial noise directed to the eavesdropper.

Spectrum sensing

Unlike HD radios, an FD transceiver is capable of transmission and sensing at the same time and frequency, hence showing potential for a higher resolution spectrum sensing, as well as better collision avoidance during the transmission periods. In [106] a simultaneous transmission and sensing technique is proposed, where directional antennas are used to enable the FD operation. A simultaneous sensing and communication scheme is then enabled in [107]. In [108], an energy detection scheme is analyzed where the observed spectrum is additionally distorted by thermal noise, and residual self-interference. The application of an FD transceiver as an spectrum-observing cognitive node is considered in [109] for multiple promising scenarios, where the use of FD capability is observed to enhance the spectrum usage.

Further applications

Although the presented scenarios so far, are considered to be the most promising use-cases of the FD transceivers, the gainful application of FD nodes entail a broader set of use cases. In [110] active SIC methods are considered to significantly enhance the dynamic range of electronic scanning devices, by effectively measuring and reducing the near-end reflections. In [111] FD radios are considered as promising alternatives for distributed localization and group synchronization, however, assuming a perfect SIC. The reciprocal channel among two FD radios is considered as a shared information for the generation of secret keys, thereby enhancing the key generation rate which can be

obtained using HD radios. For a broader overview on the applications of FD transceivers please see [1, 112, 113].

1.3 Thesis Outline and Contributions

The outline of this thesis, as well as the main contributions are summarized in the following.

In Chapter 2, a bidirectional wireless communication system is studied between two FD transceivers, where both nodes are equipped with multiple antennas. In particular, a multi-carrier system is studied, where the communication in opposite directions can be interchangeably accommodated on the same channel resource, in order to enhance the spectral efficiency, or can be accommodated on orthogonal subcarriers, in order to avoid interference. The impact of channel estimation error as well as the non-linear transceiver distortions, leading to the RSI and inter-carrier leakage (ICL), are jointly taken into account. The design of the linear transmit and receive filters is then studied, following a sum rate maximization, as well as minimum sum mean squared-error (MSE) approaches. A notable gain is observed, compared to the traditionally HD systems, for transceivers with accurate hardware. However, it is observed that the application of a distortion-aware design is essential, as transceiver accuracy degrades and ICL becomes a dominant factor.

In Chapter 3, a MIMO FD relaying setup is studied, where the impact of hardware distortions are taken into account in the SIC process. The end-to-end performance of the FD relay is then evaluated and optimized, by the means of linear transmit and receive strategies. In particular, by jointly considering the impact of hardware distortions at the receive and transmit chains, we observe an inter-dependent behavior of the relay transmit covariance and the RSI covariance in an AF-FD relay, i.e., the distortion loop effect. This results in a performance disadvantage for the AF-FD relaying as dynamic range degrades, e.g., compared to the DF-FD relaying where the aforementioned inter-dependency does not exist due to decoding. Moreover, it is observed that for a system with a small thermal noise variance, or a high power or high transceiver distortion, the application of a distortion-aware design is essential.

In Chapter 4, the secrecy energy efficiency (SEE) of a multiple-input multiple-output multiple-antenna eavesdropper (MIMOME) wiretap channel is studied, in terms of the securely communicated bits-per-Joule, where the legitimate receiver is equipped with full-duplex (FD) capability. Hence, the transmitter and the legitimate receiver are capable of transmitting AN to the eavesdropper, while exchanging information. In particular, it is investigated: if and how the application of an FD jammer can enhance the system SEE, when considering the additional power used for jamming and SIC, as well as the degrading effect of RSI. In this regard, an optimized allocation of resources is proposed for the information and jamming transmissions, with the goal of maximizing

the system SEE, assuming the availability of perfect, or partial CSI. Numerical simulations indicate only a marginal SEE gain for a wide range of system conditions. However, under the condition that the SI can be efficiently mitigated, a significant gain is observed for the scenarios with a small distance between the FD node and the eavesdropper, a system with a high signal to noise ratio (SNR) condition, or for a bidirectional FD communication setup.

In Chapter 5, gainful utilization of FD capability for cellular communication systems is studied. In the first part, an overview on the application of FD capability in the radio access network is given, where UL and DL connections are scheduled on the same channel, aiming at a higher spectral efficiency. The coordination among the infrastructure nodes is observed to be effective in achieving a higher spectral efficiency, however, resulting in a higher data traffic on the backhaul network. In the second part, the application of FD wireless links is studied as a spectrum-saving mechanism for wireless backhaul solutions, leading to a reduced overall network cost. In particular, the coexistence of multiple wireless links at the same channel resource is enabled, utilizing an environment-aware interference management scheme together with the FD capability, leading to a reduced overall cost. Moreover, a reactive network re-tuning method is proposed which reacts to small changes in the network data, e.g., quality of service (QoS) requirements or SIC level, via transmit power adjustment on each wireless link. Numerical simulations suggest that for a dense urban deployment where the environment information is accurately accessible, the proposed methodologies lead to a reduced overall network cost, thanks to the FD capability at the radio links.

A summary of the main findings and an outlook for the future related research directions are given in Chapter 6. The contributions of this thesis are based on the works already published, or under consideration for publication in [28, 36, 37, 39, 47, 50, 51, 56, 59, 60, 74, 114–132].

1.4 Mathematical Notations and Conventions

The following mathematical notations and conventions are used throughout this thesis. Scalar values are denoted as italic normal letters, e.g., x. Column vectors and matrices are respectively denoted as lower-case and upper-case bold letters, e.g., $\mathbf{x}, \mathbf{X}$. An all-zero (all-one) matrix with size $m \times n$ is denoted as $\mathbf{0}_{m\times n}$ ($\mathbf{1}_{m\times n}$). The identity matrix with dimension K is denoted as $\mathbf{I}_K$.

1.4.1 Sets

The set $\mathbb{F}_K$ is defined as $\{1, 2, \ldots, K\}$. The set of real, positive real, and complex numbers are respectively denoted as $\mathbb{R}, \mathbb{R}^+, \mathbb{C}$. The size of the set $\mathbb{X}$ is denoted as $|\mathbb{X}|$. The set of all positive semi-definite matrices is denoted by $\mathcal{H}$.

1.4.2 Matrix and vector operations

Trace, inverse, determinant, transpose, conjugate and Hermitian transpose of the matrix $\mathbf{X}$ are respectively denoted by $\mathrm{tr}(\mathbf{X})$, $\mathbf{X}^{-1}$, $|\mathbf{X}|$, $\mathbf{X}^T$, $\mathbf{X}^*$ and $\mathbf{X}^H$. The Kronecker product is denoted by $\otimes$. $\mathrm{vec}(\mathbf{X})$ stacks the elements of $\mathbf{X}$ into a vector. Euclidean and Frobenius norms are respectively denoted as $\|\mathbf{x}\|_2$ and $\|\mathbf{X}\|_F$. $\mathrm{diag}(\mathbf{X})$ returns a diagonal matrix by putting the off-diagonal elements to zero. $\lfloor \mathbf{X}_i \rfloor_{i=1,\ldots,K}$ denotes a tall matrix, obtained by stacking the matrices $\mathbf{X}_i,\ i = 1, \ldots, K$. The range, i.e., column space, of the matrix $\mathbf{X}$ is denoted as $\mathcal{R}\{\mathbf{X}\}$. The value of $\{x\}^+$ is defined as

$$\{x\}^+ = \begin{cases} x & x \geq 0 \\ 0 & x < 0, \end{cases}$$

and the matrix $\{\mathbf{X}\}^+$ is similarly obtained by replacing the negative matrix elements by zero. The dominant eigenvalue, and the corresponding eigenvector of the matrix $\mathbf{X}$ are calculated via the operators $\lambda_{\max}\{\mathbf{X}\}$, and $\boldsymbol{\lambda}_{\max}\{\mathbf{X}\}$, respectively. $\boldsymbol{\Gamma}_M^l$ is an $M \times M$ zero matrix except for the l-th diagonal element equal to 1. The gradient of the function $F \in \mathbb{R}$ with respect to the matrix $\mathbf{X}$ and at the point $\mathbf{X}_0$ is denoted as $\nabla_{\mathbf{X}} F(\mathbf{X}_0)$. $\mathbf{S}_{\mathrm{D}}^M \in \{0,1\}^{M^2 \times M^2}$ is a selection matrix with one or zero elements such that $\mathbf{S}_{\mathrm{D}}^M \mathrm{vec}(\mathbf{X}) = \mathrm{vec}(\mathrm{diag}(\mathbf{X}))$, for $\mathbf{X} \in \mathbb{C}^{M \times M}$. $\mathbf{S}_{\mathrm{K}} \in \{0,1\}^{M^2N^2 \times M^2N^2}$ is a permutation matrix such that

$$\mathrm{vec}(\mathbf{X}_1 \otimes \mathbf{X}_2) = \mathbf{S}_{\mathrm{K}} \mathrm{vec}\left(\mathrm{vec}(\mathbf{X}_1)\mathrm{vec}(\mathbf{X}_2)^T\right),$$

for any $\mathbf{X}_1, \mathbf{X}_2 \in \mathbb{C}^{M \times N}$. Similarly, $\mathbf{S}_{\mathrm{T}} \in \{0,1\}^{MN \times MN}$, such that $\mathbf{S}_{\mathrm{T}} \mathrm{vec}(\mathbf{X}) = \mathrm{vec}(\mathbf{X}^T)$.

1.4.3 Statistical notations

Mathematical expectation is denoted as $\mathbb{E}\{\cdot\}$. The statistical independence is denoted as $\perp$. $\mathcal{CN}(\mathbf{x}, \mathbf{X})$ denotes a complex normal distribution with mean $\mathbf{x}$ and covariance $\mathbf{X}$.

2 Full-Duplex Bidirectional MIMO OFDM Communications

2.1 Overview

FD transceivers can accommodate a bidirectional communication on the same channel resource, hence showing potential to save the spectrum. On the other hand, FD systems suffer from the RSI, which may greatly impact the resulting system performance. Although successful instances of SIC have been demonstrated for a bidirectional setup, such methods are still far from perfect in a realistic environment mainly due to *i)* aging and inherent inaccuracy of the hardware (analog) elements, as well as *ii)* inaccurate CSI in the SI path, due to noise and limited channel coherence time. In this regard, inaccuracy of the analog hardware elements used in subtracting the dominant SI path in the RF domain, e.g., via signal injection methods, may result in severe degradation of the SIC quality. This issue becomes more relevant in a realistic scenario, where unlike the demonstrated setups in the lab environment, analog components are prone to aging, temperature fluctuations, and occasional physical damage. Moreover, an FD link is vulnerable to CSI inaccuracy at the SI path in environments with a small channel coherence time. A good example of such challenge is a high-speed vehicle that passes close to an FD device, and results in additional reflective SI paths[1].

In order to combat the aforementioned issues, an FD transceiver may adapt its Tx and Rx strategies to the expected nature of the CSI inaccuracy, e.g., by directing the transmit beams away from the moving objects or operating in the directions with smaller impact of CSI error. Moreover, the accuracy of the Tx and Rx chain elements can be considered, e.g., by dedicating less power, or ignoring the chains with noisier elements in the signal processing. In this regard, a widely used model for the operation of a multiple-antenna FD transceiver is proposed in [32], assuming a single-carrier communication system, where CSI inaccuracy as well as the impact of hardware impairments are taken into account. A gradient projection (GP)-based method is then proposed in the same work for maximizing the sum rate in an FD bidirectional setup. Building upon the proposed benchmark, a convex optimization design framework is introduced in [27,28] by defining a price/threshold for the SI power, assuming the availability of perfect CSI and accurate transceiver operation. While this approach reduces the design computational complexity, it does not provide a reliable performance for a scenario with erroneous

[1]Since the object is moving rapidly, the reflective paths are more difficult to be accurately estimated.

CSI, particularly regarding the SI path [126]. Consequently, the consideration of CSI and transceiver error in an FD bidirectional system is further studied in [35, 36] by maximizing the system sum rate, in [133] by minimizing the sum MSE, and in [38, 39] for minimizing the system power consumption under a required quality of service.

The aforementioned works focus on modeling and design methodologies for single-carrier FD bidirectional systems under frequency-flat channel assumptions. In this regard, the importance of extending the previous designs for a multi carrier (MC) system with a frequency selective channel is threefold. Firstly, due to the increasing rate demand of the wireless services, and following the same rationale for the promotion of FD systems, the usage of larger bandwidths becomes necessary. This, in turn, invalidates the usual frequency-flat assumption and calls for updated design methodologies. Secondly, unlike the half-duplex (HD) systems where the operation of different subcarriers can be safely separated in the digital domain, an FD system is highly prone to the ICL due to the impact of hardware distortions on the strong SI channel[2]. This, in particular, calls for a proper modeling of the ICL effect as a result of non-linear hardware distortions for FD transceivers. And finally, the channel frequency selectivity shall be opportunistically exploited to enhance the system performance.

2.1.1 Related works on FD multi-carrier systems

In the early work by Riihonen *et al.* [134], the performance of a combined analog and digital SIC scheme is evaluated for an FD orthogonal frequency-division multiplexing (OFDM) transceiver, taking into account the impact of hardware distortions, e.g., limited ADC accuracy. The problems of resource allocation and performance analysis for FD MC communication systems are then addressed in [53, 135–140], however, assuming a single-antenna transceiver. Specifically, an FD MC system is studied in [135–137] in the context of FD relaying, in [53, 139] and [138] in the context of FD cellular systems with non-orthogonal multiple access (NOMA) capability, and in [140] for rate region analysis of a hybrid HD and FD link. Moreover, an MC relaying system with hybrid DF and AF operation is studied in [141], with the goal of maximizing the system sum rate via scheduling and resource allocation. However, in all of the aforementioned designs, the behavior of the RSI signal is modeled as a purely linear system. As a result, the impacts of the hardware distortions leading to ICL, as observed in [134], are neglected.

2.1.2 Chapter outline and contributions

The main contributions of this chapter are as follows:

[2]For instance, a high-power transmission in one of the subcarriers will result in a higher RSI in all of the sub-channels due to, e.g., a higher quantization and power amplifier noise levels.

- In the seminal work by Day *et al.* [32], an FD MIMO transceiver is modeled considering the impacts of limited dynamic range in Tx and Rx chains, however, assuming a single-carrier setup with a frequency-flat channel. In this chapter, the similar experimental results on MIMO OFDM systems [142–144] are utilized, indicating the Gaussian and statistically independent nature of distortion signals at different chains and different time samples, and extending the available model to an FD MC system. As a result, in Section 2.2, the explicit impact of hardware distortions on RSI and ICL is formulated in relation to the intended Tx and Rx signals.

- Building on the obtained model, linear transmit and receive strategies are proposed in order to enhance the system performance. In Section 2.3, an alternating quadratic convex programing (QCP) method, denoted as AltQCP, is proposed in order to obtain a minimum weighted MSE transceiver design. The known weighted minimum mean squared-error (WMMSE) method [145] is then utilized to extend the alternating quadratic convex programming (AltQCP) framework for maximizing the system sum rate. For both algorithms, a monotonic performance improvement is observed at each step, leading to a necessary convergence.

- In Section 2.4 the proposed design in Section 2.3 is extended by also taking into account the impact of CSI error. This is done by updating the system model proposed in Section 2.2. Moreover, a worst-case minimum mean squared-error (MMSE) design is proposed as an alternating semi-definite programming (SDP), denoted as AltSDP. Similar to the previous methods, a monotonic performance improvement is observed at each step, leading to a necessary convergence.

- FD systems are vulnerable to the CSI error due to, e.g., additional reflections from a moving object, particularly due to the impact of residual self-interference. It is hence beneficial to obtain the worst-case CSI error conditions for the purpose of worst-case performance evaluation. Moreover, other than the usual approach of optimizing system parameters independently for each frame [35, 36, 38, 39, 133], such knowledge can be used for prevention purposes, e.g., updating the channel training sequence to prevent destructive CSI error conditions. To facilitate this, in Section 2.5, a methodology to obtain the least favorable CSI error matrices is proposed by transforming the resulting non-convex quadratic problem into a convex problem.

Numerical simulations show that the application of a distortion-aware design is essential, as transceiver accuracy degrades, and ICL becomes a dominant factor. Part of this chapter is based on the works which are published or under consideration for publication in [28, 36, 37, 39, 123–127].

2.2 System Model

A bidirectional OFDM communication between two MIMO FD transceivers is considered. Each communication direction is associated with N_i transmit and M_i receive antennas, where $i \in \mathbb{I}$, and $\mathbb{I} := \{1, 2\}$ represents the set of the communication directions. The desired channel in the communication direction i and subcarrier $k \in \mathbb{F}_K$ is denoted as $\mathbf{H}_{ii}^k \in \mathbb{C}^{M_i \times N_i}$ where K is the number of subcarriers. The SI channel from i to j-th communication direction is denoted as $\mathbf{H}_{ji}^k \in \mathbb{C}^{M_j \times N_i}$. All channels are quasi-static[3], and frequency-flat in each subcarrier.

The transmitted signal in the direction i, subcarrier k is formulated as

$$\mathbf{x}_i^k = \underbrace{\mathbf{V}_i^k \mathbf{s}_i^k}_{=:\mathbf{v}_i^k} + \mathbf{e}_{\mathrm{t},i}^k, \quad \sum_{k \in \mathbb{F}_K} \mathbb{E}\left\{\|\mathbf{x}_i^k\|_2^2\right\} \leq P_i, \tag{2.1}$$

where $\mathbf{s}_i^k \in \mathbb{C}^{d_i}$ and $\mathbf{V}_i^k \in \mathbb{C}^{N_i \times d_i}$ respectively represent the vector of the data symbols and the transmit precoding matrix, and $P_i \in \mathbb{R}^+$ imposes the maximum affordable transmit power constraint. The number of the data streams in each subcarrier and in direction i is denoted as d_i, and $\mathbb{E}\{\mathbf{s}_i^k \mathbf{s}_i^{k\,H}\} = \mathbf{I}_{d_i}$. Moreover, $\mathbf{v}_i^k \in \mathbb{C}^{N_i}$ represents the desired signal to be transmitted, where $\mathbf{e}_{\mathrm{t},i}^k$ models the inaccurate behavior of the transmit chain elements, i.e, transmit distortion, see Subsection 2.2.1 for more details.

The received signal at the destination can be consequently written as

$$\mathbf{y}_i^k = \underbrace{\mathbf{H}_{ii}^k \mathbf{x}_i^k + \mathbf{H}_{ij}^k \mathbf{x}_j^k + \mathbf{n}_i^k}_{=:\mathbf{u}_i^k} + \mathbf{e}_{\mathrm{r},i}^k, \tag{2.2}$$

where $\mathbf{n}_i^k \sim \mathcal{CN}\left(\mathbf{0}_{M_i}, \sigma_{i,k}^2 \mathbf{I}_{M_i}\right)$ is the additive thermal noise. Similar to the transmit signal model, $\mathbf{e}_{\mathrm{r},i}^k$ represents the receiver distortion and models the inaccuracies of the receive chain elements. The *known*, i.e., distortion-free, part of the SI is then subtracted from the received signal, employing an SIC scheme. This is formulated as

$$\tilde{\mathbf{y}}_i^k := \mathbf{y}_i^k - \mathbf{H}_{ij}^k \mathbf{V}_j^k \mathbf{s}_j^k = \mathbf{H}_{ii}^k \mathbf{V}_i^k \mathbf{s}_i^k + \boldsymbol{\nu}_i^k, \tag{2.3}$$

where $\tilde{\mathbf{y}}_i^k$ is the received signal in direction i and subcarrier k, after SIC. Moreover, the aggregate interference-plus-noise term is denoted as $\boldsymbol{\nu}_i^k \in \mathbb{C}^{M_i}$, where

$$\boldsymbol{\nu}_i^k = \mathbf{H}_{ij}^k \mathbf{e}_{\mathrm{t},j}^k + \mathbf{H}_{ii}^k \mathbf{e}_{\mathrm{t},i}^k + \mathbf{e}_{\mathrm{r},i}^k + \mathbf{n}_i^k, \quad j \neq i. \tag{2.4}$$

Finally, the estimated data vector is obtained at the receiver as

$$\tilde{\mathbf{s}}_i^k = \left(\mathbf{U}_i{}^k\right)^H \tilde{\mathbf{y}}_i^k, \tag{2.5}$$

where $\mathbf{U}_i^k \in \mathbb{C}^{M_i \times d_i}$ is the linear receive filter.

[3]It indicates that the channel is constant in each communication frame, but may vary from one frame to another frame.

2.2.1 Limited dynamic range in an FD OFDM system

In the seminal works in [32, 78] a model for the operation of an FD MIMO system is proposed, relying on the experimental results and modeling on the impact of hardware distortions. In this part, we rely on the similar experimental results conducted on a MIMO OFDM system, see [143] regarding the measurements on receiver chain distortions and [142, 144] for transmit distortions, as well as the recent characterizations of FD transceivers [134, 146] in order to provide a reasonable abstraction. The results of the aforementioned experiments led to four major indications:

(a) The collective distortion signal in each chain is approximated by an additive zero-mean Gaussian term,

(b) The variance of the distortion signal is proportional to the power of the intended transmit or receive signal,

(c) The distortion signal is statistically independent from the intended transmit or receive signal at each chain,

(d) The distortion signal is statistically independent for different chains, and at different time samples,

where (a) is substantiated in [142], and (c)-(d) are obtained in [142, Section IV], [143], see [32, Section II], [78, Section II], [35, 38, 79, 147, 148] for a similar assumption set. Please note that the accuracy of the above-mentioned assumptions varies for different implementations of FD transceivers, depending on the complexity and the used SIC method. In this regard, the statistical independence of distortion elements defined in (c) and (d) holds also for an advanced implementation of an FD transceiver, assuming a high signal processing capability[4]. However, the linear dependence of the remaining distortion signal variance to the desired signal strength, and the choice of distortion coefficients may vary for different SIC techniques.

Following the above arguments, the inaccuracy of the transmit chain elements, e.g., digital-to-analog converter (DAC) error, power amplifier (PA) and oscillator phase noise, are jointly modeled for each antenna as an additive distortion, and written as $x_l(t) = v_l(t) + e_{\mathrm{t},l}(t)$, see Fig. 2.1, such that

$$e_{\mathrm{t},l}(t) \sim \mathcal{CN}\Big(0, \kappa_l \mathbb{E}\Big\{ |v_l(t)|^2 \Big\}\Big), \tag{2.6}$$

$$e_{\mathrm{t},l}(t) \perp v_l(t), \;\; e_{\mathrm{t},l}(t) \perp e_{\mathrm{t},l'}(t), \;\; e_{\mathrm{t},l}(t) \perp e_{\mathrm{t},l}(t'), \quad l \neq l' \in \mathbb{L}_T, \;\; t \neq t', \tag{2.7}$$

where t denotes the instance of time, and v_l, x_l, and $e_{\mathrm{t},l} \in \mathbb{C}$ are respectively the baseband time-domain representation of the intended transmit signal, the actual transmit

[4]This is since any correlation structure in the distortion signal can be exploited and removed in order to reduce the residual self-interference via advanced signal processing, see [2, Subsection 3.2].

signal, and the additive transmit distortion at the l-th transmit chain. The set $\mathbb{L}_T$ represents the set of all transmit chains. Moreover, $\kappa_l \in \mathbb{R}^+$ represents the distortion coefficient for the l-th transmit chain, relating the collective power of the distortion signal, over the active spectrum, to the intended transmit power.

In the receiver side, the combined effects of the inaccurate hardware elements, i.e., ADC error, automatic gain control (AGC) and oscillator phase noise, are presented as additive distortion terms and written as $y_l(t) = u_l(t) + e_{\mathrm{r},l}(t)$ such that

$$e_{\mathrm{r},l}(t) \sim \mathcal{CN}\Big(0, \beta_l \mathbb{E}\big\{ |u_l(t)|^2 \big\}\Big), \tag{2.8}$$

$$e_{\mathrm{r},l}(t) \perp u_l(t), \;\; e_{\mathrm{r},l}(t) \perp e_{\mathrm{r},l'}(t), \;\; e_{\mathrm{r},l}(t) \perp e_{\mathrm{r},l}(t'), \quad l \neq l' \in \mathbb{L}_R, \;\; t \neq t', \tag{2.9}$$

where u_l, $e_{\mathrm{r},l}$, and $y_l \in \mathbb{C}$ are respectively the baseband representation of the intended (distortion-free) received signal, additive receive distortion, and the received signal from the l-th receive antenna. The set $\mathbb{L}_R$ represents the set of all receive chains. Similar to the transmit chain characterization, $\beta_l \in \mathbb{R}^+$ is the distortion coefficient for the l-th receive chain, see Fig. 2.1. For each communication block, the frequency domain representation of the sampled time domain signal is obtained as

$$x_l^k = \frac{1}{\sqrt{K}} \sum_{m=0}^{K-1} x_l(mT_{\mathrm{s}}) e^{-\frac{j2\pi mk}{K}} = \underbrace{\frac{1}{\sqrt{K}} \sum_{m=0}^{K-1} v_l(mT_{\mathrm{s}}) e^{-\frac{j2\pi mk}{K}}}_{=:v_l^k} + \underbrace{\frac{1}{\sqrt{K}} \sum_{m=0}^{K-1} e_{\mathrm{t},l}(mT_{\mathrm{s}}) e^{-\frac{j2\pi mk}{K}}}_{=:e_{\mathrm{t},l}^k}, \tag{2.10}$$

and

$$y_l^k = \frac{1}{\sqrt{K}} \sum_{m=0}^{K-1} y_l(mT_{\mathrm{s}}) e^{-\frac{j2\pi mk}{K}} = \underbrace{\frac{1}{\sqrt{K}} \sum_{m=0}^{K-1} u_l(mT_{\mathrm{s}}) e^{-\frac{j2\pi mk}{K}}}_{=:u_l^k} + \underbrace{\frac{1}{\sqrt{K}} \sum_{m=0}^{K-1} e_{\mathrm{r},l}(mT_{\mathrm{s}}) e^{-\frac{j2\pi mk}{K}}}_{=:e_{\mathrm{r},l}^k}, \tag{2.11}$$

where T_{s} is the sampling time, and KT_{s} is the OFDM block duration prior to the cyclic extension, see [149] for a detailed discussion on OFDM technology.

Lemma 2.2.1. *The impact of hardware distortions in the frequency domain is characterized as*

$$e_{t,l}^k \sim \mathcal{CN}\left(0, \frac{\kappa_l}{K} \sum_{m \in \mathbb{F}_K} \mathbb{E}\left\{ |v_l^m|^2 \right\}\right), \;\; e_{t,l}^k \perp v_l^k, \;\; e_{t,l}^k \perp {e_{t,l'}}^k, \tag{2.12}$$

$$e_{r,l}^k \sim \mathcal{CN}\left(0, \frac{\beta_l}{K} \sum_{m \in \mathbb{F}_K} \mathbb{E}\left\{ |u_l^m|^2 \right\}\right), \;\; e_{r,l}^k \perp u_l^k, \;\; e_{r,l}^k \perp {e_{r,l'}}^k, \tag{2.13}$$

transforming the statistical independence, as well as the proportional variance properties from the time domain.

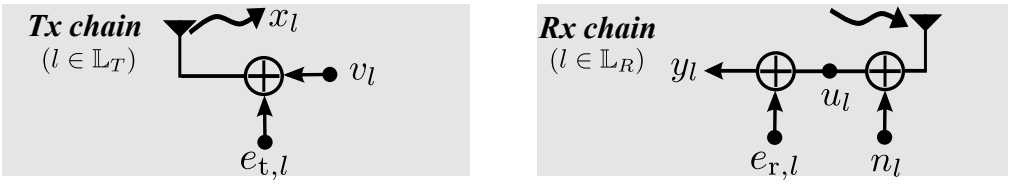

Figure 2.1: Limited dynamic range is modeled by injecting additive distortion terms at each transmit or receive chain. $e_{\mathrm{t},l}$ and $e_{\mathrm{r},l}$ denote the distortion terms, and n_l represent the additive thermal noise.

Proof. See Appendix 7. □

The above lemma indicates that the distortion signal variance at each subcarrier, relates to the total distortion power at the corresponding chain, indicating the impact of ICL. This can be interpreted as a variance-dependent thermal noise, where the temporal independence of signal samples results in a flat power spectral density over the active communication bandwidth. In this part we consider a general framework where the transmit (receive) distortion coefficients are not necessarily identical for all transmit (receive) chains belonging to the same transceiver, i.e., different chains may hold different accuracy due to occasional damage and aging. This assumption is relevant in practice since it enables the design algorithms to reduce communication task, e.g., transmit power, on the chains with noisier elements. Following Lemma 2.2.1, the statistics of the distortion terms, introduced in (2.1), (2.2) can be inferred as

$$\mathbf{e}_{\mathrm{t},i}^{k} \sim \mathcal{CN}\left(\mathbf{0}_{N_i}, \boldsymbol{\Theta}_{\mathrm{tx},i} \sum_{k\in\mathbb{F}_K} \mathrm{diag}\left(\mathbb{E}\left\{\mathbf{v}_i^k \mathbf{v}_i^{k\,H}\right\}\right)\right), \tag{2.14}$$

$$\mathbf{e}_{\mathrm{r},i}^{k} \sim \mathcal{CN}\left(\mathbf{0}_{M_i}, \boldsymbol{\Theta}_{\mathrm{rx},i} \sum_{k\in\mathbb{F}_K} \mathrm{diag}\left(\mathbb{E}\left\{\mathbf{u}_i^k \mathbf{u}_i^{k\,H}\right\}\right)\right), \tag{2.15}$$

where $\boldsymbol{\Theta}_{\mathrm{tx},i} \in \mathbb{R}^{N_i \times N_i}$ ($\boldsymbol{\Theta}_{\mathrm{rx},i} \in \mathbb{R}^{M_i \times M_i}$) is a diagonal matrix including distortion coefficients κ_l/K (β_l/K) for the corresponding chains[5].

Via the application of (2.14)-(2.15) on (2.4), the covariance of the received collective interference-plus-noise signal is obtained as

$$\begin{aligned}\boldsymbol{\Sigma}_i^k :&\approx \mathbb{E}\left\{\boldsymbol{\nu}_i^k \boldsymbol{\nu}_i^{k\,H}\right\} \\ &= \sum_{j\in\mathbb{I}} \mathbf{H}_{ij}^k \boldsymbol{\Theta}_{\mathrm{tx},j} \mathrm{diag}\left(\sum_{l\in\mathbb{F}_K} \mathbf{V}_j^l \mathbf{V}_j^{l\,H}\right) \mathbf{H}_{ij}^{k\,H} \\ &+ \boldsymbol{\Theta}_{\mathrm{rx},i} \mathrm{diag}\left(\sum_{l\in\mathbb{F}_K}\left(\sigma_{i,l}^2 \mathbf{I}_{M_i} + \sum_{j\in\mathbb{I}} \mathbf{H}_{ij}^l \mathbf{V}_j^l \mathbf{V}_j^{l\,H} \mathbf{H}_{ij}^{l\,H}\right)\right) + \sigma_{i,k}^2 \mathbf{I}_{M_i}, \quad k \in \mathbb{F}_K, \end{aligned} \tag{2.16}$$

[5] A simpler mathematical presentation can be obtained by assuming the same transceiver accuracy over all antennas, similar to [32, 78]. In such a case, the defined diagonal matrices can be replaced by a scalar.

where $\mathbf{\Sigma}_i^k \in \mathbb{C}^{M_i \times M_i}$ is obtained considering $0 \leq \beta_l \ll 1$, $0 \leq \kappa_l \ll 1$, and hence ignoring the terms containing higher orders of the distortion coefficients in (2.16).

2.2.2 Remarks

- In this section, we have assumed the availability of perfect CSI, and focused on the impact of non-linear transceiver distortions. This assumption is relevant for the scenarios with stationary channel, e.g., a backhaul directive link with zero mobility [150], where an adequately long training sequence can be applied, see [32, Subsection III.A]. The impact of the CSI inaccuracy is later addressed in Section 2.4.
- As expected, the role of the distortion signals on the RSI, including the resulting ICL, is evident from (2.16). It is the main goal of the remaining parts of this chapter to incorporate and evaluate this impact on the design of the defined MC system.

2.3 Linear Transceiver Design for Multi-Carrier Communications

Via the application of $\mathbf{V}_i^k$ and $\mathbf{U}_i^k$, as the linear transmit precoder and receive filters, the MSE matrix of the defined system is calculated as

$$\begin{aligned}\mathbf{E}_i^k :&= \mathbb{E}\left\{\left(\tilde{\mathbf{s}}_i^k - \mathbf{s}_i^k\right)\left(\tilde{\mathbf{s}}_i^k - \mathbf{s}_i^k\right)^H\right\} \\ &= \left(\mathbf{U}_i^{kH}\mathbf{H}_{ii}^k\mathbf{V}_i^k - \mathbf{I}_{d_i}\right)\left(\mathbf{U}_i^{kH}\mathbf{H}_{ii}^k\mathbf{V}_i^k - \mathbf{I}_{d_i}\right)^H + \mathbf{U}_i^{kH}\mathbf{\Sigma}_i^k\mathbf{U}_i^k, \end{aligned} \tag{2.17}$$

where $\mathbf{\Sigma}_i^k$ is given in (2.16). In the following two design strategies are introduced for the defined system via an alternating QCP framework.

2.3.1 Weighted MSE minimization via Alternating QCP (AltQCP)

An optimization problem for minimizing the weighted sum MSE is written as

$$\min_{\mathbb{V},\mathbb{U}} \quad \sum_{i\in\mathbb{I}}\sum_{k\in\mathbb{F}_K} \mathrm{tr}\left(\mathbf{S}_i^k\mathbf{E}_i^k\right) \tag{2.18a}$$

$$\text{s.t.} \quad \mathrm{tr}\left(\left(\mathbf{I}_{N_i} + K\mathbf{\Theta}_{\mathrm{tx},i}\right)\sum_{l\in\mathbb{F}_K}\mathbf{V}_i^l\mathbf{V}_i^{lH}\right) \leq P_i, \quad \forall i \in \mathbb{I}, \tag{2.18b}$$

where $\mathbb{X} := \{\mathbf{X}_i^k,\ \forall i \in \mathbb{I},\ \forall k \in \mathbb{F}_K\}$, with $\mathbb{X} \in \{\mathbb{U}, \mathbb{V}\}$, and (2.18b) represents the transmit power constraint. It is worth mentioning that the application of $\mathbf{S}_i^k \succ 0$, as a weight matrix associated with $\mathbf{E}_i^k$ is two-folded. Firstly, it may appear as a diagonal matrix, emphasizing the importance of different data streams and communication directions. Secondly, it can be applied as an auxiliary variable which later relates the defined weighted MSE minimization to a sum-rate maximization problem, see Subsection 2.3.2.

It is observed that (2.18) is not a jointly convex problem. Nevertheless, it holds a QCP structure separately over the sets $\mathbb{V}$ and $\mathbb{U}$, when other variables are fixed. In this regard, the objective (2.18a) can be decomposed over $\mathbb{U}$ for different communication directions, and for different subcarriers. The optimal MMSE receive filter can be hence calculated in closed form as

$$\mathbf{U}_{i,\text{mmse}}^k = \left(\mathbf{\Sigma}_i^k + \mathbf{H}_{ii}^k \mathbf{V}_i^k \mathbf{V}_i^{k\,H} \mathbf{H}_{ii}^{k\,H}\right)^{-1} \mathbf{H}_{ii}^k \mathbf{V}_i^k. \tag{2.19}$$

Nevertheless, the defined problem is coupled over $\mathbf{V}_i^k$, due to the impact of ICL, as well as the power constraint (2.18b). The Lagrangian function, corresponding to the optimization problem (2.18) over $\mathbb{V}$ is expressed as

$$\mathcal{L}\left(\mathbb{V}, \boldsymbol{\iota}\right) := \sum_{i \in \mathbb{I}} \left(\iota_i \mathcal{P}_i\left(\mathbb{V}\right) + \sum_{k \in \mathbb{F}_K} \text{tr}\left(\mathbf{S}_i^k \mathbf{E}_i^k\right) \right), \tag{2.20}$$

$$\mathcal{P}_i\left(\mathbb{V}\right) := -P_i + \text{tr}\left(\left(\mathbf{I}_{N_i} + K\mathbf{\Theta}_{\text{tx},i}\right) \sum_{l \in \mathbb{F}_K} \mathbf{V}_i^l \mathbf{V}_i^{l\,H} \right), \tag{2.21}$$

where $\boldsymbol{\iota} := \{\iota_i,\ i \in \mathbb{I}\}$ is the set of dual variables. The dual function, corresponding to the above Lagrangian is defined as

$$\mathcal{F}\left(\boldsymbol{\iota}\right) : = \min_{\mathbb{V}}\ \ \mathcal{L}\left(\mathbb{V}, \boldsymbol{\iota}\right), \tag{2.22}$$

where the optimal $\mathbf{V}_i^k$ is obtained as

$$\mathbf{V}_i^{k\star} = \left(\mathbf{J}_i^k + \iota_i \left(\mathbf{I}_{N_i} + K\mathbf{\Theta}_{\text{tx},i}\right) + \mathbf{H}_{ii}^{k\,H} \mathbf{U}_i^k \mathbf{S}_i^k \mathbf{U}_i^{k\,H} \mathbf{H}_{ii}^k\right)^{-1} \mathbf{H}_{ii}^{k\,H} \mathbf{U}_i^k \mathbf{S}_i^k, \tag{2.23}$$

and

$$\mathbf{J}_i^k : = \sum_{l \in \mathbb{F}_K} \sum_{j \in \mathbb{I}} \left(\mathbf{H}_{ji}^{k\,H} \text{diag}\left(\mathbf{U}_j^l \mathbf{S}_j^l \mathbf{U}_j^{l\,H} \mathbf{\Theta}_{\text{rx},j}\right) \mathbf{H}_{ji}^k + \text{diag}\left(\mathbf{H}_{ji}^{l\,H} \mathbf{U}_j^l \mathbf{S}_j^l \mathbf{U}_j^{l\,H} \mathbf{H}_{ji}^l \mathbf{\Theta}_{\text{tx},i}\right) \right). \tag{2.24}$$

Due to the convexity of the original problem (2.18) over $\mathbb{V}$, the defined dual problem is a concave function over $\boldsymbol{\iota}$, with $\mathcal{P}_i(\mathbb{V})$ as a subgradient, see [151, Eq. (6.1)]. As a result, the optimal $\boldsymbol{\iota}$ is obtained from the maximization

$$\boldsymbol{\iota}^\star = \underset{\boldsymbol{\iota} \geq 0}{\text{argmax}}\ \mathcal{F}\left(\boldsymbol{\iota}\right), \tag{2.25}$$

following a standard subgradient update [151, Subsection 6.3.1].

Utilizing the proposed optimization framework, the alternating optimization over $\mathbb{V}$ and $\mathbb{U}$ is continued until a stable point is obtained. Note that due to the monotonically non-increasing nature of the objective in each step, and the fact that (2.18a) is non-negative and hence bounded from below, the defined procedure converges necessarily. Algorithm 1 defines the necessary optimization steps.

Algorithm 1 Alternating QCP (AltQCP) for weighted MSE minimization

1: $\ell \leftarrow 0$; (set iteration number to zero);
2: $\mathbb{V} \leftarrow$ right singular matrix initialization, see [152, Appendix A];
3: $\mathbb{U} \leftarrow$ solve (2.19);
4: **repeat**
5: $\quad \ell \leftarrow \ell + 1$;
6: $\quad \mathbb{V} \leftarrow$ solve (2.23) or QCP (2.18), with fixed $\mathbb{U}$;
7: $\quad \mathbb{U} \leftarrow$ solve (2.19) or QCP (2.18) with fixed $\mathbb{V}$;
8: **until** a stable point, or maximum number of ℓ reached
9: **return** $\{\mathbb{U}, \mathbb{V}\}$;

2.3.2 Weighted MMSE (WMMSE) design for sum rate maximization

Via the utilization of $\mathbf{V}_i^k$ as the transmit precoders, the resulting communication rate for the k-th subcarrier and for the i-th communication direction is written as

$$I_i^k = \log_2 \left| \mathbf{I}_{d_i} + \mathbf{V}_i^{k\,H} \mathbf{H}_{ii}^{k\,H} \left(\mathbf{\Sigma}_i^k \right)^{-1} \mathbf{H}_{ii}^k \mathbf{V}_i^k \right|, \tag{2.26}$$

where $\mathbf{\Sigma}_i^k$ is defined in (2.16). The sum rate maximization problem can be hence presented as

$$\max_{\mathbb{V}} \quad \sum_{i \in \mathbb{I}} \sum_{k \in \mathbb{F}_K} I_i^k, \ \text{ s.t. } (2.18\text{b}). \tag{2.27}$$

The optimization problem (2.27) is intractable in the current form. In the following an iterative optimization solution is proposed following the WMMSE method [145].
Via the application of the MMSE receive linear filters from (2.19), the resulting MSE matrix is obtained as

$$\mathbf{E}_{i,\text{mmse}}^k = \left(\mathbf{I}_{d_i} + \mathbf{V}_i^{k\,H} \mathbf{H}_{ii}^{k\,H} \left(\mathbf{\Sigma}_i^k \right)^{-1} \mathbf{H}_{ii}^k \mathbf{V}_i^k \right)^{-1}. \tag{2.28}$$

By recalling (2.26), and upon utilization of $\mathbf{U}_{i,\text{mmse}}^k$, the following useful connection to the rate function is observed

$$I_i^k = -\log_2 \left| \mathbf{E}_{i,\text{mmse}}^k \right|, \tag{2.29}$$

which facilitates the decomposition of rate function via the following lemma, see also [145, Eq. (9)].

Lemma 2.3.1. *Let* $\mathbf{E} \in \mathbb{C}^{d\times d}$ *be a positive definite matrix. The maximization of the term* $-log|\mathbf{E}|$ *is equivalent to the maximization*

$$\max_{\mathbf{E},\mathbf{S}} - tr(\mathbf{SE}) + log|\mathbf{S}| + d, \tag{2.30}$$

where $\mathbf{S} \in \mathbb{C}^{d\times d}$ *is a positive definite matrix, and we have*

$$\mathbf{S} = \mathbf{E}^{-1}, \tag{2.31}$$

at the optimality.

Proof. See [153, Lemma 2]. □

By recalling (2.29), and utilizing Lemma 2.3.1, the original optimization problem over $\mathbb{V}$ can be equivalently formulated as

$$\max_{\mathbb{V},\mathbb{U},\mathbb{S}} \sum_{k\in\mathbb{F}_K}\sum_{i\in\mathbb{I}} \left(\log\left|\mathbf{S}_i^k\right| + d_i - \mathrm{tr}\left(\mathbf{S}_i^k\mathbf{E}_i^k\right)\right) \text{ s.t. (2.18b)}, \tag{2.32}$$

where $\mathbb{S} := \{\mathbf{S}_i^k \succ 0,\ \forall i \in \mathbb{I},\ \forall k \in \mathbb{F}_K\}$. The obtained optimization problem (2.32) is not a jointly convex problem. Nevertheless, it is a QCP over $\mathbb{V}$ when other variables are fixed, and can be obtained with a similar structure as for (2.18). Moreover, the optimization over $\mathbb{U}$ and $\mathbb{S}$ is respectively obtained from (2.19), and (2.31) as $\mathbf{S}_i^k = \left(\mathbf{E}_i^k\right)^{-1}$. This facilitates an alternating optimization where in each step the corresponding problem is solved to optimality, see Algorithm 2. The defined alternating optimization steps result in a necessary convergence in the value of the objective. This is due to the monotonically non-decreasing nature of the objective in each step, and the fact that the eventual system sum rate is bounded from above.

Algorithm 2 AltQCP-WMMSE design for sum rate maximization

Algorithm 1, Steps 1-2 (initialization);
repeat
  Algorithm 1, Steps 5-7;
  $\mathbb{S} \leftarrow \mathbf{S}_i^k = \left(\mathbf{E}_i^k\right)^{-1}$;
until a stable point, or maximum number of ℓ reached
return $\{\mathbb{V}\}$;

2.4 Robust Design with Imperfect CSI

In many realistic scenarios the CSI matrices can not be estimated or communicated accurately due to the limited channel coherence time as a result of, e.g., reflections from a moving object, or due to dedicating limited resource on the training and feedback

process. This issue becomes more significant in an FD system, due to the strong SI channel which calls for dedicated silent times for tuning and training process, see [32, Subsection III.A]. In particular, the impact of CSI error on the defined MC FD system is threefold. Firstly, similar to the usual HD scenarios, it results in the erroneous equalization in the receiver, as the communication channels are not accurately known. Secondly, it results in an inaccurate estimation of the received signal from the self-interference path, and thereby degrades the SIC quality. Finally, due to the CSI error, the impact of the distortion signals may not be accurately known, as the statistics of the distortion signals directly depend on the channel situation. In this part we extend the proposed designs in Section 2.3 such that the aforementioned uncertainties, resulting from CSI error, are also taken into account.

2.4.1 Norm-bounded CSI error

In this part we update the defined system model in Section 2.2 to the scenario where the CSI is known erroneously. In this respect we follow the so-called deterministic model [154], where the error matrices are not known but located, with a sufficiently high probability, within a known feasible error region. This is expressed as

$$\mathbf{H}_{ij}^k = \tilde{\mathbf{H}}_{ij}^k + \mathbf{\Delta}_{ij}^k, \quad \mathbf{\Delta}_{ij}^k \in \mathbb{D}_{ij}^k, \quad i,j \in \mathbb{I}, \tag{2.33}$$

and

$$\mathbb{D}_{ij}^k := \left\{ \mathbf{\Delta}_{ij}^k \;\middle|\; \|\mathbf{D}_{ij}^k \mathbf{\Delta}_{ij}^k\|_F \leq \zeta_{ij}^k \right\}, \quad \forall i,j \in \mathbb{I},\ k \in \mathbb{F}_K, \tag{2.34}$$

where $\tilde{\mathbf{H}}_{ij}^k$ is the estimated channel matrix and $\mathbf{\Delta}_{ij}^k$ represents the channel estimation error. Moreover, $\mathbf{D}_{ij}^k \succeq 0$ and $\zeta_{ij}^k \geq 0$ jointly define a feasible ellipsoid region for $\mathbf{\Delta}_{ij}^k$ which generally depends on the noise and interference statistics, and the used channel estimation method. For further elaboration on the used error model see [154] and the references therein.
The aggregate interference-plus-noise signal at the receiver is hence updated as

$$\boldsymbol{\nu}_i^k = \mathbf{H}_{ij}^k \mathbf{e}_{\mathrm{t},j}^k + \mathbf{H}_{ii}^k \mathbf{e}_{\mathrm{t},i}^k + \mathbf{e}_{\mathrm{r},i}^k + \mathbf{\Delta}_{ij}^k \mathbf{V}_j^k \mathbf{s}_j^k + \mathbf{n}_i^k, \quad j \neq i \in \mathbb{I}, \tag{2.35}$$

where $\mathbf{\Sigma}_i^k$, representing the covariance of $\boldsymbol{\nu}_i^k$, is expressed as

$$\begin{aligned} \mathbf{\Sigma}_i^k = {} & \mathbf{\Delta}_{ij}^k \mathbf{V}_j^k {\mathbf{V}_j^k}^H {\mathbf{\Delta}_{ij}^k}^H + \sum_{j \in \mathbb{I}} \mathbf{H}_{ij}^k \mathbf{\Theta}_{\mathrm{tx},j} \mathrm{diag}\left(\sum_{l \in \mathbb{F}_K} \mathbf{V}_j^l {\mathbf{V}_j^l}^H \right) {\mathbf{H}_{ij}^k}^H \\ & + \mathbf{\Theta}_{\mathrm{rx},i} \mathrm{diag}\Big(\sum_{l \in \mathbb{F}_K} \Big(\sigma_{i,l}^2 \mathbf{I}_{M_i} + \sum_{j \in \mathbb{I}} \mathbf{H}_{ij}^l \mathbf{V}_j^l {\mathbf{V}_j^l}^H {\mathbf{H}_{ij}^l}^H \Big) \Big) + \sigma_{i,k}^2 \mathbf{I}_{M_i}. \end{aligned} \tag{2.36}$$

2.4.2 Alternating SDP (AltSDP) for worst-case MSE minimization

An optimization problem for minimizing the worst-case MSE under the defined norm-bounded CSI error is written as

$$\begin{aligned}\min_{\mathbb{V},\mathbb{U}} \ \max_{\mathbb{C}} \ & \sum_{i\in\mathbb{I}}\sum_{k\in\mathbb{F}_K} \mathrm{tr}\left(\mathbf{S}_i^k\mathbf{E}_i^k\right), \\ & \text{s.t.} \quad (2.18\text{b}), \ \ \boldsymbol{\Delta}_{ij}^k \in \mathbb{D}_{ij}^k, \ \ \forall i,j\in\mathbb{I}, \ \ k\in\mathbb{F}_K, \end{aligned} \tag{2.37}$$

where $\mathbb{C} := \{\boldsymbol{\Delta}_{ij}^k, \ \forall i,j\in\mathbb{I}, \ \forall k\in\mathbb{F}_K\}$, and $\mathbf{E}_i^k$ is obtained from (2.17) and (2.36). Note that the above problem is intractable due to the inner maximization of quadratic convex objective over $\mathbb{C}$, which also invalidates the observed convex QCP structure in (2.18). In order to formulate the objective into a tractable form, we calculate

$$\begin{aligned}&\sum_{k\in\mathbb{F}_K} \mathrm{tr}\left(\mathbf{S}_i^k\mathbf{E}_i^k\right) \\ &= \sum_{k\in\mathbb{F}_K}\Bigg(\left\|\mathbf{W}_i^{kH}\left(\mathbf{U}_i^{kH}\mathbf{H}_{ii}^k\mathbf{V}_i^k - \mathbf{I}_{d_i}\right)\right\|_F^2 \\ &\quad + \left\|\mathbf{W}_i^{kH}\mathbf{U}_i^{kH}\boldsymbol{\Delta}_{i3-i}^k\mathbf{V}_{3-i}^k\right\|_F^2 + \sigma_{i,k}^2\left\|\mathbf{W}_i^{kH}\mathbf{U}_i^{kH}\right\|_F^2 \\ &\quad + \sum_{j\in\mathbb{I}}\sum_{l\in\mathbb{F}_{N_j}}\sum_{m\in\mathbb{F}_K}\left\|\mathbf{W}_i^{kH}\mathbf{U}_i^{kH}\mathbf{H}_{ij}^k\left(\boldsymbol{\Theta}_{\mathrm{tx},j}\right)^{\frac{1}{2}}\boldsymbol{\Gamma}_{N_j}^l\mathbf{V}_j^m\right\|_F^2 \\ &\quad + \sum_{j\in\mathbb{I}}\sum_{l\in\mathbb{F}_{M_i}}\sum_{m\in\mathbb{F}_K}\left\|\mathbf{W}_i^{kH}\mathbf{U}_i^{kH}\left(\boldsymbol{\Theta}_{\mathrm{rx},i}\right)^{\frac{1}{2}}\boldsymbol{\Gamma}_{M_i}^l\mathbf{H}_{ij}^m\mathbf{V}_j^m\right\|_F^2 \\ &\quad + \left\|\mathbf{W}_i^{kH}\mathbf{U}_i^{kH}\left(\boldsymbol{\Theta}_{\mathrm{rx},i}\sum_{q\in\mathbb{F}_K}\sigma_{i,q}^2\right)^{\frac{1}{2}}\right\|_F^2\Bigg) \qquad (2.38) \\ &= \sum_{j\in\mathbb{I}}\sum_{k\in\mathbb{F}_K}\left\|\mathbf{c}_{ij}^k + \mathbf{C}_{ij}^k\mathrm{vec}\left(\boldsymbol{\Delta}_{ij}^k\right)\right\|_2^2, \qquad (2.39)\end{aligned}$$

where $\boldsymbol{\Gamma}_M^l$ is an $M\times M$ zero matrix except for the l-th diagonal element equal to 1. In the above expressions $\mathbf{W}_i^k = \left(\mathbf{S}_i^k\right)^{\frac{1}{2}}$, and

$$\mathbf{c}_{ij}^k := \begin{bmatrix} \delta_{ij}\mathrm{vec}\left(\mathbf{W}_i^{kH}\left(\mathbf{U}_i^{kH}\tilde{\mathbf{H}}_{ij}^k\mathbf{V}_j^k - \mathbf{I}_{d_j\delta_{ij}}\right)\right) \\ \left.\mathrm{vec}\left(\mathbf{W}_i^{kH}\mathbf{U}_i^{kH}\tilde{\mathbf{H}}_{ij}\left(\boldsymbol{\Theta}_{\mathrm{tx},j}\right)^{\frac{1}{2}}\boldsymbol{\Gamma}_{N_j}^l\mathbf{V}_j^m\right)\right|_{l\in\mathbb{F}_{N_j},m\in\mathbb{F}_K} \\ \left.\mathrm{vec}\left(\mathbf{W}_i^{mH}\mathbf{U}_i^{mH}\left(\boldsymbol{\Theta}_{\mathrm{rx},i}\right)^{\frac{1}{2}}\boldsymbol{\Gamma}_{M_i}^l\tilde{\mathbf{H}}_{ij}^k\mathbf{V}_j^k\right)\right|_{l\in\mathbb{F}_{M_i},m\in\mathbb{F}_K} \\ \delta_{ij}\mathrm{vec}\left(\mathbf{W}_i^{kH}\mathbf{U}_i^{kH}\left(\sigma_{i,k}^2\mathbf{I}_{M_i} + \boldsymbol{\Theta}_{\mathrm{rx},i}\sum_{m\in\mathbb{F}_K}\sigma_{i,m}^2\right)^{\frac{1}{2}}\right) \end{bmatrix}, \tag{2.40}$$

$$\mathbf{C}_{ij}^{k}:=\begin{bmatrix} \mathbf{V}_{j}^{k^T}\otimes\left(\mathbf{W}_{i}^{k^H}\mathbf{U}_{i}^{k^H}\right) \\ \left.\left(\left(\boldsymbol{\Theta}_{\mathrm{tx},j}\right)^{\frac{1}{2}}\boldsymbol{\Gamma}_{N_j}^{l}\mathbf{V}_{j}^{m}\right)^{T}\otimes\left(\mathbf{W}_{i}^{k^H}\mathbf{U}_{i}^{k^H}\right)\right|_{l\in\mathbb{F}_{N_j},m\in\mathbb{F}_K} \\ \left.\mathbf{V}_{j}^{k^T}\otimes\left(\mathbf{W}_{i}^{m^H}\mathbf{U}_{i}^{m^H}\left(\boldsymbol{\Theta}_{\mathrm{rx},i}\right)^{\frac{1}{2}}\boldsymbol{\Gamma}_{M_i}^{l}\right)\right|_{l\in\mathbb{F}_{M_i},m\in\mathbb{F}_K} \\ \mathbf{0}_{M_id_i\times M_iN_i} \end{bmatrix}, \tag{2.41}$$

where δ_{ij} is the Kronecker delta where $\delta_{ij}=1$ for $i=j$ and zero otherwise. Moreover, we have $\mathbf{c}_{ij}^{k}\in\mathbb{C}^{\tilde{d}_{ij}\times 1}$, and $\mathbf{C}_{ij}^{k}\in\mathbb{C}^{\tilde{d}_{ij}\times M_iN_j}$ such that

$$\tilde{d}_{ij}:=d_id_j\left(1+K\left(N_j+M_i\right)\right)+d_iM_i. \tag{2.42}$$

Please note that (2.38) is obtained by recalling (2.17) and (2.36) and the known matrix equality [155, Eq. (516)], and (2.40)-(2.41) are calculated via the application of [155, Eq. (496), (497)].

By applying the Schur's complement lemma on the epigraph form of the quadratic norm (2.39), i.e., $\left\|\mathbf{c}_{ij}^{k}+\mathbf{C}_{ij}^{k}\mathrm{vec}\left(\boldsymbol{\Delta}_{ij}^{k}\right)\right\|_2^2\leq\tau_{ij}^{k}$, the optimization problem (2.37) is equivalently written as

$$\min_{\mathbb{V},\mathbb{U},\mathbb{T}}\ \max_{\mathbb{C}}\ \sum_{i\in\mathbb{I}}\sum_{k\in\mathbb{F}_K}\tau_{ij}^{k},\quad\text{s.t.}\quad(2.18\text{b}),\quad\|\mathbf{b}_{ij}^{k}\|_F\leq\zeta_{ij}^{k}, \tag{2.43a}$$

$$\begin{bmatrix} 0 & \mathbf{b}_{ij}^{k^H}\tilde{\mathbf{D}}_{ij}^{k^H}\mathbf{C}_{ij}^{k^H} \\ \mathbf{C}_{ij}^{k}\tilde{\mathbf{D}}_{ij}^{k}\mathbf{b}_{ij}^{k} & \mathbf{0}_{\tilde{d}_{ij}\times\tilde{d}_{ij}} \end{bmatrix}+\begin{bmatrix} \tau_{ij}^{k} & \mathbf{c}_{ij}^{k^H} \\ \mathbf{c}_{ij}^{k} & \mathbf{I}_{\tilde{d}_{ij}} \end{bmatrix}\succeq 0, \tag{2.43b}$$

where $\mathbb{T}:=\{\tau_{ij}^{k},\ \forall i,j\in\mathbb{I},\ \forall k\in\mathbb{F}_K\}$ and

$$\tilde{\mathbf{D}}_{ij}^{k}:=\mathbf{I}_{N_j}\otimes\left(\mathbf{D}_{ij}^{k}\right)^{-1}, \tag{2.44}$$

$$\tilde{\boldsymbol{\Delta}}_{ij}^{k}:=\mathbf{D}_{ij}^{k}\boldsymbol{\Delta}_{ij}^{k},\quad\mathbf{b}_{ij}^{k}:=\mathrm{vec}\left(\tilde{\boldsymbol{\Delta}}_{ij}^{k}\right), \tag{2.45}$$

are defined for notational simplicity. The problem (2.43) is still intractable due to the inner maximization. The following lemma can be used to convert this structure into a tractable form.

Lemma 2.4.1. *Generalized Petersen's sign-definiteness lemma: Let* $\mathbf{Y}=\mathbf{Y}^H$, *and* $\mathbf{X},\mathbf{P},\mathbf{Q}$ *are arbitrary matrices with complex valued elements. Then we have*

$$\mathbf{Y}\succeq\mathbf{P}^H\mathbf{X}\mathbf{Q}+\mathbf{Q}^H\mathbf{X}^H\mathbf{P},\ \ \forall\mathbf{X}\ :\ \|\mathbf{X}\|_F\leq\zeta, \tag{2.46}$$

if and only if

$$\exists\lambda\geq 0,\ \begin{bmatrix} \mathbf{Y}-\lambda\mathbf{Q}^H\mathbf{Q} & -\zeta\mathbf{P}^H \\ -\zeta\mathbf{P} & \lambda\mathbf{I} \end{bmatrix}\succeq 0. \tag{2.47}$$

Proof. See [156, Proposition 2], [157]. □

By choosing the matrices in Lemma 2.4.1 such that $\mathbf{X} = \mathbf{b}_{ij}^k$, $\mathbf{Q} = \left[-1,\ \mathbf{0}_{1\times \tilde{d}_{ij}}\right]$ and

$$\mathbf{Y} = \begin{bmatrix} \tau_{ij}^k & \mathbf{c}_{ij}^{k\,H} \\ \mathbf{c}_{ij}^k & \mathbf{I}_{\tilde{d}_{ij}} \end{bmatrix}, \mathbf{P} = \begin{bmatrix} \mathbf{0}_{M_i N_j \times 1}, & \tilde{\mathbf{D}}_{ij}^{k\,H} \mathbf{C}_{ij}^{k\,H} \end{bmatrix},$$

the optimization problem in (2.43) is equivalently written as

$$\min_{\mathbb{V},\mathbb{U},\mathbb{T},\mathbb{M}} \quad \sum_{i,j\in\mathbb{I}} \sum_{k\in\mathbb{F}_K} \tau_{ij}^k \tag{2.48a}$$

$$\text{s.t.} \quad \mathbf{F}_{i,j}^k \succeq 0,\ \mathbf{G}_i \succeq 0,\ \ \forall i,j \in \mathbb{I},\ k \in \mathbb{F}_K, \tag{2.48b}$$

where $\mathbb{M} := \{\lambda_{ij}^k,\ \forall i,j \in \mathbb{I}, k \in \mathbb{F}_K\}$, and

$$\mathbf{G}_i := \begin{bmatrix} P_i & \tilde{\mathbf{v}}_i^H \\ \tilde{\mathbf{v}}_i & \mathbf{I} \end{bmatrix},\ \tilde{\mathbf{v}}_i := \left\lfloor \mathrm{vec}\left(\left(\mathbf{I} + K\boldsymbol{\Theta}_{\mathrm{tx},i}\right)^{\frac{1}{2}} \mathbf{V}_i^k \right) \right\rfloor_{k\in\mathbb{F}_K},$$

$$\mathbf{F}_{i,j}^k := \begin{bmatrix} \tau_{ij}^k - \lambda_{ij}^k & \mathbf{c}_{ij}^{k\,H} & \mathbf{0}_{1\times M_i N_j} \\ \mathbf{c}_{ij}^k & \mathbf{I}_{\tilde{d}_{ij}} & -\zeta_{ij}^k \mathbf{C}_{ij}^{k} \tilde{\mathbf{D}}_{ij}^k \\ \mathbf{0}_{M_i N_j \times 1} & -\zeta_{ij}^k \tilde{\mathbf{D}}_{ij}^{k\,H} \mathbf{C}_{ij}^{k\,H} & \lambda_{ij}^k \mathbf{I}_{M_i N_j} \end{bmatrix}.$$

Similar to (2.32), the obtained problem in (2.48) is not a jointly, but a separately convex problem over $\mathbb{V}$ and $\mathbb{U}$ when the other variables are fixed. In particular, the optimization over $\mathbb{V}, \mathbb{T}, \mathbb{M}$ is cast as an SDP, assuming a fixed $\mathbb{U}$. Afterwards, the optimization over $\mathbb{U}, \mathbb{T}, \mathbb{M}$ is solved as an SDP, assuming a fixed $\mathbb{V}$. The described alternating steps are continued until a stable point is achieved[6], see Algorithm 3 for the detailed procedure.

Algorithm 3 Alternating SDP (AltSDP) for worst-case MMSE design under CSI error.

1: $\ell \leftarrow 0$; (set iteration number to zero);
2: $\mathbb{V}, \mathbb{U} \leftarrow$ similar initialization as Algorithm 1;
3: **repeat**
4: $\quad \ell \leftarrow \ell + 1$;
5: $\quad \mathbb{V}, \mathbb{T}, \mathbb{M} \leftarrow$ solve SDP (2.48), with fixed $\mathbb{U}$;
6: $\quad \mathbb{U}, \mathbb{T}, \mathbb{M} \leftarrow$ solve SDP (2.48), with fixed $\mathbb{V}$;
7: **until** a stable point, or maximum number of ℓ reached
8: **return** $\{\mathbb{U}, \mathbb{V}\}$;

[6]Due to the monotonically non-increasing nature of the objective at each optimization step, and the fact that the objective value is bounded from below, the proposed iterative updates converge eventually. Please note that the convergence is obtained in the sense that the objective reaches a stable value with an arbitrarily small tolerance margin. Although the resulting optimization variables do not converge necessarily, the potentially different solutions are equally favorable, i.e., they are all feasible and result in the same objective value.

2.4.3 WMMSE for sum rate maximization

Under the impact of CSI error, the worst-case rate maximization problem is written as

$$\max_{\mathbb{V}} \min_{\mathbb{C}} \quad \sum_{i\in\mathbb{I}} \sum_{k\in\mathbb{F}_K} I_i^k \tag{2.49a}$$

$$\text{s.t. } (2.18\text{b}), \quad \boldsymbol{\Delta}_{ij}^k \in \mathbb{D}_{ij}^k, \ \ \forall i,j \in \mathbb{I}, \ \ k \in \mathbb{F}_K. \tag{2.49b}$$

Via the application of Lemma 2.3.1, and (2.29) the rate maximization problem is equivalently written as

$$\max_{\mathbb{V}} \min_{\mathbb{C}} \max_{\mathbb{U},\mathbb{W}} \sum_{i\in\mathbb{I}} \sum_{k\in\mathbb{F}_K} \left(\log\left|\mathbf{W}_i^k \mathbf{W}_i^{kH}\right| + d_i - \operatorname{tr}\left(\mathbf{W}_i^{kH} \mathbf{E}_i^k \mathbf{W}_i^k\right) \right) \tag{2.50a}$$

$$\text{s.t. } (2.49\text{b}), \tag{2.50b}$$

where $\mathbb{W} := \{\mathbf{W}_i^k, \ \forall i \in \mathbb{I}, \ \forall k \in \mathbb{F}_K\}$. The above problem is not tractable in the current form due to the inner min-max structure. Following the max-min exchange introduced in [153, Section III], and undertaking similar steps as in (2.39)-(2.48a) the problem (2.50) is turned into

$$\max_{\mathbb{V},\mathbb{U},\mathbb{W},\mathbb{T},\mathbb{M}} \quad \sum_{i\in\mathbb{I}} \sum_{k\in\mathbb{F}_K} \left(2\log\left|\mathbf{W}_i^k\right| + d_i - \sum_{j\in\mathbb{I}} \tau_{ij}^k \right) \tag{2.51a}$$

$$\text{s.t.} \qquad \mathbf{F}_{i,j}^k \succeq 0, \ \mathbf{G}_i \succeq 0, \ \ \forall i,j \in \mathbb{I}, \ k \in \mathbb{F}_K, \tag{2.51b}$$

where $\mathbf{F}_{i,j}^k$ and $\mathbf{G}_i$ are defined in (2.48). It is observable that the transformed problem holds a separately, but not a jointly, convex structure over the optimization variable sets. In particular, the optimization over $\mathbb{V}, \mathbb{T}, \mathbb{M}$ and $\mathbb{U}, \mathbb{T}, \mathbb{M}$ are cast as SDP in each case when other variables are fixed. Moreover, the optimization over $\mathbb{W}$ can be efficiently implemented using the MAX-DET algorithm [158], see Algorithm 4. Similar to Algorithm 3, due to the monotonically non-decreasing nature of the objective in each optimization iteration the algorithm convergences. See [153, Section III] for arguments regarding convergence and optimization steps for a problem with a similar variable separation.

Algorithm 4 AltSDP-WMMSE algorithm for worst-case rate maximization under CSI error

1: Algorithm 1, Steps 1-3 (initialization);
2: **repeat**
3: $\quad \mathbb{W}, \mathbb{T}, \mathbb{M} \leftarrow$ solve MAX-DET (2.48), with fixed $\mathbb{V}, \mathbb{U}$;
4: $\quad$ Algorithm 3, Steps 4-6;
5: **until** a stable point, or maximum number of ℓ reached
6: **return** $\{\mathbb{U}, \mathbb{V}\}$;

2.5 Discussions

In this section useful insights are provided regarding the proposed designs in Section 2.3 and 2.4, from the aspects of the required computational complexity, as well as the worst-case CSI error matrices.

2.5.1 Worst case CSI error

It is beneficial to obtain the least favorable CSI error matrices, as they provide guidelines for the future channel estimation strategies. For instance, this helps us to choose a channel training sequence that reduces the radius of the CSI error feasible regions in the most destructive directions. Moreover, such knowledge is a necessary step for cutting-set-based methods [159] which aim to reduce the design complexity by iteratively identifying the most destructive error matrices and explicitly incorporating them into the future design steps. In the current setup, the worst-case channel error matrices are identified by maximizing the weighted MSE objective in (2.37) within their defined feasible region. This is expressed as

$$\max_{\mathbb{C}} \ \sum_{i\in\mathbb{I}} \sum_{k\in\mathbb{F}_K} \mathrm{tr}\left(\mathbf{W}_i^{kH}\mathbf{E}_i^k\mathbf{W}_i^k\right), \tag{2.52a}$$

$$\text{s.t.} \ \ \left\|\mathbf{D}_{ij}^k\boldsymbol{\Delta}_{ij}^k\right\|_F \leq \zeta_{ij}^k, \ \ \forall i,j\in\mathbb{I},\ k\in\mathbb{F}_K. \tag{2.52b}$$

Due to the uncoupled nature of the error feasible set, and the value of the objective function over $\boldsymbol{\Delta}_{ij}^k$, following (2.39), the above problem is decomposed as

$$\min_{\mathbf{b}_{ij}^k} \ -\left\|\mathbf{C}_{ij}^k\tilde{\mathbf{D}}_{ij}^k\mathbf{b}_{ij}^k\right\|_2^2 - 2\mathrm{Re}\left\{\mathbf{b}_{ij}^{k\,H}\tilde{\mathbf{D}}_{ij}^{k\,H}\mathbf{C}_{ij}^{k\,H}\mathbf{c}_{ij}^k\right\} - \mathbf{c}_{ij}^{k\,H}\mathbf{c}_{ij}^k \tag{2.53a}$$

$$\text{s.t.} \ \ \mathbf{b}_{ij}^{k\,H}\mathbf{b}_{ij}^k \leq \zeta_{ij}^{k\,2}, \tag{2.53b}$$

where $\mathrm{Re}\{\cdot\}$ represents the real part of a complex value. Note that the objective in (2.53a) is a non-convex function and can not be minimized using the usual numerical solvers in the current form. Following the zero duality gap results for the non-convex quadratic problems [160], we focus on the dual function of (2.53). The corresponding Lagrangian function to (2.53) is constructed as

$$\mathcal{L}\left(\mathbf{b}_{ij}^k,\rho_{ij}^k\right) = \mathbf{b}_{ij}^{k\,H}\mathbf{A}_{ij}^k\mathbf{b}_{ij}^k - 2\mathrm{Re}\left\{\mathbf{b}_{ij}^{k\,H}\tilde{\mathbf{D}}_{ij}^{k\,H}\mathbf{C}_{ij}^{k\,H}\mathbf{c}_{ij}^k\right\} - \mathbf{c}_{ij}^{k\,H}\mathbf{c}_{ij}^k - \rho_{ij}^k\zeta_{ij}^{k\,2}, \tag{2.54}$$

where ρ_{ij}^k is the dual variable and

$$\mathbf{A}_{ij}^k := \rho_{ij}^k\mathbf{I}_{N_jM_i} - \tilde{\mathbf{D}}_{ij}^{k\,H}\mathbf{C}_{ij}^{k\,H}\mathbf{C}_{ij}{}^k\tilde{\mathbf{D}}_{ij}^k. \tag{2.55}$$

Consequently, the value of the dual function is obtained as

$$\mathbf{g}\left(\rho_{ij}^k\right) = -\mathbf{c}_{ij}^{k\,H}\mathbf{C}_{ij}^k\tilde{\mathbf{D}}_{ij}^k\left(\mathbf{A}_{ij}^k\right)^{-1}\tilde{\mathbf{D}}_{ij}^{k\,H}\mathbf{C}_{ij}^{k\,H}\mathbf{c}_{ij}^k - \mathbf{c}_{ij}^{k\,H}\mathbf{c}_{ij}^k - \rho_{ij}^k\zeta_{ij}^{k\,2},$$

if $\mathbf{A}_{ij}^k \succeq 0$, and $\tilde{\mathbf{D}}_{ij}^{k\,H}\mathbf{C}_{ij}^{k\,H}\mathbf{c}_{ij}^k \in \mathcal{R}\{\mathbf{A}_{ij}^k\}$, and otherwise is unbounded from below[7]. By applying the Schur's complement lemma, the maximization of the dual function is written using the epigraph form as

$$\max_{\rho_{ij}^k \geq 0,\, \phi_{ij}^k} \quad -\phi_{ij}^k \tag{2.56a}$$

$$\text{s.t.} \quad \begin{bmatrix} \phi_{ij}^k - \mathbf{c}_{ij}^{k\,H}\mathbf{c}_{ij}^k - \rho_{ij}^k \zeta_{ij}^{k\,2} & \mathbf{c}_{ij}^{k\,H}\mathbf{C}_{ij}^k\tilde{\mathbf{D}}_{ij}^k \\ \tilde{\mathbf{D}}_{ij}^{k\,H}\mathbf{C}_{ij}^{k\,H}\mathbf{c}_{ij}^k & \mathbf{A}_{ij}^k \end{bmatrix} \succeq 0, \tag{2.56b}$$

where $\phi_{ij}^k \in \mathbb{R}$ is an auxiliary variable[8]. By plugging the obtained dual variable ρ_{ij}^k into (2.54), and considering the fact that $-\tilde{\mathbf{D}}_{ij}^{k\,H}\mathbf{C}_{ij}^{k\,H}\mathbf{C}_{ij}^k\tilde{\mathbf{D}}_{ij}^k + \rho_{ij}^{k\,\star}\mathbf{I}_{N_jM_i} \succeq 0$ as a result of (2.56), the optimal value of $\mathbf{b}_{ij}^k$ is obtained from (2.54) as

$$\mathbf{b}_{ij}^{k\,\star} = \left(-\tilde{\mathbf{D}}_{ij}^{k\,H}\mathbf{C}_{ij}^{k\,H}\mathbf{C}_{ij}^k\tilde{\mathbf{D}}_{ij}^k + \rho_{ij}^{k\,\star}\mathbf{I}_{N_jM_i}\right)^{-1}\tilde{\mathbf{D}}_{ij}^{k\,H}\mathbf{C}_{ij}^{k\,H}\mathbf{c}_{ij}^k,$$

where $(\cdot)^\star$ represents the optimality and the worst case $\boldsymbol{\Delta}_{ij}^k$ is consequently calculated via $\text{vec}(\boldsymbol{\Delta}_{ij}^k) = \tilde{\mathbf{D}}_{ij}^k\mathbf{b}_{ij}^{k\,\star}$.

2.5.2 Computational complexity

The proposed designs in Section 2.3 and 2.4 are based on the alternating design of the optimization variables. Furthermore, it is observed that the consideration of non-linear hardware distortions, leading to ICL, as well as the impact of CSI error, result in a higher problem dimension and thereby complicate the structure of the resulting optimization. In this part, we analyze the arithmetic complexity associated with the Algorithm 2.4. Note that Algorithm 2.4 is considered as a general framework, containing Algorithm 2.3 as a special case, since it takes into account the impacts of hardware distortion jointly with CSI error.

The optimization over $\mathbb{V}, \mathbb{U}$ are separately cast as SDP. A general SDP problem is defined as

$$\min_{\mathbf{z}} \ \mathbf{p}^T\mathbf{z}, \ \text{ s.t. } \ \mathbf{z} \in \mathbb{R}^n, \ \mathbf{Y}_0 + \sum_{i=1}^n z_i\mathbf{Y}_i \succeq 0, \ \|\mathbf{z}\|_2 \leq q,$$

where the fixed matrices $\mathbf{Y}_i$ are symmetric block-diagonal, with M diagonal blocks of the sizes $l_m \times l_m$, $m \in \mathbb{F}_M$, and define the specific problem structure, see [161, Subsection 4.6.3]. The arithmetic complexity of obtaining an ϵ-solution to the defined problem, i.e., the convergence to the ϵ-distance vicinity of the optimum is upper-bounded

[7] If one of the aforementioned conditions is not satisfied, an infinitely large value of $\mathbf{b}_{ij}$ can be chosen in the negative direction of $\mathbf{A}_{ij}$, if $\mathbf{A}_{ij}^k$ is not positive semi-definite, or in the direction $\tilde{\mathbf{D}}_{ij}^{k\,H}\mathbf{C}_{ij}^{k\,H}\mathbf{c}_{ij}^k$ within the null-space of $\mathbf{A}_{ij}^k$.

[8] Note that the semi-definite presentation in (2.56b) automatically satisfies $\mathbf{A}_{ij}^k \succeq 0$, and $\tilde{\mathbf{D}}_{ij}^{k\,H}\mathbf{C}_{ij}^{k\,H}\mathbf{c}_{ij}^k \in \mathcal{R}\{\mathbf{A}_{ij}^k\}$.

by

$$\mathcal{O}(1)\left(1+\sum_{m=1}^{M} l_m\right)^{\frac{1}{2}}\left(n^3+n^2\sum_{m=1}^{M} l_m^2+n\sum_{m=1}^{M} l_m^3\right)\text{digit}\left(\epsilon\right),$$

where digit(ϵ) is obtained from [161, Subsection 4.1.2] and affected by the required solution precision. The required computation of each step is hence determined by size of the variable space and the corresponding block diagonal matrix structure, which is obtained in the following:

Optimization over $\mathbb{V},\mathbb{T},\mathbb{M}$

The size of the variable space is given as $n = 2K\left(4+\sum_{i\in\mathbb{I}} d_i N_i\right)$. Moreover, the block sizes are calculated as $l_m = 2+2Kd_iN_i,\ \forall i \in \mathbb{I}$, corresponding to the semi-definite constraint on $\mathbf{G}_i$, and as $l_m = 2+2\tilde{d}_{ij}+2M_iN_j,\ \forall i,j \in \mathbb{I}, k \in \mathbb{F}_K$, corresponding to the semidefinite constraint on $\mathbf{F}_{i,j}^k$ from (2.48). The overall number of the blocks is calculated as $M = 2+4K$.

Optimization over $\mathbb{U},\mathbb{T},\mathbb{M}$

The size of the variable space is given as $n = 2K\left(4+\sum_{i\in\mathbb{I}} d_i M_i\right)$. The block sizes are calculated as $l_m = 2+2\tilde{d}_{ij}+2M_iN_j,\ \forall i,j \in \mathbb{I}, k \in \mathbb{F}_K$, corresponding to the semidefinite constraint on $\mathbf{F}_{i,j}^k$ from (2.48). The overall number of the blocks is calculated as $M = 4K$.

Remarks

The above analysis intends to show how the bounds on computational complexity are related to different dimensions in the problem structure. Nevertheless, the actual computational load may vary in practice due to the structure simplifications and depending on the used numerical solver. Furthermore, the overall algorithm complexity also depends on the number of optimization iterations required for convergence. See Subsection 2.6.1 for a study on the convergence behavior, as well as a numerical evaluation of the algorithm computational complexity.

2.6 Simulation Results

In this section we evaluate the behavior of the studied FD MC system via numerical simulations[9]. In particular, we evaluate the proposed designs in Sections 2.3 and 2.4

[9] I would like to thank my colleague M.Sc. Vimal Radhakrishnan for his help in running the numerical simulations regarding the Algorithms 1-4.

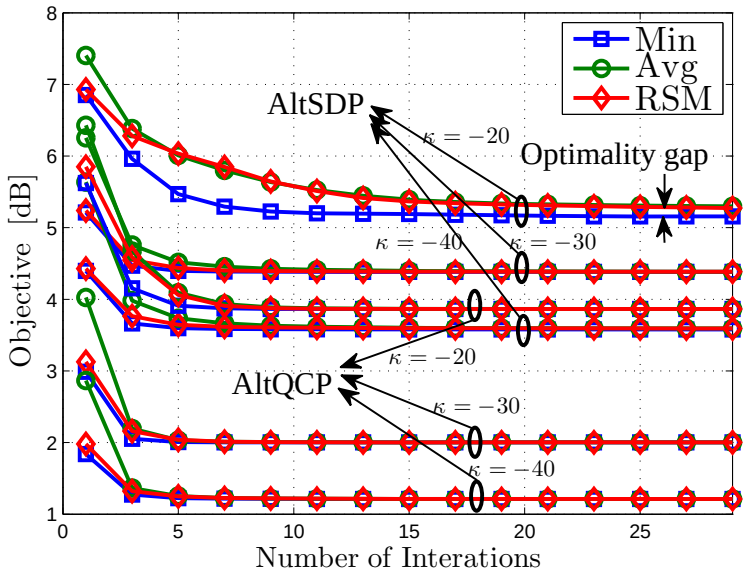

Figure 2.2: Average convergence behavior for AltQCP and AltSDP algorithms. AltQCP converges with fewer steps, and leads to a smaller optimality gap compared to AltSDP. Both algorithms converge in 10-30 iterations.

for various system situations and under the impact of transceiver inaccuracy and CSI error. Communication channels $\mathbf{H}_{ii}^{k}$ follow an uncorrelated Rayleigh flat fading model with variance ρ. For the SI channel we follow the characterization reported in [146]. In this respect, we have $\mathbf{H}_{ij} \sim \mathcal{CN}\left(\sqrt{\frac{\rho_{\text{si}} K_R}{1+K_R}}\mathbf{H}_0, \frac{\rho_{\text{si}}}{1+K_R}\mathbf{I}_{M_i} \otimes \mathbf{I}_{N_j}\right)$ where ρ_{si} represents the SI channel strength, $\mathbf{H}_0$ is a deterministic term,[10] and K_R is the Rician coefficient. For each channel realization, the resulting performance is evaluated by employing different design strategies and for various system parameters. The overall system performance is then averaged over 100 channel realizations. Unless otherwise is stated, the following values are used to define the default setup: $K = 4$, $K_R = 10$, $M := M_i = N_j = 2$, $\rho = -20$ dB, $\rho_{\text{si}} = 1$, $\sigma_{\text{n}}^2 := \sigma_{i,k}^2 = -30$ dB, $P_{\max} := P_i = 1$, $d_i = 1$, $\kappa = -30$ dB where $\mathbf{\Theta}_{\text{rx},i} = \kappa \mathbf{I}_{M_i}$ and $\mathbf{\Theta}_{\text{tx},i} = \kappa \mathbf{I}_{N_i}$, and $\zeta_{ij}^{k} = -15$ dB, $\forall i, j \in \mathbb{I}$, $k \in \mathbb{F}_K$.

2.6.1 Algorithm analysis

Due to the alternating structure, the convergence behavior of the proposed algorithms is of interest, both as a verification for algorithm operation as well as an indication of the algorithm efficiency in terms of the required computational effort. In this part, the performance of AltQCP and AltSDP algorithms are studied in terms of the average convergence behavior and computational complexity. Moreover, the impact of the choice

[10] For simplicity, we choose $\mathbf{H}_0$ as a matrix of all-1 elements.

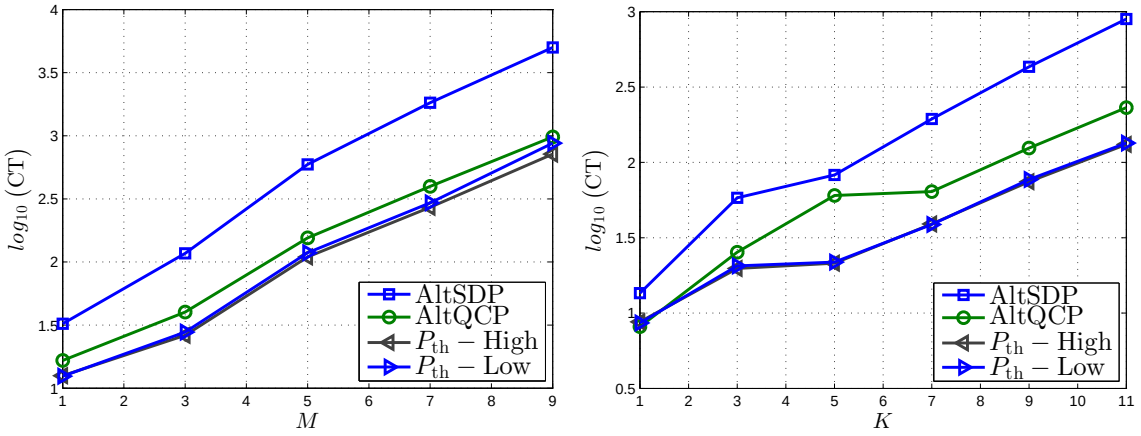

(a) CPU Time vs M (b) CPU Time vs K

Figure 2.3: Comparison of the algorithm computational complexities, in terms of the required CT, for different system dimensions, i.e., different K and M.

of the algorithm initialization is evaluated.
In Fig. 2.2 the average convergence behavior is depicted for different values of κ [dB]. In particular, "Min" and "Avg" curves respectively represent the minimum and the average value of the algorithm objective at the corresponding optimization step over the choice of 20 random initializations. Moreover, "RSM" represents the right-singular matrix initialization proposed in [152, Appendix A]. It is observed that the algorithms converge, within $10 - 30$ optimization iterations. Although the global optimality of the final solution can not be verified due to the possibility of local solutions, the numerical experiments suggest that the applied RSM initialization shows a better convergence behavior compared to a random initialization. Moreover, it is observed that a higher transceiver inaccuracy results in a slower convergence and a gap with optimality. This is expected, as larger κ leads to a more complex problem structure. Note that the algorithm AltQCP shows a smaller value of objective compared to that of AltSDP for any value of κ, since the impact of CSI error is not considered in the algorithm objective.

In addition to the algorithm convergence behavior, the required computational complexity is affected by the problem dimension, and the required per-iteration complexity, see Subsection 2.5.2. In Fig. 2.3, the required computation time (CT) is depicted for different number of antennas, as well as different number of subcarriers[11]. It is observed that the AltSDP results in a significantly higher CT compared to AltQCP. This is expected as the consideration of CSI error in AltSDP results in a larger problem dimension and hence higher complexity. Moreover, the obtained closed-form solution expressions in AltQCP result in a more efficient implementation. Nevertheless, the required CT for AltQCP is still higher than the threshold-based low-complexity approaches, see Sub-

[11]The reported CT is obtained using an Intel Core i5 – 3320M processor with the clock rate of 2.6 GHz and 8 GB of random access memory (RAM). As software platform, MATLAB 2013a is used, on a 64-bit operating system.

section 2.6.2, due to the expanded problem dimension associated with the impact of RSI and ICL.

2.6.2 Performance comparison

In this part we evaluate the performance of the proposed AltSDP and AltQCP algorithms in terms of the resulting worst-case MSE, see Subsection 2.5.1, under various system conditions.

Comparison benchmarks

In order to facilitate a meaningful comparison, we consider popular approaches for the design of FD single-carrier bidirectional systems, or the available designs for other MC systems with simplified assumptions, see Subsection 2.1.1. The following approaches are hence implemented as the evaluation framework:

- *AltSDP*: The AltSDP algorithm proposed in Section 2.4. The impact of the hardware distortions leading to ICL, as well as CSI error are taken into account.

- *AltQCP*: The AltQCP algorithm proposed in Section 2.3. The algorithm operates on the simplified assumption that the CSI error does not exist, i.e., $\zeta = 0$, and hence focuses on the impact of hardware distortions.

- *HD*: The AltSDP algorithm is used on an equivalent HD setup, where the communication directions are separated via a time division duplexing (TDD) scheme.

- $\kappa = 0$: The impact of CSI error is taken into account similar to, e.g., [126, 141]. Nevertheless the impact of hardware distortion, leading to ICL, is ignored.

- *SC*: The optimal single carrier design applied to the defined MC system, following a similar approach as in [32,35]. The impact of CSI error and hardware distortions are taken into account.

Other than the approaches that directly deal with the impact of RSI, e.g., [32, 35], a low complexity design framework is proposed in [27, 28], by introducing an interference power threshold, denoted as P_{th}. In this approach, it is assumed that the SI signal can be perfectly subtracted, given that the SI power is kept below P_{th}.

- $P_{th} - \{\infty, High, Low\}$: representing a design by respectively choosing $P_{\text{th}} = \infty$, P_i, $P_i/10$, representing a system with perfect, high, and low dynamic range conditions.

Visualization

In Figs. 2.4 (a)-(e) the average performance of the defined benchmark algorithms in terms of the worst case (WC) MSE are depicted. The average sum rate behavior of the system is depicted in Fig. 2.5 (a)-(c).

In Fig. 2.4 (a) the impact of transceiver inaccuracy is depicted on the resulting WC-MSE. It is observed that the estimation accuracy is degraded as κ increases. For the low-complexity algorithms, where the impact of hardware distortion is not considered, the resulting MSE goes to infinity as κ increases. Nevertheless, the resulting MSE reaches a saturation point for the distortion-aware algorithms, i.e., AltSDP and AltQCP. This is since, the decoder matrices are set to zero for the data streams affected with a large distortion intensity, which limits the resulting MSE to the magnitude of the data symbols. Moreover, the AltSDP method outperforms the other performance benchmarks for all values of κ. It is worth mentioning that the significant gain of an FD system with low κ over the HD counterpart disappears for larger levels of hardware distortion where AltSDP and HD result in a close performance.

In Fig. 2.4 (b) the impact of the CSI error is depicted. It is observed that the estimation MSE increases for a larger value of ζ. For the low-complexity algorithms where the impact of CSI error is not considered, the resulting MSE goes to infinity, as ζ increases. Nevertheless, the performance of the AltSDP method saturates by choosing zero decoder matrices, following a similar concept as for Fig. 2.4 (a). It is observed that the performance of the AltSDP and AltQCP methods deviate as ζ increases, however, they obtain a similar performance for a small ζ. Similar to Fig. 2.4 (a), a significant gain is observed in comparison to the HD and SC cases for a system with accurate CSI.

In Fig. 2.4 (c) the impact of the thermal noise variance is depicted. It is observed that the resulting performance degrades for the distortion-aware algorithms, as the noise variance increases. Nevertheless, we observe a significant performance degradation for the threshold-based algorithms, particularly $P_{\text{th}} - \text{Low}$, in the low noise regime. This is since the imposed interference power threshold tends to reduce the transmit power, which results in a larger decoder matrices in a low-noise regime. This, in turn, results in an increased impact of distortion. Nevertheless, as the noise variance increases, the algorithm chooses decoding matrices with a smaller norm in order to reduce the impact of noise. This also reduces the impact of hardware distortions. Similar to Fig. 2.4 (a), the proposed AltSDP method outperforms the other comparison benchmarks. It is observed that the performance degradation caused by ignoring the CSI error in AltQCP, or by applying a simplified single carrier design, is significant particularly for a system with a small noise variance.

In Fig. 2.4 (d) the impact of the number of antennas is observed. As expected, a higher number of antennas results in an increased performance for all of the performance benchmarks. In particular, a higher number of antennas enables the system to better

overcome the CSI error, for a fixed ζ, and also to direct the transmit power in the desired channel and not in the self-interference path.

In Fig. 2.4 (e) the impact of the number of subcarriers is observed on the resulting MSE. It is observed that a higher number of subcarriers result in a higher error for all benchmark methods. This is expected as a higher number of subcarriers enables a higher number of communication streams, resulting in a lower available per-stream power. The performance of the SC design reaches optimality of a single carrier system, as expected. Nevertheless the performance of the SC scheme deviates from optimality as K increases, and results in the highest MSE in comparison to the evaluated benchmarks for $K \geq 5$. This is expected, as higher independent subcarriers represent a channel with a higher frequency selectivity which calls for a specialized MC design.

In Fig. 2.5 the average sum rate behavior of the system depicted under the impact of noise and transceiver distortion. In Fig. 2.5-(a), the impact of hardware inaccuracy is depicted. It is observed that a higher κ results in a smaller sum rate. Moreover, the obtained gains via the application of the defined MC design in comparison to the designs with frequency-flat assumption, and via the application of FD setup in comparison to HD setup, are evident for a system with accurate hardware conditions. Conversely, it is observed that a design with consideration of hardware impairments is essential as κ increases. In Figs. 2.5-(b) and (c), the opposite impacts of noise level, and the maximum transmit power are observed on the system sum rate. It is observed that the system sum rate increases as noise level decreases, or as the maximum transmit power increases. In both cases, the gain of AltQCP method, in comparison to the methods which ignore the impact of hardware distortions are observed for a high SNR conditions, i.e., for a system with a high transmit power or a low noise level.

2.7 Conclusion

The application of bidirectional FD communication presents a potential for improving the spectral efficiency. Nevertheless, such systems are limited by the impact of residual self-interference. This issue becomes more crucial in a multi-carrier system, where the residual self-interference spreads over multiple carriers due to the impact of hardware distortion. In this chapter, a modeling and design framework for an FD MIMO OFDM system is presented, taking into account the impact of hardware distortions leading to inter-carrier leakage, as well as the impact of CSI error.

It is observed that the application of a distortion-aware design is essential as transceiver accuracy degrades and inter-carrier leakage becomes a dominant factor. Moreover, a significant gain is observed compared to the usual single-carrier approaches for a channel with frequency selectivity. However, the aforementioned improvements are obtained at the expense of a higher design computational complexity.

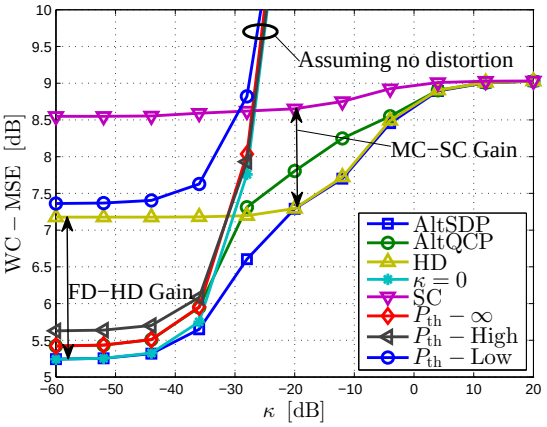

(a) Sum rate MSE vs. transceiver inaccuracy (κ)

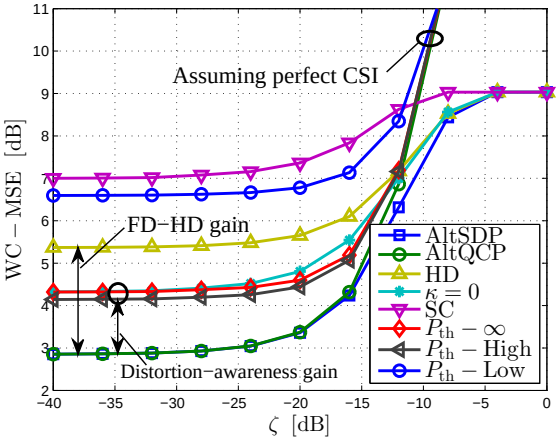

(b) Sum rate MSE vs. feasible CSI error radius (ζ)

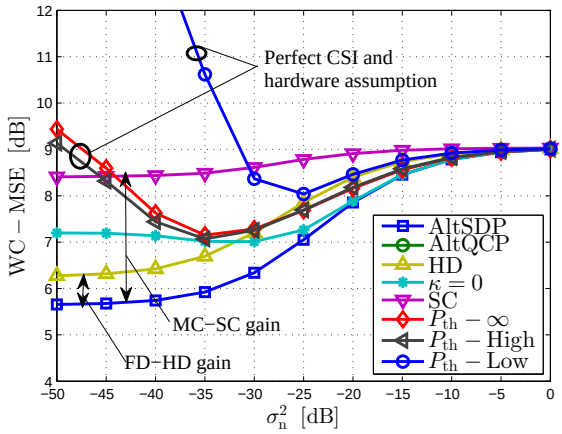

(c) Sum rate MSE vs. thermal noise variance (σ_{n}^2)

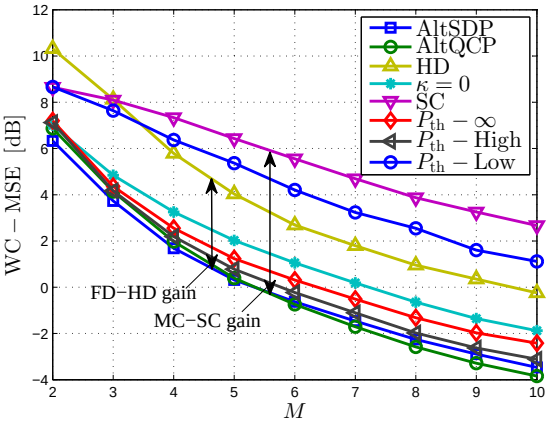

(d) Sum rate MSE vs. number of antennas (M)

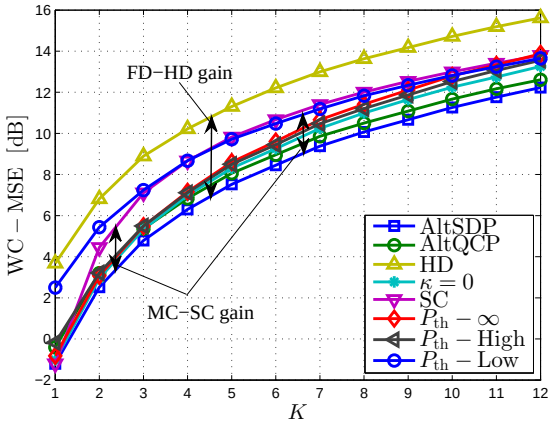

(e) Sum rate MSE vs. number of independent subcarriers (K)

Figure 2.4: WC MSE vs. different system parameters.

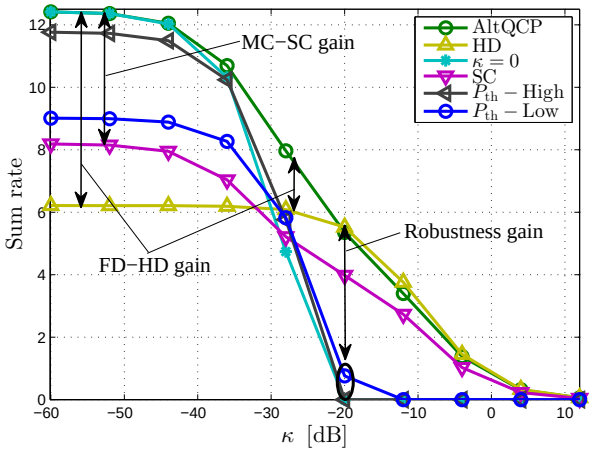

(a) Sum rate vs. hardware inaccuracy (κ)

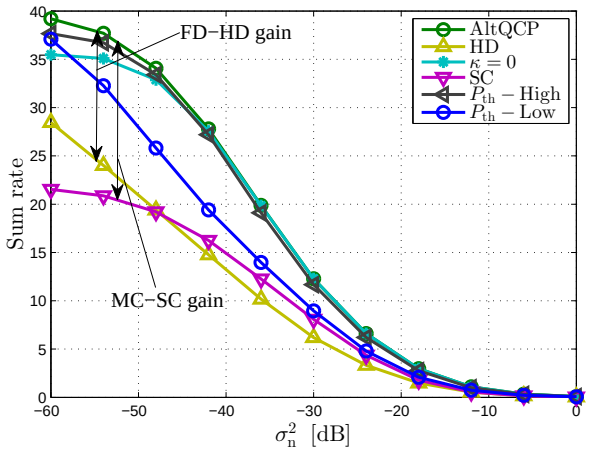

(b) Sum rate vs. noise variance (σ_{n}^2)

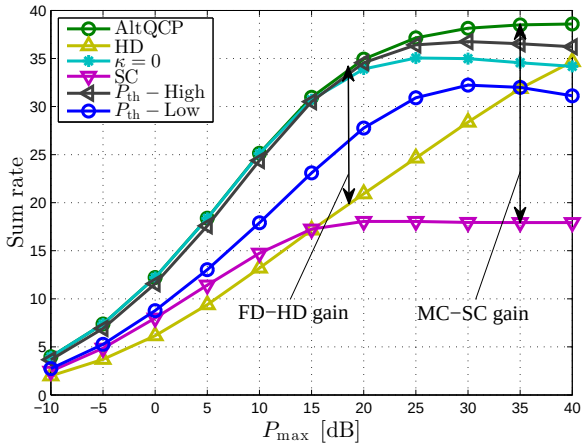

(c) Sum rate vs. maximum transmit power (P_{max})

Figure 2.5: Average sum rate for different system conditions. The gain of a distortion-aware design is apparent for a high SNR, or a high distortion region. The default parameter set is $\kappa = -50$ dB, $\sigma_{\text{n}}^2 := \sigma_{i,k}^2 = -30$ dB, $P_{\text{max}} := P_i = 1, \zeta = 0$.

3 Linear Transceiver Optimization for Full-Duplex Relaying under Hardware Impairments

3.1 Overview

An FD relay is capable of receiving the signal from the source, while simultaneously communicating to the destination. This capability, not only reduces the required time slots for an end-to-end communication, but also reduces the end-to-end latency compared to the known TDD-based HD relays. In the early work by Riihonen. et. al. [58] the relay operation with a generic processing protocol is modeled and many insights have been provided regarding the multiple-antenna strategies for reducing the impact of SI. The design methodologies and performance evaluation for FD relays with DF operation have been then studied in [78–82], where the effects of hardware impairments as well as channel estimation errors in digital domain are taken into account. For the FD relaying systems with AF operation, single antenna relaying scenarios are studied in [59–64]. The AF relays are interesting due to their implementation simplicity and acceptable performance. In the aforementioned works, the effect of the CSI error has been incorporated in [61], where the impact of non-linear hardware distortions have been addressed in [59, 60].

While the aforementioned literature introduces the importance of an accurate transceiver modeling with respect to the effects of hardware impairments for an AF-FD relay, such works have not been extended for the relays with multiple antennas. This stems from the fact that in an AF-FD relay, the inter-dependent behavior of the transmit power from the relay and the RSI intensity results in a distortion loop effect, see Subsection 3.2.4. This results in a rather complicated mathematical description when relay is equipped with multiple antennas. As a result, related studies resort to simplified models to reduce the consequent design complexity. In [65–73] a multiple-antenna AF-FD relay system is studied where a perfect SIC is assumed; via estimating and subtracting the interference in the receiver [65–67], or via spatial zero-forcing of the SI signal assuming that the number of transmit antennas exceeds the number of receive antennas at the relay [68–73]. For the scenarios where the number of transmit antennas is not higher than the receive antennas, a general framework is proposed in [162, 163], assu-

ming a fixed and known RSI statistics. Also in [74, 75], a perfect SIC[1] is assumed via a combined analog and digital SIC scheme, on the condition that the self-interference power does not exceed a certain threshold. In [76, 77] the RSI signal is related to the transmit signal via a known and linear function, assuming a distortion-free hardware.

3.1.1 Chapter outline and contributions

In this chapter, we study a MIMO AF-FD relay, where the explicit impact of hardware distortions in the receiver and transmit chains are taken into account in the SIC process. Our goal is to enhance the instantaneous end-to-end performance via optimized linear transmit and receive strategies. The main contributions of this chapter are as follows:

- Due to the joint consideration of hardware distortions in the receiver and transmit chains, we observe an inter-dependent behavior between the relay transmit covariance and the RSI covariance in an AF-FD relay, i.e., the distortion loop effect. Note that this behavior may not be captured from the works based on simplified RSI models due to e.g., assuming a known (fixed) residual interference statistics [74, 75, 162, 163], or assuming a distortion-less hardware operation [65–73, 76, 77]. In Section 3.3, the relay operation is analyzed under the effect of distortion loop, and the instantaneous end-to-end signal to distortion-plus-noise ratio (SDNR) is formulated in relation to the statistics of the noise and hardware impairments.

- Building on the obtained analysis, we propose linear transmit and receive strategies in order to maximize the SDNR. The instantaneous CSI is utilized to control the impact of distortion and to enhance the quality of the desired signal. In this regard, an SDNR maximization problem is formulated which shows an intractable mathematical structure due to the impact of the distortion loop. A GP-based solution is then proposed in Section 3.4 to act as a benchmark for the achievable performance, however, imposing a high computational complexity.

- In order to reduce the design computational complexity, a sub-optimal multi-stage rank-one (MuStR1) solution is introduced in Section 3.5, by assuming a rank-1 relay amplification matrix and separating the design of the relay process into multiple stages. In this regard, a non-alternating algorithm is proposed by locally maximizing the resulting SDNR for each stage. Moreover, the performance of MuStR1 is improved by introducing an alternating update, denoted as alternating multi-stage rank-one (AltMuStR1) at the cost of a slightly higher computational complexity compared to MuStR1.

- In Section 3.6, the permanence of a similar setup is studied assuming that the relay is operating with DF processing protocol, under the impact of hardware im-

[1]RSI is assumed to be buried in the thermal noise, following a known statistics.

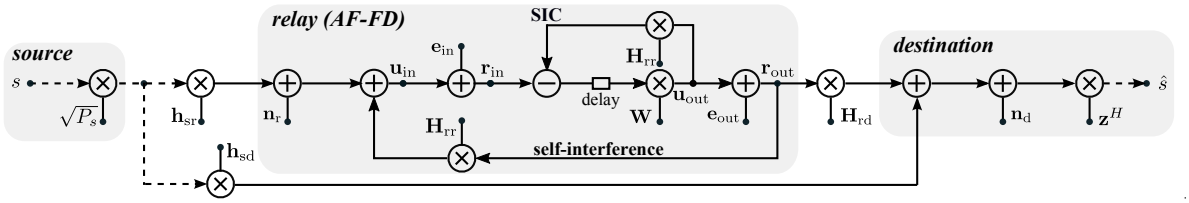

Figure 3.1: The signal model for an amplify-and-forward FD MIMO relay. The impact of hardware inaccuracies from the transmitter ($\mathbf{e}_{\text{out}}$) and receiver ($\mathbf{e}_{\text{in}}$) chains is observable on the relay process. The bold arrows represent the vector signals while the dashed arrows represent the scalars.

pairments. Similarly, optimized linear transmit and receive strategies are obtained in order to act as a comparison benchmark.

Numerical simulations show that for a system with a small thermal noise variance, or a high power or high transceiver distortion, application of a distortion-aware design is essential. Moreover, the AF-FD relaying suffers from a significant performance gap, compared to the DF-FD relaying, as relay dynamic range decreases. Parts of this chapter are based on the works already published or under consideration for publication in [59, 60, 74, 118–122].

3.2 System Model

In this part, we investigate a system where a single-antenna HD source communicates with an HD destination node equipped with M_{d} antennas, via an FD relay. The relay is assumed to have M_{t} (M_{r}) transmit (receive) antennas and operates in AF mode. The channels between the source and the relay, between the relay and the destination, and between the source and the destination are denoted as $\mathbf{h}_{\text{sr}} \in \mathbb{C}^{M_{\text{r}}}$, $\mathbf{H}_{\text{rd}} \in \mathbb{C}^{M_{\text{d}} \times M_{\text{t}}}$, and $\mathbf{h}_{\text{sd}} \in \mathbb{C}^{M_{\text{d}}}$, respectively. The self-interference channel, which is the channel between the relay's transmit and receive ends is denoted by $\mathbf{H}_{\text{rr}} \in \mathbb{C}^{M_{\text{r}} \times M_{\text{t}}}$. All channels are following the flat-fading model.

3.2.1 Source-to-relay communication

The relay continuously receives and amplifies the received signal from the source, while estimating and subtracting the SI signal from its own transmitter, see Fig. 3.1. The received signal at the relay is expressed as

$$\mathbf{r}_{\text{in}} = \underbrace{\mathbf{h}_{\text{sr}}\sqrt{P_{\text{s}}}s + \mathbf{H}_{\text{rr}}\mathbf{r}_{\text{out}} + \mathbf{n}_{\text{r}}}_{=:\mathbf{u}_{\text{in}}} + \mathbf{e}_{\text{in}}, \tag{3.1}$$

where $\mathbf{r}_{\text{in}} \in \mathbb{C}^{M_{\text{r}}}$ and $\mathbf{r}_{\text{out}} \in \mathbb{C}^{M_{\text{t}}}$ respectively represent the received and transmitted signal from the relay and $\mathbf{n}_{\text{r}} \sim \mathcal{CN}(\mathbf{0}, \sigma_{\text{nr}}^2 \mathbf{I}_{M_{\text{r}}})$ represents the additive thermal noise at the relay. The transmitted data symbol from the source is denoted as $s \in \mathbb{C}$, $\mathbb{E}\{|s|^2\} = 1$. $P_{\text{s}} \in \mathbb{R}^+$ is the source transmit power and $\mathbf{u}_{\text{in}} \in \mathbb{C}^{M_{\text{r}}}$ represents the *undistorted* received signal at the relay.

The receiver distortion, denoted by $\mathbf{e}_{\text{in}} \in \mathbb{C}^{M_{\text{r}}}$, represents the combined effects of receiver chain impairments and modeled similar to Section 2.2. Please note that while the aforementioned impairments are usually assumed to be ignorable for an HD transceiver, they play an important role in our system due to high strength of the self-interference path. The known, i.e., distortion-free, part of the self-interference signal is then suppressed in the receiver by utilizing the recently developed SIC techniques in analog and digital domains, e.g., [2, 7]. The remaining signal is then amplified to constitute the relay's output:

$$\mathbf{r}_{\text{out}} = \mathbf{u}_{\text{out}} + \mathbf{e}_{\text{out}}, \quad \mathbf{u}_{\text{out}}(t) = \mathbf{W}\mathbf{r}_{\text{supp}}(t - \tau), \tag{3.2}$$

$$\mathbf{r}_{\text{supp}} = \mathbf{r}_{\text{in}} - \mathbf{H}_{\text{rr}}\mathbf{u}_{\text{out}}, \tag{3.3}$$

where $\mathbf{r}_{\text{supp}} \in \mathbb{C}^{M_{\text{r}}}$ and $\mathbf{W} \in \mathbb{C}^{M_{\text{t}} \times M_{\text{r}}}$ respectively represent the interference-suppressed version of the received signal and the relay amplification matrix, $t \in \mathbb{R}^+$ represents the time instance[2], and $\tau \in \mathbb{R}^+$ is the relay processing delay, see Subsection 3.2.5. The *intended* transmit signal is denoted as $\mathbf{u}_{\text{out}} \in \mathbb{C}^{M_{\text{t}}}$. Similar to the defined additive distortion in the receiver chains, the combined effects of the transmit chain impairments, e.g., limited DAC accuracy, oscillator phase noise, and power amplifier noise is denoted by $\mathbf{e}_{\text{out}} \in \mathbb{C}^{M_{\text{r}}}$. Furthermore, in order to take into account the transmit power limitations we impose

$$\mathbb{E}\{\|\mathbf{r}_{\text{out}}\|_2^2\} \leq P_{\text{r,max}}, \; P_{\text{s}} \leq P_{\text{s,max}}, \tag{3.4}$$

where $P_{\text{r,max}}$ and $P_{\text{s,max}}$ respectively represent the maximum transmit power from the relay and from the source.

3.2.2 Distortion signal statistics

The impact of hardware elements inaccuracy in each chain can be modeled as additive and Gaussian-distributed independent distortion terms, see Section 2.2 for more elaboration. In the defined relaying system it is expressed as

$$\mathbf{e}_{\text{in}} \sim \mathcal{CN}\Big(\mathbf{0}, \beta \text{diag}\Big(\mathbb{E}\left\{\mathbf{u}_{\text{in}}\mathbf{u}_{\text{in}}^H\right\}\Big)\Big), \;\; \mathbf{e}_{\text{in}}(t) \perp \mathbf{e}_{\text{in}}(t'), \;\; \mathbf{e}_{\text{in}}(t) \perp \mathbf{u}_{\text{in}}(t), \tag{3.5}$$

and

$$\mathbf{e}_{\text{out}} \sim \mathcal{CN}\Big(\mathbf{0}, \kappa \text{diag}\Big(\mathbb{E}\left\{\mathbf{u}_{\text{out}}\mathbf{u}_{\text{out}}^H\right\}\Big)\Big), \;\; \mathbf{e}_{\text{out}}(t) \perp \mathbf{e}_{\text{out}}(t'), \;\; \mathbf{e}_{\text{out}}(t) \perp \mathbf{u}_{\text{out}}(t), \tag{3.6}$$

[2]The argument indicating time instance, i.e., t, is dropped for simplicity for signals with a same time reference.

where $t \neq t^{'}$ and $\beta, \kappa \in \mathbb{R}^{+}$ are the receive and transmit distortion coefficients which respectively relate the *undistorted* receive and transmit signal covariance to the covariance of the corresponding distortion. Note that the defined statistics in (3.5), (3.6) indicate that unlike the traditional additive white noise model, a higher transmit (receive) signal power results in a higher transmit (receive) distortion intensity in the corresponding chain. As it will be further elaborated, this effect plays an important role in the performance of an AF-FD relay.

3.2.3 Relay-to-destination communication

The transmitted signal from the relay node propagates through the relay to destination channel and constitutes the received signal at the destination:

$$\mathbf{y} = \mathbf{H}_{\mathrm{rd}}\mathbf{r}_{\mathrm{out}} + \mathbf{h}_{\mathrm{sd}}\sqrt{P_{\mathrm{s}}}s + \mathbf{n}_{\mathrm{d}}, \quad \hat{s}(t-\tau) = \mathbf{z}^{H}\mathbf{y}(t), \tag{3.7}$$

where $\mathbf{y} \in \mathbb{C}^{M_{\mathrm{d}}}$ is the received signal, and $\mathbf{n}_{\mathrm{d}} \sim \mathcal{CN}\left(\mathbf{0}, \sigma_{\mathrm{nd}}^{2}\mathbf{I}_{M_{\mathrm{d}}}\right)$ is the additive thermal noise at the destination. The linear receiver filter and the estimated received symbol is denoted as $\mathbf{z} \in \mathbb{C}^{M_{\mathrm{d}}}$ and $\hat{s}$, respectively.

3.2.4 Distortion loop

As the transmit power from the relay increases, the power of the error components increases at the transmit and receive chains, see (3.1) in connection to (3.5)-(3.6). On the other hand, these errors are amplified in the relay process and further increase the relay transmit power, see (3.1) in connection to (3.2) and (3.3). The aforementioned effect results in a distortion loop, i.e., the inter-dependent behavior of the relay transmit covariance and the RSI covariance for an AF-FD relay, which deteriorates the impact of RSI. In the following sections, this impact is analytically studied and an optimization strategy is proposed in order to alleviate this effect.

3.2.5 Remarks

CSI estimation

In this chapter it is assumed that the CSI is known by dedicating an adequately long training sequence at the relay. Therefore, the studied framework serves best for the scenarios with a stationary channel where long training sequences can be utilized, e.g., relay channel in a static backhaul link with a directive LOS connection [150]. An effective channel estimation method is presented in [78, Subsection III.A] for a FD

relaying setup in the presence of hardware impairments[3]. It is observed that an accurate CSI can be obtained on the condition of employing a sufficiently long training sequence, see [78, Eq. (9)], and also [32, Eq. (10)] for a similar argument. For the scenarios where the CSI cannot be accurately obtained, the results of this chapter can be treated as theoretical guidelines on the effects of hardware impairments, if CSI were accurately known.

Hardware impairments

Compared to many HD scenarios, the impact of hardware impairments is severe in FD transceivers due to the strong self-interference, see, e.g., specifications of SIC for 802.11ac PHY [2]. This is since on one hand, the distortions originating from the transmit chains pass through a strong self-interference channel and become significant. On the other hand, the receiver chains are more prone to distortion due to the high-power received signal. In this chapter, we focus on the impact of hardware impairments for the FD relay transceiver, and otherwise model the inaccuracies as an additive thermal noise.

Direct link

In this chapter, it is assumed that the direct link is weak and consider the source-destination path as a source of interference, similar to [61, 78]. For the scenarios where the direct link is strong, it is shown in [164] that the receiver strategy can be gainfully updated as a RAKE receiver [165] to temporally align the desired signal in the direct and relay links. This can be considered as a future possible extension.

Processing delay

The relay output signals, i.e., $\mathbf{u}_{\text{out}}$ and $\mathbf{r}_{\text{out}}$, are generated from the received signals with a relay processing delay τ, see (3.2). This delay is assumed to be long enough, e.g., more than a symbol duration, such that the source signal is decorelated, i.e., $s(t) \perp s(t-\tau)$ [164, 166]. The zero-mean and statistical independence of the samples from data signal, i.e., $s(t)$ and $s(t-\tau)$, as well as the noise and distortion signals are basis for the analysis in the following section.

[3] A two-phase estimation is suggested to avoid interference; first, source transmits the pilot where relay is silent, thereby estimating the source-relay and source-destination channels, and then relay transmits pilot and source remain silent, hence estimating the self-interference and relay-destination channels.

3.3 Performance Analysis of MIMO AF-FD Relaying with Hardware Impairments

In this part, the end-to-end system performance is analyzed as a function of the relay amplification matrix $\mathbf{W}$, receive linear filter at the destination $\mathbf{z}$, as well as the transmit power from the source P_{s}. By incorporating (3.1), (3.5) and (3.6) into (3.2) and (3.3) we have

$$\begin{aligned}\mathbf{Q} &= \mathbf{W}\Big(P_{\mathrm{s}}\mathbf{h}_{\mathrm{sr}}\mathbf{h}_{\mathrm{sr}}^{H} + \sigma_{\mathrm{nr}}^{2}\mathbf{I}_{M_{\mathrm{r}}} + \mathbb{E}\left\{\mathbf{e}_{\mathrm{in}}\mathbf{e}_{\mathrm{in}}^{H}\right\} + \mathbf{H}_{\mathrm{rr}}\mathbb{E}\{\mathbf{e}_{\mathrm{out}}\mathbf{e}_{\mathrm{out}}^{H}\}\mathbf{H}_{\mathrm{rr}}^{H}\Big)\mathbf{W}^{H} \\ &= \mathbf{W}\Big(P_{\mathrm{s}}\mathbf{h}_{\mathrm{sr}}\mathbf{h}_{\mathrm{sr}}^{H} + \sigma_{\mathrm{nr}}^{2}\mathbf{I}_{M_{\mathrm{r}}} + \beta\mathrm{diag}\Big(\mathbb{E}\left\{\mathbf{u}_{\mathrm{in}}\mathbf{u}_{\mathrm{in}}^{H}\right\}\Big) + \kappa\mathbf{H}_{\mathrm{rr}}\mathrm{diag}\Big(\mathbf{Q}\Big)\mathbf{H}_{\mathrm{rr}}^{H}\Big)\mathbf{W}^{H}, \end{aligned} \tag{3.8}$$

where $\mathbf{Q} \in \mathcal{H}$ is the covariance matrix of the undistorted transmit signal from the relay, i.e., $\mathbf{Q} := \mathbb{E}\{\mathbf{u}_{\mathrm{out}}\mathbf{u}_{\mathrm{out}}^{H}\}$. Furthermore, the undistorted receive covariance matrix can be formulated from (3.1)-(3.3) as

$$\mathbb{E}\{\mathbf{u}_{\mathrm{in}}\mathbf{u}_{\mathrm{in}}^{H}\} = P_{\mathrm{s}}\mathbf{h}_{\mathrm{sr}}\mathbf{h}_{\mathrm{sr}}^{H} + \sigma_{\mathrm{nr}}^{2}\mathbf{I}_{M_{\mathrm{r}}} + \mathbf{H}_{\mathrm{rr}}\mathbb{E}\{\mathbf{r}_{\mathrm{out}}\mathbf{r}_{\mathrm{out}}^{H}\}\mathbf{H}_{\mathrm{rr}}^{H}. \tag{3.9}$$

It is worth mentioning that due to the proximity of the Rx and Tx antennas on the FD device, the loopback SI signal is much stronger than the desired signal which is coming from a distant location, and hence constitutes the dominant part in (3.9). By recalling (3.2) and (3.6) the relay transmit covariance matrix can be formulated as

$$\mathbb{E}\{\mathbf{r}_{\mathrm{out}}\mathbf{r}_{\mathrm{out}}^{H}\} = \mathbf{Q} + \kappa\mathrm{diag}\left(\mathbf{Q}\right), \tag{3.10}$$

and consequently from (3.8) and (3.9) it follows

$$\mathbf{Q} = \mathbf{W}\mathcal{V}\left(\mathbf{Q}\right)\mathbf{W}^{H}, \tag{3.11}$$

where

$$\begin{aligned}\mathcal{V}\left(\mathbf{Q}\right) :&= P_{\mathrm{s}}\mathbf{h}_{\mathrm{sr}}\mathbf{h}_{\mathrm{sr}}^{H} + \sigma_{\mathrm{nr}}^{2}\mathbf{I}_{M\,\mathrm{r}} + \beta\mathrm{diag}\left(P_{\mathrm{s}}\mathbf{h}_{\mathrm{sr}}\mathbf{h}_{\mathrm{sr}}^{H} + \sigma_{\mathrm{nr}}^{2}\mathbf{I}_{M_{\mathrm{r}}}\right) \\ &\quad + \beta\mathrm{diag}\Big(\mathbf{H}_{\mathrm{rr}}\Big(\mathbf{Q} + \kappa\mathrm{diag}\left(\mathbf{Q}\right)\Big)\mathbf{H}_{\mathrm{rr}}^{H}\Big) + \kappa\mathbf{H}_{\mathrm{rr}}\mathrm{diag}\left(\mathbf{Q}\right)\mathbf{H}_{\mathrm{rr}}^{H}. \end{aligned} \tag{3.12}$$

Note that the above derivations (3.8)-(3.11) hold as the noise, the desired signal at subsequent symbol durations, and the distortion components are zero-mean and mutually independent. Unfortunately, a direct expression of $\mathbf{Q}$ in terms of $\mathbf{W}$ cannot be achieved from (3.11), (3.12) in the current form. In order to facilitate further analysis, we resort to the vectorized presentation of $\mathbf{Q}$. By applying the famous matrix equality $\mathrm{vec}(\mathbf{A}_1\mathbf{A}_2\mathbf{A}_3) = (\mathbf{A}_3^{\mathrm{T}} \otimes \mathbf{A}_1)\mathrm{vec}(\mathbf{A}_2)$, the identity (3.10) can be written as

$$\mathrm{vec}\left(\mathbb{E}\{\mathbf{r}_{\mathrm{out}}\mathbf{r}_{\mathrm{out}}^{H}\}\right) = \left(\mathbf{I}_{M_{\mathrm{t}}^2} + \kappa\mathbf{S}_{\mathrm{D}}^{M_{\mathrm{t}}}\right)\mathrm{vec}\left(\mathbf{Q}\right), \tag{3.13}$$

where $\mathbf{S}_{\mathrm{D}}^{M} \in \{0,1\}^{M^2 \times M^2}$ is a selection matrix with one or zero elements such that $\mathbf{S}_{\mathrm{D}}^{M_{\mathrm{t}}} \mathrm{vec}\,(\mathbf{Q}) = \mathrm{vec}\,(\mathrm{diag}(\mathbf{Q}))$. Similarly from (3.11) we obtain

$$\mathrm{vec}\,(\mathbf{Q}) = \Big(\mathbf{I}_{M_{\mathrm{t}}^2} - (\mathbf{W}^* \otimes \mathbf{W})\,\mathbf{C}\Big)^{-1} (\mathbf{W}^* \otimes \mathbf{W})\,\mathbf{c}, \tag{3.14}$$

where

$$\mathbf{C} := \beta \mathbf{S}_{\mathrm{D}}^{M_{\mathrm{r}}} (\mathbf{H}_{\mathrm{rr}}^* \otimes \mathbf{H}_{\mathrm{rr}}) \Big(\mathbf{I}_{M_{\mathrm{t}}^2} + \kappa \mathbf{S}_{\mathrm{D}}^{M_{\mathrm{t}}}\Big) + \kappa\,(\mathbf{H}_{\mathrm{rr}}^* \otimes \mathbf{H}_{\mathrm{rr}})\,\mathbf{S}_{\mathrm{D}}^{M_{\mathrm{t}}}, \tag{3.15}$$

$$\mathbf{c} := \Big(\mathbf{I}_{M_{\mathrm{r}}^2} + \beta \mathbf{S}_{\mathrm{D}}^{M_{\mathrm{r}}}\Big)\,\mathrm{vec}\,\Big(P_{\mathrm{s}} \mathbf{h}_{\mathrm{sr}} \mathbf{h}_{\mathrm{sr}}^H + \sigma_{\mathrm{nr}}^2 \mathbf{I}_{M_{\mathrm{r}}}\Big)\,. \tag{3.16}$$

The direct dependence of the relay transmit covariance matrix and $\mathbf{W}$ can be consequently obtained from (3.13) and (3.14) as

$$\mathrm{vec}\,\Big(\mathbb{E}\{\mathbf{r}_{\mathrm{out}} \mathbf{r}_{\mathrm{out}}^H\}\Big) = \boldsymbol{\Theta}\Big(\mathbf{W}, \mathbf{H}_{\mathrm{rr}}, \kappa, \beta\Big)\mathrm{vec}\Big(P_{\mathrm{s}} \mathbf{h}_{\mathrm{sr}} \mathbf{h}_{\mathrm{sr}}^H + \sigma_{\mathrm{nr}}^2 \mathbf{I}_{M_{\mathrm{r}}}\Big)\,, \tag{3.17}$$

where

$$\boldsymbol{\Theta}\Big(\mathbf{W}, \mathbf{H}_{\mathrm{rr}}, \kappa, \beta\Big) := \Big(\mathbf{I}_{M_{\mathrm{t}}^2} + \kappa \mathbf{S}_{\mathrm{D}}^{M_{\mathrm{t}}}\Big) \Big(\mathbf{I}_{M_{\mathrm{t}}^2} - (\mathbf{W}^* \otimes \mathbf{W})\,\mathbf{C}\Big)^{-1} (\mathbf{W}^* \otimes \mathbf{W}) \Big(\mathbf{I}_{M_{\mathrm{r}}^2} + \beta \mathbf{S}_{\mathrm{D}}^{M_{\mathrm{r}}}\Big) \tag{3.18}$$

represents the transfer function of the relay that relates the distortion-less input $P_{\mathrm{s}} \mathbf{h}_{\mathrm{sr}} \mathbf{h}_{\mathrm{sr}}^H + \sigma_{\mathrm{nr}}^2 \mathbf{I}_{M_{\mathrm{r}}}$ to the distorted transmit covariance. It can be observed that $\boldsymbol{\Theta}\,(\mathbf{W}, \mathbf{H}_{\mathrm{rr}}, 0, 0) = \mathbf{W}^* \otimes \mathbf{W}$, which is similar to the known AF-FD relay operation with a perfect hardware, i.e., $\kappa = \beta = 0$.

3.3.1 Optimization problem

The received signal power at the destination, after application of $\mathbf{z}$, can be separated as

$$\begin{aligned} P_{\mathrm{des}} &= \mathbb{E}\left\{\left|\mathbf{z}^H \mathbf{H}_{\mathrm{rd}} \mathbf{W} \mathbf{h}_{\mathrm{sr}} \sqrt{P_s} s\right|^2\right\} \\ &= P_s \mathbf{z}^H \mathbf{H}_{\mathrm{rd}} \mathbf{W} \mathbf{h}_{\mathrm{sr}} \mathbf{h}_{\mathrm{sr}}^H \mathbf{W}^H \mathbf{H}_{\mathrm{rd}}^H \mathbf{z}, \end{aligned} \tag{3.19}$$

$$\begin{aligned} P_{\mathrm{tot}} &= \mathbb{E}\left\{\left|\mathbf{z}^H \left(\mathbf{H}_{\mathrm{rd}} \mathbf{r}_{\mathrm{out}} + \mathbf{h}_{\mathrm{sd}} \sqrt{P_s} s + \mathbf{n}_{\mathrm{d}}\right)\right|^2\right\} = \\ &\quad \mathbf{z}^H \left(\mathbf{H}_{\mathrm{rd}} \Big(\mathbf{Q} + \kappa \mathrm{diag}\,(\mathbf{Q})\Big) \mathbf{H}_{\mathrm{rd}}^H + \sigma_{\mathrm{nd}}^2 \mathbf{I}_{M_{\mathrm{d}}} + P_{\mathrm{s}} \mathbf{h}_{\mathrm{sd}} \mathbf{h}_{\mathrm{sd}}^H\right) \mathbf{z}, \end{aligned} \tag{3.20}$$

$$P_{\mathrm{err}} = P_{\mathrm{tot}} - P_{\mathrm{des}}, \tag{3.21}$$

where P_{des} and P_{err} respectively represent the power of the desired and distortion-plus-noise parts of the estimated signal $\hat{\mathbf{s}}$, and $P_{\mathrm{tot}} := \mathbb{E}\{|\hat{s}|^2\}$. The corresponding optimization problem for maximizing the resulting SDNR is written as

$$\max_{P_{\mathrm{s}}, \mathbf{z}, \mathbf{W}} \quad \frac{P_{\mathrm{des}}}{P_{\mathrm{err}}} =: \mathrm{SDNR}\,(P_{\mathrm{s}}, \mathbf{z}, \mathbf{W}) \tag{3.22a}$$

$$\text{s.t.} \quad (3.14), \quad \mathbf{Q} \in \mathcal{H}, \quad \mathrm{tr}\,(\mathbf{Q}) \leq \tilde{P}_{\mathrm{r,max}}, \quad 0 \leq P_{\mathrm{s}} \leq P_{\mathrm{s,max}}, \tag{3.22b}$$

where (3.22b) limits the feasible set of $\mathbf{W}$ to those resulting in a feasible $\mathbf{Q}$. Note that $\tilde{P}_{\mathrm{r,max}} := \frac{P_{\mathrm{r,max}}}{1+\kappa}$ and the power constraint in (3.22b) follows as $\mathrm{tr}\left(\mathbf{Q} + \kappa \mathrm{diag}(\mathbf{Q})\right) = (1+\kappa)\mathrm{tr}\left(\mathbf{Q}\right)$.

As it can be observed, the optimization problem (3.22a)-(3.22b) is a non-convex optimization problem and cannot be solved analytically, due to the structure imposed by (3.14). In order to approach the solution, we propose a GP-based optimization method in the following section.

3.4 Gradient Projection for SDNR maximization

In this part, an iterative solution to (3.22a)-(3.22b) is proposed, based on the gradient projection method [32, 167]. In this regard, the optimization variables are updated in the increasing direction of the objective function (3.22a).

3.4.1 Iterative update for relay amplification

The update rule for $\mathbf{W}$ is defined following the GP method, where detailed instructions are inspired from [78]. This includes the update of $\mathbf{W}$ in the steepest ascent direction, and occasional projection due to constraints violation. This is expressed as

$$\bar{\mathbf{W}}^{[l]} = \mathcal{P}\left(\mathbf{W}^{[l]} + \delta \nabla_{\left(\mathbf{W}^{[l]}\right)^*}\left(\mathrm{SDNR}\right)\right). \tag{3.23}$$

$$\mathbf{W}^{[l+1]} = \mathbf{W}^{[l]} + \gamma^{[l]}\left(\bar{\mathbf{W}}^{[l]} - \mathbf{W}^{[l]}\right), \tag{3.24}$$

where $\mathcal{P}\left(\cdot\right)$ represents the projection to the feasible solution space, l is the iteration index, $\nabla_{\mathbf{X}}\left(\cdot\right)$ represents the gradient with respect to $\mathbf{X}$, and $\delta, \gamma \in \mathbb{R}^{+}$ represent the step size variables. The update direction is obtained from the calculated gradients in (3.26) and (3.27), and the fact that

$$\nabla_{\mathbf{W}^*}\left(\mathrm{SDNR}\right) = \left(\nabla_{\mathbf{W}^*}\left(P_{\mathrm{des}}\right) P_{\mathrm{err}} - \nabla_{\mathbf{W}^*}\left(P_{\mathrm{err}}\right) P_{\mathrm{des}}\right) / {P_{\mathrm{err}}}^2. \tag{3.25}$$

The stepsize value γ is chosen according to the Armijo's step size rule [168]. This is expressed as

$$\mathrm{SDNR}\left(\mathbf{W}^{[l+1]}\right) - \mathrm{SDNR}\left(\mathbf{W}^{[l]}\right) \geq \sigma \nu^m \mathrm{tr}\left(\left\{\nabla_{\left(\mathbf{W}^{[l]}\right)^*}\left(\mathrm{SDNR}\right)\right\}^H \left(\bar{\mathbf{W}}^{[l]} - \mathbf{W}^{[l]}\right)\right),$$

where $\gamma^{[l]} = \nu^m$, such that m is the smallest non-negative integer satisfying the above inequality, and $\nu = 0.5$, $\sigma = 0.1$ and $\delta = 0.1$.

Projection rule

Once an updated $\mathbf{W}$ in the steepest ascend direction, i.e., $\mathbf{W}^{[l]}+\delta\nabla_{\left(\mathbf{W}^{[l]}\right)^*}$ (SDNR), and the corresponding $\mathbf{Q}$ calculated from (3.14), violate the problem constrains, i.e., when $\mathbf{Q}$ contains a negative eigenvalue or violates the relay power constraint (3.22b), they are projected into the feasible set. Due to the convexity of the feasible variable space in $\mathbf{Q}$, similar to the suggested procedure in [169], we follow a projection rule which results in a minimum Euclidean distance to the feasible set, i.e., minimum Frobenius norm of the matrix difference. In order to obtain this, let $\mathbf{W}_{\text{old}}$ and $\mathbf{Q}_{\text{old}}$ be the updated relay amplification matrix prior to the projection and the corresponding undistorted transmit covariance calculated from (3.14). Moreover, let $\mathbf{U}_{\text{old}}\mathbf{\Lambda}_{\text{old}}\mathbf{U}_{\text{old}}^H$ be an eigenvalue decomposition of the matrix $\mathbf{Q}_{\text{old}}$, such that $\mathbf{U}_{\text{old}}$ is a unitary matrix, and $\mathbf{\Lambda}_{\text{old}}$ is a diagonal matrix containing the eigenvalues. The feasible relay undistorted transmit covariance matrix, i.e., $\mathbf{Q}_{\text{new}}$, with minimum Euclidean distance to $\mathbf{Q}_{\text{old}}$ is then obtained as

$$\mathbf{Q}_{\text{new}} \leftarrow \mathbf{U}_{\text{old}} \underbrace{\left(\mathbf{\Lambda}_{\text{old}} - \zeta_{\text{gp}}\mathbf{I}_{M_{\text{t}}}\right)^+}_{=:\mathbf{\Lambda}_{\text{new}}} \mathbf{U}_{\text{old}}^H, \quad \zeta_{\text{gp}} \in \mathbb{R}, \tag{3.29}$$

where $\{\cdot\}^+$ substitutes the negative elements by zero and $\zeta_{\text{gp}} \in \mathbb{R}$ is the minimum non-negative value that satisfies $\text{tr}\left(\mathbf{\Lambda}_{\text{new}}\right) \leq \tilde{P}_{\text{r,max}}$, see [169, Eq. (25)-(27)]. The projected version of $\mathbf{W}_{\text{old}}$, i.e., $\mathbf{W}_{\text{new}}$ is then calculated as

$$\mathbf{W}_{\text{new}} \leftarrow \mathbf{Q}_{\text{new}}^{\frac{1}{2}}\mathbf{V}\mathbf{U}_{\text{r,new}}\left(\mathbf{\Sigma}_{\text{r,new}}\right)^{-\frac{1}{2}}\mathbf{U}_{\text{r,new}}^H, \tag{3.30}$$

where $\mathbf{Q}_{\text{new}}^{\frac{1}{2}} = \mathbf{U}_{\text{old}}\mathbf{\Lambda}_{\text{new}}^{\frac{1}{2}}\mathbf{U}_{\text{old}}^H$, $\mathbf{V}$ is an arbitrary unitary matrix such that $\mathbf{V}\mathbf{V}^H = \mathbf{I}_{M_{\text{t}}}$, and $\mathbf{U}_{\text{r,new}}\mathbf{\Sigma}_{\text{r,new}}\mathbf{U}_{\text{r,new}}^H$ is the eigenvalue decomposition of $\mathcal{V}(\mathbf{Q}_{\text{new}})$, see (3.12).

Note that the resulting amplification matrix $\mathbf{W}_{\text{new}}$ consequently results in $\mathbf{Q}_{\text{new}}$ as the relay covariance matrix, see (3.11), and hence belongs to the feasible set of (3.22b). Moreover, the choice of $\mathbf{V}$ does not affect the corresponding $\mathbf{Q}_{\text{new}}$ and hence does not

---

$$\text{vec}\left(\nabla_{\mathbf{W}^*}P_{\text{err}}\right)^T = \text{vec}\left(\left(\mathbf{H}_{\text{rd}}^H\mathbf{z}\mathbf{z}^H\mathbf{H}_{\text{rd}}\right)^T\right)^T\left(\mathbf{I}_{M_{\text{t}}^2} + \kappa\mathbf{S}_{\text{D}}^{M_{\text{t}}}\right)\Bigg(\left[\mathbf{c} + \mathbf{C}\left(\mathbf{I}_{M_{\text{t}}^2} - \left(\mathbf{W}^*\otimes\mathbf{W}\right)\mathbf{C}\right)^{-1}\left(\mathbf{W}^*\otimes\mathbf{W}\right)\mathbf{c}\right]^T$$
$$\otimes\left(\mathbf{I}_{M_{\text{t}}^2} - \left(\mathbf{W}^*\otimes\mathbf{W}\right)\mathbf{C}\right)^{-1}\Bigg)\mathbf{S}_{\text{K}}\left(\mathbf{w}\otimes\mathbf{I}_{M_{\text{r}}M_{\text{t}}}\right) - \left(\mathbf{z}^T\mathbf{H}_{\text{rd}}^*\right)\otimes\left(P_{\text{s}}\mathbf{z}^H\mathbf{H}_{\text{rd}}\mathbf{W}\mathbf{h}_{\text{sr}}\mathbf{h}_{\text{sr}}^H\right)\mathbf{S}_{\text{T}}, \tag{3.26}$$

$$\text{vec}\left(\nabla_{\mathbf{W}^*}P_{\text{des}}\right)^T = \left(\mathbf{z}^T\mathbf{H}_{\text{rd}}^*\right)\otimes\left(P_{\text{s}}\mathbf{z}^H\mathbf{H}_{\text{rd}}\mathbf{W}\mathbf{h}_{\text{sr}}\mathbf{h}_{\text{sr}}^H\right)\mathbf{S}_{\text{T}},$$

$$\text{where } \mathbf{w} := \text{vec}(\mathbf{W}),\ \mathbf{S}_{\text{K}} \in \{0,1\}^{M_{\text{r}}^2M_{\text{t}}^2\times M_{\text{r}}^2M_{\text{t}}^2},\ \mathbf{S}_{\text{T}} \in \{0,1\}^{M_{\text{r}}M_{\text{t}}\times M_{\text{r}}M_{\text{t}}}, \tag{3.27}$$

$$\text{such that: } \text{vec}\left(\mathbf{W}^*\otimes\mathbf{W}\right) = \mathbf{S}_{\text{K}}\text{vec}\left(\mathbf{w}^*\mathbf{w}^T\right), \text{ and } \mathbf{S}_{\text{T}}\text{vec}(\mathbf{W}) = \text{vec}(\mathbf{W}^T). \tag{3.28}$$

affect the feasibility. Thus, it can be chosen similar to that of $\mathbf{W}_{\text{old}}$, with no need for modification in the projection process:

$$\mathbf{V} = (\mathbf{Q}_{\text{old}})^{-\frac{1}{2}} \mathbf{W}_{\text{old}} \mathbf{U}_{\text{r,old}} (\mathbf{\Sigma}_{\text{r,old}})^{\frac{1}{2}} \mathbf{U}_{\text{r,old}}^{H}, \tag{3.31}$$

where $\mathbf{U}_{\text{r,old}} \mathbf{\Sigma}_{\text{r,old}} \mathbf{U}_{\text{r,old}}^{H}$ is the eigenvalue decomposition of $\mathcal{V}(\mathbf{Q}_{\text{old}})$.

3.4.2 Iterative update for source Tx power

For fixed values of $\mathbf{W}$ and $\mathbf{z}$, an increase in P_{s} results in an increase in the desired received power, see (3.19). On the other hand, it also results in an increase in P_{err}, due to the direct source-destination interference as well as the increase in the received power at the relay. This results in an amplified distortion effect. As a result, the impact of the choice of P_{s} on the end-to-end SDNR is not clear. The following lemma provides an answer to this question.

Lemma 3.4.1. *For fixed values of* $\mathbf{W}$ *and* $\mathbf{z}$ *the resulting SDNR is a concave and increasing function of* P_s*. Hence, the optimum* P_s *is given as*

$$P_s^{\star} = min\left\{P_{s,max}, \tilde{P}_{s,max}(\mathbf{W})\right\}, \tag{3.32}$$

where $\tilde{P}_{s,max}(\mathbf{W})$ *represents the value of* P_s *that results in the maximum relay transmit power* $P_{r,max}$*, with* $\mathbf{W}$ *as the relay amplification matrix.*

Proof. See Appendix 7. □

It is worth mentioning that for a setup with a weak direct link, i.e., $\|\mathbf{h}_{\text{sd}}\|_2 \approx 0$, we have $P_{\text{s}}^{\star} = P_{\text{s,max}}$ for a jointly optimal choice of $\mathbf{W}$ and P_{s}. This is grounded on the fact that for any $P_{\text{s}} < P_{\text{s,max}}$, the joint variable update $P_{\text{s}} \leftarrow P_{\text{s,max}}$ and $\mathbf{W} \leftarrow \mathbf{W}\sqrt{\frac{P_{\text{s}}}{P_{\text{s,max}}}}$ result in the same P_{des}, see (3.19), while decreasing the P_{err}, see (3.21) in connection to (3.17).

3.4.3 Iterative update for destination Rx filter

It is apparent that the relay transmit covariance, and hence the constraints in (3.22b) are invariant to the choice of receive linear filter. The optimal choice of $\mathbf{z}$ for a given $\mathbf{W}$ and P_{s} is obtained as

$$\mathbf{z}^{\star} = \left(\mathbf{H}_{\text{rd}}\Big(\mathbf{Q} + \kappa \text{diag}\left(\mathbf{Q}\right)\Big)\mathbf{H}_{\text{rd}}^{H} + \sigma_{\text{nd}}^{2}\mathbf{I}_{M_{\text{d}}} + P_{\text{s}}\mathbf{h}_{\text{sd}}\mathbf{h}_{\text{sd}}^{H}\right)^{-1} \sqrt{P_{\text{s}}}\mathbf{H}_{\text{rd}}\mathbf{W}\mathbf{h}_{\text{sr}}. \tag{3.33}$$

The value of $\mathbf{z}$ is updated according to (3.33) after the updates for $\mathbf{W}, P_{\text{s}}$. The update iterations continue until a stable point is achieved or a certain number of iterations is expired, see Algorithm 5.

3.4.4 Convergence

The proposed GP algorithm leads to a necessary convergence, due to the monotonically non-decreasing nature of the SDNR after each variable update and the fact that the objective is bounded from above[4]. However, due to the non-convexity of the problem, the global optimality of the obtained solution is not guaranteed, and the converging point depends on the used initialization [32, 78]. In Subsection 3.7.1 a numerical evaluation of the optimal performance is obtained by repeating the GP algorithm with several initializations.

Algorithm 5 Iterative SDNR maximization algorithm based on GP. Number of algorithm iterations are determined by $c_1 \in \mathbb{R}^+$ and $C_1 \in \mathbb{N}$.

Counter $\leftarrow 0$
repeat (running for multiple initializations)
  Counter $\leftarrow$ Counter $+ 1$;
  $l \leftarrow 0$;
  $P_{\mathrm{s}}^{[0]} \leftarrow P_{\mathrm{s,max}} \times 10^{-4}$;
  $\mathbf{Q}^{[0]} \leftarrow$ random init., see (3.22b);
  $\mathbf{W}^{[0]} \leftarrow \mathbf{Q}^{[0]\,\frac{1}{2}} \mathcal{V}^{\frac{-1}{2}} \left(\mathbf{Q}^{[0]}\right)$, see (3.30), (3.12);
  repeat
    $l \leftarrow l + 1$;
    $\left(\mathbf{W}^{[l]}, P_{\mathrm{s}}^{[l]}, \mathbf{z}^{[l]}\right) \leftarrow$ update, see (3.24), (3.30), (3.32), (3.33);
    $\mathrm{SDNR}^{[l]} \leftarrow$ (3.22a);
  until $\mathrm{SDNR}^{[l]} - \mathrm{SDNR}^{[l-1]} \geq c_1$ (until SDNR improves)
  $\mathcal{A} \leftarrow$ save $\left(\mathrm{SDNR}^{[l]}, \mathbf{W}^{[l]}, \mathbf{z}^{[l]}\right)$;
until Counter $\leq C_1$
return $(\mathbf{W}, \mathbf{z}, \mathrm{SDNR}) \leftarrow \max\ \mathrm{SDNR} \in \mathcal{A}$;

3.5 An Intuitive Approach: Distortion-Aware Multi-Stage Rank-1 Relay Amplification (MuStR1)

The proposed method in Section 3.4 directly deals with the SDNR as optimization objective, which also leads to the maximization of end-to-end mutual information for Gaussian signal codewords. Nevertheless, the proposed procedure imposes a high computational complexity, due to the number of the required iterations. In this section, a simpler design is introduced by considering a rank-one relay amplification matrix. Note that the near-optimality of rank-one relay amplification matrices for single stream

[4]Please note that the convergence is obtained in the sense that the objective reaches a stable value with an arbitrarily small tolerance margin. Although the resulting optimization variables do not necessarily converge, the potentially different obtained solutions are equally favorable, i.e., they are all feasible and result in the same objective value.

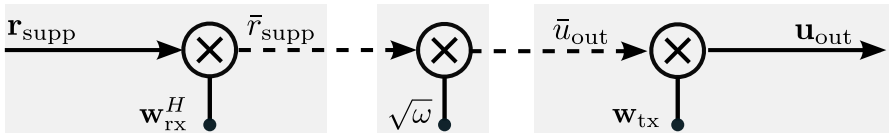

Figure 3.2: The relay amplification is divided into three parts: $\mathbf{w}_{\text{rx}}$ and $\mathbf{w}_{\text{tx}}$, respectively, represent the reception and transmit filters, while ω represents the scaling factor. The bold arrows represent the vector signals while the dashed arrows represent the scalars. The overall process can be described as $\mathbf{W} = \omega \mathbf{w}_{\text{tx}} \mathbf{w}_{\text{rx}}^H$.

communication has been established, see the arguments in [74, Subsection 3.2] and [73, Section III]. Nevertheless, in the aforementioned works, the impacts of transmit and receive distortion have not been considered in the FD transceiver. A rank-one relay amplification process is expressed as

$$\mathbf{W} = \sqrt{\omega} \mathbf{w}_{\text{tx}} \mathbf{w}_{\text{rx}}^H, \tag{3.34}$$

where $\mathbf{w}_{\text{rx}} \in \mathbb{C}^{M_{\text{r}}}$, $\|\mathbf{w}_{\text{rx}}\|_2 = 1$ and $\mathbf{w}_{\text{tx}} \in \mathbb{C}^{M_{\text{t}}}$, $\|\mathbf{w}_{\text{tx}}\|_2 = 1$, respectively act as the receive and transmit linear filters at the relay, while $\omega \in \mathbb{R}^+$ acts as a scaling factor, see Fig. 3.2. The idea is to separately design the transmit (receive) filters to maximize the SDNR at each segment. Afterwards, the value of ω is optimized. A detailed role and design strategy for the aforementioned parts is elaborated in the following.

3.5.1 Transmit filter

The role of $\mathbf{w}_{\text{tx}}$ is to direct the relay transmit beam towards the destination, while imposing minimal distortion on the receiver end of the relay and destination nodes. For this purpose we define the following optimization problem

$$\max_{\mathbf{w}_{\text{tx}}} \quad \frac{\mathbb{E}\{\|\mathbf{H}_{\text{rd}} \mathbf{u}_{\text{out}}\|_2^2\}}{\mathbb{E}\{\|\mathbf{H}_{\text{D,tx}} \mathbf{u}_{\text{out}}\|_2^2\} + \text{tr}\left(P_{\text{s}} \mathbf{h}_{\text{sd}} \mathbf{h}_{\text{sd}}^H + \sigma_{\text{nd}}^2 \mathbf{I}_{M_{\text{d}}}\right)}, \quad \text{s.t.} \quad \|\mathbf{w}_{\text{tx}}\|_2 = 1, \tag{3.35}$$

where the numerator is the desired received power from the relay-destination path and $\mathbf{H}_{\text{D,tx}}$ is the equivalent distortion channel observed from the relay transmitter, see Appendix 7. The optimization problem (3.35) can be hence formulated as[5]

$$\max_{\mathbf{w}_{\text{tx}}} \quad \frac{\mathbf{w}_{\text{tx}}^H \left(\mathbf{H}_{\text{rd}}^H \mathbf{H}_{\text{rd}}\right) \mathbf{w}_{\text{tx}}}{\mathbf{w}_{\text{tx}}^H \left(\mathbf{H}_{\text{D,tx}}^H \mathbf{H}_{\text{D,tx}} + N_{\text{tx}} \mathbf{I}_{M_{\text{t}}}\right) \mathbf{w}_{\text{tx}}}, \quad \text{s.t.} \quad \|\mathbf{w}_{\text{tx}}\|_2 = 1, \tag{3.36}$$

[5]For the calculation of the spatial filters $\mathbf{w}_{\text{tx}}$ and $\mathbf{w}_{\text{rx}}$, it is assumed that the relay operates with maximum power, to emphasize the impact of hardware distortions. The relay transmit power is afterwards adjusted by the choice of ω. An alternating adjustment of the spatial filters with the optimized relay power is later discussed in Subsection 3.5.5.

which holds a generalized Rayleigh quotient structure [170], and

$$N_{\mathrm{tx}} := \left(M_{\mathrm{d}}\sigma_{\mathrm{nd}}^2 + P_{\mathrm{s}}\|\mathbf{h}_{\mathrm{sd}}\|_2^2\right)/P_{\mathrm{r,max}}. \tag{3.37}$$

The optimal transmit filter is hence obtained as

$$\mathbf{w}_{\mathrm{tx}}^{\star} = \boldsymbol{\lambda}_{\max}\left\{\left(\mathbf{H}_{\mathrm{D,tx}}^H\mathbf{H}_{\mathrm{D,tx}} + N_{\mathrm{tx}}\mathbf{I}_{M_{\mathrm{t}}}\right)^{-1}\left(\mathbf{H}_{\mathrm{rd}}^H\mathbf{H}_{\mathrm{rd}}\right)\right\}. \tag{3.38}$$

3.5.2 Receive filter

The role of $\mathbf{w}_{\mathrm{rx}}$, is to accept the desired received signal from the source, while rejecting the received distortion-plus-noise terms at the relay. Similar to (3.35) this is expressed as

$$\max_{\mathbf{w}_{\mathrm{rx}}} \quad \frac{\mathbf{w}_{\mathrm{rx}}^H\left(\mathbf{h}_{\mathrm{sr}}\mathbf{h}_{\mathrm{sr}}^H\right)\mathbf{w}_{\mathrm{rx}}}{\mathbf{w}_{\mathrm{rx}}^H\left(\boldsymbol{\Phi} + \sigma_{\mathrm{nr}}^2\mathbf{I}_{M_{\mathrm{r}}}\right)\mathbf{w}_{\mathrm{rx}}}, \quad \text{s.t.} \quad \|\mathbf{w}_{\mathrm{rx}}\|_2 = 1, \tag{3.39}$$

where

$$\boldsymbol{\Phi} := \kappa P_{\mathrm{r,max}}\mathbf{H}_{\mathrm{rr}}\mathrm{diag}\left(\mathbf{w}_{\mathrm{tx}}\mathbf{w}_{\mathrm{tx}}^H\right)\mathbf{H}_{\mathrm{rr}}^H + \beta P_{\mathrm{r,max}}\mathrm{diag}\left(\mathbf{H}_{\mathrm{rr}}\mathbf{w}_{\mathrm{tx}}\mathbf{w}_{\mathrm{tx}}^H\mathbf{H}_{\mathrm{rr}}^H\right), \tag{3.40}$$

gives the covariance of the received distortion signal at the relay. The optimal solution to $\mathbf{w}_{\mathrm{rx}}$ can be hence obtained as

$$\mathbf{w}_{\mathrm{rx}}^{\star} = \boldsymbol{\lambda}_{\max}\left\{\left(\boldsymbol{\Phi} + \sigma_{\mathrm{nr}}^2\mathbf{I}_{M_{\mathrm{r}}}\right)^{-1}\left(\mathbf{h}_{\mathrm{sr}}\mathbf{h}_{\mathrm{sr}}^H\right)\right\}. \tag{3.41}$$

3.5.3 Relay amplification

The role of ω is to adjust the amplification intensity at the relay. This plays a significant role, considering the fact that even with optimally designed spatial filters, i.e., $\mathbf{w}_{\mathrm{tx}}$ and $\mathbf{w}_{\mathrm{rx}}$, a weak amplification at the relay reduces the desired signal strength at the destination, resulting in a low signal-to-noise ratio. On the other hand, a strong amplification may lead to instability and (theoretically) infinite distortion transmit power, i.e., low signal-to-distortion ratio. Hence, similar to (3.22), we focus on maximizing the end-to-end SDNR, assuming that $\mathbf{w}_{\mathrm{tx}}$ and $\mathbf{w}_{\mathrm{rx}}$ are given from the previous parts. The end-to-end SDNR and the transmit power from the relay corresponding to a value of ω are, respectively, approximated as f_1 and f_2, where

$$f_1(\omega) = a_{\mathrm{d}}\omega\left(a_0 + \sum_{k\in\mathbb{F}_K} a_k\omega^k\right)^{-1}, \tag{3.42}$$

and

$$f_2(\omega) = \sum_{k\in\mathbb{F}_K} b_k \omega^k, \tag{3.43}$$

where

$$a_{\mathrm{d}} = P_{\mathrm{s}} \mathbf{d}_{M_{\mathrm{d}}}^T \left(\mathbf{H}_{\mathrm{rd}}^* \otimes \mathbf{H}_{\mathrm{rd}}\right) \tilde{\mathbf{W}} \mathrm{vec}\left(\mathbf{h}_{\mathrm{sr}} \mathbf{h}_{\mathrm{sr}}^H\right), \tag{3.44}$$

$$a_0 = \mathbf{d}_{M_{\mathrm{d}}}^T \mathrm{vec}\left(\sigma_{\mathrm{nd}}^2 \mathbf{I}_{M_{\mathrm{d}}} + P_{\mathrm{s}} \mathbf{h}_{\mathrm{sd}} \mathbf{h}_{\mathrm{sd}}^H\right), \tag{3.45}$$

$$a_1 = -a_{\mathrm{d}} + \mathbf{d}_{M_{\mathrm{d}}}^T \left(\mathbf{H}_{\mathrm{rd}}^* \otimes \mathbf{H}_{\mathrm{rd}}\right) \left(\mathbf{I}_{M_{\mathrm{t}}^2} + \kappa \mathbf{S}_{\mathrm{D}}^{M_{\mathrm{t}}}\right) \tilde{\mathbf{W}} \mathbf{c}, \tag{3.46}$$

$$a_k = \mathbf{d}_{M_{\mathrm{d}}}^T \left(\mathbf{H}_{\mathrm{rd}}^* \otimes \mathbf{H}_{\mathrm{rd}}\right) \left(\mathbf{I}_{M_{\mathrm{t}}^2} + \kappa \mathbf{S}_{\mathrm{D}}^{M_{\mathrm{t}}}\right) \left(\tilde{\mathbf{W}} \mathbf{C}\right)^{k-1} \tilde{\mathbf{W}} \mathbf{c},\ k \in \{2 \dots K\}, \tag{3.47}$$

$$b_k = \mathbf{d}_{M_{\mathrm{t}}}^T \left(\mathbf{I}_{M_t{}^2} + \kappa \mathbf{S}_{\mathrm{D}}^{M_{\mathrm{t}}}\right) \left(\tilde{\mathbf{W}} \mathbf{C}\right)^{k-1} \tilde{\mathbf{W}} \mathbf{c},\ k \in \mathbb{F}_K, \tag{3.48}$$

see Appendix 7 for more details. In the above expressions, K is the approximation order and $\mathbf{d}_M \in \{0,1\}^{M^2}$ is defined such that $\mathrm{tr}(\mathbf{A}) = \mathbf{d}_M^T \mathrm{vec}(\mathbf{A})$, $\mathbf{A} \in \mathbb{C}^{M\times M}$. Furthermore $\mathbf{C}, \mathbf{c}, \tilde{\mathbf{W}}$ are, respectively, defined in (3.15), (3.16) and Appendix 7. The corresponding optimization problem can be written as

$$\max_{\omega} \quad f_1(\omega) \tag{3.49a}$$

$$\text{s.t.} \quad 0 \le \omega \le \min\{\omega_{\mathrm{infty}}, \omega_{\max}\} = \omega_{\max}, \tag{3.49b}$$

where $\omega_{\max}$ corresponds to the relay amplification that results in a tight transmit power constraint, i.e., $f_2(\omega_{\max}) = P_{\mathrm{r,max}}$. Moreover, ω_{infty} is the smallest pole of $f_2(\omega)$ in the real positive domain which yields to instability of the relay distortion loop, i.e., infinite relay transmit power. It is observed that while $f_1(\omega)$ remains positive and differentiable in the range $[0, \omega_{\mathrm{infty}})$, we have $\underset{\omega\to 0}{f_1}(\omega) \to 0$ and $\underset{\omega\to\omega_{\mathrm{infty}}}{f_1}(\omega) \to 0$. This concludes the existence of (at least) one local maximum point in this domain, see Fig. 3.3 for a visual description. By setting the derivative of (3.42) to zero, it is observed that the resulting extremum points are necessarily located such that

$$a_0 = \sum_{k\in\mathbb{F}_K} (k-1) a_k \omega^k. \tag{3.50}$$

While the left side of (3.50) is a constant, the right side of the equality is monotonically increasing with respect to $\omega \in \mathbb{R}^+$, as $a_k \ge 0, \forall k$. This readily results in the exactly one extremum point[6] in the positive domain of ω. Hence, the optimality occurs either at the obtained extremum point, i.e., a local maximum in the range $[0, \omega_{\max})$, see Fig. 3.3-a, or at the point where the relay transmit power constraint is tight, see Fig. 3.3-b. The optimum ω can be hence formulated as

$$\omega^\star = \min\{\omega_0, \omega_{\max}\}, \tag{3.51}$$

[6]Note that both $f_2(\omega_{\max}) = P_{\mathrm{r,max}}$ or (3.50) result in exactly one solution for ω in $\mathbb{R}^+$, as $a_k, b_k \ge 0, \forall k$. In this regard, values of $\omega_{\max}$ and ω_0 can be obtained via a bi-section search, or can be obtained in closed-form for small values of K, i.e., $K \le 3$, as a known polynomial root.

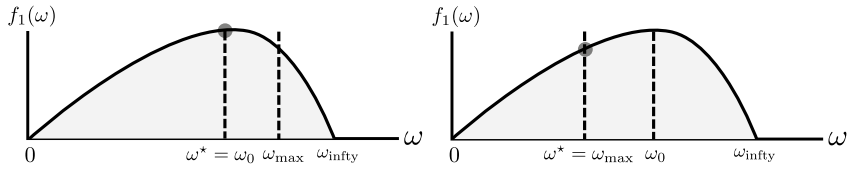

(a) $\omega_0 \leq \omega_{\max}$ (b) $\omega_0 > \omega_{\max}$

Figure 3.3: Possible situations of ω_0 with respect to $\omega_{\max}$, considering the feasible region of ω. The dark circle indicates the position of the optimum point.

where ω_0 is the only solution of (3.50) in the positive region.

Note that the proposed design for ω, also subsumes the problem of optimal power adjustment at the relay for a setup with a single-antenna source, relay and destination nodes. Please refer to [60] for the optimal relay selection and power adjustment problem on a single-antenna AF-FD relay under hardware impairments, and [59] for an extension to a distributed beamforming problem among multiple single-antenna AF-FD relays.

3.5.4 Design of destination Rx filter

The optimal design of $\mathbf{z}$ is given in (3.33) as a closed form expression. Note that the solution of $\mathbf{z}$ is dependent on the choice of other optimization variables. However, as the proposed designs for the other optimization variables do not depend on $\mathbf{z}$, there is no need for further alternation among the design parameters. The Algorithm 6 defines the required steps.

Algorithm 6 Distortion Aware Multi-Stage Rank-1 Relay amplification (MuStR1) for SDNR maximization. The solution is obtained

1: $P_{\text{s}} \leftarrow P_{\text{s,max}}$
2: $\mathbf{w}_{\text{tx}} \leftarrow$ calculate Tx filter, see (3.38);
3: $\mathbf{w}_{\text{rx}} \leftarrow$ calculate Rx filter, see (3.41);
4: $\omega \leftarrow$ adjust amplification intensity, see Subsection 3.5.3;
5: $\mathbf{z} \leftarrow$ see (3.33);
6: **return** $\left(\mathbf{z},\ \mathbf{W} = \omega \mathbf{w}_{\text{tx}} \mathbf{w}_{\text{rx}}^H\right)$;

3.5.5 Alternating enhancement of MuStR1 (AltMuStR1)

The proposed MuStR1 design is accomplished with no alternation among the optimization variables, see Algorithm 6. In this part, an alternating enhancement of MuStR1 is proposed, which results in an increased performance at the expense of a higher computational complexity. In order to accomplish this purpose, similar to (3.19) and (3.21) we focus on the signal and power values at the destination, after the application of $\mathbf{z}$.

In this respect, the values of $\mathbf{w}_{\text{tx}}, \mathbf{w}_{\text{rx}}, \mathbf{z}$ and ω will be calculated as a joint alternating optimization. This is done by replacing $\mathbf{H}_{\text{rd}}$ with $\mathbf{z}^H\mathbf{H}_{\text{rd}}$ in the design of $\mathbf{w}_{\text{tx}}$, and $\mathbf{d}^T$ with $\left(\mathbf{z}^T \otimes \mathbf{z}^H\right)$ in (3.44)-(3.47). The steps 2-6 in Algorithm 6 are then repeated until a stable point is achieved or a maximum number of iterations is expired. The performance of the proposed (Alt)MuStR1 algorithms in terms of the resulting communication rate, convergence, and computational complexity are studied via numerical simulations in Subsection 3.7.1. In particular, it is observed that the performance of the AltMuStR1 algorithm reaches close to the performance of GP with a significantly lower computational complexity.

3.5.6 Convergence

Due to the proposed SDNR approximation as well as the sub-optimal solutions for $\mathbf{w}_{\text{tx}}$ and $\mathbf{w}_{\text{tx}}$ at each iteration, the convergence of the AltMuStR1 algorithm is not theoretically guaranteed. However, it is observed via numerical simulations in Subsection 3.7.1, that the algorithm shows a fast average convergence, with a performance close to the proposed GP method for a wide range of system parameters.

3.6 FD Decode-and-Forward Relaying Under Residual Self-Interference

In the previous sections, the behavior of an AF-FD relay is studied under the impact of hardware impairments. While an AF relaying is known to provide a simple strategy, it particularly suffers from the observed distortion loop effect, especially when the hardware impairments are not negligible, see Subsection 3.2.4. In this part, a similar study is provided for a setup where the relay operates with DF protocol, in order to act as a comparison benchmark. In a DF relay, the discussed distortion loop is significantly alleviated as the decoding process eliminates the inter-dependency of the received residual interference intensity to the relay transmit signal power. Note that optimization strategies for FD relays with DF process have been discussed in the literature, see [78–80, 82], for different relaying setups and assumptions. In order to adopt the available designs to our setup, we follow a modified version of the approach given in [80, 82], where an SDNR maximization problem is studied at a MIMO DF relay. Note that the proposed design in [80, 82] considers a maximization of the SDNR at the relay input and output, taking advantage of spatial and temporal filters. In contrast, we focus on the resulting performance from the source to the destination, after the application of the receive filter $\mathbf{z}$, and hence including P_{s} and $\mathbf{z}$ as optimization variables. Afterwards, similar to [82], a joint optimization is proposed where in each step a subset of the variables are updated. A detailed model update and design strategy is given in the following.

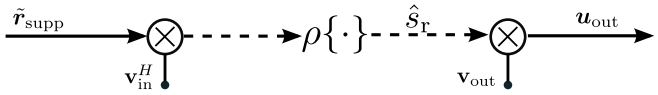

Figure 3.4: A schematic of a decode-and-forward relaying process. $\rho\{\cdot\}$ and $\hat{s}_{\text{r}}$ represent the decoding process, and the estimate of the transmitted symbol, s, at the relay. The receive and transmit spatial filters are represented as $\mathbf{v}_{\text{in}}$ and $\mathbf{v}_{\text{out}}$, respectively. The bold arrows represent the vector signals while the dashed arrows represent the scalars.

3.6.1 DF relaying

We define $\mathbf{v}_{\text{in}} \in \mathbb{C}^{M_{\text{r}}}$ as linear filter at the relay input, $\hat{s}_{\text{r}} \in \mathbb{C}$ as the decoded symbol such that $\mathbb{E}\{|\hat{s}_{\text{r}}|^2\} = 1$, and $\mathbf{v}_{\text{out}} \in \mathbb{C}^{M_{\text{t}}}$ as the beamforming vector to transmit the decoded data symbol, see Fig. 3.4. The end-to-end rate maximization can be equivalently formulated as

$$\max_{\mathbf{v}_{\text{in}},\mathbf{z},\mathbf{Q}\in\mathcal{H},P_{\text{s}}} \quad \min\left(\zeta_{\text{sr}}, \zeta_{\text{rd}}\right), \tag{3.52a}$$

$$\text{s.t.} \quad \text{tr}\left(\mathbf{Q}\right) \leq \tilde{P}_{\text{r,max}},\ P_{\text{s}} \leq P_{\text{s,max}},\ \text{rank}(\mathbf{Q}) = 1, \tag{3.52b}$$

where the rank-one constraint is imposed to ensure the structure $\mathbf{Q} := \mathbb{E}\{\mathbf{u}_{\text{out}}\mathbf{u}_{\text{out}}^H\} = \mathbf{v}_{\text{out}}\mathbf{v}_{\text{out}}^H$. The values ζ_{sr} and ζ_{rd}, respectively represent the resulting SDNR in source-to-relay and relay-to destination links which can be calculated as

$$\zeta_{\text{sr}} \approx \frac{P_{\text{s}}\mathbf{v}_{\text{in}}^H\mathbf{h}_{sr}\mathbf{h}_{sr}^H\mathbf{v}_{\text{in}}}{\mathbf{v}_{\text{in}}^H\Big(\sigma_{\text{nr}}^2\mathbf{I}_{M_{\text{r}}}+\kappa\mathbf{H}_{\text{rr}}\text{diag}(\mathbf{Q})\mathbf{H}_{\text{rr}}^H+\beta\text{diag}\left(\mathbf{H}_{\text{rr}}\mathbf{Q}\mathbf{H}_{\text{rr}}^H\right)\Big)\mathbf{v}_{\text{in}}}, \tag{3.53}$$

$$\zeta_{\text{rd}} = \frac{\mathbf{z}^H\mathbf{H}_{\text{rd}}\mathbf{Q}\mathbf{H}_{\text{rd}}^H\mathbf{z}}{\mathbf{z}^H\Big(\sigma_{\text{nd}}^2\mathbf{I}_{M_{\text{d}}} + \kappa\mathbf{H}_{\text{rd}}\text{diag}(\mathbf{Q})\mathbf{H}_{\text{rd}}^H + P_{\text{s}}\mathbf{h}_{\text{sd}}\mathbf{h}_{\text{sd}}^H\Big)\mathbf{z}}, \tag{3.54}$$

where the approximation in (3.53) follows from the fact that the self-interference signal constitutes the dominant part of the received power in $\mathbf{u}_{\text{in}}$, see also (3.9). Note that (3.52) is not a convex optimization problem and also cannot be solved in a closed form. Nevertheless, recognizing the generalized Rayleigh quotient structure in (3.53) and (3.54) we obtain

$$\mathbf{z}^\star = \Big(\sigma_{\text{nd}}^2\mathbf{I}_{M_{\text{d}}} + \kappa\mathbf{H}_{\text{rd}}\text{diag}(\mathbf{Q})\mathbf{H}_{\text{rd}}^H + P_{\text{s}}\mathbf{h}_{\text{sd}}\mathbf{h}_{\text{sd}}^H\Big)^{-1}\mathbf{H}_{\text{rd}}\mathbf{v}_{\text{out}}, \tag{3.55}$$

$$\mathbf{v}_{\text{in}}^\star = \Big(\sigma_{\text{nr}}^2\mathbf{I}_{M_{\text{r}}} + \kappa\mathbf{H}_{\text{rr}}\text{diag}(\mathbf{Q})\mathbf{H}_{\text{rr}}^H + \beta\text{diag}\left(\mathbf{H}_{\text{rr}}\mathbf{Q}\mathbf{H}_{\text{rr}}^H\right)\Big)^{-1}\mathbf{h}_{\text{sr}}\sqrt{P_{\text{s}}}, \tag{3.56}$$

where $\mathbf{z}^\star$ and $\mathbf{v}_{\text{in}}^\star$ represent the optimum $\mathbf{z}$ and $\mathbf{v}_{\text{in}}$ for a fixed $\mathbf{Q}$ and P_{s}. In order to obtain the optimal $\mathbf{Q}, P_{\text{s}}$, the problem in (3.52) can be re-formulated as

$$\max_{P_{\text{s}},\zeta\in\mathbb{R}^+,\mathbf{Q}\in\mathcal{H}} \quad \zeta \tag{3.57a}$$

$$\text{s.t.} \quad \zeta \leq \zeta_{\text{sr}},\ \zeta \leq \zeta_{\text{rd}}, \tag{3.57b}$$

$$\mathbf{Q} \in \mathcal{H},\ \text{tr}\left(\mathbf{Q}\right) \leq \tilde{P}_{\text{r,max}},\ \text{rank}(\mathbf{Q}) = 1, \tag{3.57c}$$

where the values of $\mathbf{v}_{\text{in}}$ and $\mathbf{z}$ are fixed. By temporarily relaxing the rank constraint, the above problem can be written as a convex feasibility check over $\mathbf{Q}, P_{\text{s}}$, for each value of ζ as

$$\text{find} \quad \mathbf{Q}, P_{\text{s}} \tag{3.58a}$$

$$\text{s.t.} \quad \text{tr}\left(\mathbf{Q}\right) \leq \tilde{P}_{\text{r,max}},\ \ P_{\text{s}} \geq 0,\ \mathbf{Q} \in \mathcal{H}, \tag{3.58b}$$

$$\text{tr}\left(\mathbf{\Psi}_{\text{sr}} + \mathbf{\Phi}_{\text{sr}}\mathbf{Q}\right) \geq 0,\ \text{tr}\left(\mathbf{\Psi}_{\text{rd}} + \mathbf{\Phi}_{\text{rd}}\mathbf{Q}\right) \geq 0, \tag{3.58c}$$

where

$$\mathbf{\Psi}_{\text{rd}} := -\zeta\mathbf{z}\mathbf{z}^H\left(\sigma_{\text{nd}}^2\mathbf{I}_{M_{\text{d}}} + P_{\text{s}}\mathbf{h}_{\text{sd}}\mathbf{h}_{\text{sd}}^H\right), \tag{3.59}$$

$$\mathbf{\Psi}_{\text{sr}} := \mathbf{v}_{\text{in}}\mathbf{v}_{\text{in}}^H\left(P_{\text{s}}\mathbf{h}_{\text{sr}}\mathbf{h}_{\text{sr}}^H - \zeta\sigma_{\text{nr}}^2\mathbf{I}_{M_{\text{r}}}\right), \tag{3.60}$$

$$\mathbf{\Phi}_{\text{rd}} := \mathbf{H}_{\text{rd}}^H\mathbf{z}\mathbf{z}^H\mathbf{H}_{\text{rd}} - \zeta\kappa\text{diag}\left(\mathbf{H}_{\text{rd}}^H\mathbf{z}\mathbf{z}^H\mathbf{H}_{\text{rd}}\right), \tag{3.61}$$

$$\mathbf{\Phi}_{\text{sr}} := -\zeta\left(\kappa\text{diag}\left(\mathbf{H}_{\text{rr}}^H\mathbf{v}_{\text{in}}\mathbf{v}_{\text{in}}^H\mathbf{H}_{\text{rr}}\right) + \beta\mathbf{H}_{\text{rr}}^H\text{diag}\left(\mathbf{v}_{\text{in}}\mathbf{v}_{\text{in}}^H\right)\mathbf{H}_{\text{rr}}\right). \tag{3.62}$$

Note that the iterations of the defined feasibility check will be continued, following a bi-section search procedure until an optimum ζ is obtained with a sufficient accuracy. Fortunately, for the special structure of (3.58) as a complex-valued semi-definite program with three linear constraints, an optimal rank-1 $\mathbf{Q} \in \mathcal{H}$ can be achieved following [171, Theorem 3.2]. The optimal $\mathbf{v}_{\text{in}}$ is hence obtained as

$$\mathbf{v}_{\text{out}}^\star = \mathbf{Q}^{\star\frac{1}{2}}, \tag{3.63}$$

where $\mathbf{Q}^\star$ represents the obtained $\mathbf{Q}$ for the highest feasible ζ.

Algorithm initialization

The initial value of $\mathbf{Q}$ is obtained by setting $\mathbf{v}_{\text{out}}$ as the dominant eigenvector of $\mathbf{H}_{\text{rd}}$, resulting in a maximum ratio transmission (MRT) and assuming a maximum transmit power at the relay. The initial values of $\mathbf{v}_{\text{in}}$ and $\mathbf{z}$ are then obtained from the maximum ratio combining (MRC) in (3.55) and (3.56). Moreover, the feasible values of ζ are necessarily located in the region $[0, \zeta_{\text{max}}]$ where

$$\zeta_{\text{max}} := \min\left\{\frac{P_{\text{s,max}}\|\mathbf{h}_{sr}\|_2^2}{\sigma_{\text{nr}}^2}, \frac{P_{\text{r,max}}\boldsymbol{\lambda}_{\text{max}}\left\{\mathbf{H}_{\text{rd}}\mathbf{H}_{\text{rd}}^H\right\}}{\sigma_{\text{nd}}^2}\right\} \tag{3.64}$$

corresponds to the minimum of the individual link qualities, assuming $\beta = \kappa = 0$, and will be used as the initial bounds for the aforementioned bi-section search.

Algorithm 7 An iterative rate maximization algorithm for decode-and-forward relaying. $C_{\mathrm{DF}}, C_2 \in \mathbb{N}$ respectively represent the number of the main optimization steps and the bi-section process, and $c_1 \in \mathbb{R}^+$ determines the stability condition.

$P_{\mathrm{s}} \leftarrow P_{\mathrm{s,max}} \times 10^{-2}$;
$\mathrm{counter}_1 \leftarrow 0$;
repeat (main optimization steps)
  $\mathrm{counter}_1 \leftarrow \mathrm{counter}_1 + 1$;
  $\mathbf{v}_{\mathrm{in}} \leftarrow \mathbf{v}_{\mathrm{in}}^{\star}$, see (3.56);
  $\mathbf{z} \leftarrow \mathbf{z}^{\star}$, see (3.55);
  $\mathrm{counter}_2 \leftarrow 0$;
  $\zeta_{\min} \leftarrow 0$;
  $\zeta_{\max} \leftarrow$ see (3.64);
  repeat (bi-section search steps)
    $\zeta \leftarrow (\zeta_{\min} + \zeta_{\max})/2$;
    if (3.58a)-(3.58b) is feasible **then**
      $\zeta_{\min} \leftarrow \zeta$;
    else
      $\zeta_{\max} \leftarrow \zeta$;
    end if
  until $\mathrm{counter}_2 \leq C_2$
  $\zeta^{\mathrm{counter}_1} \leftarrow (\zeta_{\min} + \zeta_{\max})/2$;
  $P_{\mathrm{s}} \leftarrow P_{\mathrm{s}}^{\star}$, see (3.57);
  $\mathbf{v}_{\mathrm{out}} \leftarrow \mathbf{v}_{\mathrm{out}}^{\star}$, see (3.63);
until $\mathrm{counter}_1 \leq C_{\mathrm{DF}}$ or $\zeta^{\mathrm{counter}_1} - \zeta^{\mathrm{counter}_1 - 1} \leq c_1$
return $(P_{\mathrm{s}}, \mathbf{z}, \mathbf{v}_{\mathrm{in}}, \mathbf{v}_{\mathrm{our}})$;

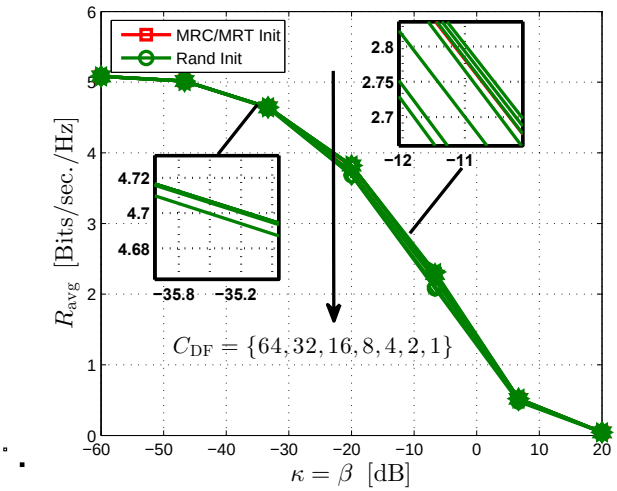

Figure 3.5: Evaluation of the DF relaying performance with C_{DF} random initializations, compared to the used MRC-MRT initialization.

Convergence and optimality gap

The solutions in (3.55)-(3.63) result in a necessary improvement of ζ, since in each step the defined sub-problem is solved to optimality. Moreover, since the performance of the studied relay system is bounded from above, see (3.64), the defined iterative update results in a necessary convergence. However, the global optimality of the obtained solution is not guaranteed, since the problem is not a jointly convex optimization problem. Hence, the resulting solution depends on the used initialization. In order to evaluate this, Algorithm 7 is repeated with several random initializations in Fig. 3.5, in comparison to the initialization defined in Subsection 3.6.1. It is observed that the proposed initialization in Algorithm 7 reaches close to the best achievable performance via several initializations. Hence, it is used as the performance benchmark for an achievable SDNR in an DF-FD relaying system.

3.7 Simulation Results

In this section, the behavior of the studied AF-FD relaying setup is evaluated via numerical simulations[7]. In particular, the proposed GP design in Section 3.4 as well as the (Alt)MuStR1 algorithms in Section 3.5 are evaluated, under the impact of hardware inaccuracies, and compared to the available relevant methods in the literature. It is assumed that $\mathbf{h}_{\mathrm{sr}}, \mathbf{H}_{\mathrm{rd}}$ and $\mathbf{h}_{\mathrm{sd}}$ follow an uncorrelated Rayleigh flat-fading model, where ρ_{sr}, ρ_{rd} and $\rho_{\mathrm{sd}} \in \mathbb{R}^{+}$ represent the path loss. For the SI channel, the characterization reported in [146] is used. In this respect, we have

$$\mathbf{H}_{\mathrm{rr}} \sim \mathcal{CN}\left(\sqrt{\frac{\rho_{\mathrm{rr}} K_R}{1+K_R}}\mathbf{H}_0, \frac{1}{1+K_R}\mathbf{I}_{M_{\mathrm{t}}} \otimes \mathbf{I}_{M_{\mathrm{r}}}\right), \tag{3.65}$$

where ρ_{rr} represents the SI channel strength, $\mathbf{H}_0$ is a deterministic term[8] and K_R is the Rician coefficient. For each channel realization the resulting performance in terms of the communication rate, i.e., $\log_2(1+\mathrm{SDNR})$, is evaluated by employing different design strategies and for various system parameters. The overall system performance in terms of the average rate, i.e., R_{avg}, is then evaluated via Monte-Carlo simulations by employing 500 channel realizations. Unless explicitly stated, the following parameters are used as the default setup: $M := M_{\mathrm{t}} = M_{\mathrm{r}} = M_{\mathrm{d}} = 4$, $\kappa = \beta = -40$ dB, $P_{\max} := P_{\mathrm{s,max}} = P_{\mathrm{r,max}} = 0$ dBW, $\sigma_{\mathrm{n}}^2 := \sigma_{\mathrm{nr}}^2 = \sigma_{\mathrm{nd}}^2 = -40$ dBW, $\rho_{\mathrm{rr}} = 1$, $\rho_{\mathrm{sr}} = \rho_{\mathrm{rd}} = -30$ dB, $\rho_{\mathrm{sd}} = -60$ dB, $K_R = 10$.

[7] I would like to thank my colleague M.Sc. Tianyu Yang for his help in running the numerical simulations regarding the Algorithms 5-7.

[8] For simplicity, $\mathbf{H}_0$ is chosen as a matrix of all-1 elements.

3.7.1 Algorithm analysis

In this subsection, the behavior of the proposed iterative algorithms, i.e., GP and (Alt)MuStR1, is studied in terms of the convergence speed, approximation accuracy, and computational complexity. Moreover, the gap of the proposed GP method with the optimality is evaluated with the help of an extensive numerical simulation.

Convergence

Both GP and AltMuStR1 operate based on iterative update of the variables, until a stable point is obtained. A study on the convergence behavior of these algorithms is hence necessary in order to verify the algorithm function and also as a measure of the required computational effort.

In Fig. 3.6 (a) the average convergence behavior of the GP algorithm is depicted. At each iteration, the obtained performance is depicted as a percentage of the final performance after convergence, where $\text{SDNR}^\star$ is the SDNR at the convergence. It is observed that the convergence speed differs for different values of transceiver inaccuracy. This is expected, as a higher distortion results in the complication of the mathematical structure by signifying non-quadratic terms, see (3.17), and requires the application of the projection procedure (Subsection 3.4.1) more often. It is observed from the simulations that the algorithm requires 10^2 to 10^4 number of iterations to converge, depending on the value of the distortion coefficients κ and β.

In Fig. 3.6 (b) the average convergence behavior of the proposed AltMuStR1 is depicted. Note that unlike GP, AltMuStR1 operates based on the local increase of SDNR in the defined relaying segments, see Section 3.5. Hence, a theoretical guarantee on the monotonic increase of the overall SDNR in each iteration is not available. Nevertheless, the numerical evaluation shows that the algorithm converges within much fewer number of iterations, with an effective increase in each step. Similar to GP, higher values of κ and β result in a slower convergence.

Computational complexity

Other than the required number of iterations, the computational demand of an algorithm is impacted by the required per-iteration complexity. In Fig. 3.6 (c), the required CPU time of the proposed algorithms are depicted as the number of antennas increase. The reported CPU time is obtained using an Intel Core $\text{i5}-3320\text{M}$ processor with the clock rate of 2.6 GHz and 8 GB of random-access memory (RAM). As the software platform, MATLAB 2013a is used on a 64-bit operating system. While the GP method is considered as the performance benchmark, the proposed (Alt)MuStR1 algorithms show a significant advantage to the GP algorithm in terms of computational complexity.

Approximation accuracy

The proposed (Alt)MuStR1 algorithms are based on the used approximation (3.47) and (3.48). In this regard, the choice of the approximation order K leads to a trade-off between algorithm complexity and the resulting performance. In Fig. 3.6-(d) the exact, and approximated SDNR values are depicted for a pessimistic case of $\kappa = 0.1$. By repeating such experiments, $K = 5$ is empirically chosen as a good balance between approximation accuracy and the resulting complexity.

GP optimality gap

Via the application of the gradient ascend, the proposed GP converges with a monotonically increasing objective. Nevertheless, the global optimality of the resulting stationary point may not be guaranteed due to the possibility of a local extrema. In Fig. 3.6 (e) the performance of GP algorithm is evaluated with multiple random initializations, where the best converging point is considered as the algorithm solution. It is observed that the occurrence of a non-optimum solutions is more likely for higher values of κ and β, as a larger number of initial points results in a better performance. Nevertheless, it is observed that no significant performance improvement is observed by employing more than $C_1 = 10$ number of random initial points. The obtained performance of the GP algorithm with $C_1 = 10$ is considered as a performance benchmark for AF-FD relaying, hereinafter.

Rank profile

In the proposed (Alt)MuStR1 method, a rank-1 relay amplification is assumed. Hence, it is interesting to observe how the solution to the GP method behaves in terms of the matrix rank. In Fig. 3.6 (f) the energy distribution of the singular values of the obtained relay amplification from the GP method is depicted. It is observed that for most of the distortion conditions, the highest singular value holds almost all of the energy, indicating an approximately rank-1 property.

3.7.2 Performance comparison

In this part the performance of the proposed designs is evaluated in comparison with the available designs in the literature.

Available design approaches

We divide the relevant available literature on the AF-FD relaying design into three main approaches. Firstly, as considered in [65, 66], SIC is purely relegated to the relay receiver end via combined time domain analog and digital cancellation techniques. The aforementioned approach imposes no design constraint on the self-interference power, i.e., $P_{\text{intf}} \leq \infty$, where P_{intf} represents the self-interference power prior to analog and digital cancellation[9]. Secondly, the SIC is purely done via transmit beamforming at the null space of the relay receive antennas, e.g., [68–73], hence imposing a zero interference power constraint for transmit beamforming design, i.e., $P_{\text{intf}} \leq 0$. Finally, as a generalization of the aforementioned extreme approaches, a combined transmit beamforming and SIC at the receiver is considered in [74, 75]. In the aforementioned case it is assumed that the received self-interference power should not exceed the threshold P_{th}, i.e., $P_{\text{intf}} \leq P_{\text{th}}$. In all of the aforementioned cases, due to the perfect hardware assumptions, and upon imposition of the required self-interference power constraint, the SIC is assumed to be perfect. In the simulations, the generalized approach in [74, 75] is evaluated by once assuming a high self-interference power threshold, i.e., $P_{\text{th}} = P_{\text{r,max}}$, denoted as '$P_{\text{th}}$-High', and once assuming a low self-interference power threshold, i.e., $P_{\text{th}} = 0.01 \times P_{\text{r,max}}$, denoted as '$P_{\text{th}}$-Low'[10]. Moreover, the proposed approach in [172] is evaluated as a sub-optimal solution, where a power adjustment method is done at the relay, assuming MRC-MRT linear filters. The performance of an AF-FD relay with perfect hardware, i.e., $\kappa = 0$, is also illustrated as 'FD-Perf.'.

Decoding gain

Other than the defined approaches for AF-FD relaying, it is interesting to evaluate the impact of decoding in the studied system. This is since in a DF relay, the discussed distortion loop is significantly alleviated as the decoding process eliminates the interdependency of the received residual interference to the relay transmit covariance.

Visualization

In Figs. 3.7 (a)-(f) the average communication rate, i.e., $\log_2(1 + \text{SDNR})$, is evaluated under various system parameters.

In Fig. 3.7 (a) the impact of the transceiver inaccuracy is depicted. It is observed that as $\kappa = \beta$ increase, the communication performance decreases for all methods. In this

[9] This approach is equivalent to ignoring the impact of SIC in the beamforming design.

[10] Note that the application of $P_{\text{th}} = 0$, and $P_{\text{th}} = \infty$ are not feasible in this scenario. This is due to the fact that $P_{\text{th}} = 0$ strictly requires that $M_{\text{t}} > M_{\text{r}}$, and the $P_{\text{th}} = \infty$ often results in a non-stable relay function due to the impact of distortion. Nevertheless, the chosen scenarios 'P_{th}-High' and 'P_{th}-Low' closely capture the nature of the aforementioned designs.

respect, the HD setup remains more robust against the hardware distortions, and outperforms the FD setup for large values of $\kappa = \beta$. This is since the strong self-interference channel, as the main cause of distortion, is not present for a HD setup. Relative to the benchmark performance for the AF-FD relaying (GP), a significant decoding gain is observed for the big values of κ, where the system performance is dominated by the impact of distortion loop, see Subsection 3.2.4. Moreover, it is observed that the proposed AltMuStR1 method performs close to the GP method for different values of κ. The performance of 'P_{th}-High' reaches close to optimality for a small κ, where the 'P_{th}-Low' reaches a relatively better performance as κ increases. Nevertheless, both of the aforementioned methods degrade rapidly for higher values of κ. This is expected, as the impacts of hardware inaccuracies are not taken into account in the aforementioned approaches.

In Fig. 3.7 (b) and (c), the opposite impact of the thermal noise variance $\sigma_{\text{n}}^2 = \sigma_{\text{nr}}^2 = \sigma_{\text{nd}}^2$ and the maximum transmit power $P_{\max} = P_{\text{s,max}} = P_{\text{r,max}}$ is observed on the average system performance. This is expected, as an increase (decrease) in $P_{\max}$ (σ_{n}^2) increases the signal-to-noise ratio, while keeping the signal-to-distortion ratio intact. Furthermore, it is observed that in a low noise (high power) region the performance of the methods with perfect hardware assumptions saturate. This is since the role of hardware distortions become dominant for a high power or a low noise system.

In Fig. 3.7 (d), the resulting system performance is depicted with respect to the number of antennas. It is observed that the performance of all methods increase as the number of antennas increase. Moreover, the performance of the proposed (Alt)MuStR1 methods remain close to the benchmark GP performance. This is promising, considering the increasing computational complexity of the GP method as the number of antennas increases.

In Fig. 3.7 (e), the impact of the relay position is observed. In this regard, it is assumed that the source is located with the distance d_{sr} from the relay where the relay is located with the distance $d_{\text{rd}} = 20 - d_{\text{sr}}$ from the source. The path loss value for each link is then obtained as $\rho_X = \frac{0.1}{d_X^2}$, $X \in \{\text{sr}, \text{rd}\}$. As expected, the decoding gain decreases when the relay is positioned close to the source or destination. Interestingly, the performance of the (Alt)MuStR1 methods are slightly outperformed by 'P_{th}-High', when relay is positioned very close to the source. The reason is that in such a situation the bottleneck shifts to the relay-destination path as the source-relay channel is very strong and is not degraded by the impact of distortion from the self-interference path. Nevertheless, the distortion awareness in (Alt)MuStR1 destructively limits the performance of the relay-destination path in order to avoid distortion on the relay receiver. It is worth mentioning that this mismatch does not appear for the GP method, where the end-to-end SDNR is considered as the optimization objective.

In Fig. 3.7 (f), the impact of the self-interference channel intensity is depicted. It is observed that the performance of the FD relay operation, for all design methods, degrades as the ρ_{rr} increase while the performance of the HD method is not changed.

As expected, the performance of the methods with perfect hardware assumptions degrades faster compared to the proposed methods. Moreover, the performance of the proposed AltMuStR1 method remains close to that of GP for different values of the self-interference channel intensity. It is observed that the MRC-MRT method suffers from a rapid degradation, when κ or ρ_{rr} increases, also see Fig. 3.7 (a). This is expected, since the transmit and receive filters are designed with no consideration of the impact of distortion, e.g., the instantaneous CSI regarding the self-interference channel is not effectively used to control the impact of distortion.

3.8 Conclusion

The impact of hardware inaccuracies is of particular importance for an FD transceiver, due to the high strength of the SI channel. In particular, for an AF-FD relaying system such impact is significant due to the inter-dependency of the relay transmit covariance and the residual self-interference covariance, which results in a distortion loop effect. In this chapter, the aforementioned effect is analytically observed and optimization strategies are proposed to alleviate the resulting degradation. It is observed that the proposed GP algorithm can be considered as the performance benchmark, though, imposing a high computational complexity. On the other hand, the proposed (Alt)MuStR1 methods provide a significant reduction in the complexity at the expense of a slightly lower performance. In particular, the comparison to the available schemes in the literature reveals that for a system with a small thermal noise variance or a high transceiver inaccuracy the application of a distortion-aware design is essential. Moreover, it is observed that a DF-FD relay is more robust against the increase of hardware distortions, compared to an AF-FD relay. This is expected, since the observed distortion loop for AF-FD relays does not exist for a DF-FD relay due to decoding.

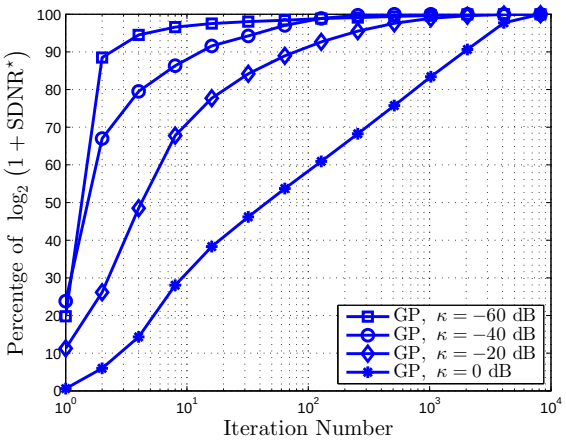

(a) Convergence-GP

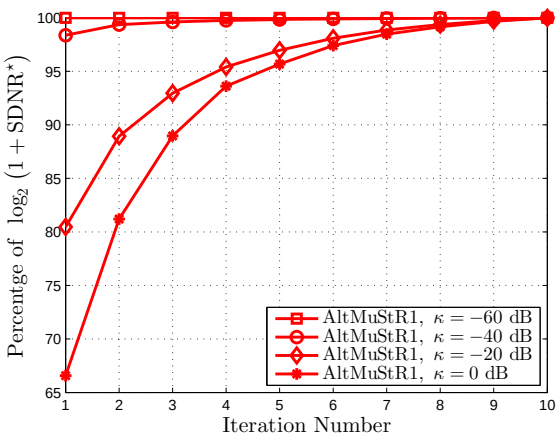

(b) Convergence-AltMuStR1

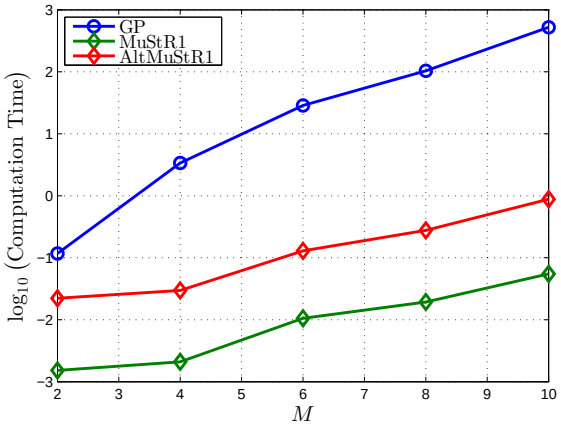

(c) CPU Time

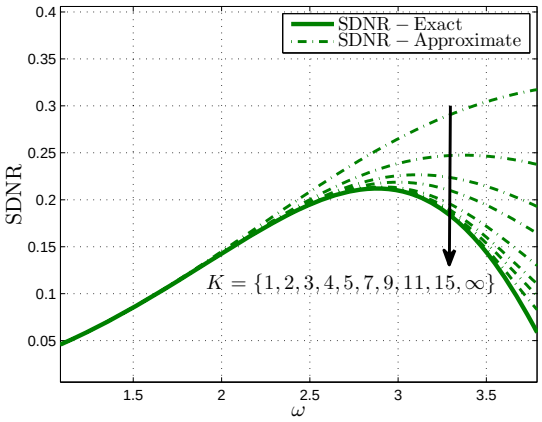

(d) SDNR Approximation

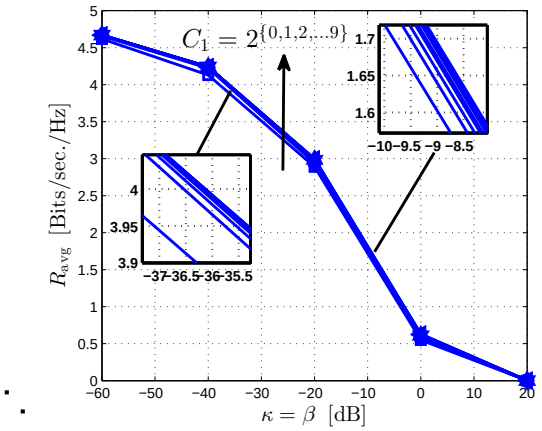

(e) GP-Initialization

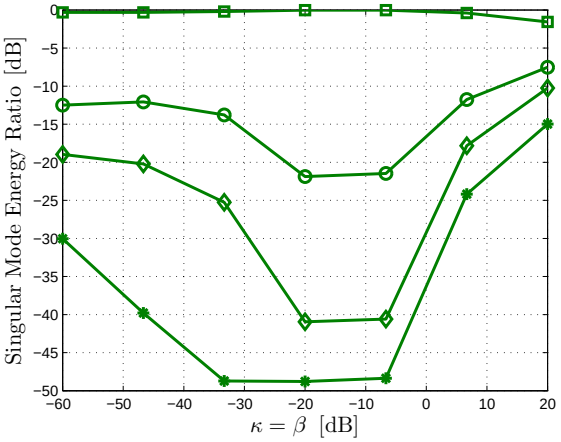

(f) Singular energy distribution

Figure 3.6: Numerical algorithm analysis including the average convergence behavior of the proposed GP algorithm (a), the AltMuStR1 algorithm (b), a comparison on computational complexity (c), accuracy of the SDNR approximation (d), impact of algorithm initialization on the GP method (e) and the singular mode energy profile for the obtained $\mathbf{W}$ from the GP method (f).

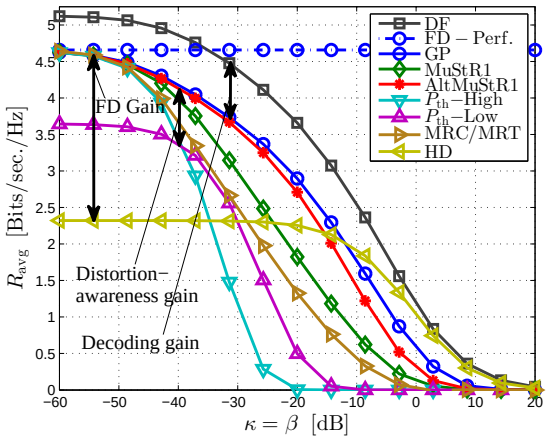

(a) R_{avg} vs. Distortion

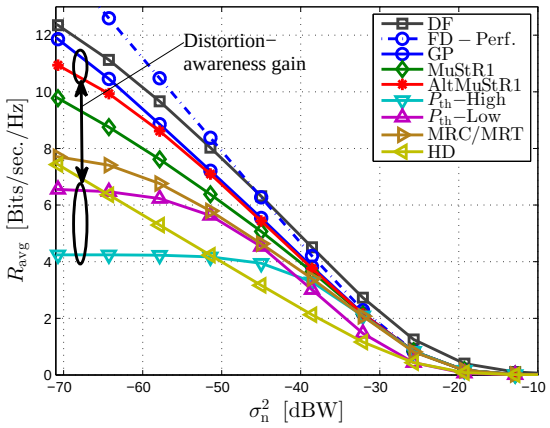

(b) R_{avg} vs. Noise

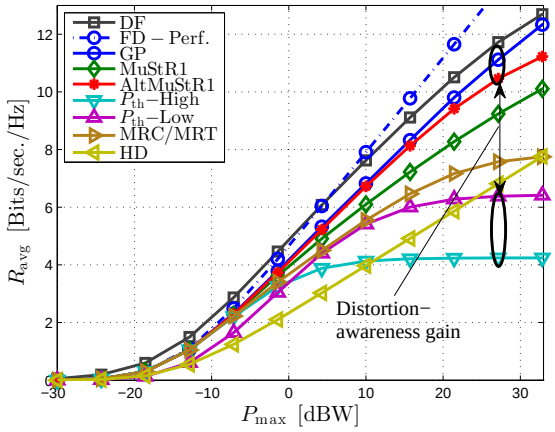

(c) R_{avg} vs. Max. Tx power

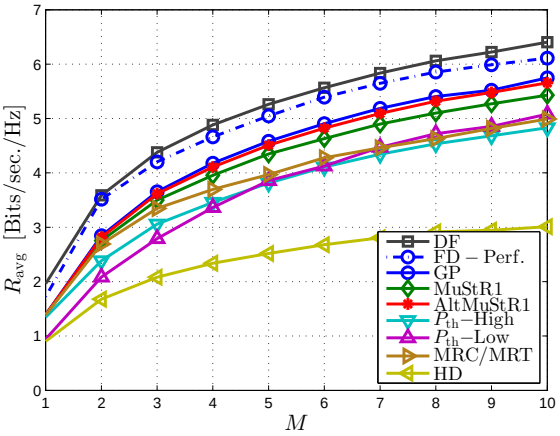

(d) R_{avg} vs. M

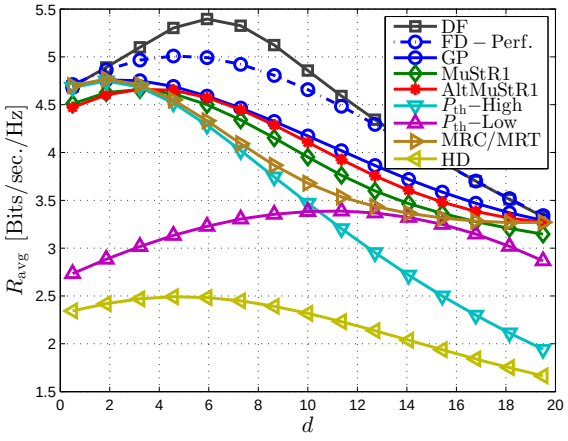

(e) R_{avg} vs. Relay position

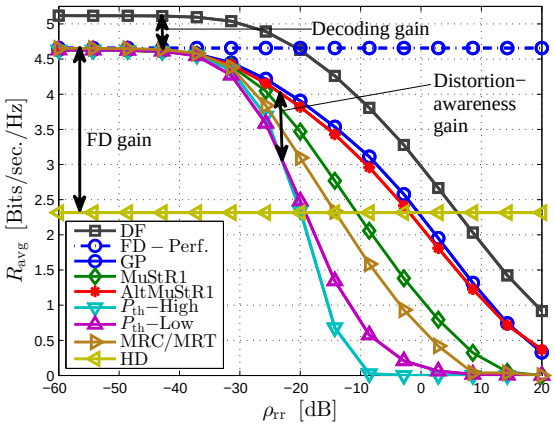

(f) R_{avg} vs. ρ_{rr}

Figure 3.7: The comparison of average system performance R_{avg} under different parameter ranges.

4 Secrecy Energy Efficiency of an FD MIMOME Wiretap Channel: Does FD Jamming Reduce the Energy-Cost of a Secure Bit?

4.1 Scope

The information security of wireless communication systems is currently provided via cryptographic approaches at the upper layers of the protocol stack. However, these approaches are vulnerable to the ever-increasing computational capability of the digital processors, and suffer due to the issues regarding management and distribution of secret keys [102, 173]. Alternatively, physical layer security takes advantage of physical characteristics of the communication medium in order to provide a secure data exchange between the information transmitter (Alice) and the legitimate receiver (Bob). In the seminal work by Wyner [174], the concept of secrecy capacity is introduced for a three-node degraded wiretap channel, as the maximum information rate that can be exchanged under perfect secrecy condition. It is shown that a positive secrecy capacity is achievable when the physical channel to the eavesdropper is weaker in comparison to the channel to the legitimate receiver. The arguments of [174] have since been extended in the directions of secrecy rate region analysis for various wiretap channel models [175–177], construction of capacity achieving channel codes [178–180], as well as signal processing techniques for enhancing the secrecy capacity of wireless communication systems, see [181–185] and references therein.

As a promising method to enhance the secrecy capacity of wireless systems, Goel and Negi [182] have introduced the idea of friendly jamming, i.e., the transmission of AN with the intention of degrading the decoding capability of the eavesdropper. This can be implemented via *i)* the joint transmission of information and AN from Alice, however, requiring an effective beamforming capability at Alice and sharing the communication and jamming resources [181, 182], *ii)* utilization of external (cooperative) jammers, nonetheless, resulting in the issues of jammer mobility, synchronization, and trustworthiness [176, 183–185], and *iii)* via the application of FD transceivers [102]. An FD

transceiver is capable of transmission and reception at the same time and frequency. Hence, an FD Bob can act as a friendly jammer, while simultaneously receiving information from Alice. Note that an FD jammer does not occupy the communication resources from Alice, nor does it rely on the external helpers, resolving the related drawbacks. The problems regarding secrecy rate region analysis and resource optimization have been hence addressed in [99, 102, 114, 186–188]. It is observed that a significant gain is achievable, in terms of the resulting secrecy capacity, via the utilization of an FD jamming strategy under the condition that the SI signal can be attenuated effectively.

Although the available literature introduces a gainful utilization of FD transceivers for enhancing the system secrecy capacity, the aforementioned gain comes at the expense of a higher power consumption due to *i)* the degrading impact of RSI on the desired communication link *ii)* the implementation of an SIC scheme at the FD transceiver, incurring additional digital processing and analog circuitry, as well as *iii)* the power consumed for the transmission of AN. As a result, it is not clear how the FD jamming-enabled systems perform in terms of the SEE. Note that the issue of energy efficiency is recently raised as a key criteria in the design of wireless communication systems. This is justified due to the exponential increase of the information and communication technology (ICT) services, currently generating around 5% of global CO_2 emissions and with 75% expected share of wireless systems in 2020, which calls for novel energy efficient ICT solutions [189, 190]. Hence, it is the main purpose of this chapter to investigate if and how the application of FD jammers can enhance the system's SEE, in terms of the secure bits per Joul (SBPJ).

4.1.1 Chapter outline and contributions

In this chapter we study a set of SEE maximization problems for a MIMOME wiretap channel, assuming the availability of perfect or statistical CSI, where Alice and an FD Bob are jointly capable of transmitting AN. The main contributions of this chapter are as follows:

- In contrast to the available designs [99, 186–188], utilizing FD transceivers for secrecy capacity enhancement, in Section 4.3, an SEE maximization problem is formulated. Due to the intractable structure, a successive general inner approximation (SUIAP) algorithm is proposed, with a guaranteed convergence to a point satisfying Karush-Kuhn-Tucker (KKT) conditions of optimality.
- The joint utilization of FD capability, both on Alice and Bob for jamming and bidirectional information exchange, shows additional potentials for the improvement of SEE. This is grounded on the fact that *i)* the FD jamming power is reused for both communication directions, resulting in a power-efficient jamming, and *ii)* the coexistence of two communication directions on the same channel may degrade Eve's decoding capability. Motivated by this, the proposed SUIAP algorithm is extended in Section 4.4 for an FD bidirectional setup.

- In order to account for the channel uncertainties, the consideration of statistical CSI regarding the channels to Eve has been introduced in [191] for maximizing system secrecy and in [192] for enhancing the system SEE, considering HD nodes. However, the aforementioned works limit the studied setups to a single antenna Eve, where CSI statistics follow a fast-fading nature. In this chapter an SEE maximization problem is studied for an FD-enabled MIMOME setup, where the channels to Eve follow an arbitrary statistical distribution. Note that unlike the fast-fading conditions, which assumes the CSI is not available due to mobility, the consideration of an arbitrary statistical distribution also accounts for the scenarios where Eve's condition is stationary, but the CSI can not be obtained due to the lack of collaboration from Eve. Hence, in Section 4.5, a successive selection and statistical lower bound maximization (SSSLM) algorithm is proposed, utilizing a combination of ensemble average approximation (SAA) [193], together with the successive lower bound approximation method [194], with the goal of maximizing the statistical average of SEE. The algorithm is proven to converge to a point satisfying KKT conditions. It is worth mentioning that the studied problem also subsumes the problem for the maximization of secrecy capacity under the same assumption set.

The numerical results show that the utilization of FD transceivers is able to provide a significant SEE gain for a system with a small distance between the FD node and the eavesdropper, a high SNR or for a bidirectional FD communication setup, under the condition that the SI can be effectively and efficiently mitigated. Contributions of this chapter are based on the works published or under consideration for publication in [114–117].

4.2 System Model

We consider a multiple-input multiple-output multiple-antenna eavesdropper (MIMOME) wiretap channel that consists of a legitimate transmitter, i.e., Alice, a legitimate receiver, i.e., Bob, and an eavesdropper, i.e., Eve, see Fig. 4.1. Alice and Eve are equipped with N_A transmit and M_E receive antennas, respectively. Bob is respectively equipped with N_B and M_B transmit and receive antennas and is capable of FD operation. Channels are assumed to follow a quasi-stationary and flat-fading model. In this regard, channels from Alice to Bob, Alice to Eve, and Bob to Eve (jamming channel) are respectively denoted as $\mathbf{H}_{ab} \in \mathbb{C}^{M_B \times N_A}$, $\mathbf{H}_{ae} \in \mathbb{C}^{M_E \times N_A}$, $\mathbf{H}_{be} \in \mathbb{C}^{M_E \times N_B}$. The channel from Bob to Bob, i.e., SI channel, is denoted as $\mathbf{H}_{bb} \in \mathbb{C}^{M_B \times N_B}$.

4.2.1 Signal model

The transmission from Alice includes the information-containing signal, intended for Bob, and an AN, intended to degrade the reception by Eve. This is expressed as

$$\mathbf{x}_a = \underbrace{\mathbf{q}_a + \mathbf{w}_a}_{\mathbf{u}_a} + \mathbf{e}_{\mathrm{tx},a}, \tag{4.1}$$

where $\mathbf{u}_a \in \mathbb{C}^{N_A}$ is the intended transmit signal, $\mathbf{q}_a \sim \mathcal{CN}(\mathbf{0}_{N_A}, \mathbf{Q}_a)$ and $\mathbf{w}_a \sim \mathcal{CN}(\mathbf{0}_{N_A}, \mathbf{W}_a)$ respectively represent the information-containing and AN signal, and $\mathbf{x}_a \in \mathbb{C}^{N_A}$ is the combined transmitted signal from Alice. The transmit distortion, denoted as $\mathbf{e}_{\mathrm{tx},a} \in \mathbb{C}^{N_A}$ models collective impact of transmit chain inaccuracies, similarly modeled as in Section 2.2. Note that the role of hardware inaccuracies becomes important in a system with FD transceivers, due to the impact of a strong SI channel. Similar to the transmission from Alice, the transmission of AN by Bob is expressed as

$$\mathbf{x}_b = \mathbf{w}_b + \mathbf{e}_{\mathrm{tx},b}, \tag{4.2}$$

where $\mathbf{w}_b \sim \mathcal{CN}(\mathbf{0}_{N_B}, \mathbf{W}_b)$ is the transmitted artificial noise and $\mathbf{e}_{\mathrm{tx},b} \in \mathbb{C}^{N_B}$ represents the transmit distortions from Bob. Via the application of (4.1) and (4.2) the received signal at Eve is expressed as

$$\mathbf{y}_e = \mathbf{H}_{ae}\mathbf{x}_a + \mathbf{H}_{be}\mathbf{x}_b + \mathbf{n}_e = \mathbf{H}_{ae}\mathbf{q}_a + \mathbf{c}_e, \tag{4.3}$$

where $\mathbf{n}_e \sim \mathcal{CN}\left(\mathbf{0}_{M_E}, \sigma^2_{\mathrm{n},e}\mathbf{I}_{M_E}\right)$ is the additive thermal noise and

$$\mathbf{c}_e := \mathbf{H}_{ae}\mathbf{w}_a + \mathbf{H}_{be}\mathbf{w}_b + \mathbf{H}_{ae}\mathbf{e}_{\mathrm{tx},a} + \mathbf{H}_{be}\mathbf{e}_{\mathrm{tx},b} + \mathbf{n}_e \tag{4.4}$$

is the collective interference-plus-noise at Eve.

Similarly, the received signal at Bob is formulated as

$$\mathbf{y}_b = \underbrace{\mathbf{H}_{ab}\mathbf{x}_a + \mathbf{H}_{bb}\mathbf{x}_b + \mathbf{n}_b}_{=:\mathbf{u}_b} + \mathbf{e}_{\mathrm{rx},b}, \tag{4.5}$$

where $\mathbf{n}_b \sim \mathcal{CN}\left(\mathbf{0}_{M_B}, \sigma^2_{\mathrm{n},b}\mathbf{I}_{M_B}\right)$ is the additive thermal noise, and $\mathbf{u}_b$ is the undistorted received signal. Similar to the transmit side, the receiver distortion, denoted as $\mathbf{e}_{\mathrm{rx},b} \in \mathbb{C}^{M_B}$, models the collective impact of receiver chain inaccuracies, similarly modeled as in Section 2.2. Note that $\mathbf{y}_b$ includes the received SI signal at Bob, originating from the same transceiver. Hence, the *known*, i.e., distortion-free, part of the SI signal can be subtracted applying an SIC method. The received signal at Bob, after the application of SIC is hence written as

$$\begin{aligned}\tilde{\mathbf{y}}_b &= \mathbf{y}_b - \mathbf{H}_{bb}\mathbf{w}_b \\ &= \mathbf{H}_{ab}\mathbf{x}_a + \mathbf{H}_{bb}\mathbf{e}_{\mathrm{tx},b} + \mathbf{e}_{\mathrm{rx},b} + \mathbf{n}_b = \mathbf{H}_{ab}\mathbf{q}_a + \mathbf{c}_b,\end{aligned} \tag{4.6}$$

where

$$\mathbf{c}_b := \mathbf{H}_{ab}\mathbf{w}_a + \mathbf{H}_{ab}\mathbf{e}_{\mathrm{tx},a} + \mathbf{H}_{bb}\mathbf{e}_{\mathrm{tx},b} + \mathbf{e}_{\mathrm{rx},b} + \mathbf{n}_b, \tag{4.7}$$

is the collective interference-plus-noise at Bob.

$$\mathbf{\Sigma}_b = \mathbb{E}\{\mathbf{c}_b\mathbf{c}_b^H\} = \mathbf{H}_{ab}\mathbf{W}_a\mathbf{H}_{ab}^H + \kappa_a\mathbf{H}_{ab}\mathrm{diag}\left(\mathbf{Q}_a + \mathbf{W}_a\right)\mathbf{H}_{ab}^H + \kappa_b\mathbf{H}_{bb}\mathrm{diag}\left(\mathbf{W}_b\right)\mathbf{H}_{bb}^H + \beta_b\mathrm{diag}\Big(\mathbf{H}_{ab}\left(\mathbf{Q}_a + \mathbf{W}_a\right)\mathbf{H}_{ab}^H + \mathbf{H}_{bb}\mathbf{W}_b\mathbf{H}_{bb}^H + \sigma_{\mathrm{n},b}^2\mathbf{I}_{M_B}\Big) + \sigma_{\mathrm{n},b}^2\mathbf{I}_{M_B}, \quad (4.8)$$

$$\mathbf{\Sigma}_e = \mathbb{E}\{\mathbf{c}_e\mathbf{c}_e^H\} = \mathbf{H}_{ae}\mathbf{W}_a\mathbf{H}_{ae}^H + \mathbf{H}_{be}\mathbf{W}_b\mathbf{H}_{be}^H + \kappa_a\mathbf{H}_{ae}\mathrm{diag}\left(\mathbf{Q}_a + \mathbf{W}_a\right)\mathbf{H}_{ae}^H + \kappa_b\mathbf{H}_{be}\mathrm{diag}\left(\mathbf{W}_b\right)\mathbf{H}_{be}^H + \sigma_{\mathrm{n},e}^2\mathbf{I}_{M_E}. \quad (4.9)$$

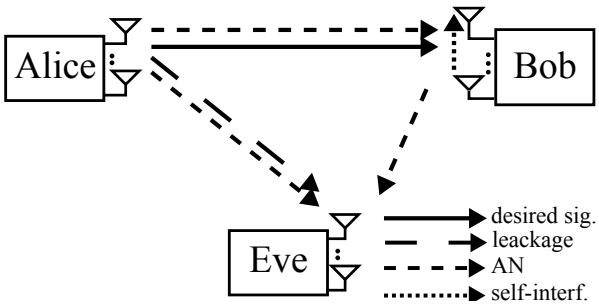

Figure 4.1: The studied wiretap channel. Alice and the FD-Bob are jointly enabled with jamming capability.

4.2.2 Distortion signal statistics

The impact of hardware elements inaccuracy in each chain can be modeled as additive and Gaussian-distributed independent distortion terms, see Section 2.2 for more elaboration. This is expressed in our system as

$$\mathbf{e}_{\mathrm{tx},a} \sim \mathcal{CN}\Big(\mathbf{0}_{N_A}, \kappa_a\mathrm{diag}\Big(\mathbb{E}\left\{\mathbf{u}_a\mathbf{u}_a^H\right\}\Big)\Big), \quad \mathbf{e}_{\mathrm{tx},a}\perp\mathbf{u}_a, \quad (4.10)$$

$$\mathbf{e}_{\mathrm{tx},b} \sim \mathcal{CN}\Big(\mathbf{0}_{N_B}, \kappa_b\mathrm{diag}\Big(\mathbb{E}\left\{\mathbf{w}_b\mathbf{w}_b^H\right\}\Big)\Big), \quad \mathbf{e}_{\mathrm{tx},b}\perp\mathbf{w}_b, \quad (4.11)$$

$$\mathbf{e}_{\mathrm{rx},b} \sim \mathcal{CN}\Big(\mathbf{0}_{M_B}, \beta_b\mathrm{diag}\Big(\mathbb{E}\left\{\mathbf{u}_b\mathbf{u}_b^H\right\}\Big)\Big), \quad \mathbf{e}_{\mathrm{rx},b}\perp\mathbf{u}_b, \quad (4.12)$$

where $\kappa_a, \kappa_b, \beta_b \in \mathbb{R}^+$ are distortion coefficients, relating the variance of the distortion terms to the intended signal power, and $\mathbf{u}_a$ and $\mathbf{u}_b$ are defined in (4.1) and (4.5), respectively. For further elaborations on the used distortion model please see [32,78–80], and the references therein.

4.2.3 Power consumption model

The consumed power of a wireless transceiver can be segmented into three parts. First, the power consumed at the PA, which is related to the effective transmit power via PA efficiency, see [195, Eq. (2)]. Secondly, the zero-state power, i.e., the power consumed

by other circuit blocks, independent from transmission status[1], see [195, Eq. (3)]. And finally, the power consumed for the implementation of an SIC scheme, for enabling FD operation. The aforementioned power varies for different SIC methods, and by definition, is not relevant for HD transceivers.

The consumed power for Alice and Bob can be hence expressed as

$$P_A = \frac{1}{\mu_A}\mathbb{E}\left\{\|\mathbf{x}_a\|_2^2\right\} + P_{A,0}, \quad P_A \leq P_{A,\max} \tag{4.13}$$

and

$$P_B = \frac{1}{\mu_B}\mathbb{E}\left\{\|\mathbf{x}_b\|_2^2\right\} + P_{B,0} + P_{\mathrm{FD}}, \quad P_B \leq P_{B,\max}. \tag{4.14}$$

In the above arguments, $P_{\mathcal{X}}, P_{\mathcal{X},0}, \mu_{\mathcal{X}}$, and $P_{\mathcal{X},\max}$, where $\mathcal{X} \in \{A, B\}$, respectively represent the consumed power, the zero-state power, PA efficiency, and the maximum allowed power consumption for each node. The additional required power for the implementation of an SIC scheme is denoted by P_{FD}. From (4.13), (4.14), the total system power consumption is obtained as

$$P_{\mathrm{tot}} = P_A + P_B. \tag{4.15}$$

4.2.4 Secrecy energy efficiency

Following [102, 177, 182], the achievable secrecy rate[2] for Alice-Bob communication is expressed as $C_{ab} = \left\{\tilde{C}_{ab}\right\}^+$, such that

$$\tilde{C}_{ab} = \log\left|\mathbf{I} + \mathbf{H}_{ab}\mathbf{Q}_a\mathbf{H}_{ab}^H\boldsymbol{\Sigma}_b^{-1}\right| - \log\left|\mathbf{I} + \mathbf{H}_{ae}\mathbf{Q}_a\mathbf{H}_{ae}^H\boldsymbol{\Sigma}_e^{-1}\right|, \tag{4.16}$$

where $\boldsymbol{\Sigma}_b$, $\boldsymbol{\Sigma}_e$ are given in (4.8), (4.9), and represent the covariance of the interference-plus-noise terms at Bob and Eve, respectively. The secrecy energy efficiency (SEE), as a measure of securely communicated information per energy unit, is consequently expressed as

$$\mathrm{SEE} = \frac{C_{ab}}{P_{\mathrm{tot}}}. \tag{4.17}$$

It is the intention of the remaining parts of this chapter to improve the efficiency of the defined wiretap channel, in terms of the SEE, and provide comparison to the usual HD strategies.

[1] This includes, e.g., the power consumed at receiver chain, and for base band processing.

[2] The system secrecy capacity is lower bounded by all achievable secrecy rates resulting from different choices of transmit covariance matrices, see [177, Theorem 1], [182, Equation (6)].

$$\tilde{\mathrm{SEE}}_p\left(\mathbb{Q}^{[k,l]},\mathbb{Q}^{[0,l]},\lambda^{[k,l]}\right)=\log\left|\mathbf{\Sigma}_b^{[k,l]}+\mathbf{H}_{ab}\mathbf{Q}_a^{[k,l]}\mathbf{H}_{ab}^H\right|-\log\left|\mathbf{\Sigma}_b^{[0,l]}\right|+\mathrm{tr}\left(\left(\mathbf{\Sigma}_b^{[0,l]}\right)^{-1}\left(\mathbf{\Sigma}_b^{[0,l]}-\mathbf{\Sigma}_b^{[k,l]}\right)\right)$$
$$+\log\left|\mathbf{\Sigma}_e^{[k,l]}\right|-\log\left|\mathbf{\Sigma}_e^{[0,l]}+\mathbf{H}_{ae}\mathbf{Q}_a^{[0,l]}\mathbf{H}_{ae}^H\right|+\mathrm{tr}\Big(\left(\mathbf{\Sigma}_e^{[0,l]}+\mathbf{H}_{ae}\mathbf{Q}_a^{[0,l]}\mathbf{H}_{ae}^H\right)^{-1}\Big(\mathbf{\Sigma}_e^{[0,l]}-\mathbf{\Sigma}_e^{[k,l]}+\mathbf{H}_{ae}\Big(\mathbf{Q}_a^{[0,l]}$$
$$-\mathbf{Q}_a^{[k,l]}\Big)\mathbf{H}_{ae}^H\Big)\Big)-\lambda^{[k,l]}\left(\frac{1+\kappa_a}{\mu_a}\mathrm{tr}\left(\mathbf{Q}_a^{[k,l]}+\mathbf{W}_a^{[k,l]}\right)+\frac{1+\kappa_b}{\mu_b}\mathrm{tr}\left(\mathbf{W}_b^{[k,l]}\right)+P_{A,0}+P_{B,0}+P_{\mathrm{FD}}\right) \tag{4.18}$$

4.2.5 Remarks

- In this part we have assumed the availability of the perfect CSI for all channels. However, it may be difficult to estimate the channels associated to Eve, due to mobility, or the lack of collaboration from Eve. The scenario with the availability of partial CSI is discussed in Section 4.5.
- Unlike the data symbols, which follow a known constellation, the AN is generated from a psedu-random sequence which is not known to the receivers, see [182, Section III]. This is to prevent Eve from decoding the AN.

4.3 Secrecy Energy Efficiency Maximization

In this part we intend to enhance the system SEE, assuming the availability of CSI for all channels. In particular, we look for an optimized information transmit covariance from Alice, i.e., $\mathbf{Q}_a$, and jamming transmit covariances from Alice and Bob, i.e., respectively, $\mathbf{W}_a$ and $\mathbf{W}_b$, with the goal of maximizing the resulting system SEE. The corresponding optimization problem is defined as

$$\max_{\mathbf{Q}_a,\mathbf{W}_a,\mathbf{W}_b}\quad \mathrm{SEE}\left(\mathbf{Q}_a,\mathbf{W}_a,\mathbf{W}_b\right) \tag{4.19a}$$
$$\text{s.t.}\quad \frac{1+\kappa_a}{\mu_a}\mathrm{tr}\left(\mathbf{Q}_a+\mathbf{W}_a\right)+P_{A,0}\leq P_{A,\max}, \tag{4.19b}$$
$$\frac{1+\kappa_b}{\mu_b}\mathrm{tr}\left(\mathbf{W}_b\right)+P_{B,0}+P_{\mathrm{FD}}\leq P_{B,\max}, \tag{4.19c}$$
$$\mathbf{Q}_a,\mathbf{W}_a,\mathbf{W}_b\in\mathcal{H}, \tag{4.19d}$$

where (4.19b) and (4.19c) represent the power constraints at Alice and Bob. The defined problem in (4.19) is not tractable in the current form, due to the non-convex and non-smooth objective. In order to obtain a tractable structure, without loss of optimality, we remove the non-linear operator $\{\}^+$ from the definition of SEE[3]. The modified SEE,

[3]Note that at the optimality of (4.19), the resulting C_{s}, and consequently the SEE is non-negative. This is since a non-negative SEE is immediately obtained by setting $\mathbf{Q}_a=\mathbf{0}$, see [102, 192] for similar arguments.

named SEE_p hereinafter, can hence be formulated as

$$\mathrm{SEE}_p\left(\mathbf{Q}_a, \mathbf{W}_a, \mathbf{W}_b\right) = \frac{\Sigma_{\mathcal{X}\in\{b,e\}}\alpha_{\mathcal{X}}\left(\log\left|\mathbf{\Sigma}_{\mathcal{X}} + \mathbf{H}_{a\mathcal{X}}\mathbf{Q}_a\mathbf{H}_{a\mathcal{X}}^H\right| - \log\left|\mathbf{\Sigma}_{\mathcal{X}}\right|\right)}{P_{\mathrm{tot}}\left(\mathbf{Q}_a, \mathbf{W}_a, \mathbf{W}_b\right)}, \tag{4.20}$$

where $\alpha_b = 1$ and $\alpha_e = -1$. It is observed that SEE_p is a difference of concave (DC) over affine fractional function which is intractable in the current form. In the following, we propose a successive general inner approximation algorithm (SUIAP) to obtain an optimal solution to (4.19).

4.3.1 SUIAP algorithm

The proposed SUIAP algorithm consists of two nested loops. In each outer iteration, an effective lower bound to SEE_p is constructed following the successive inner approximation (SIA) method [196], applying the inequality

$$-\log\left|\mathbf{X}\right| \geq -\log\left|\mathbf{Y}\right| + \mathrm{tr}\left(\mathbf{Y}^{-1}\left(\mathbf{Y}-\mathbf{X}\right)\right) \tag{4.21}$$

as the first-order Taylor approximation of the convex terms $-\log|\cdot|$ in (4.20) at the point $\mathbf{Y}$. Please note that via the elimination of the convex terms from the numerator, the proposed lower bound holds a concave over affine fractional structure, which is a psedu-concave function [197]. Hence, in the inner loop, the well-known Dinkelbach's algorithm [198] can be applied to iteratively maximize the obtained lower bound. The proposed SUIAP algorithm, for the lth outer iteration and kth inner iteration is hence formulated as

$$\max_{\mathbb{Q}^{[k,l]}} \quad \tilde{\mathrm{SEE}}_p\left(\mathbb{Q}^{[k,l]}, \mathbb{Q}^{[0,l]}, \lambda^{[k,l]}\right) \tag{4.22a}$$

$$\text{s.t.} \quad \text{(4.19b), (4.19c), (4.19d),} \tag{4.22b}$$

where $\mathbb{Q} := \{\mathbf{Q}_a, \mathbf{W}_a, \mathbf{W}_b\}$, $\tilde{\mathrm{SEE}}_p$ is defined in (4.18), λ is an auxiliary variable, and $\mathbf{\Sigma}_b^{[k,l]}, \mathbf{\Sigma}_e^{[k,l]}$ are calculated from (4.8), (4.9) at the iteration instance represented by k, l.

It is observed that $\tilde{\mathrm{SEE}}_p$ is a jointly concave function over $\mathbf{Q}_a^{[k,l]}, \mathbf{W}_a^{[k,l]}, \mathbf{W}_b^{[k,l]}$ for a fixed $\lambda^{[k,l]}$. In particular, the maximization over $\mathbb{Q}^{[k,l]}$ is efficiently implemented via the MAX-DET algorithm, see [158]. Afterwards, in each inner algorithm iteration, the value of $\lambda^{[k,l]}$ is uniquely updated by solving the identity

$$\tilde{\mathrm{SEE}}_p\left(\mathbb{Q}^{[k,l]}, \mathbb{Q}^{[0,l]}, \lambda^{[k,l]}\right) = 0, \tag{4.23}$$

see [199, Subsection 3.2], [198] for more elaboration regarding the Dinkelbach's algorithm. The defined algorithm steps, both outer and inner loop iterations, are continued until a jointly stable point is obtained, see Algorithm 8 for more details.

4.3.2 Convergence

It is observed that the proposed steps in the inner loop lead to a necessary convergence, due to the monotonically increasing update of λ and the fact that a feasible value of λ is bounded from above. Moreover, it is proven in [199, Proposition 3.2] that for the studied concave-over-affine fractional structure, the converging point of the Dinkelbach's algorithm is indeed the global optimum point. The global optimality result of the inner loop iterations also results in a necessary convergence in the outer loop, by ensuring a monotonic improvement. Please note that the obtained lower bound via the utilization of (4.21) is a tight and global lower bound to SEE_p. Moreover, it shares the same slope as the SEE_p function at the point of approximation. The aforementioned properties, and the fact that inner iterations are solved to the optimality, results in the convergence of the outer loop iterations to a point satisfying the KKT conditions of the original problem, see [196, Theorem 1]. However, the converging KKT point of the original problem is not necessarily the global optimum. This optimality gap is numerically analyzed in Section 4.6 by examining multiple initializations.

4.3.3 Initialization

In order to obtain an efficient initialization we separate the design of spatial beams and power allocation for different transmissions, thereby obtaining a low-complexity but sub-optimal solution. In the first step the spatial beams are designed to maximize the ratio of the desired received power, to the distortion-plus-leakage power. Afterwards, the transmitted power is adjusted for each transmission, with the goal of maximizing the resulting SEE. The detailed initialization procedure is given in [200].

4.3.4 Computational complexity

Each outer iteration consists of the calculation of $\mathbf{\Sigma}_b^{[0,l]}$ and $\mathbf{\Sigma}_e^{[0,l]} + \mathbf{H}_{ae}\mathbf{Q}_a^{[0,l]}\mathbf{H}_{ae}^H$ via (4.8), (4.9), and the inverse terms via Cholesky decomposition incurring in total

$$\mathcal{O}\Big(\gamma_{\text{out}}\Big(M_E^3 + M_B^3 + N_A M_B\left(4M_B + N_A\right) + 5N_A M_E(N_A + M_E) + N_B M_B\left(2N_B + 4M_B\right) + 4N_B M_E\left(M_E + N_B\right)\Big)\Big)$$

arithmetic operations [201], where γ_{in} (γ_{out}) is the total number of the required inner (outer) iterations until convergence. However, the computational complexity of the algorithm is dominated by the steps of the determinant maximization in the inner loop, see Algorithm 8, Step 8. A general form of a MAX-DET problem is defined as

$$\min_{\mathbf{z}} \ \mathbf{p}^T\mathbf{z} + \log\left|\mathbf{Y}(\mathbf{z})^{-1}\right|, \ \text{ s.t. } \ \mathbf{Y}(\mathbf{z}) \succ 0, \ \mathbf{F}(\mathbf{z}) \succeq 0, \tag{4.24}$$

where $\mathbf{z} \in \mathbb{R}^n$, and $\mathbf{Y}(\mathbf{z}) \in \mathbb{R}^{n_Y \times n_Y} := \mathbf{Y}_0 + \sum_{i=1}^{n} z_i \mathbf{Y}_i$ and $\mathbf{F}(\mathbf{z}) \in \mathbb{R}^{n_F \times n_F} := \mathbf{F}_0 + \sum_{i=1}^{n} z_i \mathbf{F}_i$. An upper bound to the computational complexity of the above problem is given as

$$\mathcal{O}\Big(\gamma_{\text{in}} \sqrt{n} \big(n^2 + n_Y^2\big) n_F^2\Big), \tag{4.25}$$

see [158, Section 10]. In our problem $n = 2N_A^2 + N_B^2$ representing the dimension of real valued scalar variable space, and $n_Y = 2M_B + 2M_E$ and $n_F = 2N_B + 4N_A + 2$, representing the dimension of the determinant operation and the constraints space, respectively.

Remark

The above analysis intends to show how the bounds on computational complexity are related to different problem dimensions. Nevertheless, the computational load may vary in practice, depending on the implementation and the used numerical solver. Furthermore, the overall algorithm complexity also depends on the number of optimization iterations required to obtain convergence. Please see Section 4.6 for a numerical analysis on the convergence behavior, as well as the algorithm computational complexity.

Algorithm 8 Successive inner approximation algorithm (SUIAP) for SEE maximization. $C_{\min}$ ($\lambda_{\min}$) represents the convergence threshold for the outer (inner) iterations.

$l, k \leftarrow 0$;
$\lambda^{[0,0]} \leftarrow \mathbf{0}, \mathbb{Q}^{[0,0]} \leftarrow$ Subsection 4.3.3; ▷ initialization
repeat ▷ outer loop
  $l \leftarrow l + 1$; $\lambda^{[0,l]} \leftarrow \lambda^{[k,l-1]}$; $\mathbb{Q}^{[0,l]} \leftarrow \mathbb{Q}^{[k,l-1]}$;
  $k \leftarrow 0$,
  repeat ▷ inner loop (Dinkelbach alg.)
    $k \leftarrow k + 1$;
    $\mathbb{Q}^{[k,l]} \leftarrow$ MAX-DET [158], see (4.22);
    $C \leftarrow \tilde{\text{SEE}}_p\left(\mathbb{Q}^{[k,l]}, \mathbb{Q}^{[0,l]}, \lambda^{[k-1,l]}\right)$; $\lambda^{[k,l]} \leftarrow$ (4.23);
  until $C \leq C_{\min}$
until $\lambda^{[k,l]} - \lambda^{[0,l]} \leq \lambda_{\min}$
return $\left\{\mathbb{Q}^{[k,l]}, \lambda^{[k-1,l]}\right\}$

4.4 Secure Bidirectional Communication: Joint Full-Duplex Operation at Alice and Bob

In this part we study the case that a bidirectional communication is established between Alice and Bob, where both Alice and Bob are enabled with FD capability. An FD bidirectional setup is interesting as it enables the usage of the same channel for both communication directions, and leads to a higher spectral efficiency [32]. Moreover, the jamming power at both Alice and Bob can be reused to improve security at both

directions[4] and potentially improve the resulting SEE. However, the coexistence of the multiple signal transmissions on a single channel results in a higher number of interference paths, which calls for a smart design regarding the signal and jamming transmit strategies at Alice and Bob.

In order to update the defined setup to a bidirectional one, we denote the number of receive antennas, and the self-interference channel at Alice as M_A, $\mathbf{H}_{aa}$, respectively. Moreover, we denote that the data transmission from Bob as $\mathbf{q}_b \sim \mathcal{CN}(\mathbf{0}_{N_B}, \mathbf{Q}_b)$. Following the same signal model for the transmission of data and jamming signals as in (4.1) - (4.12), the received interference-plus-noise covariance matrix at Bob and Eve are updated respectively as

$$\mathbf{\Sigma}_b^{\mathrm{BD}} = \mathbf{\Sigma}_b + \kappa_b \mathbf{H}_{bb} \mathrm{diag}\left(\mathbf{Q}_b\right) \mathbf{H}_{bb}^H + \beta_b \mathrm{diag}\left(\mathbf{H}_{bb} \mathbf{Q}_b \mathbf{H}_{bb}^H\right), \tag{4.26}$$

$$\mathbf{\Sigma}_e^{\mathrm{BD}} = \mathbf{\Sigma}_e + \kappa_b \mathbf{H}_{be} \mathrm{diag}\left(\mathbf{Q}_b\right) \mathbf{H}_{be}^H, \tag{4.27}$$

where $\mathbf{\Sigma}_b, \mathbf{\Sigma}_e$ are given from (4.8), (4.9). Please note that in the formulation of (4.27) we consider a worst-case scenario where the interference on Eve, due to the transmission of data signals, i.e., $\mathbf{q}_a$ and $\mathbf{q}_b$, can be decoded [202]. Similarly, the received interference-plus-noise signal covariance at Alice is written as

$$\begin{aligned}\mathbf{\Sigma}_a^{\mathrm{BD}} &= \mathbf{H}_{ba} \mathbf{W}_b \mathbf{H}_{ba}^H + \sigma_{\mathrm{n},a}^2 \mathbf{I}_{M_A} + \kappa_b \mathbf{H}_{ba} \mathrm{diag}\left(\mathbf{Q}_b + \mathbf{W}_b\right) \mathbf{H}_{ba}^H + \kappa_a \mathbf{H}_{aa} \mathrm{diag}\left(\mathbf{W}_a + \mathbf{Q}_a\right) \mathbf{H}_{aa}^H \\ &+ \beta_a \mathrm{diag}\Big(\mathbf{H}_{ba}\left(\mathbf{Q}_b + \mathbf{W}_b\right) \mathbf{H}_{ba}^H + \mathbf{H}_{aa}\left(\mathbf{W}_a + \mathbf{Q}_a\right) \mathbf{H}_{aa}^H + \sigma_{\mathrm{n},a}^2 \mathbf{I}_{M_A}\Big),\end{aligned} \tag{4.28}$$

where $\beta_a \in \mathbb{R}^+$ is the distortion coefficient for the reception at Alice, and $\sigma_{\mathrm{n},a}^2$ represents the thermal noise variance at Alice. The SEE for the defined BD system is then obtained as

$$\mathrm{SEE}^{\mathrm{BD}} = \frac{\left\{\tilde{C}_{ab}\right\}^+ + \left\{\tilde{C}_{ba}\right\}^+}{P_{\mathrm{tot}}}, \tag{4.29}$$

where $\tilde{C}_{ab}$ is obtained by applying (4.26), (4.27) into (4.17), and

$$\tilde{C}_{ba} = \log\left|\mathbf{I} + \mathbf{H}_{ba} \mathbf{Q}_b \mathbf{H}_{ba}^H \left(\mathbf{\Sigma}_a^{\mathrm{BD}}\right)^{-1}\right| - \log\left|\mathbf{I} + \mathbf{H}_{be} \mathbf{Q}_b \mathbf{H}_{be}^H \left(\mathbf{\Sigma}_e^{\mathrm{BD}}\right)^{-1}\right|, \tag{4.30}$$

is defined similar to (4.16) but for the opposite direction.

Lemma 4.4.1. *The values $\tilde{C}_{ab}$ and $\tilde{C}_{ba}$ in the numerator of (4.29) are non-negative for an optimal choice of $\mathbf{Q}_a, \mathbf{Q}_b$, under some mild practical assumptions.*

Proof. The proof is obtained via contradiction, assuming that an optimal choice of $\mathbf{Q}_a$ results in a negative $\tilde{C}_{ab}$[5]. A feasible, non-negative value of $\tilde{C}_{ab}$ can be obtained

[4] This is since the jamming sent to Eve from each single node degrades Eves reception quality from both communication directions.

[5] The proof for $\mathbf{Q}_b$, $\tilde{C}_{ba}$ for the opposite direction can be obtained similarly.

by setting $\mathbf{Q}_a = \mathbf{0}$. Note that this choice reduces the residual self-interference terms, i.e., $\kappa_a \mathbf{H}_{aa} \text{diag}(\mathbf{Q}_a) \mathbf{H}_{aa}^H + \beta_a \text{diag}\left(\mathbf{H}_{aa}\mathbf{Q}_a\mathbf{H}_{aa}^H\right)$, which impacts $\tilde{C}_{ba}$ positively. Conversely, it eliminates the received distortion terms at Eve, i.e., $\kappa_a \mathbf{H}_{ae} \text{diag}(\mathbf{Q}_a) \mathbf{H}_{ae}^H$, hence impacting $\tilde{C}_{ba}$ in the degrading direction. However, this degradation is negligible considering $\kappa_a \ll 1$, and $\|\mathbf{H}_{ae}\|_F \ll \|\mathbf{H}_{aa}\|_F$ which are common assumptions for any practical implementation of an FD transceiver[6]. This concludes that a non-negative value of $\tilde{C}_{ba}$ holds at the optimality under some mild practical assumptions. □

4.4.1 Extended SUIAP for bidirectional-SEE maximization

In the first step we remove the nonlinear operator $\{\}^+$ from the numerator of (4.29), following the result of Lemma 4.4.1, hence turning the BD-SEE objective into a DC over affine fraction. Moreover, it is observed that the SEE^{BD} maximization holds a similar mathematical structure in relation to the transmit covariance matrices, i.e., $\mathbf{Q}_{\mathcal{X}}, \mathbf{W}_{\mathcal{X}}, \mathcal{X} \in \{a, b\}$ as addressed for (4.19). Hence, a similar procedure as in the SUIAP algorithm is employed to obtain an optimal solution, with a guaranteed convergence to a point satisfying KKT conditions. The computational complexity of each Dinkelbach step is obtained similar to (4.25), where $n = 2N_A^2 + 2N_B^2$, $n_Y = 2M_B + 2M_A + 2M_E$ and $n_F = 4N_B + 4N_A + 2$.

4.5 Secrecy Energy Efficiency Maximization with Statistical CSI

It is usually challenging to obtain an accurate estimate of $\mathbf{H}_{ae}$ and $\mathbf{H}_{be}$ due to the lack of collaboration from Eve and mobility. In this part, we consider the case where the channel matrices are known only partially, i.e., only a statistical knowledge of $\mathbf{H}_{ae}, \mathbf{H}_{be}$ is available, considering a similar setup as defined in Section 4.2. An optimization problem for maximizing the statistical expectation of SEE is written as

$$\max_{\mathbb{Q}} \ \mathbb{E}_{\mathbf{H}_{ae},\mathbf{H}_{be}} \{\text{SEE}(\mathbb{Q})\} \tag{4.31a}$$

$$\text{s.t.} \quad (4.19b), (4.19c), (4.19d). \tag{4.31b}$$

It is worth mentioning that the consideration of statistical CSI on secrecy capacity with single antenna receivers is studied in [191], considering a fast-fading channel case and extended for SEE maximization in [192], assuming HD operation of the nodes. In this work, we consider a more general case, where the channel to Eve may be stationary but

[6]This is since the self-interference channel is much stronger than the communication channels, up to 100 dB, due to the proximity of the transmit and receiver chains on the same device [32]. Moreover, the power of the transmit noise is much smaller than the actually transmitted signal, in the margin of $40 - 60$ dB, see [2].

not accurately known due to the lack of collaboration from Eve. In order to turn (4.31) into a tractable form we write

$$\mathbb{E}_{\mathbf{H}_{ae},\mathbf{H}_{be}}\left\{\mathrm{SEE}\right\}=\frac{\mathbb{E}_{\mathbf{H}_{ae},\mathbf{H}_{be}}\left\{\left\{\tilde{C}_{ab}\left(\mathbb{Q}\right)\right\}^{+}\right\}}{P_{\mathrm{tot}}\left(\mathbb{Q}\right)}\approx\frac{\frac{1}{|\mathbb{G}_C|}\sum_{i\in\mathbb{G}_C}\left\{\tilde{C}_{\mathrm{s},i}\left(\mathbb{Q}\right)\right\}^{+}}{P_{\mathrm{tot}}\left(\mathbb{Q}\right)}=:\mathrm{SAA}\left(\mathbb{Q}\right),\tag{4.32}$$

where the latter is obtained via sample average approximation (SAA) [193], such that the equality holds for $|\mathbb{G}_C|\to\infty$, $\mathbb{G}_C$ being the index set of the sampled channel realizations. Moreover, $\tilde{C}_{\mathrm{s},i}\left(\mathbb{Q}\right):=\tilde{C}_{ab}\left(\mathbb{Q},\mathbf{H}_{ae,i},\mathbf{H}_{be,i}\right)$ where $\mathbf{H}_{ae,i},\mathbf{H}_{be,i}$ represent the i-th realization of the channel matrices drawn from the given distributions. The approximated problem is hence expressed as

$$\max_{\mathbb{Q}}\quad\mathrm{SAA}\left(\mathbb{Q}\right)\quad\text{s.t.}\quad\text{(4.19b), (4.19c), (4.19d).}\tag{4.33}$$

Note that the above formulation is still challenging due to three reasons. Firstly, while the application of SAA turns the statistical expectation into a linear sum for any arbitrary channel distribution, it results in a high computational complexity as $|\mathbb{G}_C|$ increases. This calls for a smart choice of $|\mathbb{G}_C|$, compromising accuracy with algorithm complexity. Secondly, unlike the scenario with perfect CSI and also the case presented in [191, 192] considering a fast fading channel situation, the $\{\}^+$ operation may not be ignored. This is since some of the channel realizations may result in a negative $\tilde{C}_{\mathrm{s}}$, while the statistical expectation remains effectively positive. And third, similar to the studied problem in (4.19), the above objective presents a non-concave over affine fractional program which is not tractable in general.

4.5.1 Successive selection and statistical lower bound maximization

In order to address the aforementioned challenges, we propose a successive selection and statistical lower bound maximization (SSSLM) algorithm, which converges to a stationary point of (4.33). Please note that in contrast to Subsection 4.3.1, the operating objective in this part is not a differentiable one, hence invalidating the arguments given by SIA [196]. In this regard we follow a variation of SIA, i.e., the successive upper-bound minimization (SUM) method [194], generalizing the convergence arguments in SIA-based methods for non-smooth problems. The proposed SSSLM algorithm is composed of three nested loops; separation of the SAA into smooth and non-smooth parts at the outer loop, construction of an effective lower bound to SAA as the intermediate loop, and maximization of the constructed bound in the inner loop. A detailed description of the algorithm steps is given in the following.

Initialization

The algorithm starts by generating the channel instances $\mathbf{H}_{ae,i}, \mathbf{H}_{be,i}, \forall i \in \mathbb{G}_C$, drawn from the known statistical distribution of the channels. The number of channel realizations, i.e., $|\mathbb{G}_C|$, should be chosen large enough to capture the channel statistics in SAA with adequate accuracy, however, should be kept small to reduce computational complexity. The analytical expression for the choice of $|\mathbb{G}_C|$ is given in [203, Theorem 5.18], depending on the required statistical accuracy and the given probability distribution. For the initialization of $\mathbb{Q}$, we follow the approximation

$$\mathbb{E}_{\mathbf{H}_{ae},\mathbf{H}_{be}} \left\{ \mathrm{SEE}\left(\mathbb{Q}, \mathbf{H}_{ae}, \mathbf{H}_{be}\right) \right\} \approx \mathrm{SEE}\left(\mathbb{Q}, \mathbb{E}\left\{\mathbf{H}_{ae}\right\}, \mathbb{E}\left\{\mathbf{H}_{be}\right\}\right), \tag{4.34}$$

where the expectations $\mathbb{E}\left\{\mathbf{H}_{ae}\right\}, \mathbb{E}\left\{\mathbf{H}_{be}\right\}$ are obtained from the statistical distribution of the channels. Note that the right side of the approximation corresponds to the objective addressed in Subsection 4.3.1, where SUAIP algorithm is applied to obtain an optimal solution. The obtained solution from SUAIP is then used as an initialization to the SSSLM algorithm.

Outer loop

In each outer iteration, the objective is decomposed as

$$\mathrm{SAA}\left(\mathbb{Q}\right) = \frac{\sum_{i\in\mathbb{G}_{C_1}} \left\{\tilde{C}_{\mathrm{s},i}\left(\mathbb{Q}\right)\right\}^{+} + \sum_{i\in\mathbb{G}_{C_2}} \left\{\tilde{C}_{\mathrm{s},i}\left(\mathbb{Q}\right)\right\}^{+}}{|\mathbb{G}_C| P_{\mathrm{tot}}\left(\mathbb{Q}\right)} \tag{4.35}$$

by separating the set of channel realizations into the disjoint sets $\mathbb{G}_{C_1}$ and $\mathbb{G}_{C_2}$, such that $\mathbb{G}_C = \mathbb{G}_{C_1} \cup \mathbb{G}_{C_2}$. In particular, the set $\mathbb{G}_{C_1}$ is updated in each outer iteration as

$$\mathbb{G}_{C_1}^{(\mathrm{new})} \leftarrow \left\{ \forall i \;\middle|\; i \in \mathbb{G}_{C_1} \;\text{ or }\; \tilde{C}_{\mathrm{s},i}\left(\mathbb{Q}\right) = 0 \right\}, \tag{4.36}$$

where $\mathbb{Q}$ is given from the last intermediate loop, and results in the separation of smooth and non-smooth parts of the objective in (4.35). The algorithm converges when the constructed set $\mathbb{G}_{C_1}$ does not change. As it will be elaborated, the set members in $\mathbb{G}_{C_1}$ incur a high computational complexity, but are capable of resolving the non-smooth points by maintaining the same directional derivative as to SAA. On the other hand, the set members in $\mathbb{G}_{C_2}$ are resolved with lower computational complexity, however, they are not capable of handling non-smooth situations.

Intermediate loop

In each intermediate iteration a lower bound is constructed from the original objective SAA, namely SAA_{LB}, using the value of $\mathbb{Q}$ from the last inner loop, i.e., $\mathbb{Q}_0$. In order to construct SAA_{LB} we undertake three steps. Firstly, the operator $\{\}^{+}$ is removed from SAA for $i \in \mathbb{G}_{C_2}$, which results in a global lower bound. Secondly, concave and

tight lower bounds of the functions $\tilde{C}_{\mathrm{s},i}$ are constructed at the point $\mathbb{Q}_0$, denoted as $\hat{C}_{\mathrm{s},i}\left(\mathbb{Q},\mathbb{Q}_0\right)$, by applying the inequality (4.21) on the convex parts. Please note that the values of $\tilde{C}_{\mathrm{s},i}$ may be negative at $\mathbb{Q}_0$ for some $i \in \mathbb{G}_{C_2}$, resulting in a bias to the original objective. In order to obtain a tight lower bound, we define the set

$$\mathbb{G}_{C_2^+} := \left\{ \forall i \;\middle|\; i \in \mathbb{G}_{C_2},\ \tilde{C}_{\mathrm{s},i}\left(\mathbb{Q}_0\right) \geq 0 \right\}, \tag{4.37}$$

representing the subset of channel realizations resulting in a non-negative $\tilde{C}_{\mathrm{s},i}$ at $\mathbb{Q}_0$. The corresponding lower bound function is then obtained as

$$\mathrm{SAA}_{LB}\left(\mathbb{Q},\mathbb{Q}_0\right) := \frac{\sum_{i\in\mathbb{G}_{C_1}} \left\{\hat{C}_{\mathrm{s},i}\left(\mathbb{Q},\mathbb{Q}_0\right)\right\}^+ + \sum_{i\in\mathbb{G}_{C_2^+}} \hat{C}_{\mathrm{s},i}\left(\mathbb{Q},\mathbb{Q}_0\right)}{|\mathbb{G}_C| P_{\mathrm{tot}}\left(\mathbb{Q}\right)}. \tag{4.38}$$

It can be verified that the constructed lower bound is tight at the point of approximation, i.e., $\mathrm{SAA}\left(\mathbb{Q}_0\right) = \mathrm{SAA}_{LB}\left(\mathbb{Q}_0,\mathbb{Q}_0\right)$, see Appendix 7. The obtained lower bound is then optimally maximized in the inner loop. The iterations of the intermediate loop converge when $\mathbb{Q}_0$, and hence SAA_{LB}, does not change in subsequent intermediate iterations.

Inner loop

The inner loop is dedicated to optimally maximize SAA_{LB}, under the original problem constrains (4.33). Note that the SAA_{LB} is not tractable in the current form, due to the $\{\}^+$ operation. In order to obtain the optimum solution we equivalently write the maximization problem in the inner loop as

$$\max_{a_i\in\{0,1\}, i\in\mathbb{G}_{C_1}} \ \max_{\mathbb{Q}} \ \overline{\mathrm{SAA}_{LB}}, \quad \text{s.t.} \quad \text{(4.19b), (4.19c), (4.19d)}, \tag{4.39}$$

where $\overline{\mathrm{SAA}_{LB}}$ is obtained by replacing the terms $\left\{\hat{C}_{\mathrm{s},i}\right\}^+$ in (4.38) by $a_i\hat{C}_{\mathrm{s},i}$. Please note that for fixed values of a_i, $i \in \mathbb{G}_{C_1}$, the function $\overline{\mathrm{SAA}_{LB}}$ is a concave over affine fraction, and can be maximized to optimality via the application of the Dinkelbach algorithm. Hence (4.39) can be solved by repeating the Dinkelbach algorithm for all $2^{|\mathbb{G}_{C_1}|}$ possible combinations of a_i, $i \in \mathbb{G}_{C_1}$, however, requiring a large number of Dinkelbach iterations. The optimization problem corresponding to the k-th inner iteration is expressed as

$$\max_{\mathbf{a}^{[k]}\in\mathbb{A}^{[k]}} \max_{\mathbb{Q}^{[k]}} \ \overline{\mathrm{SAA}_{\overline{LB}}}\left(\mathbb{Q}^{[k]},\mathbb{Q}^{[0]},\mathbf{a}^{[k]}\right) - \lambda^{[k-1]} P_{\mathrm{tot}}\left(\mathbb{Q}^{[k]}\right) \tag{4.40a}$$

$$\text{s.t.} \quad \text{(4.19b), (4.19c), (4.19d)}. \tag{4.40b}$$

where $\overline{\mathrm{SAA}_{\overline{LB}}}$ is the numerator in $\overline{\mathrm{SAA}_{LB}}$, and $\mathbb{Q}^{[0]}$ is the point for the construction of SAA_{LB}, given from the intermediate loop. Moreover, the vector $\mathbf{a} \in \{0,1\}^{|\mathbb{G}_{C_1}|}$ stacks the values of $a_i, \forall i \in \mathbb{G}_{C_1}$, and $\mathbb{A}^{[k]} \subset \{0,1\}^{|\mathbb{G}_{C_1}|}$. It is observed that for a given $\mathbf{a}^{[k]}$ and $\lambda^{[k-1]}$, (4.40) is a jointly convex optimization problem, and is solved to optimality

via MAX-DET algorithm [158]. Hence, the optimum $\mathbf{a}^{[k]}$ and $\mathbb{Q}^{[k]}$ are obtained by repeating the MAX-DET algorithm for all combinations $\mathbf{a}^{[k]} \in \mathbb{A}^{[k]}$. The value of λ is then updated by applying the obtained $\mathbb{Q}^{[k]}$ and $\mathbf{a}^{[k]}$ as

$$\lambda^{[k]} = \overline{\mathrm{SAA}_{\overline{LB}}}\left(\mathbb{Q}^{[k]}, \mathbb{Q}^{[0]}, \mathbf{a}^{[k]}\right) / P_{\mathrm{tot}}\left(\mathbb{Q}^{[k]}\right). \tag{4.41}$$

Please note that the set $\mathbb{A}^{[k]}$, is initialized as $\{0,1\}^{|\mathbb{G}_{C_1}|}$ but is reduced in each iteration. The following lemma clarifies this reduction.

Lemma 4.5.1. *Let $g_k(\mathbf{a}_0)$ be the optimal value of the objective (4.40) at inner iteration k, for the given combination $\mathbf{a}^{[k]} = \mathbf{a}_0$. Then, if $g_k(\mathbf{a}_0)$ is negative, then the combination $\mathbf{a}_0$ will not be an optimum combination.*

Proof. Due to the monotonic improvement of λ in every iteration, and the fact that $P_{\mathrm{tot}} \geq 0$, the value of $g_k(\mathbf{a}_0)$ will never improve after further iterations. This also results in a negative value of $g_k(\mathbf{a}_0)$ at the optimality. Since at least one of the combinations $\mathbf{a} \in \{0,1\}^{|\mathbb{G}_{C_1}|}$ equalizes the objective to zero at the optimality, the combination $\mathbf{a}_0$ will never be optimal. □

As a result of Lemma 4.5.1, once a combination $\mathbf{a}_0$ results in a negative value of the objective, then it is safely removed from $\mathbb{A}$ for the next iteration, see Algorithm 9. Note that the above process reduces the required computational complexity, compared to separately applying the Dinkelbach method on all combinations, in two ways. Firstly, the parameter λ is only updated jointly, for all combinations $\mathbf{a} \in \mathbb{A}$. Secondly, the monotonic reduction in $|\mathbb{A}|$ in each iteration results in a smaller computational demand in finding the solution to (4.40).

Convergence

The proposed SSSLM algorithm converges to a stationary point of the optimization problem (4.33). In order to observe this, we first verify the convergence of the algorithm. Afterwards, we show that the converging point is also a stationary point of (4.33).

It is observed that the constructed lower bound in each step of the intermediate loop is maximized to the optimality via the application of the Dinkelbach algorithm. On the other hand, after the construction of the new lower bound in each intermediate iteration, the value of $\mathrm{SAA}_{LB}(\mathbb{Q})$ experiences an improvement. This is grounded on the re-calculation of $\hat{C}_{\mathrm{s},i}$ at the point of approximation, and elimination of the channel instances from $\mathbb{G}_{C_2}$ which result in a negative $\tilde{C}_{\mathrm{s},i}$. Since the both aforementioned updates result in a monotonic improvement of $\mathrm{SAA}_{LB}(\mathbb{Q})$ and as the SAA is bounded from above, the iterations of inner and intermediate loop will result in a necessary convergence. The convergence of the intermediate loop subsequently results in the necessary convergence of the outer loop, due to the monotonic increase of $|\mathbb{G}_{C_1}|$ after each outer iteration, and the fact that $|\mathbb{G}_{C_1}| \leq |\mathbb{G}_C|$.

In order to argue the properties of the converging point on the original objective, we observe that neither the SAA nor $\mathrm{SAA}_{LB}(\mathbb{Q})$ are necessarily differentiable at the point of convergence. This invalidates the convergence arguments used for SUAIP algorithm from [196]. In this regard, we follow the guidelines given by SUM method [194], generalizing the convergence arguments in SIA-based methods for non-smooth problems.

Lemma 4.5.2. *Let $\mathbb{Q}^\star$ be a solution of SSSLM. Then the function SAA, i.e., original problem objective, and SAA_{LB}, i.e., the constructed lower bound at the last intermediate iteration, are tight and share the same directional derivatives at $\mathbb{Q}^\star$.*

Proof. See Appendix 7. □

The results of Lemma 4.5.2, together with the fact that $\mathrm{SAA}_{LB}(\mathbb{Q}) \leq \mathrm{SAA}(\mathbb{Q})$ for any feasible $\mathbb{Q}$, jointly satisfy the required assumption set [194, Assumption 1], and guarantee that the obtained converging point is indeed a stationary point of the original problem.

Computational complexity

The computational complexity of the algorithm is dominated by the maximization defined in (4.40), solved via the MAX-DET algorithm in each inner iteration. The associated arithmetic complexity is hence upper-bounded similar to (4.25), where $\gamma_{\text{in}} \propto 2^{|\mathbb{G}_{C_1}|}$, $n = 2N_A^2 + N_B^2$, $n_Y = |\mathbb{G}_C|(2M_B + 2M_E)$, $n_F = 4N_A + 2N_B + 2$. The performance of the proposed SSSLM algorithm in terms of the computational complexity and convergence behavior is further studied in Subsection 4.6.1 via numerical simulations.

Algorithm 9 SEE maximization using statistical CSI, via successive selection and statistical lower bound maximization (SSSLM). $C_{\min}$ ($\lambda_{\min}$) represents the convergence threshold for the intermediate (inner) iterations.

$k, l, m, \lambda^{[0,0,0]} \leftarrow 0$; $\mathbb{G}_{C_1}^{[0]} \leftarrow \emptyset$; $\mathbb{G}_C, \mathbb{Q}^{[0,0,0]} \leftarrow$ Subsection 4.5.1; ▷ initialize
repeat ▷ outer loop
  $m \leftarrow m + 1$; $\lambda^{[0,0,m]} \leftarrow \lambda^{[k,l,m-1]}$; $\mathbb{Q}^{[0,0,m]} \leftarrow \mathbb{Q}^{[k,l,m-1]}$; $\mathbb{G}_{C_1}^{[m]} \leftarrow$ (4.36); $l \leftarrow 0$;
  repeat ▷ intermediate loop
    $l \leftarrow l + 1$; $\mathbb{G}_{C_2^+} \leftarrow$ (4.37); $\mathrm{SAA}_{LB} \leftarrow$ (4.38);
    repeat ▷ inner loop
      $k \leftarrow k + 1$; $\left\{\mathbb{Q}^{[k,l,m]}, \lambda^{[k,l,m]}\right\} \leftarrow$ Dinkelbach's alg. (4.40)-(4.41);
    until (4.40a) $\leq C_{\min}$
  until $\lambda^{[k,l,m]} - \lambda^{[0,l,m]} \leq \lambda_{\min}$
until $\mathbb{G}_{C_1}^{[m]} = \mathbb{G}_{C_1}^{[m-1]}$
return $\left\{\mathbb{Q}^{[k,l,m]}, \lambda^{[k,l,m]}\right\}$

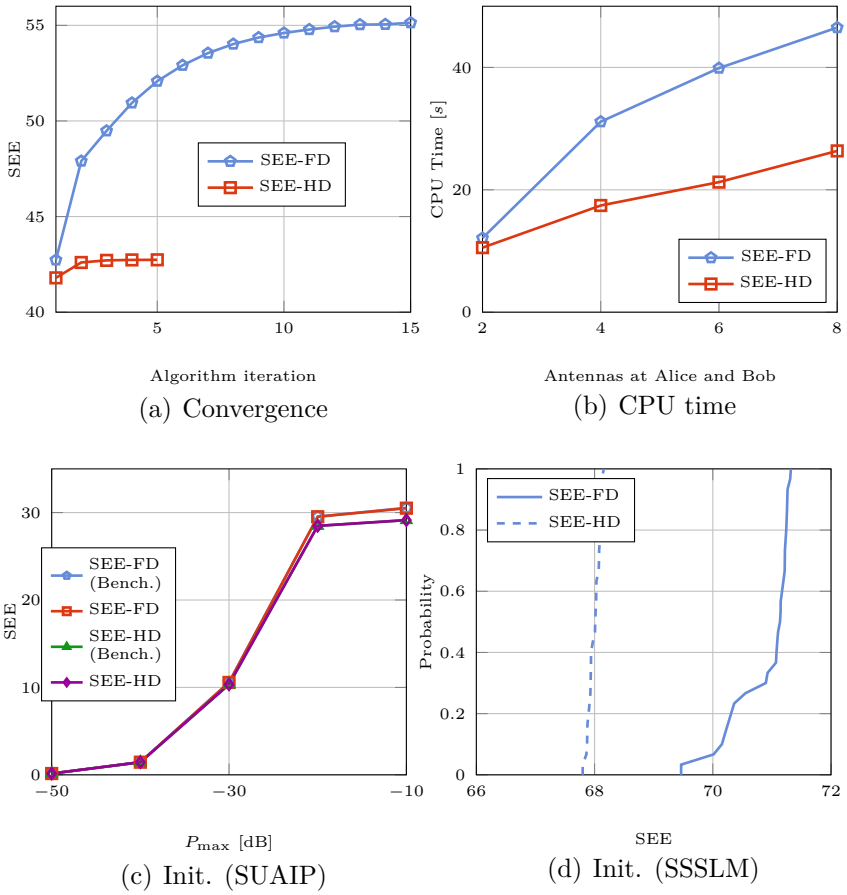

(a) Convergence (b) CPU time

(c) Init. (SUAIP) (d) Init. (SSSLM)

Figure 4.2: Numerical algorithm analysis in terms of the average convergence behavior, initialization, and computational complexity.

4.6 Simulation Results

In this section, the performance of the studied MIMOME system is evaluated in terms of the resulting SEE via numerical simulations[7]. In particular, we are interested in a comparison between the performance of an FD-enabled setup, with the case where all nodes operate in HD mode. Moreover, the evaluation of the proposed SEE-specific designs is of interest compared to the available designs, which target the maximization of the system's secrecy capacity. We assume that all communication channels follow a Rayleigh flat-fading model with variance $\rho_{\mathcal{X}} = \bar{\rho}/d_{\mathcal{X}}^2$, where $d_{\mathcal{X}}$ is the link distance and depends on the simulated geometry, and $\mathcal{X} \in \{ab, ba, ae, be\}$. Moreover, in case that only a statistical CSI is available for the channels to Eve, it is assumed assume that $\mathbf{H}_{\mathcal{X}} = \sqrt{\rho_{\mathcal{X}}}\left(\mathbf{D}_{\mathcal{X}}\bar{\mathbf{H}}_{\mathcal{X}} + \tilde{\mathbf{H}}_{\mathcal{X}}\right)$, $\mathcal{X} \in \{ae, be\}$, where $\sqrt{\rho_{\mathcal{X}}}\tilde{\mathbf{H}}_{\mathcal{X}}$ is the known channel estimate following a Rayleigh distribution with variance $\rho_{\mathcal{X}}$, and $\sqrt{\rho_{\mathcal{X}}}\mathbf{D}_{\mathcal{X}}\bar{\mathbf{H}}_{\mathcal{X}}$ is the es-

[7] I would like to thank my former student M.Sc. Peter Neuhaus for his help in running the numerical simulations regarding the Algorithms 8-9.

timation error where $\mathbf{D}$ enforces the receive-side spatial correlation, and $\bar{\mathbf{H}}_{\mathcal{X}}$ includes independent and identically distributed (i.i.d.) Gaussian elements with unit variance. For the self-interference channels, the characterization reported in [146] is followed. In this respect, we have $\mathbf{H}_{bb} \sim \mathcal{CN}\left(\sqrt{\frac{\rho_{\text{si}} K_R}{1+K_R}}\mathbf{H}_0, \frac{\rho_{\text{si}}}{1+K_R}\mathbf{I}_{M_B} \otimes \mathbf{I}_{N_B}\right)$, where ρ_{si} represents the self-interference channel strength, $\mathbf{H}_0$ is a deterministic term[8], and K_R is the Rician coefficient. The statistics of the self-interference channel on Alice, i.e., $\mathbf{H}_{aa}$, is defined similarly. The resulting system SEE is evaluated by employing different design strategies, and averaged over 100 channel realizations. Unless otherwise is stated, the default simulated setup is defined as follows: $P_{\max} := P_{\mathcal{X},\max} = 0\text{dB}$, $P_0 := P_{\mathcal{X},0} = -20\text{dB}$, $\mu := \mu_{\mathcal{X}} = 0.9$, $\kappa := \kappa_{\mathcal{X}} = \beta_{\mathcal{X}} = -40\text{dB}$, $N := N_{\mathcal{X}} = M_{\mathcal{X}} = 4$, $\mathcal{X}, \in \{A, B\}$. Moreover we set $P_{\text{FD}} = 0$, $\rho_{\text{si}} = 0\text{dB}$, $K_R = 10$, $\bar{\rho} = -20\text{dB}$, and $\sigma_{\text{n}}^2 := \sigma_{\text{na}}^2 = \sigma_{\text{nb}}^2 = \sigma_{\text{ne}}^2 = -40\text{dB}$. The three nodes are equidistantly positioned with the distance equal to one[9].

4.6.1 Algorithm analysis

Due to the iterative structure of the proposed algorithms and the possibility of local optimum points, the convergence behavior of the algorithms are of high interest both as a verification for algorithm operation as well as an indication of the required computational effort. In this part, the performance of the SUAIP and SSSLM algorithms are studied in terms of the average convergence behavior and computational complexity. Moreover, the impact of the choice of the algorithm initialization is evaluated.

In Fig. 4.2 (a), the average convergence behavior of the SUAIP algorithm is depicted. As expected, a monotonic objective improvement is observed, where convergence is achieved in 5-20 outer iterations.

In Fig. 4.2 (b), the average required CPU time is depicted[10]. It is observed that a higher antenna array size results in a higher required computational complexity, associated with larger problem dimensions. Moreover, a design with an FD-enabled jamming results in a higher CPU time, due to the additional problem complexity associated with the choice of jamming strategy and RSI.

In Figs. 4.2 (c)-(d), the impact of the proposed initializations for the SUAIP and SSSLM algorithms are depicted. In Fig. 4.2 (c) it is observed that for the SUIAP algorithm, the proposed initialization in Subsection 4.3.3 reaches close to the benchmark performance[11]. For the SSSLM algorithm, the situation is prone to more randomness. This is

[8] For simplicity, we choose $\mathbf{H}_0$ as a matrix of all-1 elements.

[9] We consider unit-less parameters to preserve a general framework. However, the obtained SEE values can be interpreted as the number of securely communicated bits per-Hz per-Joule, assuming the power values are in Watt.

[10] The reported CPU time is obtained using an Intel Core i5 3320M processor with the clock rate of 2.6 Giga Hertz (GHz) and 8 Giga bytes (GB) of RAM. As software platform, CVX [204] is used together with MATLAB 2013a on a 64-bit operating system.

[11] The benchmark performance is obtained by repeating the algorithm with several random initializations, and choosing the highest obtained SEE.

since, in addition to the choice of the algorithm initialization, the solution is dependent on the generated channel realizations used in the construction of SAA, see (4.32). In this regard, the resulting cumulative distribution function (CDF) of the resulting SEE values is depicted in Fig. 4.2 (d), by examining 100 instances of the SSSLM algorithm. It is observed that the resulting average SEE differs for different solution instances, however, within $2-3\%$ of the relative difference. This value is smaller for a system with HD nodes, due to the absence of FD jamming and the impact of RSI which results in a simpler problem structure.

4.6.2 Performance comparison

In this part, the SEE performance of the FD-enabled system is evaluated via the application of the proposed SUAIP and SSSLM algorithms, and under different system conditions. In particular, we are interested in a comparison between the performance of an FD-enabled setup, compared to the case where all nodes operate in HD mode. Moreover, the evaluation of the proposed SEE-specific designs is of interest, in comparison to the available designs which target the maximization of the system's secrecy capacity. The following benchmarks are hence implemented to provide a meaningful comparison.

- *SEE-FD*: The proposed SUAIP (SSSLM) algorithm is implemented using the exact (statistical) CSI, where Bob is capable of FD operation.
- *SEE-HD*: Similar to *SEE-FD*, but with restricting the operation of the nodes to the HD mode.
- *CS-FD*: The design with the intention of maximizing secrecy capacity. Bob is capable of FD operation.
- *CS-HD*: Similar to *CS-FD*, but with restricting the operation of the nodes to the HD mode.

FD-enabled jamming with exact CSI

In Figs. 4.3 (a)-(h), the average SEE performance of the defined benchmarks are evaluated assuming the availability of perfect CSI and FD operation at Bob. Hence, both Alice and Bob are simultaneously capable of transmitting AN, see Fig. 4.1.

In Fig. 4.3 (a), the impact of thermal noise variance is depicted. It is observed that a higher σ_{n}^2 results in a smaller SEE both for FD and HD setups. Moreover, a marginal gain for FD setup is obtained compared to the HD setup, if the noise variance is low. This is expected, since FD jamming becomes less effective when Eve is already distorted with a high thermal noise power.

In Fig. 4.3 (b), the impact of the available transmit power budget ($P_{\max}$) for each transceiver is depicted. It is observed that for small values of $P_{\max}$, the resulting SEE

is monotonically increasing with an increase in $P_{\max}$. Moreover, the performance of the benchmark algorithms essentially converge for small values of $P_{\max}$. This is grounded in the fact that for a system with low SNR condition, the positive impact of FD jamming disappears as observed from Fig. 4.3 (a). Conversely, for large values of $P_{\max}$, the traditional designs result in a rapid decrease of SEE, where the proposed SUAIP method converges to a constant value. This is expected, since the designs with the target of maximizing the secrecy rate utilize the maximum available power budget, resulting in a sever degradation of SEE. Moreover, a visible gain is observed with the application of an FD jammer for a high $P_{\max}$ region. Due to a high $P_{\max}$, the link from Alice to Eve also enjoys a better SNR condition, which justifies the application of an FD jammer.

In Fig. 4.3 (c), the impact of transceiver accuracy is depicted. As expected, a higher value of κ results in a smaller achievable SEE, both in HD and FD setups. Moreover, it is observed that FD jamming can be beneficial only for a system with an accurate hardware operation, due to the impact of RSI. However, it is observed that targeting SEE as the design objective results in a significant energy efficiency gain, compared to the traditional designs which target the maximization of secrecy rate.

In Fig. 4.3 (d), the impact of Eve's distance to Alice (d_E) is depicted. It is assumed that three nodes are positioned in a line with a total Alice-Bob distance of 100, where Eve is positioned in between. It is observed that the system SEE increases as d_E increase, and Eve gets closer to Bob. Moreover, the application of FD jamming becomes beneficial only when Eve is located in a close distance to Bob, and hence the channel between Bob and Eve, i.e., the jamming channel, is strong.

In Figs. 4.3 (e) the impact of the number of antenna elements at Eve (M_E) is depicted. As expected, a larger M_E results in a reduced SEE as it results in a stronger Alice-Eve channel. Moreover, the application of an FD jammer becomes gainful for higher values of M_E, in order to counteract the improved Eve reception capability.

In Figs. 4.3 (f)-(h), the impact of the transceiver's power efficiency is evaluated on the resulting system SEE. In particular, the impact of the zero-state power consumption (P_0) and PA efficiency (μ) are depicted respectively in Figs. 4.3 (f) and (g). The impact of the additional power consumption for SIC (P_{FD}) on the system SEE is depicted for different noise regimes in Fig. 4.3 (h), where the constant lines represent the SEE for the HD setup. It is observed that higher (lower) values of μ (P_0, P_{FD}) result in a higher SEE. Moreover, it is observed that a marginal gain with the application of an FD jammer is obtained for a high μ, and a small P_{FD} conditions. This is expected, since a small (large) value of μ (P_{FD}) results in a bigger waste of power when using an FD jamming strategy.

Secure bidirectional communication

In Fig. 4.4, a system with a bidirectional secure communication between Alice and Bob is studied. In particular, a joint FD operation at Alice and Bob is considered which

enables jamming and communication simultaneously at both directions. Two scenarios are considered regarding the decoding capability at Eve: *i*) Eve treats interference from the non-intended information path as noise, and *ii*) Eve is capable of decoding, and hence reducing, the received signal from the non-intended information link. Moreover, a setup with a HD Bob and a HD Alice is also evaluated, where TDD or FDD is employed in order to facilitate a bidirectional communication.

It is observed that the resulting SEE increases with $P_{\max}$, however, saturates for high values of maximum transmit power. Moreover, it is observed that a joint FD operation is capable of enhancing the system SEE, with a considerable margin, in the studied bidirectional setup. This is since, due to the coexistence of both communication directions on the same channel the jamming power is reused for both communication directions, leading to a higher SEE compared to the HD setup. Moreover, the Eve's decoding capability is further decreased in the FD setup considering the scenario (*i*), due to the existence of two information links at the same channel.

FD-enabled jamming with statistical CSI

In Fig. 4.5, the CDF of the resulting SEE is evaluated via the application of SSSLM algorithm on 100 problem instances[12], where only a statistical CSI is available for the channels to Eve. We choose $|\mathbb{G}_C| = 100$ in the construction of SAA, see Section 4.5, in order to limit the required computational effort. The CDF of the resulting SEE is then evaluated via the utilization of 10000 channel realizations for each problem instance, following the statistical distribution defined in the beginning of the current section and choosing $\mathbf{D}_{\mathcal{X}}$ as a matrix of all-1 elements.
In Fig. 4.5 (a), the performance of the SSSLM algorithm is compared to the case where the SUIAP algorithm is applied directly on the channel estimates, obtained from the given distribution. It is observed that a significant gain is obtained by taking into account the full channel statistics, however, at the expense of a higher computational complexity. Moreover, the superior SEE performance of the SEE specific design, compared to the secrecy rate maximizing design is observable.

In Figs. 4.5 (b)-(d) the CDF of the resulting SEE is evaluated for different levels of thermal noise (σ_{n}^2), hardware inaccuracy (κ), and the PA efficiency (μ). Similar to the observed trends for the scenario where exact CSI is available, a marginal gain is observed in the resulting SEE with the application of an optimized FD jamming strategy. In particular, the gain of the FD-enabled system is improved for a system with a high SNR, i.e., a high transmit power budget or a low noise level, and as hardware accuracy increases.

[12]Each problem instance includes a realization of $\mathbf{H}_{ab}, \mathbf{H}_{bb}$.

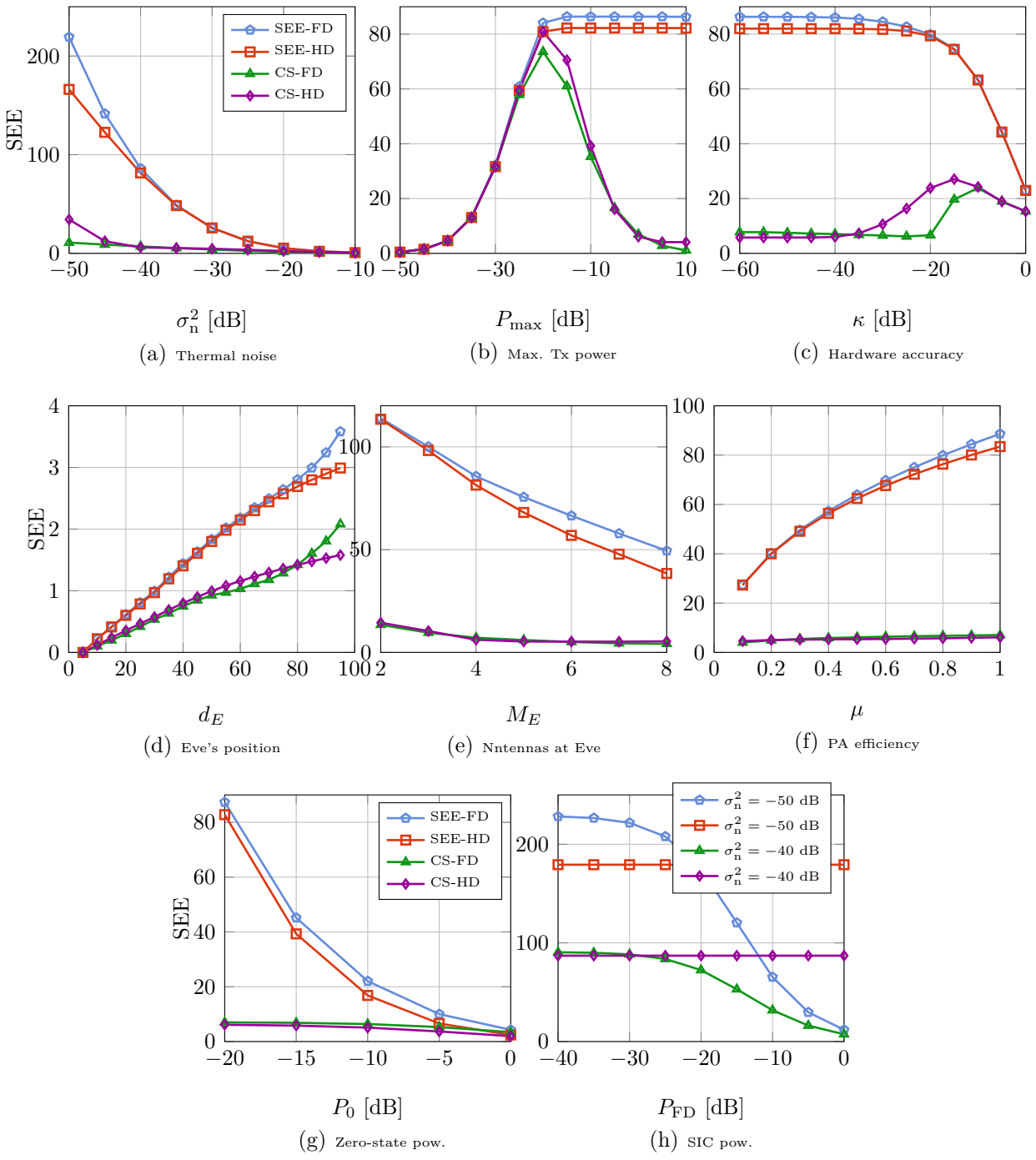

Figure 4.3: SEE performance of the secure communication system with exact CSI, via the utilization of SUAIP algorithm.

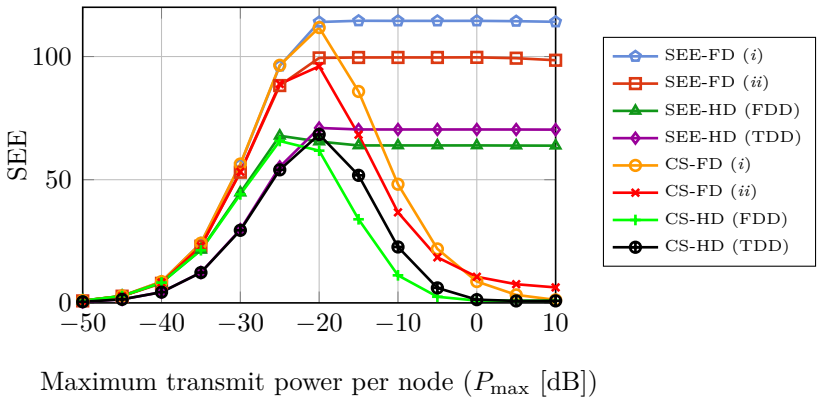

Figure 4.4: SEE performance of FD, FDD and TDD for secure bidirectional communications.

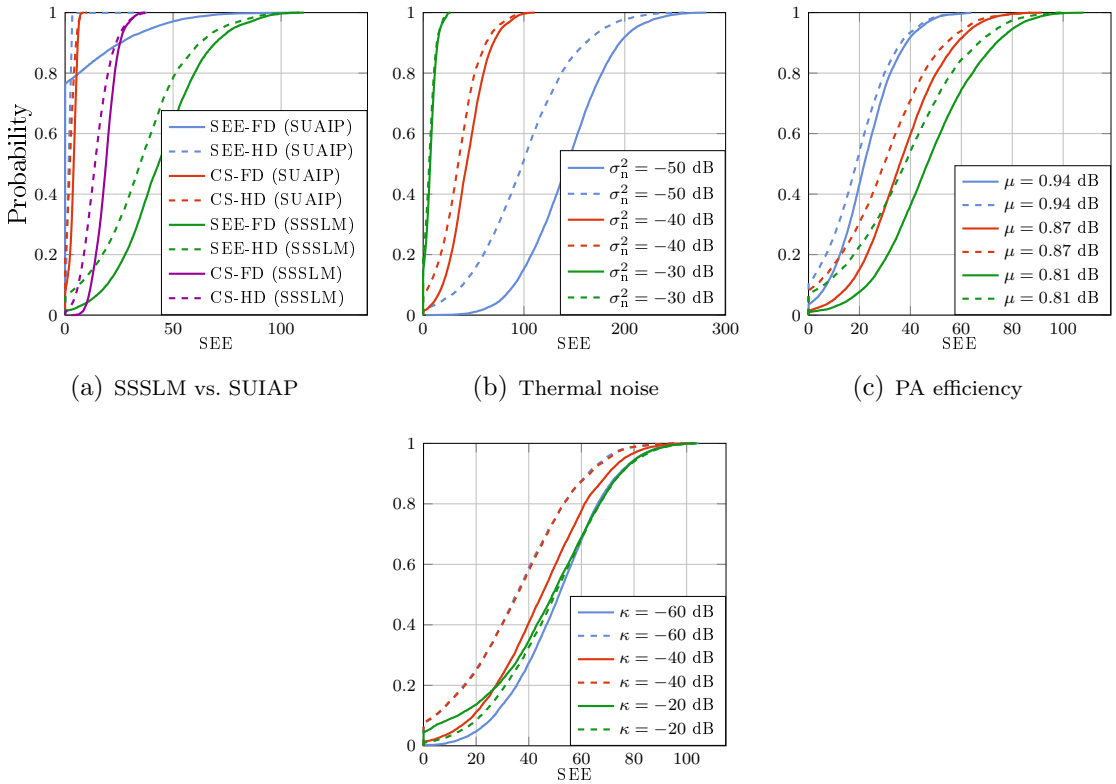

(a) SSSLM vs. SUIAP (b) Thermal noise (c) PA efficiency

(d) Hardware accuracy

Figure 4.5: CDF of the resulting SEE under various system conditions utilizing the SSSLM algorithm. The solid (dashed) lines represent the performance of the FD (HD) setups in (a)-(d).

4.7 Conclusion

The utilization of FD jamming transceivers is known to significantly enhance the secrecy capacity of wireless communication systems, by transmitting AN while exchanging information. However, this results in a higher power consumption in the system due to *i)* the degrading impact of residual self-interference on the desired communication channel, *ii)* the implementation of an SIC scheme at the FD transceiver, as well as *iii)* the power consumed for the transmission of AN. In this chapter, we have observed that the application of FD transceivers result only in a marginal gain in terms of secrecy energy efficiency, for a wide range of system conditions. However, the aforementioned SEE gain becomes significant for a system with a small distance between the FD node and the eavesdropper, or a system operating in high SNR regimes, under the condition that the self-interference can be effectively and efficiently mitigated. Moreover, a promising SEE gain is observed for an FD bidirectional communication, where jamming power can be reused for both directions. It is observed that for almost all system conditions, the application of an SEE-aware design is essential, compared to the available designs which target the maximization of secrecy capacity.

5 Full-Duplex Cellular Networking: A Minimum-Cost Wireless Backhauling Approach

5.1 Overview

Deployment of small cell base stations (SCBSs) is a necessary paradigm to meet the rapid increase of rate demand in the context of the fifth generation cellular wireless communication networks (5G). In particular, small cells enable high capacity radio access solutions due to the short distance coverage, facilitating a higher energy and spectral efficiency [205]. However, the expected dense deployments of SCBS raise challenges regarding the utilization of the already scarce spectrum resources, as well as providing backhaul connection to the SCBS sites. In this chapter, we consider the gainful utilization of FD capability for cellular communication systems in two ways. In the first part, an overview on the application of FD capability in the radio access network is given, where UL and DL connections are scheduled on the same channel, aiming at a higher spectral efficiency. It is observed that coordination among the infrastructure nodes shall be utilized to obtain a higher spectral efficiency, however, resulting in a higher traffic load on the backhaul network. In the second part, we study the application of FD wireless links as a spectrum-saving mechanism for wireless backhaul solutions, leading to a reduced overall network cost.

5.1.1 An overview on FD wireless radio access

An FD BS is capable of accommodating the UL and DL communications at the same channel resource, hence, showing potential to obtain a higher spectral efficiency. However, the coexistence of UL and DL at the same channel resource inevitably results in additional interference paths compared to the systems operating with an HD basestation. A summary of the fundamental interference paths for a cellular wireless communication system operating in HD mode is depicted in Fig. 5.1. Due to the separation of UL and DL communications into separate channel resources, the intrinsic interference paths are limited to the inter-cell UL to BS, as well as the inter-cell BS to DL interference. In addition to the interference paths depicted in Fig. 5.1, an FD cellular network suffers from the interference from UL to the DL users, as well as the interference due to the BS

co-transmissions. This includes, *i)* the self-interference at each FD base station node, *ii)* the interference due to the simultaneous transmission and reception among adjacent base stations, i.e., inter-BS interference, *iii)* interference among the uplink and downlink directions in the same cell, i.e., intra-cell UL-DL interference and *iv)* interference among the uplink and the downlink directions at the adjacent cells, i.e., inter-cell UL-DL interference, see Fig. 5.2. The aforementioned additional interference paths, if not properly controlled, lead to the degradation of the resulting system performance and eliminating the potential gain over the traditional HD networks. In this regard, a beamforming and power allocation scheme is proposed in [56], considering a multiple-antenna FD multi-cell network. In the aforementioned work, the instantaneous CSI is exploited to control and reduce the impact of interference. However, the acquisition of a perfect CSI is rather difficult, particularly for the paths between UL and DL users and the inter-cell interference paths, resulting in a disadvantage for the FD system. In [50, 51, 130] the FD capability is applied at a stand-alone BS, assuming no interference from (to) adjacent cells. In this regard, it is observed that the deteriorating interference links can be efficiently controlled, employing multiple antenna beamforming and resource allocation. However, the aforementioned scenario is valid for the cases where the operation of the adjacent cells are scheduled on orthogonal channels or physically isolated. For the scenarios with coexistence of the multiple FD BSs at the same channel, it is observed in [47, 131, 132] that the coordination among the infrastructure nodes together with an optimized resource allocation have the potential to enhance the spectral efficiency compared to the HD system counterpart. In particular, an FD cloud radio access network (C-RAN) is studied in [131, 132], where the interference among the FD BS nodes can be effectively mitigated due to the static inter-BS channel conditions, as well as the exchange of transmitted signal via a backhaul connection. Moreover, the inter-cell UL to BS, and BS-DL interference links shall be effectively mitigated, employing a joint transmission scheme[1]. However, successful implementation of the proposed interference mitigation schemes calls for a high-capacity backhaul connection, which appears to be the next-step challenge in the realization of the future wireless cellular networks.

5.1.2 FD wireless backhaul network planning

With the expected dense deployments of SCBS, the main challenge for the operators will be to provide backhaul solutions at a reasonable cost, in order to handle the data traffic to (from) the core network. In this regard, application of wireless backhaul solutions appears to be a good alternative to the traditional fiber connections due to the lower

[1]It is worth mentioning that studies in [50,51,56,130–132] focus on the below 6 GHz frequency bands for the evaluation of the gains obtained via FD operation, due the existing spectral scarcity in the aforementioned bands. The utilization of higher frequency bands, i.e., $6 - 60$ GHz, enables new potentials to mitigate the multi-cell interference which are caused due to the coexistence of UL and DL transmission. This is both due to the higher path loss and isolation properties at the higher frequency bands, as well as the possibility of applying larger antenna arrays which reduce the impact of interference via beamforming.

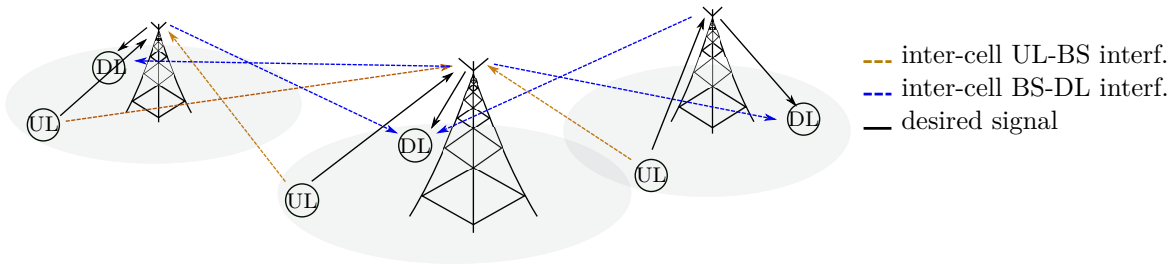

Figure 5.1: Intrinsic interference paths in an HD cellular network, with separation of UL and DL communications into orthogonal channels.

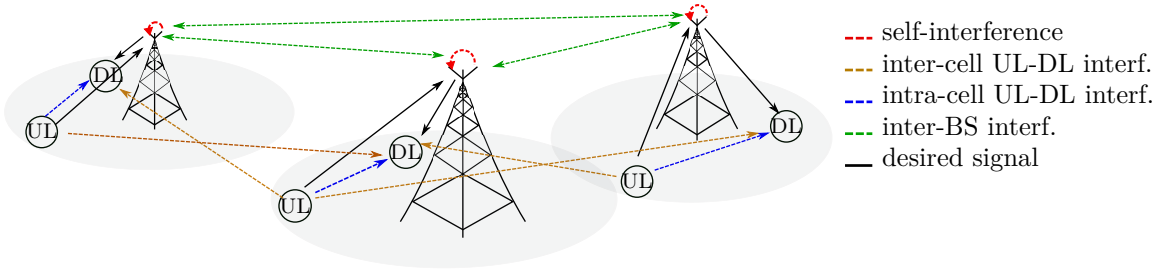

Figure 5.2: Additional interference paths emerging in an FD cellular network. UL and DL communications co-exist at the same channel.

capital expenditure and ease of deployment [206]. However, wireless backhaul links are known to suffer from occasional failure and degradation due to blockage and weather conditions, limited information capacity compared to the traditional fiber connections, as well as the additional consumption of energy and spectrum. In order to overcome the aforementioned drawbacks, several works have been dedicated to the efficient design of the wireless backhaul networks from the aspects of link and topology planning and resource allocation [207–217], as well as exploring promising technologies with the goal of enhancing the performance of the traditional LOS point-to-point microwave links. This includes, e.g., establishment of non-LOS links for resolving blockage situations [218,219], or technologies with the potential to enhance spectrum utilization, e.g., operating in unlicensed millimeter-wave bands [220], optical links [221], as well as the realization of in-band backhauling, i.e., the co-existence of access and backhaul links at the same channel [91–95, 222]. In particular, utilization of the FD capability at wireless backhaul links is presented as a promising use case, due to the zero-mobility conditions and the utilization of directive antennas, hence showing a potential to reduce the cost of spectrum [1].

5.1.3 Related works

Wireless backhaul planning

The efficient planning of a wireless access network has been the focus of several recent works [215]. In this regard, the first step is to determine the location and the required number of SCBS sites, considering the available resources from the operator, distribution of users, as well as the expected rate demands [223–225]. A proximity-based clustering method is proposed in [217], associating the groups of given SCBS sites to the available root node, i.e., a gateway node to the core network via fiber connection. Once the clusters of SCBS are identified in association with the root nodes, the remaining task is to optimally plan the backhauling network within each cluster. This includes the choice of the links to be established, identifying the network topology, as well as the link specifications, e.g., link technology and the operating frequency bands. In this regard, the problem of backhaul topology planning and optimization has been addressed with the considerations of energy efficiency [206,211,212], overall network cost [210,213–216], delay performance [226], as well as reliability and fault tolerance [207–210]. The problem of resource allocation and frequency planning for a network with a fixed topology is studied in [227,228]. In the recent works [214,215] a multi-objective design is considered, accounting for the impact of interference, delay, and system throughput. However, the aforementioned works are not yet extended for a joint frequency and topology wireless backhaul planning, which is essential for the scenarios with the high impact of interference, e.g., dense urban deployment, or the scenarios considering the coexistence of backhaul and access networks within the same spectrum.

FD-enabled backhauling

In [222] the performance of an FD in-band backhauling system is analyzed by means of stochastic geometry, where the superior performance of an FD-enabled system is observed compared to the HD counterparts. An adaptive FD/HD backhauling system is studied in [95] where FD in-band backhauling is used in a two-tier star topology. The aforementioned system is also extended with the considerations of system sum-rate analysis and optimization [94], and minimum-cost resource allocation [93]. In [91,92], a flexible frame structure is used to jointly optimize the access and backhaul parameters. In all of the aforementioned works, the FD capability is considered on a single backhaul-access link, or on a given star topology.

5.1.4 Chapter outline and contributions

In this chapter we address the joint topology design and resource allocation in a wireless backhaul network where FD capability is enabled at the wireless links, with the

goal of minimizing the collective network cost. The contributions of this chapter are summarized as follows:

- In contrast to [91–95] where FD capability is utilized to enable in-band backhauling in single backhaul link or a fixed star topology, we consider a general topology with the co-existence of multiple backhaul and access links on the same channel. However, this calls for an efficient interference management scheme. In order to facilitate this, we consider a framework where the interference conditions for backhaul-to-access, as well as the backhaul-backhaul links can be obtained via the utilization of a wave propagation simulator, suited for dense urban scenarios where relatively accurate environment information is available [229, 230]. This is in contrast to the designs in [210, 213] assuming no interference from backhaul links, or the recent works [214, 215], that simplify the impact of interference to link crossing and low arrival angle situations.
- Unlike the connected graph approaches proposed in [210,213–216] or the frequency planning on a fixed topology [227, 228], we jointly address the design of the network topology as well as the allocation of the power and frequency resources, as the aforementioned factors jointly impact the network interference pattern and the resulting link throughput. In particular, this enables a flexible usage of FD capability, when and where it is gainful. In this regard, a mixed integer-linear program (MILP) design framework is proposed to obtain a minimum cost network operation, complying with the required QoS as well as the operational network constraints.
- Due to the variable nature of the network data, e.g., change of traffic load or wireless link conditions, the networks are usually adjusted to the worst-case conditions, resulting in a reduced efficiency. In this regard, we propose a SIA design framework for adjusting the transmit power at the wireless links, with the goal of keeping the network in compliance with the changing channel or QoS conditions. In contrast to the introduced proactive measures in [207–210], where the network is designed with the consideration of a possible failure, our proposed approach is a reactive one; enabling the network to react to the partial changes with a minimal cost.

Numerical simulations show a reduction in the network cost via the utilization of the proposed designs, thanks to the coexistence of multiple links on the same channel due to the FD capability. The contributions of this chapter are based on the results already published, or under consideration for publication in [47, 50, 51, 56, 128–132].

5.2 System Model

We consider a network of backhaul nodes, including root nodes and non-root nodes, whereby the data traffic is carried to (from) the access network from (to) the core

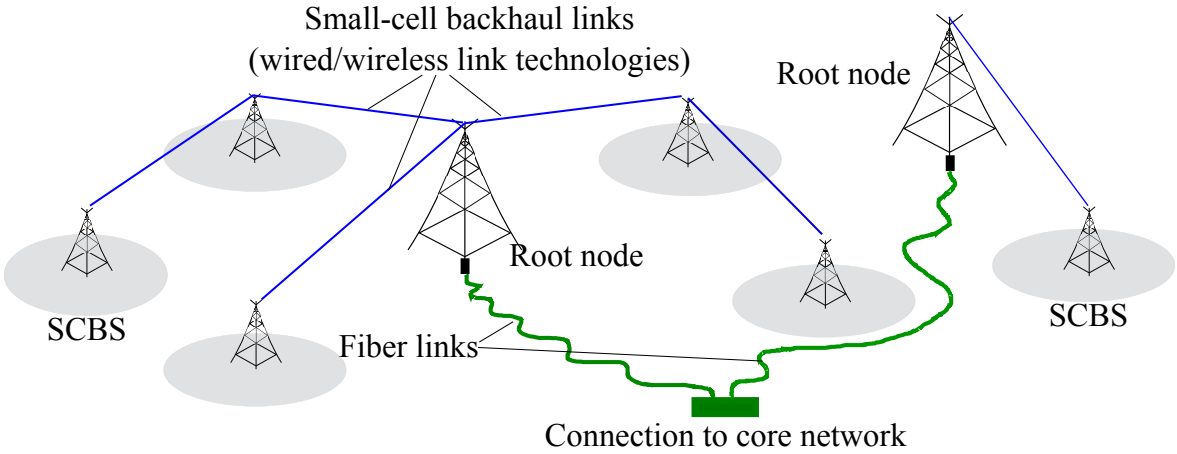

Figure 5.3: Backhauling network, including wireless and wired link technologies for small cells and fiber connections for root nodes to the core network.

network, see Fig. 5.3. Root nodes are connected to the core network via high capacity fiber connections, whereas non-root nodes set up wireless links directed to the root nodes, or to the other non-root nodes which relay their data traffic through the network. The goal of the network is hence to deliver the required uplink (downlink) information rate from (to) the non-root nodes to (from) the core network, while complying with the operational network constraints. For each wireless link the transmit power can be adjusted for different frequency subchannels, thereby facilitating an effective interference control and spectrum-saving mechanism. The wireless channels associated with each link, as well as the interference channels between different links are assumed to be frequency-flat at each sub-channel.

5.2.1 Acquisition of network information

In order to deliver a mathematical description of the network operation, the following information is obtained via direct observations and measurements, or via post-processing of the observable data:

Node locations

The topology of the network is partly determined by the location of the root and non-root nodes. Moreover, based on the location of the nodes, the potential wireless links are determined. This can be identified via the existence of a LOS between two nodes, and that the corresponding link does not exceed a maximum distance limit [214, 215]. The set of root nodes, non-root nodes, and all nodes are respectively denoted as $\mathbb{R}, \mathbb{M}$ and $\mathbb{N}$. The set of all potential links is denoted as $\mathbb{L}$.

Available spectrum

The information regarding the provisioned operational spectrum, including the spectrum dedicated for backhaul and access are obtained. The set of all frequency subchannels, and those used in the access network are denoted as $\mathbb{F}, \mathbb{F}_a$, respectively.

Large-scale channel parameters

The large-scale channel parameters associated with the desired and interference paths are obtained for each potential wireless link, and used as the basis for network planning. This includes the estimated channel strength, i.e., ratio between the transmit and receive power at each link. Note that the exact channel information may not be obtained via direct measurements, as all of the potential links may not exist prior to the network planning and realization. However, the large-scale channel conditions can be estimated at each link via the application of a wave propagation simulator [230] utilizing the used antenna specifications as well as the related environment information, e.g., city map and node locations. It is worth mentioning that for the studied system this process reaches a high accuracy, considering the static wireless links with LOS connections and almost zero mobility, which reduces the randomness. The interference channel strength between a link and the access network, e.g., from a wireless link to a remote BS, can be obtained by following a similar methodology. The desired channel strength associated with the wireless backhaul link $(i, j) \in \mathbb{L}$ and the interference channel strength from the wireless link $(l, k) \in \mathbb{L}$ to the link (i, j) are denoted as $\Lambda_{ij,f}$ and $\Gamma_{ij,lk,f}$, respectively. Moreover, the interference channel strength from the wireless link (i, j) to the access network associated with node m is denoted as $\Omega_{ij,m,f}$, where $f \in \mathbb{F}$ and $i, j, m \in \mathbb{N}$.

SIC level

Due to the full-duplex capability, a node may transmit and receive via separate wireless links at the same frequency, however, resulting in a strong SI. Such interference can be reduced via the application of state of the art SIC schemes, e.g., [2, 7]. As mentioned, a wireless backhaul link is particularly interesting for the utilization of FD capability due to the almost zero-mobility condition and the high cost of spectrum. However, the SIC may not be perfect due to the impact of hardware inaccuracies, as well as the reflections from the moving objects. In this regard, the imperfect SIC can be modeled as the attenuation factor $\Gamma_{ij,ki,f}$, relating the transmission power to the resulting residual self-interference power at the node $i \in \mathbb{N}$ and from the link (i, j) to $(k, i) \in \mathbb{L}$.

Average processing delay

The processing delay at the intermediate nodes, denoted as $d_i,\ i \in \mathbb{N}$, plays a dominant role in the overall delay for the transfer of information from (to) the core network [226].

Please note that the average processing delay can be considered as a function of the available processing and storage resources at each node, and is assumed to be a known information.

Power budget

The maximum transmit power at each wireless link, denoted as $P_{\max,ij}$ as well as the total consumed power at each node, denoted as $P_{\max,i}$, should be considered in the design of network parameters. Note that the value of $P_{\max,ij}$ is usually limited by the range of the transmit chain elements, e.g., power amplifier, whereas the $P_{\max,i}$ is limited by the available power sources, e.g., when the node is battery-powered or relies on the harvesting sources.

Required information rate

The required information rate at each node is denoted as $R_{\text{ul},i}$, representing the UL traffic requirement, and as $R_{\text{dl},i}$, as the DL traffic requirement, $i \in \mathbb{N}$. The values of $R_{\text{ul},i}$, $R_{\text{dl},i}$ can be estimated considering the number of users associated with a backhaul node, or by learning the previous network demands.

Pre-existing links

Other than the wireless backhaul links, the network may make use of the pre-existing wired links, e.g, pre-existing cooper connections. The available collective link capacity from the other technologies is denoted as $C_{ij,0}$, for the link $(i,j) \in \mathbb{L}$.

Interference temperature threshold

Interference temperature threshold, denoted as $I_{\text{th},k,f}$, gives a trade-off between the protection of the access network against the interference from backhaul wireless links, and the coexistence possibility for backhaul and access links at the same frequency. For instance, it can be chosen equal to the the noise variance, i.e., keeping the interference below the noise floor.

5.2.2 Wireless link throughput

Once a wireless link is established, the link quality in terms of signal to interference-plus-noise ratio (SINR) is obtained as

$$\gamma_{ij,f} = \frac{\Lambda_{ij,f} X_{ij,f}}{\sum_{(l,k)\in\{\mathbb{L}\setminus(i,j)\}} \Gamma_{ij,lk,f} X_{lk,f} + W_{ij,f}}, \tag{5.1}$$

where $X_{ij,f}$ and $W_{ij,f}$ respectively represent the transmit power and the thermal noise variance for the link $(i,j) \in \mathbb{L}$ at the subchannel $f \in \mathbb{F}$. $\gamma_{ij,f}$ is the SINR, resulting in

$$C_{ij,f} = B \log_2 (1 + \gamma_{ij,f}), \tag{5.2}$$

where B is the bandwidth of each frequency subchannel, and $C_{ij,f}$ is the achievable information rate. Note that the equality (5.2) holds only for a Gaussian transmit signaling and for an arbitrarily long coding block length, and can be otherwise treated as an approximation.

5.2.3 Role of planning

As mentioned, each node may setup a wireless link among the identified feasible set $\mathbb{L}$, as a usual planning choice in the context of wireless backhaul planning. In this part, we also assume that the available spectrum is divided into multiple frequency subchannels, where the transmit power for each link can be adjusted at each frequency subchannel. The aforementioned flexibility enables the planning algorithm with two enhancements compared to the usual planning strategies [210, 213–216]. Firstly, an effective interference management is enabled, regarding the interference to the other links, the SI in the FD mode, as well as the interference to the access network. In particular, it facilitates a proper incorporation of the FD capability by enabling different duplexing modes which are chosen depending on the interference conditions, SIC quality, and QoS requirements, see Fig. 5.4. Moreover, the required transmission rates can be obtained by adjusting the transmit powers, reducing un-necessary additional costs due to excessive spectrum and energy consumption. Note that the expressions in (5.1)-(5.2) formulate the achievable information rate of each wireless link, given the transmit strategies throughout the network. This is the goal of the remaining parts of this chapter to identify how the aforementioned planning choices should be made, in order to satisfy the network QoS requirements with a minimum overall costs.

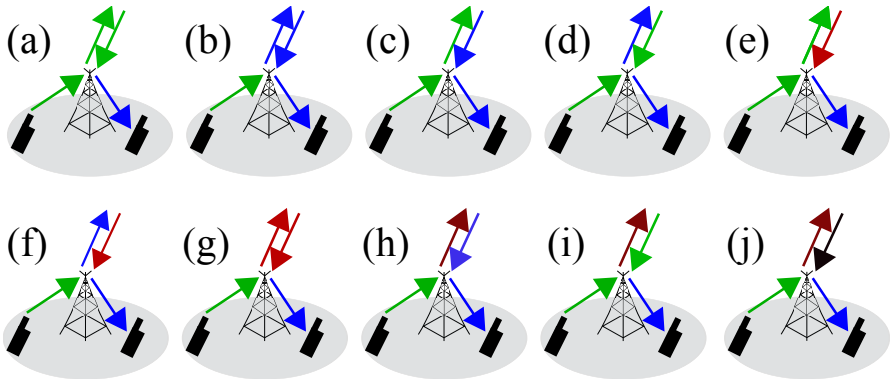

Figure 5.4: Possible frequency duplexing modes for wireless backhaul connections. Different colors represent different frequency bands. This includes the possibility of multiple coexisting links at the same frequency, e.g., (a), (b), or a complete separation of the links at different bands (j).

5.3 Minimum Cost Network Planning and Optimization

In this part, two design strategies are proposed considering the defined wireless backhaul network. First, a full-scale network planning and optimization method is proposed, employing an MILP framework, where the planning choices explained in Subsection 5.2.3 including the network topology, operational frequency bands, and the transmit power of wireless links are determined in order to setup a minimum-cost wireless backhaul network. However, this approach demands major re-configurations of the network parameters, e.g., topology, which may be only practical in the initialization phase of the network setup. Hence, as the second design strategy, the transmit power of the wireless links are adjusted in order to cope with slight changes in the network information, e.g., channel situation, SIC quality, or a slightly increased rate demand. The latter design acts as a network re-tunning method, assuming that the major network parameters including network topology and the functioning frequency bands are already fixed.

5.3.1 Decision variables

The following decision variables are considered as the outcome of our design, see Table 5.1:

Table 5.1: Set of decision variables

Set	Description
$\mathbb{P}$	Set of the variables $X_{ij,f},\ \forall(i,j) \in \mathbb{L},\ f \in \mathbb{F}$
$\mathbb{C}_U(\mathbb{C}_D)$	Set of the variables $C_{\text{ul},ij}(C_{\text{dl},ij}), \forall(i,j) \in \mathbb{L}$
$\mathbb{J}_L(\mathbb{J}_F)$	Set of the all link (subchannel) activity indicator binary variables

Transmit power $X_{ij,f}$

The decision variables $X_{ij,f},\ (i,j) \in \mathbb{L},\ f \in \mathbb{F}$, determine the transmit power of the wireless links, and at each frequency band.

Used link capacity for UL (DL) $C_{\mathbf{ul},ij}(C_{\mathbf{dl},ij})$

These variables determine the information flow within the network, regarding the used capacity of each link $(i,j) \in \mathbb{L}$ dedicated to UL (DL) traffic.

Auxiliary variables: link and subchannel activity indicators J_{ij}, J_f

The binary variables $J_{ij} \in \{0,1\}$ indicate the usage of the link $(i,j) \in \mathbb{L}$, where the binary variable $J_f \in \{0,1\}$ indicates the activeness of a frequency subchannel. A wireless link (subchannel) is active iff the transmit power associated with any of the associated subchannels (links) is non-zero.

5.3.2 Network cost model

The main required expenditures for the successful function of the wireless backhaul network can be expressed into the following three parts:

Power consumption

The cost of power can be formulated as $W_p \sum_{(i,j)\in\mathbb{L}} \sum_{f\in\mathbb{F}} X_{ij,f}$, where W_p is the price of power. Note that the value of W_p may be chosen with the direct consideration of the energy market price or with an extra emphasis on energy saving in order to reduce the consequent CO_2 emissions, which is a rising criteria for the design of wireless networks [189, 190].

Wireless links

The establishment of the wireless links is considered as one of the main capital expenditure (CAPEX) of a wireless backhaul network, including the establishment of directive antennas suitable for backhaul links, as well as the corresponding transmit and receive chains. This can be expressed as $W_l \sum_{(i,j)\in\mathbb{L}} J_{ij}$, where W_l is the overall cost of establishing a wireless link.

Spectrum usage

With almost all of the sub-6 GHz spectrum already utilized, obtaining a dedicated spectrum license is considered as a major cost of a wireless network, motivating research regarding efficient spectrum utilization as well as the usage of higher frequency bands [220,221]. The overall cost of spectrum can be expressed as $W_f \sum_{f\in\mathbb{F}\setminus\mathbb{F}_a} J_f$ where W_f represent the cost of spectrum for each frequency subchannel dedicated to backhaul.

Consequently, the collective network cost is expresses in relation to the decision variables as

$$\mathcal{V}\left(\mathbb{P},\mathbb{J}_L,\mathbb{J}_F\right) = W_p \sum_{(i,j)\in\mathbb{L}} \sum_{f\in\mathbb{F}} X_{ij,f} + W_l \sum_{(i,j)\in\mathbb{L}} J_{ij} + W_f \sum_{f\in\mathbb{F}\setminus\mathbb{F}_a} J_f. \tag{5.3}$$

5.3.3 Constraints

Formulation of the system constraints are essential in order to ensure a feasible solution; considering the operational limits, e.g., maximum transmit power, as well as the service requirements, e.g., successful transportation of the required UL and DL traffic under an acceptable delay range.

Auxiliary variables

The value of the defined auxiliary variables are inferred from the main decision variables $X_{ij,f}$, via the imposition of the following constraints:

$$\begin{aligned}
&\text{C0:} \quad X_{ij,f} \geq 0, \forall (i,j) \in \mathbb{L},\ f \in \mathbb{F},\\
&\text{C1:} \quad \sum_{f\in\mathbb{F}} X_{ij,f} \ \leq J_{ij}\tilde{P}_{\max},\ J_{ij} \in \{0,1\},\ \forall (i,j) \in \mathbb{L},\\
&\text{C2:} \quad \sum_{(i,j)\in\mathbb{L}} X_{ij,f} \leq J_f \tilde{P}_{\max},\ J_f \in \{0,1\},\ \forall f \in \mathbb{F},
\end{aligned}$$

where C0 enforces the domain of the power values, and $\tilde{P}_{\max}$ is any arbitrary upper bound on the total network power consumption, e.g., $\tilde{P}_{\max} = \sum_{i\in\mathbb{N}} P_{\max,i}$. The value of J_{ij} (J_f) is 1 if any of the corresponding power values are non-zero. Moreover, they are

forced to 0, if the corresponding link (frequency subchannel) is inactive, to reduce the cost function.

Transmit power constraints

The per-link power constraint as well as the constraint on the power budget at each node are respectively formulated as

$$\text{C3:} \quad \sum_{f\in\mathbb{F}} X_{ij,f} \leq P_{\max,ij}, \quad \forall (i,j) \in \mathbb{L},$$
$$\text{C4:} \quad \sum_{(i,x)\in\mathbb{L}} \sum_{f\in\mathbb{F}} X_{ix,f} \leq P_{\max,i}, \quad \forall i \in \mathbb{N},$$

see Subsection 5.2.1.

Average delay constraint

Related to many applications, latency is considered as an important feature of communication quality in the context of next generation communication systems [226]. The delay associated with the transfer of information from (to) the core network to (from) the backhaul nodes is dominated by the processing delay, see Subsection 5.2.1. In this regard, the average network latency is formulated in relation to the per-node delay as

$$\text{C5:} \quad \frac{\sum_{i\in\mathbb{N}} d_i \sum_{(i,x)\in\mathbb{L}} C_{\mathcal{X},ix}}{\sum_{i\in\mathbb{N}} R_{\mathcal{X},i}} \leq \bar{d}_{\mathcal{X}}, \quad \mathcal{X} \in \{ul, dl\},$$

where $\bar{d}_{ul}$ ($\bar{d}_{dl}$) is the tolerable average UL (DL) delay.

Interference threshold on access network

The coexistence of the backhaul and access network is conditioned on complying with the tolerable collective interference threshold $I_{\text{th},l,f}$, see Subsection 5.2.1. This is expressed as

$$\text{C6:} \quad \sum_{(i,j)\in\mathbb{L}} \Omega_{ij,l,f} X_{ij,f} \leq I_{\text{th},l,f}, \quad \forall f \in \mathbb{F}_a,\ l \in \mathbb{N}.$$

Link information flow constraint

The physical information capacity on each link, including the wired and wireless connections, need to be sufficient for the dedicated UL and DL information rates, i.e., $C_{\text{ul},ij}, C_{\text{dl},ij}$. This is expressed as

$$\text{C7:} \quad C_{\text{ul},ij} + C_{\text{dl},ij} \leq C_{0,ij} + \sum_{f \in \mathbb{F}} C_{ij,f}, \quad \forall (i,j) \in \mathbb{L},$$

where $C_{ij,f}$ is related to the other variables from (5.2), and $C_{0,ij}$ indicates the available link capacity via wired technologies.

Network information flow constraint

The preservation of the network information flow, separately at the root nodes and non root nodes are formulated as

$$\begin{aligned}
\text{C8:} \quad & R_{\text{ul},i} = \sum_{(i,x) \in \mathbb{L}} C_{\text{ul},ix} - \sum_{(y,i) \in \mathbb{L}} C_{\text{ul},yi}, \quad \forall i \in \mathbb{M}, \\
\text{C9:} \quad & R_{\text{dl},i} = \sum_{(x,i) \in \mathbb{L}} C_{\text{dl},xi} - \sum_{(i,y) \in \mathbb{L}} C_{\text{dl},iy}, \quad \forall i \in \mathbb{M}, \\
\text{C10:} \quad & \sum_{i \in \mathbb{M}} R_{\text{ul},i} = \sum_{i \in \mathbb{R}} \sum_{(j,i) \in \mathbb{L}} C_{\text{ul},ji}, \\
\text{C11:} \quad & \sum_{i \in \mathbb{M}} R_{\text{dl},i} = \sum_{i \in \mathbb{R}} \sum_{(i,j) \in \mathbb{L}} C_{\text{dl},ij},
\end{aligned}$$

where C8-9 indicate the flow conservation at each node, and C10-11 represent the conservation of the information over the network.

5.3.4 Network planning: an MILP model

In this part we provide an MILP framework, addressing a minimum cost wireless backhaul network design. The corresponding optimization problem is formulated as

$$\underset{\mathbb{P}, \mathbb{C}_U, \mathbb{C}_D, \mathbb{J}_L, \mathbb{J}_F}{\text{minimize}} \; \mathcal{V}(\mathbb{P}, \mathbb{J}_L, \mathbb{J}_F) \quad \text{s.t. C0-C11}, \tag{5.4a}$$

where the sets $\mathbb{P}, \mathbb{C}_U, \mathbb{C}_D, \mathbb{J}_L, \mathbb{J}_F$ represent the decision variables, see Table 5.1. It is observed that the cost function, as well as the constraints C0-C6 and C8-C11 comply with the intended mixed linear structure. However, the above problem is not an MILP due to the non-linear constraint C7. In order to observe this, we recall from (5.2) that the achievable information rate at each link is related to the power of the desired and interfering links as

$$C_{ij,f} = f_1(\mathbb{P}) - f_2(\mathbb{P}), \tag{5.5}$$

where

$$f_1(\mathbb{P}) := B\log\left(\sum_{(l,k)\in\{\mathbb{L}\}} \Gamma_{ij,lk,f} X_{lk,f} + W_{ij,f}\right), \tag{5.6}$$

$$f_2(\mathbb{P}) := B\log\left(\sum_{(l,k)\in\{\mathbb{L}\setminus(i,j)\}} \Gamma_{ij,lk,f} X_{lk,f} + W_{ij,f}\right), \tag{5.7}$$

which holds a difference of concave functions over the decision variables $\mathbb{P}$. Unfortunately, this formulation is challenging for the standard numerical solvers due to *i)* the non-convexity of the resulting feasible set in C7, and *ii)* the logarithmic concave-convex expressions. In order to comply with the intended MILP framework, we undertake three steps. Firstly, we introduce the achievable link capacity $C_{ij,f}$ as an auxiliary variable in the optimization and directly impose (5.5) as a constraint, thereby linierizing the constraint set C0-C11. Secondly, the equality in (5.5) is relaxed as an inequality constraint, however, it is easily verified that the constraint will be tight for an optimal system design, resulting in zero relaxation gap[2]. And third, we apply linear conservative approximations on the non-linear terms f_1 and f_2. In this respect, the logarithmic term f_1 is approximated as a piecewise linear function, i.e., approximating the concave expression as a maximum of multiple affine functions, denoted as $\mathcal{L}_p\left(\mathbb{P};\mathbb{P}_0\right)$, such that

$$\mathcal{L}_p\left(\mathbb{P};\mathbb{P}_0\right) \leq f_1(\mathbb{P}), \quad \mathcal{L}_p\left(\mathbb{P}_0;\mathbb{P}_0\right) = f_1(\mathbb{P}_0). \tag{5.8}$$

Moreover, the logarithmic term f_2 is approximated as an over-estimating affine, denoted as $\mathcal{L}\left(\mathbb{P};\mathbb{P}_0\right)$, such that

$$\mathcal{L}\left(\mathbb{P};\mathbb{P}_0\right) \geq f_2(\mathbb{P}), \quad \mathcal{L}\left(\mathbb{P}_0;\mathbb{P}_0\right) = f_2(\mathbb{P}_0), \tag{5.9}$$

which is directly obtained via the first-order Taylor's expansion at the point $\mathbb{P}_0$[3]. Note that the collective approximation generates a tight and piecewise affine function, which bounds the original nonlinear function from above, see (*b*). The wireless link capacity constraint can be hence satisfied by imposing

$$C_{ij,f} \leq \mathcal{L}_p\left(\mathbb{P}_0,\mathbb{P}\right) - \mathcal{L}\left(\mathbb{P}_0,\mathbb{P}\right), \tag{5.10}$$

where $\mathbb{P}_0$ is the point of approximation. Note that the satisfaction of (5.10) consequently ensures that the wireless link realizes the capacity value $C_{ij,f}$, due to the proposed conservative approximation. However, this may result in an inefficient solution, due to the approximation gap[4]. In this regard, an iterative update is applied, where the

[2]The proof is obtained via contradiction; if for an optimal design of network parameters the constraint is not tight for the link (i,j) and at the subchannel f, then the transmit power value $X_{ij,f}$ can reduced until the constraint is tight. This will reduce the objective (cost), while does not violate any of the design constraints.

[3]A tight affine approximation of a convex (concave) function obtained via Taylor's approximation, is also a global lower (upper) bound [231].

[4]A large deviation of approximated piecewise linear function $\mathcal{L}_p - \mathcal{L}$ with the original nonlinear expression results in the under-utilization of the wireless link capacity, and consequently additional costs.

obtained variable set $\mathbb{P}$ at each iteration is set as the approximation point, i.e., $\mathbb{P}_0$, for the next design iterations. The minimum-cost network design problem can be hence formulated as

$$\underset{\mathbb{V}^{[m]}}{\text{minimize}} \quad \mathcal{V}\left(\mathbb{P}^{[m]}, \mathbb{J}_L^{[m]}, \mathbb{J}_F^{[m]}\right) \tag{5.11a}$$

$$\text{s.t.} \quad C_{ij,f} \leq \mathcal{L}_p\left(\mathbb{P}^{[m]}; \mathbb{P}^{[m-1]}\right) - \mathcal{L}\left(\mathbb{P}^{[m]}; \mathbb{P}^{[m-1]}\right), \quad \forall (i,j) \in \mathbb{L}, \quad \forall f \in \mathbb{F}, \tag{5.11b}$$

$$\text{C0-C11}, \tag{5.11c}$$

where

$$\mathbb{V}^{[m]} := \left\{\mathbb{P}^{[m]}, \mathbb{C}_U^{[m]}, \mathbb{C}_D^{[m]}, \tilde{\mathbb{C}}^{[m]}, \mathbb{J}_L^{[m]}, \mathbb{J}_F^{[m]}\right\}, \tag{5.12}$$

the set $\tilde{\mathbb{C}}$ represents the sets of the variables $C_{ij,f}$, and m denotes the iteration index, see Algorithm 10. The algorithm stops as a stable set of decision variables is obtained, or a maximum number of iterations is expired.

Numerical implementation

As intended, the obtained optimization framework (5.11) is an MILP in each iteration. Note that due to the combinatorial structure, such problems are not convex, and hence the popular interior point methods may not be applied [231]. However, efficient variations of branch and bound methods [167] have been recently developed and implemented in the framework of the standard numerical solvers, e.g., CPLEX, Gurobi, resulting in efficient numerical solutions for the MILP problems with large dimensions.

Algorithm initialization

The algorithm starts by activating all feasible physical links, frequency sub channels, as well as the maximum power consumptions at all wireless links, respecting the constraints C0-2. Note that this initialization choice corresponds to a strong link and network capacity. However, it corresponds with the maximum utilization of the network resources, resulting in the maximum cost.

Convergence

The convergence behavior of the algorithm is of interest, due to the proposed iterative cost reduction. Due to the application of the branch and bound update by the numerical solver, the solution experiences a non-decreasing change in each iteration, within a fixed tolerance region. Note that such monotonic reduction of the cost function holds at the internal solver iterations, as well as the external iterations by updating the approximations, see Algorithm 10, step 4. This results in a necessary algorithm convergence, due

to the fact that the problem objective is bounded from below[5]. Further analysis regarding the algorithm convergence behavior and computational complexity is conducted via numerical simulations in Section 5.4.

Algorithm 10 MILP-based minimum cost network planning.

$m \leftarrow 0$; $\mathbb{P}^{[0]} \leftarrow$ Subsection 5.3.4; ▷ initialization
repeat
  $m \leftarrow m + 1$;
  $\mathbb{P}^{[m]}, \mathbb{C}_U^{[m]}, \mathbb{C}_D^{[m]}, \tilde{\mathbb{C}}^{[m]}, \mathbb{J}_L^{[m]}, \mathbb{J}_F^{[m]} \leftarrow$ solve MILP (5.11);
until a stable point, or a maximum number of m reached
return $\left\{\mathbb{P}^{[m]}, \mathbb{C}_{UL}^{[m]}, \mathbb{C}_{DL}^{[m]}, \mathbb{J}_L^{[m]}, \mathbb{J}_F^{[m]}\right\}$

5.3.5 Network re-tuning: an SIA model

The joint consideration of the power allocation on wireless links as well as the frequency and topology planning is expected to be gainful as the aforementioned factors jointly impact the network interference pattern and information flow. In this regard, a full scale design of the wireless backhaul network is proposed in the previous part, assuming the availability of the accurate network information and integrating the FD capability. In this part, we propose a methodology to re-tune the network operation by adjusting the transmit power at the wireless links, assuming that the links, as well as the operating frequencies are already established. In particular, this approach enables the network to adapt to slight changes, e.g., change in the channel situations due to weather and temperature fluctuations, a slight increase or decrease in the required information rate, and the occasional degradation of the SIC quality. Moreover, contrary to usual planning strategies which focus on the worst-case network requirements, the provided flexibility results in a higher efficiency and reduced cost, e.g., by reducing the transmit power at a wireless link when the data traffic is low. And finally, the reduced setup complexity, as a result of the fixed network topology, is constructively used to obtain a computationally more efficient design.

Given an active set of links and frequency subchannels, the problem of adjusting the transmit powers at the wireless links is formulated as

$$\underset{\mathbb{P},\mathbb{C}_{UL},\mathbb{C}_{DL}}{\text{minimize}} \quad \sum_{(i,j)\in\mathbb{L}} \sum_{f\in\mathbb{F}} X_{ij,f}, \quad \text{C0}, \quad \text{C3-C11}. \tag{5.13}$$

It is observed that due to the elimination of the binary variable sets $\mathbb{J}_L, \mathbb{J}_F$, the problem is simplified to a non-linear program over a continuous domain, hence, the utilization of MILP-based solvers is not necessary. However, the problem (5.13) it is not a

[5]Please note that the convergence is obtained in the sense that the objective reaches a stable value with an arbitrarily small tolerance margin. Although the resulting optimization variables need not to converge, the potentially different obtained solutions are equally favorable, i.e., they are all feasible and result in the same objective value.

convex optimization problem due to the constraint C7. In this regard, we introduce an SIA framework [196], where the non-convex feasible region constructed by C7 is inner-approximated in each iteration as a convex set. In this regard, we follow the same procedure as implemented for (5.11), i.e., introduction and relaxation of (5.5) as an inequality constraint, and upper-approximation of f_2 via (5.9). However, the term f_1 can be directly applied since it does not violate the convexity. The approximated optimization problem is hence formulated as

$$\underset{\mathbb{P}^{[m]},\tilde{\mathbb{C}}^{[m]},\mathbb{C}_U^{[m]},\mathbb{C}_D^{[m]}}{\text{minimize}} \quad \sum_{(i,j)\in\mathbb{L}} \sum_{f\in\mathbb{F}} X_{ij,f} \tag{5.14a}$$

$$\text{s.t.} \quad C_{ij,f} \leq f_1\left(\mathbb{P}^{[m]}\right) - \mathcal{L}\left(\mathbb{P}^{[m]};\mathbb{P}^{[m-1]}\right), \ \ \forall (i,j)\in\mathbb{L}, \ \ \forall f\in\mathbb{F}, \tag{5.14b}$$

$$\text{C0}, \ \ \text{C3-C11}, \tag{5.14c}$$

where m denotes algorithm iteration. The iterations of (5.14) are continued until convergence, or a maximum number of algorithm iterations is expired, see Algorithm 11 for a detailed procedure.

Algorithm 11 SIC-based network re-tuning.

$m \leftarrow 0$; $\mathbb{P}^{[0]} \leftarrow$ Subsection 5.3.5; ▷ initialization
repeat
  $m \leftarrow m+1$;
  $\mathbb{P}^{[m]} \leftarrow$ solve (5.13);
until a stable point, or a maximum number of m reached
return $\left\{\mathbb{P}^{[m]}, \mathbb{C}_U^{[m]}, \mathbb{C}_D^{[m]}\right\}$

Algorithm initialization

Since the re-tuning algorithm is intended to operate on an existing network, the current state of the network including the transmit power of the wireless links is used as the initial point. In case such initial point may not be obtained, a similar initialization as introduced in Subsection 5.3.4 can be used.

Convergence and numerical implementation

Due to the convexity of the approximated problem (5.14) in each iteration, the optimum solution can be obtained via standard numerical solvers for convex problems, e.g., SeDuMi [232], SDPT3 [233], employing efficient interior point methods. Moreover, it is easily verified that the proposed linear approximation satisfies the set of properties established in [196, Theorem 1] for smooth problems, i.e., tightness and globally lower bound properties. Together with the fact that the approximated problem at each step is solved to the optimality, it certifies a necessary convergence to a stationary point of the original non-convex problem (5.13).

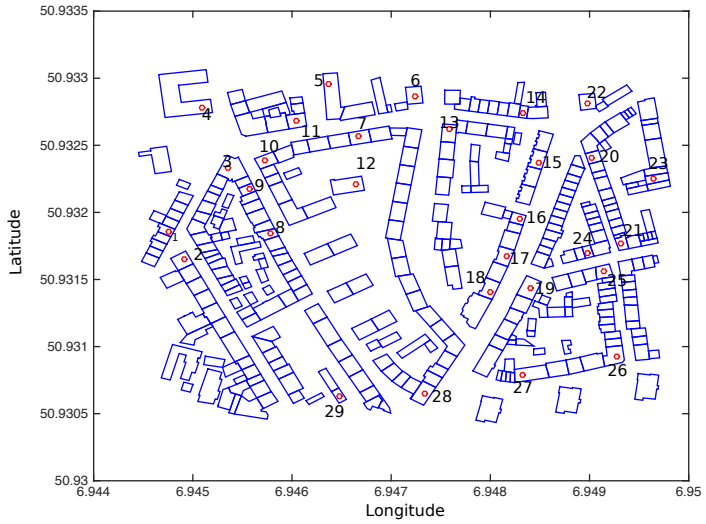

Figure 5.5: The simulated environment from Aachen city map. Red dots represent the location of the backhaul nodes, put on top of the rooftops, whereas blue squares represent the body area of the buildings.

5.4 Simulation Results

In this part, we evaluate the impact of the proposed designs in terms of the total network cost, benefiting from the FD capability at the wireless links, via numerical simulations[6]. The simulated network is obtained from the city map of Aachen, Germany, see Fig. 5.5, employing our developed wave propagation simulator [230], in combination with the urban micro-cell scenario from WINNER II model [234]. The antenna type is chosen with directivity gain of 13 dBi and directivity angle of 15 degrees in accordance with the European Standard [235]. The evaluations of the channel properties are carried by keeping the center frequency of 5 GHz and with bandwidth of each frequency sub-channel of 20 MHz. The planning algorithm determines the wireless links to be established, as well as the operating power and frequency bands at each link. Unless otherwise is stated, the following values define the default setup: $W_{ij,f} = -97$ dBm, $B = 20$ MHz, $P_{\max,ij} = 30$ dBm, $P_{\max,i} = 30$ dBm, $R_{\text{req}} = R_{\text{ul},i} = R_{\text{dl},i} = 100$ Mbits/sec, $|\mathbb{N}| = 23$, $|\mathbb{F}| = 8$, $|\mathbb{L}| = 100$, $C_{0,ij} = 0$, $I_{\text{th},k,f} = 0$, $d_i = 0$. The self-interference cancellation is assumed to be perfect, i.e., $\rho_{\text{si}} = \Gamma_{ij,li,f} = 0$. The network cost model is set following [236, 237], as $W_p = 1$, $W_l = 20$, $W_f = 10$.

In Fig. 5.6 (a), the average convergence behavior of the proposed MILP model is de-

[6]I would like to thank my colleague M.Sc. Jose Angel Leon Calvo for providing the environment-related data, and extracting the simulated channel statistics from the city map of Aachen. Moreover, I would like to thank my former students M.Sc. Praveen Sirvi, and M.Sc. Santosh Prahalada Narasimha for their constructive help in the numerical simulations for Section 5.3.4.

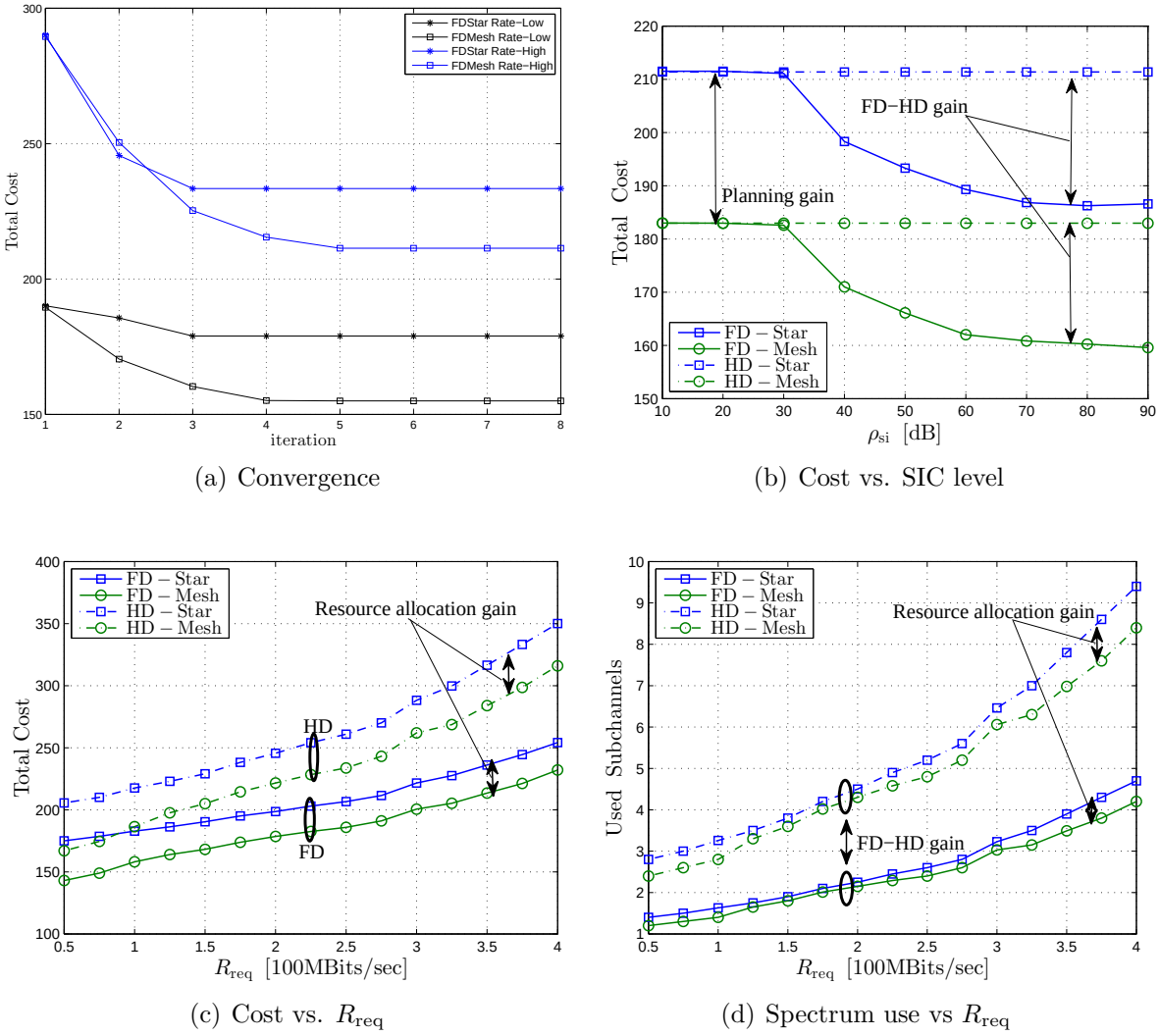

(a) Convergence

(b) Cost vs. SIC level

(c) Cost vs. R_{req}

(d) Spectrum use vs R_{req}

Figure 5.6: The algorithm convergence behavior (a), and resulting network cost for different values of R_{req} and ρ_{si}.

picted. Due to the proposed iterative improvement, the convergence behavior is interesting as an indication of the algorithm complexity as well as the achievable iterative improvement. The star topology indicates the case where each node is connected to a root node via a direct wireless link, whereas the mesh topology represents the result of the design proposed in Algorithm 10. Furthermore, the convergence curves indicate the different regimes regarding the backhaul rate requirements, i.e., $R_{\text{req}} = 100$, indicated as 'Rate-Low', and $R_{\text{req}} = 200$, indicated as 'Rate-High'. A monotonic decrease in cost is observed, where the convergence is obtained within $3 - 8$ iterations.

In Figs. 5.6 (b)-(c) the impact of the rate demand is depicted on the collective network cost. It is observed that a higher rate demand results in a higher cost. Moreover, it is observed that the application of FD capability, together with the proposed joint link/frequency planning results in the usage of less frequency subchannels, thereby

reducing the total cost compared to the half-duplex counterparts by up to $10-30\%$ depending on the traffic load.

The impact of the SIC quality on the overall network cost is depicted in Fig. 5.6 (d). It is observed that the FD gain is reduced as the SIC quality is degraded and reaches the performance of the network with half-duplex links for a poor SIC condition.

Table 5.2: Required CPU Time

$\|\mathbb{N}\|$	$\|\mathbb{L}\|$	$\|\mathbb{F}\|$	Problem Size	Execution Time in seconds
8	12	6	72	360 (MILP) 1.2 (re-tunning)
15	24	6	144	1020 (MILP) 5.6 (re-tunning)
23	40	10	400	10200 (MILP) 20.1 (re-tunning)
30	120	10	1200	30050 (MILP) 262.8 (re-tunning)

In Fig. 5.7, the optimized network topology is depicted for different cost models for a network with $\mathbb{M}=1$ and $\mathbb{R}=1$. It is observed that different network topologies result in a different power-link usage trade-off. As expected, the strategy with the focus on the cost of power prefers the establishment of a higher number of links, compared to the star topology which provides connectivity through the network with the minimum number of the wireless links.

The performance of the proposed iterative network re-tuning is depicted in Fig. 5.8 (a)-(c), for different levels of fluctuations in the channel, noise, and rate requirements. The algorithm starts with the outcome of the planning given in Algorithm 10 as the initial point, however, iteratively adjusts the transmit power to comply with the new network conditions. In particular, the ratio α_{R} indicates the level by which the specific parameters is scaled. Note that due to the infeasibility of the given initial point from the Algorithm 10, as a result of the scaled parameters, the network power consumption may raise at the initial re-tunning iteration. Nevertheless, the network power consumption is decreased monotonically after the second iteration, and converges in 3-6 iterations. Please note that the benefits of enabling the proposed retunning method is twofold. Firstly, it obtains a feasible network operation point, adjusting to the new rate requirements, noise, or channel conditions. Secondly, it enables the network to save energy, by opportunistically benefiting from the reduced rate demand, when network traffic load is not high.

In Table 5.2 the average per-iteration CPU time is reported for both Algorithms 10 and 10, for different node cluster sizes[7]. It is observed that a larger problem dimen-

[7]The simulations are performed on a Linux Debian system with processor Intel Core i7 – 3770S CPU @3.10GHz X 4, RAM of 8GB. The version 2016b of MATLAB was used along with CVX 2.1 and Gurobi 7.0 Solver

sion, i.e, $d := |\mathbb{L}| \times |\mathbb{F}|$, results in a higher computational time for both algorithms, however, remains below 10 Hrs for $d \leq 1200$ on a standard user processor. Moreover, due to the proposed SIA framework, the Algorithm11 results in a significantly smaller computational load, due to the efficient convex problem structure.

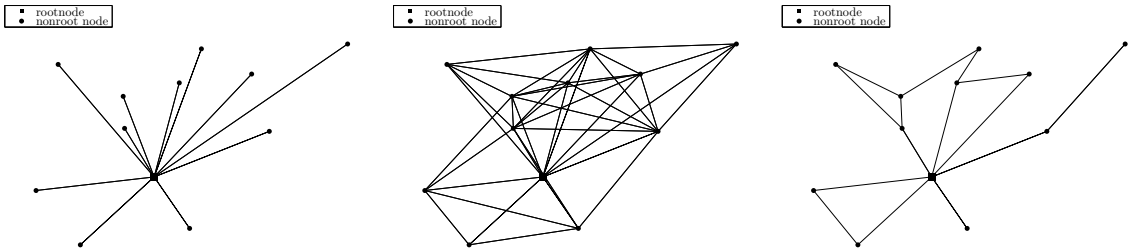

(a) $W_p = 0$, $W_l = 10$ (b) $W_p = 10$, $W_l = 1$ (c) $W_p = 10$, $W_l = 10$

Figure 5.7: Optimized network topology for different cost models. Different network topologies result in different power-link usage trade-offs.

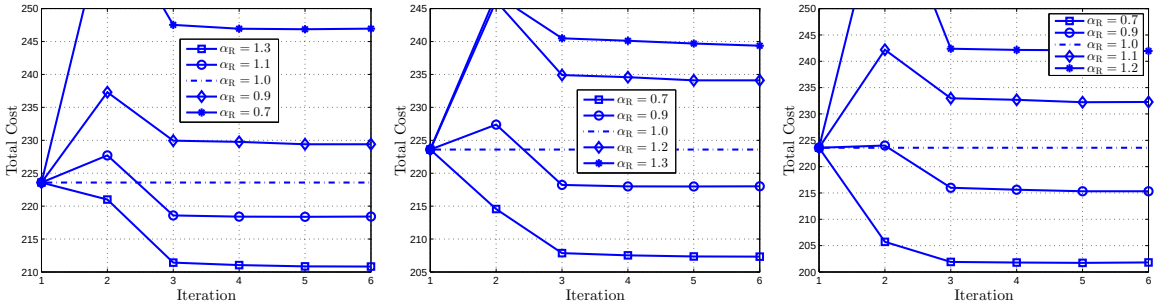

(a) channel re-tunning (b) noise re-tunning (c) rate re-tunning

Figure 5.8: Iterative network re-tuning. The network reacts to the small changes in the rate requirements and the channel and noise conditions by adjusting the transmit power at each link.

5.5 Conclusion

With almost all of the below 6 GHz spectrum already assigned, and the 1000-fold expected increase of data traffic over the next decade, the need for spectral efficient solutions is apparent in the context of cellular wireless communication systems. In the first part, an overview on the application of FD capability in the radio access network is given, where UL and DL connections are scheduled on the same channel, aiming at a higher spectral efficiency. It is observed that the existence of multiple transmissions at the same channel lead to multiple additional interference paths, which calls for advanced resource allocation and interference control mechanisms, especially

for an FD-enabled multi-cell system. Coordination among the infrastructure nodes is observed to be an effective method to attenuate the additional interference paths, however, resulting in an increased backhaul overhead. In the second part, application of FD wireless links is studied as a spectrum-saving mechanism for the wireless backhaul networks. In particular, the coexistence of multiple wireless links at the same channel resource is studied, utilizing an environment-aware interference management scheme, leading to a reduced overall cost. Moreover, a reactive network re-tuning method is proposed which reacts to small changes in the network data, e.g., QoS requirements or channel conditions, via transmit power adjustment on each wireless link. Numerical simulations suggest that for a dense urban deployment, the proposed methodologies result in reduction in the overall network cost.

6 Conclusion

This thesis covers a variety of resource allocation problems, in regard to the application of FD capability to different wireless communication scenarios. The main results and findings of this thesis, as well as a brief list of the promising future research directions are summarized in the following.

6.1 Summary

In Chapter 2, a bidirectional and multi-carrier wireless communication system is studied between two FD transceivers. The main findings of this chapter can be summarized as follows:

- A multiple-antenna beamforming together with a multi-carrier communication strategy can be effectively used to control the impact of interference. The communication in opposite directions can be interchangeably accommodated on the same channel resource (resulting in a higher spectral efficiency), or on orthogonal subcarriers (resulting in a reduced interference).

- Non-linear hardware distortions lead to residual self-interference and inter-carrier leakage. In particular, this effect is significant for an FD system due to the strong SI signal.

- A distortion-aware modeling and design is essential for the gainful use of FD transceivers in the studied multi-carrier FD bidirectional setup.

In Chapter 3, a MIMO FD relaying setup is studied. The main findings of this chapter can be summarized as follows:

- By jointly considering the impact of hardware distortions at the receive and transmit chains, we observe an inter-dependent behavior of the relay transmit covariance and the RSI covariance in an AF-FD relay, i.e., the distortion loop effect.

- As relay dynamic range decreases, the aforementioned distortion-loop results in a performance disadvantage for the AF-FD, compared to the DF-FD relaying, where the aforementioned inter-dependency does not exist due to decoding.

- Multiple-antenna linear transmit and receive strategies appear as an effective approach in order to control the impact of distortion. In particular, for a system with a small thermal noise variance or high transceiver distortion, the application of a distortion-aware design is essential.

In Chapter 4, the SEE of a MIMOME wiretap channel is studied, in terms of the securely communicated bits-per-Joule, where the legitimate receiver is equipped with FD capability. The main findings of this chapter can be summarized as follows:

- FD transceivers were previously shown to enhance the system secrecy capacity, compared to the HD counterparts, by enabling a simultaneous jamming and information exchange. However, it is observed that for a wide range of the system conditions, they result in only a marginal gain regarding the system SEE. This is due to the additional power consumption for an FD system, due to the SI cancellation and jamming, as well the degrading effect of the RSI.

- The observed SEE gain, due to the application of an FD jammer, becomes notable for the scenarios with a small distance between the FD node and the eavesdropper, and for a system with a high SNR condition, when the SI can be efficiently mitigated.

- The joint utilization of FD capability, both on Alice and Bob for jamming and bidirectional information exchange, shows a better SEE performance compared to the system with a single FD transceiver. This is grounded on the fact that the FD jamming power is reused for both communication directions, resulting in a power-efficient jamming. Moreover, the coexistence of two communication directions on the same channel may degrade Eve's decoding capability.

In Chapter 5, the gainful utilization of FD capability for cellular communication systems is investigated. The main findings of this chapter can be summarized as follows:

- Via the application of FD capability in the radio access network, UL and DL connections can be scheduled on the same channel, aiming at a higher spectral efficiency. However, it is observed that the coexistence of multiple transmissions at the same channel results in the emergence of new interference paths, calling for a strong interference control and resource optimization.

- Coordination among the infrastructure nodes is observed to be effective in controlling the impact of interference, and achieving a higher spectral efficiency. However, it results in a higher data traffic on the backhaul network.

- Utilization of FD capability on the wireless backhaul links, enables the coexistence of multiple links at the same channel. This results in a reduced overall network cost, however, calling for a smart interference management.

- Due to the static nature of the wireless backhaul links, estimation of the channel conditions can be accomplished using the available environment information together with a wave propagation simulator. Hence, the environment awareness

can be effectively utilized to act as a basis for network planning and resource allocation, resulting in a reduced overall network cost.

6.2 Outlook

The results of this thesis can be extended in a variety of new directions. In Chapter 2 the impact of hardware impairments leading to inter-carrier leakage is studied for a bidirectional MIMO FD system. Due to the significance of the role of hardware impairments in the systems with large antenna arrays, as well as the recent advancements to enable FD operation for mMIMO systems, it is relevant to extend the obtained methodologies to such scenarios. This is in particular relevant for a joint channel and beam/power scheduling in a multi-user mMIMO setup. Moreover, the obtained design frameworks in Chapter 2, addressing the rate maximization problems, can be extended into the multi-hop communication setups.

In Chapter 3, the performance of an AF-FD relaying system is studied, where the FD relay is equipped with multiple antennas. However, the studied setup is limited to the scenarios where source is equipped with a single antenna. The provided framework for performance analysis can be similarly utilized to extend the setup supporting a multiple-antenna source. Moreover, the perfect CSI assumption shall be removed, by including the impact of CSI uncertainty in the performance analysis.

In Chapter 4, the performance of a MIMOME wiretap channel is investigated in terms of the secrecy energy efficiency. It is gainful to extend the proposed design frameworks for the objectives which jointly consider the system secrecy rate as well as the system SEE, or to jointly consider the non-secure information rate as well as the secrecy rate. Rate splitting concept can be applied in the latter case to enhance the resulting joint objective.

In Chapter 5, a radio resource allocation problem is studied, where FD capability is utilized in a wireless backhauling network. Moreover, a reactive re-tunning methodology is proposed in order to counteract the performance degradation as a result of network data uncertainty. It is beneficial to extend the proposed methodologies to also incorporate proactive robust measures, e.g., considering alternative information paths to avoid network breakdown as a result of a potential link failure. Moreover, due to the high computational complexity of the proposed solutions, simplified intuitive solutions can be used for initializing the numerical model. The numerical simulations shall be also extended to evaluate the impact of latency, and interference caused by the wireless backhaul links to the access network.

7 Appendix

7.1 Proof to Lemma 2.2.1

We start the proof with the characterization of the impact of distortion on the transmit chains. The proof to the receiver characterization is obtained similarly. The statistical independence properties at the frequency domain directly follows from the time domain statistical independence $e_{\mathrm{t},l}(t) \perp v_l(t)$, and $e_{\mathrm{t},l}(t) \perp e_{\mathrm{t},l'}(t)$, and the linear nature of the transformation in (2.10). The Gaussian and zero-mean properties similarly follow for $e^k_{\mathrm{t},l}$ as a linearly weighted sum of the zero-mean Gaussian values $e_{\mathrm{t},l}(mT_s)$. The variance of $e^k_{\mathrm{t},l}$ can be hence obtained as

$$\mathbb{E}\left\{\left|e^k_{\mathrm{t},l}\right|^2\right\} = \mathbb{E}\left\{\frac{1}{K}\left(\sum_{m=0}^{K-1} e_{\mathrm{t},l}(mT_{\mathrm{s}})e^{-\frac{j2\pi mk}{K}}\right)\left(\sum_{n=0}^{K-1} e^*_{\mathrm{t},l}(nT_{\mathrm{s}})e^{\frac{j2\pi nk}{K}}\right)\right\} \tag{7.1}$$

$$= \frac{1}{K}\sum_{m=0}^{K-1}\sum_{n=0}^{K-1}\mathbb{E}\left\{e_{\mathrm{t},l}(mT_{\mathrm{s}})e^*_{\mathrm{t},l}(nT_{\mathrm{s}})\right\}e^{-\frac{j2\pi(m-n)k}{K}} \tag{7.2}$$

$$= \kappa_l\mathbb{E}\left\{|v_l(t)|^2\right\} \tag{7.3}$$

$$= \frac{\kappa_l}{K}\sum_{m=1}^{K}\mathbb{E}\left\{|v_l^m|^2\right\} \tag{7.4}$$

where (7.1) is obtained via direct application of (2.10), and (7.3) is obtained from (2.6), and the statistical independence of $e_{\mathrm{t},l}$ at the subsequent time samples from (2.7). The identity (7.4) follows from the Parseval's theorem on the energy conversation over orthonormal Fourier basis.

7.2 Proof to the Lemma 3.4.1

Let $\mathbf{W}$ and $\mathbf{z}$ be the fixed (given) relay amplification and receive filter, respectively. From (3.15)-(3.21), the SDNR at the destination can be written as a function of P_{s}

$$\mathrm{SDNR}(P_{\mathrm{s}}) = \frac{\alpha_1 P_{\mathrm{s}}}{\alpha_2 P_{\mathrm{s}} + \alpha_3}, \tag{7.5}$$

where $\alpha_1, \alpha_2, \alpha_3 \in \mathbb{R}^+$, such that

$$\begin{aligned}
\alpha_1 &:= \mathbf{z}^H \mathbf{H}_{\mathrm{rd}} \mathbf{W} \mathbf{h}_{\mathrm{sr}} \mathbf{h}_{\mathrm{sr}}^H \mathbf{W}^H \mathbf{H}_{\mathrm{rd}}^H \mathbf{z}, \quad \alpha_2 := \mathbf{q}\left(\mathbf{W}, \mathbf{z}\right) \mathrm{vec}\left(\mathbf{h}_{\mathrm{sr}} \mathbf{h}_{\mathrm{sr}}^H\right) + \mathbf{z}^H \mathbf{h}_{\mathrm{sd}} \mathbf{h}_{\mathrm{sd}}^H \mathbf{z} - \alpha_1, \\
\alpha_3 &:= \mathbf{z}^H \mathbf{z} \sigma_{\mathrm{nd}}^2 + \mathbf{q}\left(\mathbf{W}, \mathbf{z}\right) \mathrm{vec}\left(\sigma_{\mathrm{nr}}^2 \mathbf{I}_{M_{\mathrm{r}}}\right), \\
\mathbf{q}\left(\mathbf{W}, \mathbf{z}\right) &:= \left(\mathbf{z}^T \otimes \mathbf{z}^H\right) \left(\mathbf{H}_{\mathrm{rd}}^* \otimes \mathbf{H}_{\mathrm{rd}}\right) \mathbf{\Theta}\Big(\mathbf{W}, \mathbf{H}_{\mathrm{rr}}, \kappa, \beta\Big). \qquad (7.6)
\end{aligned}$$

It is observed, by taking the first and second order derivatives of the obtained function in (7.5), that SDNR is an increasing and concave function over P_{s}, which concludes the proof to the Lemma 3.4.1.

7.3 Equivalent Relay Transmit Distortion Channel Expression (3.35)

Via the application of $\mathbf{w}_{\mathrm{tx}}$, the collective received distortion power due to the relay transmission, here denoted as θ_1, is written as

$$\begin{aligned}
\theta_1 &= P_{\mathrm{r,max}} \kappa \mathrm{tr}\Big(\mathbf{H}_{\mathrm{rr}} \mathrm{diag}\left(\mathbf{w}_{\mathrm{tx}} \mathbf{w}_{\mathrm{tx}}^H\right) \mathbf{H}_{\mathrm{rr}}^H + \mathbf{H}_{\mathrm{rd}} \mathrm{diag}\left(\mathbf{w}_{\mathrm{tx}} \mathbf{w}_{\mathrm{tx}}^H\right) \mathbf{H}_{\mathrm{rd}}^H\Big) \\
&\quad + P_{\mathrm{r,max}} \beta \mathrm{tr}\Big(\mathrm{diag}\left(\mathbf{H}_{\mathrm{rr}} \mathbf{w}_{\mathrm{tx}} \mathbf{w}_{\mathrm{tx}}^H \mathbf{H}_{\mathrm{rr}}^H\right)\Big) \\
&= \sum_{i \in \mathbb{F}_{M_{\mathrm{t}}}} \sum_{X \in \{\mathrm{rr},\, \mathrm{rd}\}} P_{\mathrm{r,max}} \kappa \mathrm{tr}(\mathbf{H}_X \mathbf{\Gamma}_{M_{\mathrm{t}}}^i \mathbf{w}_{\mathrm{tx}} \mathbf{w}_{\mathrm{tx}}^H {\mathbf{\Gamma}_{M_{\mathrm{t}}}^i}^H \mathbf{H}_X^H) \\
&\quad + \sum_{i \in \mathbb{F}_{M_{\mathrm{r}}}} P_{\mathrm{r,max}} \beta \mathrm{tr}(\mathbf{\Gamma}_{M_{\mathrm{r}}}^i \mathbf{H}_{\mathrm{rr}} \mathbf{w}_{\mathrm{tx}} \mathbf{w}_{\mathrm{tx}}^H \mathbf{H}_{\mathrm{rr}}^H {\mathbf{\Gamma}_{M_{\mathrm{t}}}^i}^H) \\
&= \kappa P_{\mathrm{r,max}} \sum_{i \in \mathbb{F}_{M_{\mathrm{t}}}} \sum_{X \in \{\mathrm{rr},\, \mathrm{rd}\}} \left\| \mathbf{H}_X \mathbf{\Gamma}_{M_{\mathrm{t}}}^i \mathbf{w}_{\mathrm{tx}} \right\|_2^2 + \beta P_{\mathrm{r,max}} \sum_{i \in \mathbb{F}_{M_{\mathrm{t}}}} \left\| \mathbf{\Gamma}_{M_{\mathrm{r}}}^i \mathbf{H}_{\mathrm{rr}} \mathbf{w}_{\mathrm{tx}} \right\|_2^2 \\
&= P_{\mathrm{r,max}} \left\| \begin{bmatrix} \lfloor \sqrt{\kappa} \mathbf{H}_X \mathbf{\Gamma}_{M_{\mathrm{t}}}^i \mathbf{w}_{\mathrm{tx}} \rfloor_{i \in \mathbb{F}_{M_{\mathrm{t}}},\, X \in \{\mathrm{rr},\, \mathrm{rd}\}} \\ \lfloor \sqrt{\beta} \mathbf{\Gamma}_{M_{\mathrm{r}}}^i \mathbf{H}_{\mathrm{rr}} \mathbf{w}_{\mathrm{tx}} \rfloor_{i \in \mathbb{F}_{M_{\mathrm{r}}}} \end{bmatrix} \right\|_2^2 \\
&= P_{\mathrm{r,max}} \Bigg\| \underbrace{\begin{bmatrix} \lfloor \sqrt{\kappa} \mathbf{H}_X \mathbf{\Gamma}_{M_{\mathrm{t}}}^i \rfloor_{i \in \mathbb{F}_{M_{\mathrm{t}}},\, X \in \{\mathrm{rr},\, \mathrm{rd}\}} \\ \lfloor \sqrt{\beta} \mathbf{\Gamma}_{M_{\mathrm{r}}}^i \mathbf{H}_{\mathrm{rr}} \rfloor_{i \in \mathbb{F}_{M_{\mathrm{r}}}} \end{bmatrix}}_{=: \mathbf{H}_{\mathrm{D,tx}}} \mathbf{w}_{\mathrm{tx}} \Bigg\|_2^2,
\end{aligned}$$

where $\mathbf{\Gamma}_M^i$ is an $M \times M$ all-zero matrix, except for the i-th diagonal element equal to one, and $\mathbf{H}_{\mathrm{D,tx}}$ is viewed as the equivalent distortion channel (3.35).

7.4 Derivation of (3.42)-(3.43) and the Coefficients (3.44)-(3.48)

The desired signal power at the destination prior to the application of $\mathbf{z}$, here denoted as θ_2, can be calculated applying the known matrix equalities [155, Eq. (486), (487), (496)] as

$$\begin{aligned}\theta_2 &= P_{\mathrm{s}}\mathrm{tr}\left(\mathbf{H}_{\mathrm{rd}}\mathbf{W}\mathbf{h}_{\mathrm{sr}}\mathbf{h}_{\mathrm{sr}}^H\mathbf{W}^H\mathbf{H}_{\mathrm{rd}}^H\right)\\ &= \omega P_{\mathrm{s}}\mathrm{tr}\left(\mathbf{H}_{\mathrm{rd}}\mathbf{w}_{\mathrm{tx}}\mathbf{w}_{\mathrm{rx}}^H\mathbf{h}_{\mathrm{sr}}\mathbf{h}_{\mathrm{sr}}^H\left(\mathbf{w}_{\mathrm{tx}}\mathbf{w}_{\mathrm{rx}}^H\right)^H\mathbf{H}_{\mathrm{rd}}^H\right)\\ &= \omega P_{\mathrm{s}}\mathbf{d}_{M_{\mathrm{t}}}^T\Big(\left(\mathbf{H}_{\mathrm{rd}}^*(\mathbf{w}_{\mathrm{tx}}\mathbf{w}_{\mathrm{rx}}^H)^*\right)\otimes\left(\mathbf{H}_{\mathrm{rd}}\mathbf{w}_{\mathrm{tx}}\mathbf{w}_{\mathrm{rx}}^H\right)\Big)\mathrm{vec}\left(\mathbf{h}_{\mathrm{sr}}\mathbf{h}_{\mathrm{sr}}^H\right)\\ &= \omega P_{\mathrm{s}}\mathbf{d}_{M_{\mathrm{t}}}^T\left(\mathbf{H}_{\mathrm{rd}}^*\otimes\mathbf{H}_{\mathrm{rd}}\right)\tilde{\mathbf{W}}\mathrm{vec}\left(\mathbf{h}_{\mathrm{sr}}\mathbf{h}_{\mathrm{sr}}^H\right) = \omega a_{\mathrm{d}},\end{aligned} \tag{7.7}$$

where a_{d} and $\mathbf{d}_{M_{\mathrm{t}}}$ are respectively defined in (3.44) and immediately after (3.48), and $\tilde{\mathbf{W}} := (\mathbf{w}_{\mathrm{tx}}\mathbf{w}_{\mathrm{rx}}^H)^*\otimes(\mathbf{w}_{\mathrm{tx}}\mathbf{w}_{\mathrm{rx}}^H)$. Similarly, following (3.13)-(3.16) and the matrix identity [155, Eq. (186)] the noise+interference power at destination, here denoted as θ_3, is calculated as

$$\theta_3 = N - a_{\mathrm{d}}\omega + \mathrm{tr}\left(\mathbf{H}_{\mathrm{rd}}\mathbb{E}\{\mathbf{r}_{\mathrm{out}}\mathbf{r}_{\mathrm{out}}^H\}\mathbf{H}_{\mathrm{rd}}^H\right) \tag{7.8}$$

$$\begin{aligned}&= N - a_{\mathrm{d}}\omega + \mathbf{d}_{M_{\mathrm{d}}}^T\left(\mathbf{H}_{\mathrm{rd}}^*\otimes\mathbf{H}_{\mathrm{rd}}\right)\mathrm{vec}\left(\mathbb{E}\{\mathbf{r}_{\mathrm{out}}\mathbf{r}_{\mathrm{out}}^H\}\right)\\ &= N - a_{\mathrm{d}}\omega + \mathbf{d}_{M_{\mathrm{d}}}^T\left(\mathbf{H}_{\mathrm{rd}}^*\otimes\mathbf{H}_{\mathrm{rd}}\right)\left(\mathbf{I}_{M_{\mathrm{t}}^2} + \kappa\mathbf{S}_{\mathrm{D}}^{M_{\mathrm{t}}}\right)\times\left(\mathbf{I}_{M_{\mathrm{t}}^2} - \omega\tilde{\mathbf{W}}\mathbf{C}\right)^{-1}\omega\tilde{\mathbf{W}}\mathbf{c}\end{aligned}$$

$$= N - a_{\mathrm{d}}\omega + \mathbf{d}_{M_{\mathrm{d}}}^T\left(\mathbf{H}_{\mathrm{rd}}^*\otimes\mathbf{H}_{\mathrm{rd}}\right)\left(\mathbf{I}_{M_{\mathrm{t}}^2} + \kappa\mathbf{S}_{\mathrm{D}}^{M_{\mathrm{t}}}\right)\times\sum_{k\in\{0\cdots\infty\}}\left(\omega\tilde{\mathbf{W}}\mathbf{C}\right)^k\omega\tilde{\mathbf{W}}\mathbf{c} \tag{7.9}$$

$$\approx N - a_{\mathrm{d}}\omega + \sum_{k\in\mathbb{F}_K}\mathbf{d}_{M_{\mathrm{d}}}^T\left(\mathbf{H}_{\mathrm{rd}}^*\otimes\mathbf{H}_{\mathrm{rd}}\right)\left(\mathbf{I}_{M_{\mathrm{t}}^2} + \kappa\mathbf{S}_{\mathrm{D}}^{M_{\mathrm{t}}}\right)\times\left(\tilde{\mathbf{W}}\mathbf{C}\right)^{k-1}\tilde{\mathbf{W}}\mathbf{c}\omega^k \tag{7.10}$$

$$\approx a_0 + \sum_{k\in\mathbb{F}_K}a_k\omega^k, \tag{7.11}$$

where K represents the approximation order, $N := \sigma_{\mathrm{nd}}^2 M_{\mathrm{d}} + P_{\mathrm{s}}\|\mathbf{h}_{\mathrm{sd}}\|_2^2$, and a_k is defined in (3.45) and (3.47). Note that the identity in (7.9) holds for any feasible relay transmit strategy, see (3.22b). This stems from the fact that the effect of the distortion components are attenuated after passing through the loop process, i.e., $\omega\tilde{\mathbf{W}}\mathbf{C}$, in each consecutive symbol duration[1]. Following the same arguments as in (7.8)-(7.10) we

[1]Otherwise, the impact of distortion is accumulated, leading to an infinite distortion power and instability.

calculate the relay transmit power as

$$\begin{aligned}\operatorname{tr}\left(\mathbb{E}\{\mathbf{r}_{\text{out}}\mathbf{r}_{\text{out}}^H\}\right) &= \mathbf{d}_{M_{\text{t}}}^T\left(\mathbf{I}_{M_{\text{t}}^2}+\kappa\mathbf{S}_{\text{D}}^{M_{\text{t}}}\right)\left(\mathbf{I}_{M_{\text{t}}^2}-\omega\tilde{\mathbf{W}}\mathbf{C}\right)^{-1}\omega\tilde{\mathbf{W}}\mathbf{c}\\ &= \mathbf{d}_{M_{\text{t}}}^T\left(\mathbf{I}_{M_{\text{t}}^2}+\kappa\mathbf{S}_{\text{D}}^{M_{\text{t}}}\right)\sum_{k\in\{0\cdots\infty\}}\left(\omega\tilde{\mathbf{W}}\mathbf{C}\right)^k\omega\tilde{\mathbf{W}}\mathbf{c} \qquad (7.12)\\ &\approx \sum_{k\in\mathbb{F}_K}\mathbf{d}_{M_{\text{t}}}^T\left(\mathbf{I}_{M_{\text{t}}^2}+\kappa\mathbf{S}_{\text{D}}^{M_{\text{t}}}\right)\left(\tilde{\mathbf{W}}\mathbf{C}\right)^{k-1}\tilde{\mathbf{W}}\mathbf{c}\omega^k=\sum_{k\in\mathbb{F}_K}b_k\omega^k, \qquad (7.13)\end{aligned}$$

where b_k is defined in (3.48).

7.5 Proof to Lemma 4.5.2

7.5.1 Proof of tightness:

Tightness is obtained by observing the equivalence

$$\begin{aligned}|\mathbb{G}_C|P_{\text{tot}}\left(\mathbb{Q}^\star\right)\text{SAA}\left(\mathbb{Q}^\star\right) &= \sum_{i\in\mathbb{G}_C}\{\tilde{C}_{\text{s},i}\left(\mathbb{Q}^\star\right)\}^+\\ &= \sum_{i\in\mathbb{G}_{C_1}}\{\tilde{C}_{\text{s},i}\left(\mathbb{Q}^\star\right)\}^+ + \sum_{i\in\mathbb{G}_{C_2^+}}\tilde{C}_{\text{s},i}\left(\mathbb{Q}^\star\right) \qquad (7.14a)\\ &= \sum_{i\in\mathbb{G}_{C_1}}\{\hat{C}_{\text{s},i}\left(\mathbb{Q}^\star,\mathbb{Q}^\star\right)\}^+ + \sum_{i\in\mathbb{G}_{C_2^+}}\hat{C}_{\text{s},i}\left(\mathbb{Q}^\star,\mathbb{Q}^\star\right) \qquad (7.14b)\\ &= |\mathbb{G}_C|P_{\text{tot}}\left(\mathbb{Q}^\star\right)\text{SAA}_{LB}\left(\mathbb{Q}^\star,\mathbb{Q}^\star\right),\end{aligned}$$

where (7.14a) is obtained by applying the definition (4.37), and (7.14b) from $\tilde{C}_{\text{s},i}\left(\mathbb{Q}^\star\right)=\hat{C}_{\text{s},i}\left(\mathbb{Q}^\star,\mathbb{Q}^\star\right)$, see (4.21).

7.5.2 Proof of equal directional derivative:

Let $C_{\text{s},i}:=\{\tilde{C}_{\text{s},i}\}^+$, and $f'(x;d)$ represents the directional derivative of a function f at point x and for the direction d. The directional derivative of SAA at $\mathbb{Q}^\star$ is then

expressed as

$$
\begin{aligned}
&P_{\text{tot}}\left(\mathbb{Q}^{\star}\right)\text{SAA}^{'}\left(\mathbb{Q}^{\star};d\right)\\
&=\left(\sum_{i\in\mathbb{G}_{C_1}}C^{'}_{\text{s},i}\left(\mathbb{Q}^{\star};d\right)+\sum_{i\in\mathbb{G}_{C_2^{+}}}\tilde{C}^{'}_{\text{s},i}\left(\mathbb{Q}^{\star};d\right)\right)/|\mathbb{G}_C|-P^{'}_{\text{tot}}\left(\mathbb{Q}^{\star};d\right)\text{SAA}\left(\mathbb{Q}^{\star}\right) &\text{(7.15a)}\\
&=\left(\sum_{i\in\mathbb{G}_{C_1^{(d)}}}\hat{C}^{'}_{\text{s},i}\left(\mathbb{Q}^{\star},\mathbb{Q}^{\star};d\right)+\sum_{i\in\mathbb{G}_{C_2^{+}}}\hat{C}^{'}_{\text{s},i}\left(\mathbb{Q}^{\star},\mathbb{Q}^{\star};d\right)\right)/|\mathbb{G}_C|-P^{'}_{\text{tot}}\left(\mathbb{Q}^{\star};d\right)\text{SAA}_{LB}\left(\mathbb{Q}^{\star},\mathbb{Q}^{\star}\right) &\text{(7.15b)}\\
&=P_{\text{tot}}\left(\mathbb{Q}^{\star}\right)\text{SAA}^{'}_{LB}\left(\mathbb{Q}^{\star},\mathbb{Q}^{\star};d\right), &\text{(7.15c)}
\end{aligned}
$$

where $C_{\text{s},i}:=\{\tilde{C}_{\text{s},i}\}^{+}$ and the set $\mathbb{G}_{C_1^{(d)}}$ is defined as

$$
\mathbb{G}_{C_1^{(d)}}:=\left\{\forall i \;\middle|\; i\in\mathbb{G}_{C_1}\ \text{ and }\ C^{'}_{\text{s},i}\left(\mathbb{Q}^{\star};d\right)\neq 0\right\}. \tag{7.16}
$$

In the above arguments, (7.15a) is obtained by recalling (4.32), and the fact that $C_{\text{s},i}\left(\mathbb{Q}^{\star}\right)$ is positive and differentiable for any $i\in\mathbb{G}_{C_2^{+}}$. The identity (7.15b) is obtained by considering the possible situations for $C^{'}_{\text{s},i}\left(\mathbb{Q}^{\star};d\right)$:

- $\tilde{C}_{\text{s},i}\left(\mathbb{Q}^{\star}\right)<0$. Then, $C_{\text{s},i}$ is differentiable and $C^{'}_{\text{s},i}\left(\mathbb{Q}^{\star};d\right)=0$ for any direction d.
- $\tilde{C}_{\text{s},i}\left(\mathbb{Q}^{\star}\right)>0$. Then, $C_{\text{s},i}$ is differentiable and $C^{'}_{\text{s},i}\left(\mathbb{Q}^{\star};d\right)=\hat{C}^{'}_{\text{s},i}\left(\mathbb{Q}^{\star},\mathbb{Q}^{\star};d\right)$ for any direction d.
- $\tilde{C}_{\text{s},i}\left(\mathbb{Q}^{\star}\right)=0$ and $\tilde{C}^{'}_{\text{s},i}\left(\mathbb{Q}^{\star};d\right)>0$. Then, $C_{\text{s},i}$ is not differentiable and $C^{'}_{\text{s},i}\left(\mathbb{Q}^{\star};d\right)=\hat{C}^{'}_{\text{s},i}\left(\mathbb{Q}^{\star},\mathbb{Q}^{\star};d\right)$.
- $\tilde{C}_{\text{s},i}\left(\mathbb{Q}^{\star}\right)=0$ and $\tilde{C}^{'}_{\text{s},i}\left(\mathbb{Q}^{\star};d\right)\leq 0$. Then, $C_{\text{s},i}$ is not differentiable and $C^{'}_{\text{s},i}\left(\mathbb{Q}^{\star};d\right)=0$.

Finally, the identity (7.15c) is obtained by recalling (4.38), and the tightness property from (7.14).

List of Acronyms

ADC	Analog-to-digital converter
DAC	Digital-to-analog converter
CSI	Channel state information
MIMO	Multiple-input multiple-output
OFDM	Orthogonal frequency-division multiplexing
FD	Full-duplex
HD	Half-duplex
SI	Self-interference
RSI	Residual self-interference
SIC	Self-interference cancellation
MMSE	Minimum mean squared-error
MSE	Mean squared-error
ICL	Inter-carrier leakage
GP	Gradient projection
AF	Amplify and forward
DF	Decode and forward
NOMA	Non-orthogonal multiple access
SDP	Semi-definite programming
AltSDP	Alternating semi-definite programming
QCP	Quadratic convex programing
AltQCP	Alternating quadratic convex programming
WMMSE	Weighted minimum mean squared-error
RF	Radio frequency
Tx	Transmit

Rx	Receive
MC	Multi carrier
AGC	Automatic gain control
CT	CPU time
RAM	Random access memory
WC	Worst case
SNR	Signal to noise ratio
SINR	Signal to interference-plus-noise ratio
SDNR	Signal to distortion-plus-noise ratio
TDD	Time division duplexing
FDD	Frequency division duplexing
MuStR1	Multi-stage rank-one
AltMuStR1	Alternating multi-stage rank-one
LOS	Line-of-sight
PHY	Physical layer
MRT	Maximum ratio transmission
MRC	Maximum ratio combining
SSSLM	Successive selection and statistical lower bound maximization
SUIAP	Successive general inner approximation
KKT	Karush-Kuhn-Tucker
ICT	Information and communication technology
SEE	Secrecy energy efficiency
SBPJ	Secure bits per Joul
MIMOME	Multiple-input multiple-output multiple-antenna eavesdropper
AN	Artificial noise
SIA	Successive inner approximation
DC	Difference of concave
SAA	Ensemble average approximation
SUM	Successive upper-bound minimization

GB	Giga bytes
GHz	Giga Hertz
CDF	Cumulative distribution function
i.i.d.	Independent and identically distributed
5G	Fifth generation cellular wireless communication networks
SCBS	Small cell base station
C-RAN	Cloud radio access network
MILP	Mixed integer-linear program
CAPEX	Capital expenditure
BS	Basestation
LNA	Low noise amplifier
PCB	Printed circuit board
mMIMO	Massive multiple-input multiple-output
UL	Uplink
DL	Downlink
CCI	Co-channel interference
QoS	Quality of service
PA	Power amplifier

List of the Used Symbols

Chapter 2

k	index of subcarriers
i	index of communication direction
l	index of transmit or receive chain
K	number of subcarriers
T_{s}	sampling time
$\mathbb{I}$	set of transmit directions
$\mathbb{F}_K$	set of all subcarrier indices
$\mathbb{V}$	set of all precoder matrices
$\mathbb{U}$	set of all decoder matrices
N_i	number of transmit antennas at direction i
M_i	number of receive antennas at direction i
d_i	number of data streams at each subcarrier in direction i
$\mathbf{s}_i^k$	transmit data symbol
$\tilde{\mathbf{s}}_i^k$	estimated $\mathbf{s}_i^k$ at the receiver
$\mathbf{U}_i{}^k$	receive linear decoder
$\mathbf{V}_i{}^k$	transmit linear precoder
$\mathbf{y}_i^k$	received signal before self-interference cancellation
$\tilde{\mathbf{y}}_i^k$	received signal after self-interference cancellation
$e_{\mathrm{r},l}$	collective receiver distortion at chain l
$e_{\mathrm{t},l}$	collective transmit distortion at chain l
$\mathbf{e}_{\mathrm{r},i}^k$	receiver distortion
$\mathbf{e}_{\mathrm{t},i}^k$	transmit distortion
κ_l	transmit distortion coefficient at chain l
β_l	receive distortion coefficient at chain l
$\mathbf{\Theta}_{\mathrm{rx},i}$	matrix of receive distortion coefficients

$\mathbf{\Theta}_{\mathrm{tx},i}$	matrix of transmit distortion coefficients
$\boldsymbol{\nu}_i^k$	collective residual interference plus noise signal
$\mathbf{\Sigma}_i^k$	collective residual interference plus noise covariance
$\mathbf{n}_i^k$	thermal noise
$\sigma_{i,k}^2$	thermal noise variance
$\mathbf{u}_i^k$	received signal without receive distortion
$\mathbf{v}_i^k$	intended transmit signal without distortion
$\mathbf{x}_i^k$	transmit signal
P_i	maximum transmit power
$\mathbf{E}_i^k$	MSE matrix
$\mathbf{U}_{i,\mathrm{mmse}}^k$	MMSE linear receive filter
$\mathbf{S}_i^k$	positive definite matrix weight
ι_i	Lagrangian dual variable
I_i^k	information capacity at direction i and subcarrier k
$\tilde{\mathbf{H}}_{ij}^k$	estimated channel
$\mathbf{\Delta}_{ij}^k$	CSI error
$\mathbb{D}_{ij}^k$	CSI error region shaping matrix
ζ_{ij}^k	CSI error region radius
$\mathbf{c}_{ij}^k$	a vector stacking the impact of channel estimate on the sum MSE
$\mathbf{C}_{ij}^k$	a matrix stacking the impact of CSI error on the sum MSE
$\tilde{d}_{ij}$	length of $\mathbf{c}_{ij}^k$
$\mathbf{G}_i$	auxiliary semi-definite matrix variable
$\mathbf{F}_{i,j}^k$	auxiliary semi-definite matrix variable
$\mathbf{W}_i^k$	semi-definite matrix weight variable
$\mathbb{W}$	set of all $\mathbf{W}_i^k$ variables
τ_{ij}^k	auxiliary positive scalar variable
$\mathbb{T}$	set of all τ_{ij}^k variables
λ_{ij}^k	auxiliary real scalar variable
$\mathbb{M}$	set of all λ_{ij}^k variables
ρ_{ij}^k	Lagrangian dual variable
ϕ_{ij}^k	auxiliary real scalar variable

$\mathbf{A}_{ij}^{k}$	auxiliary semi-definite matrix variable
l_m	size of the SDP sub-block length
n	size of the SDP variable space

Chapter 3

s	transmit data symbol from the source
P_{s}	transmit power from the source
$\hat{s}$	estimated data symbol at the receiver
$P_{\mathrm{s,max}}$	maximum transmit power from the source
$P_{\mathrm{r,max}}$	maximum relay transmit power
$\tilde{P}_{\mathrm{r,max}}$	maximum undistorted relay transmit power
M_{t}	number of transmit antennas at the relay
M_{r}	number of receive antennas at the relay
M_{d}	number of antennas at the destination
$\mathbf{r}_{\mathrm{in}}$	received signal at the relay
$\mathbf{r}_{\mathrm{out}}$	transmitted signal from the relay
$\mathbf{r}_{\mathrm{supp}}$	received relay signal at the relay, after SIC
$\mathbf{h}_{\mathrm{sr}}$	source-rtelay channel
$\mathbf{H}_{\mathrm{rd}}$	relay-destination channel
$\mathbf{h}_{\mathrm{sd}}$	source-destination channel
$\mathbf{H}_{\mathrm{rr}}$	self-interference channel
$\mathbf{n}_{\mathrm{d}}$	thermal noise at the destination
σ_{nd}^2	thermal noise variance at the destination
$\mathbf{n}_{\mathrm{r}}$	thermal noise at the relay
σ_{nr}^2	thermal noise variance at the relay
κ	distortion coefficient at the relay transmit chains
β	distortion coefficient at the relay receiver chains
τ	relay processing delay
$\mathbf{e}_{\mathrm{in}}$	receive distortion at the relay
$\mathbf{y}$	received signal at the destination
$\mathbf{z}$	linear receive filter at the receiver

t	time instance
$\mathbf{W}$	relay amplification matrix
$\mathbf{Q}$	undistorted relay transmit covariance
P_{err}	received distortion-plus-noise power at the destination
P_{tot}	total received power at the destination
P_{des}	desired received power at the destination
$\mathbf{\Theta}$	relay covariance transfer function
$\mathbf{w}_{\text{tx}}$	transmit linear filter for a rank-1 AF-FD relay
$\mathbf{w}_{\text{rx}}$	receive linear filter for a rank-1 AF-FD relay
ω	scalar relay amplification
ω_{infty}	scalar relay amplification leading to instability
ω_{max}	scalar relay amplification leading to maximum allowed relay power
$f_1(\omega)$	approximate source-to-destination SDNR
$f_2(\omega)$	approximate relay transmit power
$\mathbf{H}_{\text{D,tx}}$	equivalent distortion channel from relay transmitter
ζ_{sr}	SDNR for the source-to-relay path
ζ_{rd}	SDNR for the relay-to-destination path
$\mathbf{v}_{\text{in}}$	receive linear filter for a DF-FD relay
$\mathbf{v}_{\text{out}}$	transmit linear precoder for a DF-FD relay
ρ_{sr}	path loss for the source-to-relay channel
ρ_{rd}	path loss for the relay-to-destination channel
ρ_{sd}	path loss for the source-to-destination channel
ρ_{rr}	path loss for the self-interference channel
K_R	Rician K-factor
$\mathbf{H}_0$	line of sight channel

Chapter 4

N_A	number of transmit antennas at Alice
M_A	number of receive antennas at Alice
M_E	number of receive antennas at Eve
N_B	number of transmit antennas at Bob

M_B	number of receive antennas at Bob
$\mathbf{H}_{aa}$	self-interference channel at Alice
$\mathbf{H}_{bb}$	self-interference channel at Bob
$\mathbf{H}_{ab}$	Alice to Bob channel
$\mathbf{H}_{ba}$	Bob to Alice channel
$\mathbf{H}_{ae}$	channel from Alice to Eve
$\mathbf{H}_{be}$	channel from Bob to Eve
$\mathbf{e}_{\mathrm{rx},b}$	receive distortion at the Bob
$\mathbf{e}_{\mathrm{tx},a}$	transmit distortion at Alice
$\mathbf{e}_{\mathrm{tx},b}$	transmit distortion at Bob
κ_a	transmit distortion coefficient at Alice
κ_b	transmit distortion coefficient at Bob
β_a	receive distortion coefficient at Alice
β_b	receive distortion coefficient at Bob
$\mathbf{x}_a$	transmit signal from Alice
$\mathbf{x}_b$	transmit signal from Bob
$\mathbf{w}_a$	transmit artificial noise from Alice
$\mathbf{q}_a$	transmit information-containing signal from Alice
$\mathbf{w}_b$	transmit artificial noise from Bob
$\mathbf{q}_b$	transmit information-containing signal from Bob
$\mathbf{c}_e$	collective interference-plus-noise at Eve
$\mathbf{c}_b$	collective interference-plus-noise at Bob
$\mathbf{u}_b$	undistorted receive signal at Bob
$\mathbf{y}_b$	received signal at Bob
$\mathbf{y}_e$	received signal at Eve
$\mathbf{W}_a$	covariance of the artificial noise transmitted from Alice
$\mathbf{Q}_a$	covariance of the information-containing signal transmitted from Alice
$\mathbf{W}_b$	covariance of the artificial noise transmitted from Bob
$\mathbf{Q}_b$	covariance of the information-containing signal transmitted from Bob
$\mathbf{\Sigma}_a^{(\mathrm{BD})}$	covariance of the collective bidirectional interference-plus-noise at Alice

$\mathbf{\Sigma}_b^{(\mathrm{BD})}$	covariance of the collective bidirectional interference-plus-noise at Bob
$\mathbf{\Sigma}_e^{(\mathrm{BD})}$	covariance of the collective bidirectional interference-plus-noise at Eve
$\mathbf{\Sigma}_e$	covariance of the collective interference-plus-noise at Eve
$\mathbf{\Sigma}_b$	covariance of the collective interference-plus-noise at Bob
$\mathbf{n}_a$	additive thermal noise at Alice
$\mathbf{n}_b$	additive thermal noise at Bob
$\mathbf{n}_e$	additive thermal noise at Eve
$\sigma^2_{\mathrm{n},a}$	variance of the additive thermal noise at Alice
$\sigma^2_{\mathrm{n},b}$	variance of the additive thermal noise at Bob
$\sigma^2_{\mathrm{n},e}$	variance of the additive thermal noise at Eve
P_A	total consumed power at Alice
P_B	total consumed power at Bob
μ_A	power amplifier efficiency at Alice
μ_B	power amplifier efficiency at Bob
$P_{A,0}$	zero-state power consumption at Alice
$P_{B,0}$	zero-state power consumption at Bob
$P_{A,\max}$	maximum power consumption at Alice
$P_{B,\max}$	maximum power consumption at Bob
P_{FD}	power consumption due to SIC
P_{tot}	total power consumption
C_{ab}	secrecy information capacity from Alice to Bob
C_{ba}	secrecy information capacity from Bob to Alice
SEE_p	relaxed SEE
$\tilde{\mathrm{SEE}}_p$	equivalent iterative SEE objective
$\mathbb{Q}$	set of all transmit covariance variables
a_i	selection variable for realization instance i
$\mathbf{a}$	vector of selection variables
$\mathbb{A}$	set of possible values for $\mathbf{a}$
$\mathbb{F}_{C_1}$	set of channel instances resulting in non-smooth objective
$\mathbb{F}_{C_2}$	set of channel instances resulting in smooth objective
$\mathbb{F}_{C_2^+}$	set of channel instances resulting in positive objective values

λ	auxiliary variable
SAA_{LB}	lower bound to the statistical SAA objective

Chapter 5

$X_{ij,f}$	transmit power
$\Lambda_{ij,f}$	the desired channel strength
$\Omega_{ij,k,f}$	interference channel strength to the access network
$\Gamma_{ij,lk,f}$	interference channel strength to the other backhaul links
$W_{ij,f}$	
$P_{\text{max},i}$	maximum power consumption at each node
$P_{\text{max},ij}$	maximum transmit power at each link
$R_{\text{ul},i}$	UL rate demand
$R_{\text{dl},i}$	DL rate demand
$\bar{d}_{\text{ul}}$	maximum tolerable average delay for UL traffic
$\bar{d}_{\text{dl}}$	maximum tolerable average delay for DL traffic
d_i	processing delay
$I_{\text{th},k,f}$	tolerable interference threshold from backhaul to access network
$C_{ij,0}$	link capacity from the pre-existing technologies
$C_{ij,f}$	wireless link capacity
J_{ij}	link activity indicator
J_f	frequency subchannel activity indicator
$C_{\text{ul},ij}$	used channel capacity for UL traffic
$C_{\text{dl},ij}$	used channel capacity for DL traffic
W_p	price of power
W_l	price of establishing a wireless link
W_f	price of each frequency subchannel
B	bandwidth of each frequency subchannel
$\mathbb{R}$	set of all root nodes
$\mathbb{M}$	set of all non-root nodes
$\mathbb{N}$	set of all nodes
$\mathbb{L}$	set of all potential links

$\mathbb{J}_L$	set of the variables J_{ij}
$\mathbb{J}_F$	set of the variables J_f
$\mathbb{C}_U$	set of the variables $C_{\mathrm{ul},ij}$
$\mathbb{C}_D$	set of the variables $C_{\mathrm{dl},ij}$
$\mathbb{P}$	set of transmit power values

Bibliography

[1] S. Hong, J. Brand, J. I. Choi, M. Jain, J. Mehlman, S. Katti, and P. Levis, "Applications of self-interference cancellation in 5G and beyond," *IEEE Communications Magazine*, vol. 52, no. 2, pp. 114–121, Feb 2014.

[2] D. Bharadia, E. McMilin, and S. Katti, "Full duplex radios," in *Proceedings of the ACM SIGCOMM 2013 Conference on SIGCOMM*, ser. SIGCOMM '13. New York, NY, USA: ACM, 2013, pp. 375–386. [Online]. Available: http://doi.acm.org/10.1145/2486001.2486033

[3] E. Everett, A. Sahai, and A. Sabharwal, "Passive self-interference suppression for full-duplex infrastructure nodes," *IEEE Transactions on Wireless Communications*, vol. 13, no. 2, pp. 680–694, Feb. 2014.

[4] E. Everett, M. Duarte, C. Dick, and A. Sabharwal, "Empowering full-duplex wireless communication by exploiting directional diversity," in *Signals, Systems and Computers (ASILOMAR), 2011 Conference Record of the Forty Fifth Asilomar Conference on*, 2011, pp. 2002–2006.

[5] T. Dinc, A. Chakrabarti, and H. Krishnaswamy, "A 60 GHz same-channel full-duplex CMOS transceiver and link based on reconfigurable polarization-based antenna cancellation," in *2015 IEEE Radio Frequency Integrated Circuits Symposium (RFIC)*, May 2015, pp. 31–34.

[6] M. Heino, D. Korpi, T. Huusari, E. Antonio-Rodriguez, S. Venkatasubramanian, T. Riihonen, L. Anttila, C. Icheln, K. Haneda, R. Wichman, and M. Valkama, "Recent advances in antenna design and interference cancellation algorithms for in-band full duplex relays," *IEEE Communications Magazine*, vol. 53, no. 5, pp. 91–101, May 2015.

[7] D. Bharadia and S. Katti, "Full duplex MIMO radios," in *Proceedings of the 11th USENIX Conference on Networked Systems Design and Implementation*, ser. NSDI'14, Berkeley, CA, USA, 2014, pp. 359–372.

[8] R. Askar, T. Kaiser, B. Schubert, T. Haustein, and W. Keusgen, "Active self-interference cancellation mechanism for full-duplex wireless transceivers," in *Cognitive Radio Oriented Wireless Networks and Communications (CROWNCOM), 2014 9th International Conference on*, 2014, pp. 539–544.

[9] J. I. Choi, M. Jain, K. Srinivasan, P. Levis, and S. Katti, "Achieving single channel, full duplex wireless communication," in *Proceedings of the sixteenth annual international conference on Mobile computing and networking*. ACM, 2010, pp. 1–12.

[10] M. Jain, J. I. Choi, T. Kim, D. Bharadia, K. Srinivasan, S. Seth, P. Levis, S. Katti, and P. Sinha, "Practical, real-time, full duplex wireless," in *Proceedings of 17th Annual International Conference on Mobile Computing and Networking (MobiCom)*, Las Vegas, NV, Sep. 2011.

[11] A. K. Khandani, "Methods for spatial multiplexing of wireless two-way channels," Oct. 2010, uS Patent 7,817,641.

[12] M. A. Khojastepour, K. Sundaresan, S. Rangarajan, X. Zhang, and S. Barghi, "The case for antenna cancellation for scalable full-duplex wireless communications," in *Proceedings of the 10th ACM Workshop on Hot Topics in Networks*, ser. HotNets-X. ACM, 2011, pp. 17:1–17:6.

[13] E. Aryafar, M. A. Khojastepour, K. Sundaresan, S. Rangarajan, and M. Chiang, "MIDU: Enabling MIMO full duplex," in *Proceedings of the 18th annual international conference on Mobile computing and networking*. ACM, 2012, pp. 257–268.

[14] M. Duarte and A. Sabharwal, "Full-duplex wireless communications using off-the-shelf radios: Feasibility and first results," in *Signals, Systems and Computers (ASILOMAR), 2010 Conference Record of the 44th Asilomar Conference on*, 2010, pp. 1558–1562.

[15] A. Sahai, G. Patel, and A. Sabharwal, "Pushing the limits of full-duplex: Design and real-time implementation," Rice University, Technical report, July 2011.

[16] R. Askar, B. Schubert, W. Keusgen, and T. Haustein, "Agile Full-Duplex transceiver: The concept and Self-Interference channel characteristics," in *European Wireless 2016 (EW2016)*, May 2016.

[17] M. Duarte, A. Sabharwal, V. Aggarwal, R. Jana, K. K. Ramakrishnan, C. W. Rice, and N. K. Shankaranarayanan, "Design and characterization of a full-duplex multiantenna system for wifi networks," *IEEE Transactions on Vehicular Technology*, vol. 63, no. 3, pp. 1160–1177, March 2014.

[18] A. Sahai, G. Patel, C. Dick, and A. Sabharwal, "Understanding the impact of phase noise on active cancellation in wireless full-duplex," in *Signals, Systems and Computers (ASILOMAR), 2012 Conference Record of the Forty Sixth Asilomar Conference on*, Nov. 2012, pp. 29–33.

[19] ——, "On the impact of phase noise on active cancelation in wireless full-duplex," *IEEE Transactions on Vehicular Technology*, vol. 62, no. 9, pp. 4494–4510, Nov. 2013.

[20] R. Askar, B. Schubert, W. Keusgen, and T. Haustein, "Full-Duplex wireless transceiver in presence of I/Q mismatches: Experimentation and estimation algorithm," in *IEEE GC 2015 Workshop on Emerging Technologies for 5G Wireless Cellular Networks - 4th International (GC'15 - Workshop - ET5G)*, San Diego, USA, 2015.

[21] R. Askar, N. Zarifeh, B. Schubert, W. Keusgen, and T. Kaiser, "I/Q imbalance calibration for higher self-interference cancellation levels in full-duplex wireless transceivers," in *5G for Ubiquitous Connectivity (5GU), 2014 1st International Conference on*, 2014, pp. 92–97.

[22] L. Laughlin, M. Beach, K. Morris, and J. Hainey, "Electrical balance isolation for flexible duplexing in 5G mobile devices," in *Communication Workshop (ICCW), 2015 IEEE International Conference on*, June 2015, pp. 1071–1076.

[23] L. Laughlin, M. Beach, K. Morris, and J. Haine, "Optimum single antenna full duplex using hybrid junctions," *Selected Areas in Communications, IEEE Journal on*, vol. 32, no. 9, pp. 1653–1661, Sept. 2014.

[24] Y. Hua, Y. Ma, A. Gholian, Y. Li, A. C. Cirik, and P. Liang, "Radio self-interference cancellation by transmit beamforming, all-analog cancellation and blind digital tuning," *Signal Processing*, vol. 108, pp. 322 – 340, 2015.

[25] Y. Hua, Y. Li, C. Mauskar, and Q. Zhu, "Blind digital tuning for interference cancellation in full-duplex radio," in *Signals, Systems and Computers, 2014 48th Asilomar Conference on*, Nov. 2014, pp. 1691–1695.

[26] O. Taghizadeh, J. Zhang, and M. Haardt, "Transmit beamforming aided amplify-and-forward MIMO full-duplex relaying with limited dynamic range," *Elsevier Signal Processing*, vol. 127, pp. 266–281, 2016.

[27] S. Huberman and T. Le-Ngoc, "Self-interference pricing-based MIMO full-duplex precoding," *IEEE Wireless Communications Letters*, vol. 3, no. 6, pp. 549–552, Dec 2014.

[28] J. Zhang, O. Taghizadeh, J. Luo, and M. Haardt, "Full duplex wireless communications with partial interference cancellation," *Proceedings of the 46th Asilomar Conference on Signals, Systems, and Computers, Pacific Grove, CA*, Nov. 2012.

[29] E. Everett, C. Shepard, L. Zhong, and A. Sabharwal, "Softnull: Many-antenna full-duplex wireless via digital beamforming," *IEEE Transactions on Wireless Communications*, vol. 15, no. 12, pp. 8077–8092, Dec 2016.

[30] E. Ahmed, A. Eltawil, and A. Sabharwal, "Self-interference cancellation with nonlinear distortion suppression for full-duplex systems," in *Signals, Systems and Computers, 2013 Asilomar Conference on*, 2013, pp. 1199–1203.

[31] L. Anttila, D. Korpi, V. Syrjälä, and M. Valkama, "Cancellation of power amplifier induced nonlinear self-interference in full-duplex transceivers," in *2013 Asilomar Conference on Signals, Systems and Computers*, Nov 2013, pp. 1193–1198.

[32] B. P. Day, A. R. Margetts, D. W. Bliss, and P. Schniter, "Full-duplex bidirectional MIMO: Achievable rates under limited dynamic range," *IEEE Transactions on Signal Processing*, vol. 60, no. 7, pp. 3702–3713, July 2012.

[33] A. C. Cirik, R. Wang, and Y. Hua, "Weighted-sum-rate maximization for bi-directional full-duplex MIMO systems," in *2013 Asilomar Conference on Signals, Systems and Computers*, Nov 2013, pp. 1632–1636.

[34] A. C. Cirik, J. Zhang, M. Haardt, and Y. Hua, "Sum-rate maximization for bi-directional full-duplex MIMO systems under multiple linear constraints," in *Proc. 15th Int. Workshop Signal Processing Advances in Wireless Communications (SPAWC 2014)*, Toronto, Canada, 2014.

[35] A. Cirik, R. Wang, Y. Hua, and M. Latva-aho, "Weighted sum-rate maximization for full-duplex MIMO interference channels," *Communications, IEEE Transactions on*, vol. 63, March 2015.

[36] O. Taghizadeh and R. Mathar, "Worst-Case robust sum rate maximization for Full-Duplex Bi-Directional MIMO systems under channel knowledge uncertainty," in *IEEE ICC 2017 Signal Processing for Communications Symposium (ICC'17 SPC)*, Paris, France, May 2017, pp. 5950–5956.

[37] A. C. Cirik, O. Taghizadeh, L. Lampe, R. Mathar, and Y. Hua, "Sum-power minimization under rate constraints in full-duplex MIMO systems," *VTC 2016, Montreal, Canada*, 2016.

[38] A. C. Cirik, S. Biswas, S. Vuppala, and T. Ratnarajah, "Beamforming design for full-duplex MIMO interference channels: QoS and energy-efficiency considerations," *IEEE Transactions on Communications*, vol. 64, no. 11, pp. 4635–4651, Nov 2016.

[39] O. Taghizadeh, A. C. Cirik, R. Mathar, and L. Lampe, "Sum power minimization for TDD-Enabled Full-Duplex Bi-Directional MIMO systems under channel uncertainty," in *European Wireless 2017 (EW2017)*, Dresden, Germany, May 2017, pp. 412–417.

[40] A. C. Cirik, R. Wang, Y. Rong, and Y. Hua, "Mse-based transceiver designs for full-duplex MIMO cognitive radios," *IEEE Transactions on Communications*, vol. 63, no. 6, pp. 2056–2070, June 2015.

[41] A. C. Cirik, M. C. Filippou, and T. Ratnarajaht, "Transceiver design in full-duplex MIMO cognitive radios under channel uncertainties," *IEEE Transactions on Cognitive Communications and Networking*, vol. 2, no. 1, pp. 1–14, March 2016.

[42] A. C. Cirik, Y. Rong, and Y. Hua, "Achievable rates of full-duplex MIMO radios in fast fading channels with imperfect channel estimation," *IEEE Transactions on Signal Processing*, vol. 62, no. 15, pp. 3874–3886, Aug 2014.

[43] A. C. Cirik, J. Xue, S. Biswas, T. Ratnarajah, and M. Sellathurai, "Transceiver design of optimum wirelessly powered full-duplex MIMO interference channel," in *2016 IEEE 17th International Workshop on Signal Processing Advances in Wireless Communications (SPAWC)*, July 2016, pp. 1–6.

[44] S. Han, L. Dai, Q. Sun, Z. Xu *et al.*, "Full duplex networking: Mission impossible?" *arXiv preprint arXiv:1410.5326*, 2014.

[45] D. Nguyen, L.-N. Tran, P. Pirinen, and M. Latva-aho, "On the spectral efficiency of full-duplex small cell wireless systems," *IEEE Transactions on Wireless Communications*, Sep 2014.

[46] A. Sahai, S. Diggavi, and A. Sabharwal, "On uplink/downlink full-duplex networks," in *Proc. Forty-Seventhth Asilomar Conference on Signals, Systems and Computers, Pacific Grove, CA*, Nov 2013.

[47] O. Taghizadeh and R. Mathar, "Interference mitigation via power optimization schemes for full-duplex networking," in *19th International ITG Workshop on Smart Antennas*, March 2015.

[48] Y. Sun, D. W. K. Ng, J. Zhu, and R. Schober, "Multi-objective optimization for robust power efficient and secure full-duplex wireless communication systems," *IEEE Transactions on Wireless Communications*, vol. 15, no. 8, pp. 5511–5526, Aug 2016.

[49] A. C. Cirik, S. Biswas, S. Vuppala, and T. Ratnarajah, "Robust transceiver design for full duplex multiuser MIMO systems," *IEEE Wireless Communications Letters*, vol. 5, no. 3, pp. 260–263, June 2016.

[50] A. Cirik, O. Taghizadeh, R. Mathar, and T. Ratnarajah, "QoS considerations for full duplex multi-user MIMO systems," *IEEE Wireless Communications Letters*, vol. PP, no. 99, pp. 1–1, Oct 2015.

[51] A. C. Cirik, S. Biswas, O. Taghizadeh, A. Liu, and T. Ratnarajah, "Robust transceiver design in full-duplex MIMO cognitive radios," in *IEEE ICC 2016 - Cognitive Radio and Networks Symposium (ICC'16 CRN)*, Kuala Lumpur, Malaysia, 2016, to be published after approval.

[52] Y. Sun, D. W. K. Ng, Z. Ding, and R. Schober, "Optimal joint power and subcarrier allocation for full-duplex multicarrier non-orthogonal multiple access systems," *IEEE Transactions on Communications*, vol. 65, no. 3, pp. 1077–1091, March 2017.

[53] A. C. Cirik, K. Rikkinen, Y. Rong, and T. Ratnarajah, "A subcarrier and power allocation algorithm for a full-duplex OFDM systems," in *2015 European Conference on Networks and Communications (EuCNC)*, June 2015, pp. 11–15.

[54] M. Mohammadi, B. K. Chalise, H. A. Suraweera, and Z. Ding, "Wireless information and power transfer in full-duplex systems with massive antenna arrays," in *2017 IEEE International Conference on Communications (ICC)*, May 2017, pp. 1–6.

[55] M. J. Rahman, A. C. Cirik, and L. Lampe, "Power-efficient transceiver design for full-duplex MIMO multi-cell systems with CSI uncertainty," *IEEE Access*, vol. PP, no. 99, pp. 1–1, 2017.

[56] A. C. Cirik, O. Taghizadeh, L. Lampe, R. Mathar, and Y. Hua, "Linear transceiver design for full-duplex multi-cell MIMO systems," *IEEE Access*, vol. 4, pp. 4678–4689, 2016.

[57] P. Aquilina, A. C. Cirik, and T. Ratnarajah, "Weighted sum rate maximization in full-duplex multi-user multi-cell MIMO networks," *IEEE Transactions on Communications*, vol. 65, no. 4, pp. 1590–1608, April 2017.

[58] T. Riihonen, S. Werner, and R. Wichman, "Mitigation of loopback self-interference in full-duplex MIMO relays," *IEEE Transactions on Signal Processing*, vol. 59, no. 12, pp. 5983–5993, Dec 2011.

[59] O. Taghizadeh and R. Mathar, "Cooperative strategies for distributed full-duplex relay networks with limited dynamic range," in *2014 IEEE International Conference on Wireless for Space and Extreme Environments (WiSEE)*, Oct 2014, pp. 1–7.

[60] O. Taghizadeh, M. Rothe, A. C. Cirik, and R. Mathar, "Distortion-Loop analysis for Full-Duplex Amplify-and-Forward relaying in cooperative multicast scenarios," in *2015 9th International Conference on Signal Processing and Communication Systems (ICSPCS)*, Cairns, Australia, Dec 2015, pp. 107–115.

[61] T. Riihonen, S. Werner, and R. Wichman, "Optimized gain control for single-frequency relaying with loop interference," *IEEE Transactions on Wireless Communications*, vol. 8, no. 6, pp. 2801–2806, June 2009.

[62] L. J. Rodriguez, N. H. Tran, and T. Le-Ngoc, "Optimal power allocation and capacity of full-duplex AF relaying under residual self-interference," *IEEE Wireless Communications Letters*, vol. 3, no. 2, pp. 233–236, April 2014.

[63] C. Dang, L. J. Rodríguez, N. H. Tran, S. Shelly, and S. Sastry, "Secrecy capacity of the full-duplex AF relay wire-tap channel under residual self-interference," in *2015 IEEE Wireless Communications and Networking Conference (WCNC)*, March 2015, pp. 99–104.

[64] X. Cheng, B. Yu, X. Cheng, and L. Yang, "Two-way full-duplex amplify-and-forward relaying," in *2013 IEEE Military Communications Conference (MILCOM)*, Nov 2013, pp. 1–6.

[65] K. Lee, H. Kwon, M. Jo, H. Park, and Y. Lee, "MMSE-based optimal design of full-duplex relay system," in *IEEE Vehicular Technology Conference (VTC Fall)*, Sep 2012.

[66] O. Somekh, O. Simeone, H. V. Poor, and S. Shamai, "Cellular systems with full-duplex amplify-and-forward relaying and cooperative base-stations," in *2007 IEEE International Symposium on Information Theory*, June 2007, pp. 16–20.

[67] Z. Wen, X. Liu, N. C. Beaulieu, R. Wang, and S. Wang, "Joint source and relay beamforming design for full-duplex MIMO AF relay SWIPT systems," *IEEE Communications Letters*, vol. 20, no. 2, pp. 320–323, Feb 2016.

[68] H. Suraweera, I. Krikidis, G. Zheng, C. Yuen, and P. Smith, "Low-complexity end-to-end performance optimization in MIMO full-duplex relay systems," *IEEE Transactions on Wireless Communications*, vol. 13, no. 2, pp. 913–927, Feb. 2014.

[69] D. Choi and D. Park, "Effective self interference cancellation in full duplex relay systems," *Electronics Letters*, vol. 48, no. 2, pp. 129–130, Jan. 2012.

[70] B. Chun and H. Park, "A spatial-domain joint-nulling method of self-interference in full-duplex relays," *IEEE Communications Letters*, vol. 16, no. 4, pp. 436–438, April 2012.

[71] C. Y. A. Shang, P. J. Smith, G. K. Woodward, and H. A. Suraweera, "Linear transceivers for full duplex MIMO relays," in *2014 Australian Communications Theory Workshop (AusCTW)*, Feb 2014, pp. 11–16.

[72] U. Ugurlu, T. Riihonen, and R. Wichman, "Optimized in-band full-duplex MIMO relay under single-stream transmission," *IEEE Transactions on Vehicular Technology*, vol. 65, no. 1, pp. 155–168, Jan 2016.

[73] Q. Shi, M. Hong, X. Gao, E. Song, Y. Cai, and W. Xu, "Joint source-relay design for full-duplex MIMO AF relay systems," *IEEE Transactions on Signal Processing*, vol. 64, no. 23, pp. 6118–6131, Dec 2016.

[74] O. Taghizadeh, J. Zhang, and M. Haardt, "Transmit beamforming aided amplify-and-forward MIMO full-duplex relaying with limited dynamic range," *Signal Processing*, vol. 127, pp. 266–281, 2016.

[75] Y. Y. Kang, B.-J. Kwak, and J. H. Cho, "An optimal full-duplex AF relay for joint analog and digital domain self-interference cancellation," *IEEE Transactions on Communications*, vol. 62, no. 8, pp. 2758–2772, Aug 2014.

[76] H. Shen, W. Xu, and C. Zhao, "Transceiver optimization for full-duplex massive MIMO AF relaying with direct link," *IEEE Access*, vol. 4, pp. 8857–8864, Dec 2016.

[77] T. Guo and B. Wang, "Joint transceiver beamforming design for end-to-end optimization in full-duplex MIMO relay system with self-interference," *IEEE Communications Letters*, vol. 20, no. 9, pp. 1733–1736, Sep 2016.

[78] B. P. Day, A. R. Margetts, D. W. Bliss, and P. Schniter, "Full-duplex MIMO relaying: Achievable rates under limited dynamic range," *IEEE Journal on Selected Areas in Communications*, vol. 30, no. 8, pp. 1541–1553, Sep 2012.

[79] X. Xia, D. Zhang, K. Xu, W. Ma, and Y. Xu, "Hardware impairments aware transceiver for full-duplex massive MIMO relaying," *Signal Processing, IEEE Transactions on*, vol. 63, no. 24, pp. 6565–6580, Dec 2015.

[80] E. Antonio-Rodríguez, R. López-Valcarce, T. Riihonen, S. Werner, and R. Wichman, "SINR optimization in wideband full-duplex MIMO relays under limited dynamic range," in *2014 IEEE 8th Sensor Array and Multichannel Signal Processing Workshop (SAM)*, June 2014, pp. 177–180.

[81] B. Zhong, D. Zhang, Z. Zhang, Z. Pan, K. Long, and A. V. Vasilakos, "Opportunistic full-duplex relay selection for decode-and-forward cooperative networks over rayleigh fading channels," in *2014 IEEE International Conference on Communications (ICC)*, June 2014, pp. 5717–5722.

[82] E. Antonio-Rodriguez, R. Lopez-Valcarce, T. Riihonen, S. Werner, and R. Wichman, "Subspace-constrained SINR optimization in MIMO full-duplex relays under limited dynamic range," in *IEEE 16th International Workshop on Signal Processing Advances in Wireless Communications (SPAWC)*, June 2015, pp. 281–285.

[83] H. Q. Ngo, H. A. Suraweerat, M. Matthaiou, and E. G. Larsson, "Multipair massive MIMO full-duplex relaying with MRC/MRT processing," in *2014 IEEE International Conference on Communications (ICC)*, June 2014, pp. 4807–4813.

[84] Z. Zhang, Z. Chen, M. Shen, and B. Xia, "Spectral and energy efficiency of multipair two-way full-duplex relay systems with massive MIMO," *IEEE Journal on Selected Areas in Communications*, vol. 34, no. 4, pp. 848–863, April 2016.

[85] J. Feng, Z. Shi, and S. Ma, "Sum rate of full-duplex two-way massive MIMO relay systems with channel aging," in *2016 IEEE International Conference on Communication Systems (ICCS)*, Dec 2016, pp. 1–6.

[86] A. A. Okandeji, M. R. Khandaker, K.-K. Wong, G. Zheng, Y. Zhang, and Z. Zheng, "Secure full-duplex two-way relaying for SWIPT," *arXiv preprint arXiv:1709.08237*, 2017.

[87] J. H. Lee, "Full-duplex relay for enhancing physical layer security in multi-hop relaying systems," *IEEE Communications Letters*, vol. 19, no. 4, pp. 525–528, April 2015.

[88] S. Parsaeefard and T. Le-Ngoc, "Improving wireless secrecy rate via full-duplex relay-assisted protocols," *IEEE Transactions on Information Forensics and Security*, vol. 10, no. 10, pp. 2095–2107, Oct 2015.

[89] Y. Zeng and R. Zhang, "Full-duplex wireless-powered relay with self-energy recycling," *IEEE Wireless Communications Letters*, vol. 4, no. 2, pp. 201–204, April 2015.

[90] H. Liu, K. J. Kim, K. S. Kwak, and H. V. Poor, "QoS-constrained relay control for full-duplex relaying with SWIPT," *IEEE Transactions on Wireless Communications*, vol. 16, no. 5, pp. 2936–2949, May 2017.

[91] R.-A. Pitaval, O. Tirkkonen, R. Wichman, K. Pajukoski, E. Lahetkangas, and E. Tiirola, "Full-duplex self-backhauling for small-cell 5G networks," *IEEE Wireless Communications*, vol. 22, no. 5, pp. 83–89, Oct. 2015.

[92] B. Li, D. Zhu, and P. Liang, "Small cell in-band wireless backhaul in massive MIMO systems: A cooperation of next-generation techniques," *IEEE Transactions on Wireless Communications*, vol. 14, no. 12, pp. 7057–7069, Dec. 2015.

[93] A. Rahmati, V. Shah-Mansouri, and M. Safari, "Price-based resource allocation for self-backhauled small cell networks," *Computer Communications*, 2016.

[94] D. Korpi, T. Riihonen, A. Sabharwal, and M. Valkama, "Sum-rate analysis and optimization of self-backhauling based full-duplex radio access system," *CoRR*, vol. abs/1604.06571, 2016.

[95] U. Siddique, H. Tabassum, and E. Hossain, "Adaptive in-band self-backhauling for full-duplex small cells," in *Communication Workshop (ICCW), 2015 IEEE International Conference on*, June 2015, pp. 44–49.

[96] Z. Chen, T. Q. S. Quek, and Y. C. Liang, "Spectral efficiency and relay energy efficiency of full-duplex relay channel," *IEEE Transactions on Wireless Communications*, vol. 16, no. 5, pp. 3162–3175, May 2017.

[97] G. Liu, H. Ji, F. R. Yu, Y. Li, and R. Xie, "Energy-efficient resource allocation in full-duplex relaying networks," in *2014 IEEE International Conference on Communications (ICC)*, June 2014, pp. 2400–2405.

[98] F. Zhu, F. Gao, M. Yao, and H. Zou, "Joint information- and jamming-beamforming for physical layer security with full duplex base station," *IEEE Transactions on Signal Processing*, vol. 62, no. 24, pp. 6391–6401, Dec 2014.

[99] Y. Zhou, Z. Z. Xiang, Y. Zhu, and Z. Xue, "Application of full-duplex wireless technique into secure MIMO communication: Achievable secrecy rate based optimization," *IEEE Signal Processing Letters*, vol. 21, no. 7, pp. 804–808, July 2014.

[100] W. Li, M. Ghogho, B. Chen, and C. Xiong, "Secure communication via sending artificial noise by the receiver: Outage secrecy capacity/region analysis," *IEEE Communications Letters*, vol. 16, no. 10, pp. 1628–1631, Oct. 2012.

[101] F. Zhu, F. Gao, T. Zhang, K. Sun, and M. Yao, "Physical-layer security for full duplex communications with self-interference mitigation," *IEEE Transactions on Wireless Communications*, vol. 15, no. 1, pp. 329–340, Jan 2016.

[102] G. Zheng, I. Krikidis, J. Li, A. Petropulu, and B. Ottersten, "Improving physical layer secrecy using full-duplex jamming receivers," *IEEE Transactions on Signal Processing*, Oct 2013.

[103] S. Vishwakarma and A. Chockalingam, "Sum secrecy rate in MISO full-duplex wiretap channel with imperfect CSI," in *2015 IEEE Globecom Workshops (GC Wkshps)*, Dec 2015, pp. 1–6.

[104] L. Dong, Z. Han, A. P. Petropulu, and H. V. Poor, "Improving wireless physical layer security via cooperating relays," *IEEE Transactions on Signal Processing*, vol. 58, no. 3, pp. 1875–1888, March 2010.

[105] S. Parsaeefard and T. Le-Ngoc, "Full-duplex relay with jamming protocol for improving physical-layer security," in *2014 IEEE 25th Annual International Symposium on Personal, Indoor, and Mobile Radio Communication (PIMRC)*, Sep 2014, pp. 129–133.

[106] E. Ahmed, A. Eltawil, and A. Sabharwal, "Simultaneous transmit and sense for cognitive radios using full-duplex: A first study," in *Proceedings of the 2012 IEEE International Symposium on Antennas and Propagation*, July 2012, pp. 1–2.

[107] E. Tsakalaki, O. N. Alrabadi, A. Tatomirescu, E. de Carvalho, and G. F. Pedersen, "Concurrent communication and sensing in cognitive radio devices: Challenges and an enabling solution," *IEEE Transactions on Antennas and Propagation*, vol. 62, no. 3, pp. 1125–1137, March 2014.

[108] T. Riihonen and R. Wichman, "Energy detection in full-duplex cognitive radios under residual self-interference," in *2014 9th International Conference on Cognitive Radio Oriented Wireless Networks and Communications (CROWNCOM)*, June 2014, pp. 57–60.

[109] Y. Liao, L. Song, Z. Han, and Y. Li, "Full duplex cognitive radio: a new design paradigm for enhancing spectrum usage," *IEEE Communications Magazine*, vol. 53, no. 5, pp. 138–145, May 2015.

[110] D. Bharadia, K. R. Joshi, and S. Katti, "Full duplex backscatter," in *Proceedings of the Twelfth ACM Workshop on Hot Topics in Networks*. ACM, 2013, p. 4.

[111] Y. Liu, Y. Shen, D. Guo, and M. Z. Win, "Localization and synchronization in wireless networks using full-duplex radios," in *2017 IEEE International Conference on Communications (ICC)*, May 2017, pp. 1–6.

[112] A. Sabharwal, P. Schniter, D. Guo, D. Bliss, S. Rangarajan, and R. Wichman, "In-band full-duplex wireless: Challenges and opportunities," *Selected Areas in Communications, IEEE Journal on*, vol. 32, no. 9, pp. 1637–1652, Sep 2014.

[113] D. Kim, H. Lee, and D. Hong, "A survey of in-band full-duplex transmission: From the perspective of PHY and MAC layers," *IEEE Communications Surveys & Tutorials*, vol. 17, no. 4, pp. 2017–2046, 2015.

[114] O. Taghizadeh, T. Yang, and R. Mathar, "Joint power and beam optimization in a multi-carrier MIMO wiretap channel with full-duplex jammer," in *2017 IEEE International Conference on Communications Workshops (ICC Workshops)*, May 2017, pp. 1316–1322.

[115] O. Taghizadeh, P. Neuhaus, and R. Mathar, "Can Full-Duplex jamming reduce the energy-cost of a secure bit?" in *2018 IEEE Wireless Communications and Networking Conference (WCNC'18) (accepted for publication)*, Barcelona, Spain, Apr. 2018.

[116] O. Taghizadeh, A. Zamani, and R. Mathar, "Physical-layer security for simultaneous information and power transfer in full-duplex multi-user networks," in *20th International ITG Workshop on Smart Antennas (WSA 2016)*, Munich, Germany, 2016, to be published after approval.

[117] O. Taghizadeh, P. Neuhaus, and R. Mathar, "Secrecy energy efficiency of MIMOME wiretap channels with full-duplex jamming," *IEEE Transactions on Communications (to be submitted for publication).*

[118] R. M. O. Taghizadeh, A. C. Cirik, "Hardware impairments aware transceiver design for full-duplex amplify-and-forward MIMO relaying," *IEEE Transactions on Wireless Communications*, 2017.

[119] J. Zhang, O. Taghizadeh, and M. Haardt, "Joint source and relay precoding design for one-way full-duplex MIMO relaying systems," *Proceedings of the Tenth International Symposium on Wireless Communication Systems (ISWCS)*, Aug 2013.

[120] O. Taghizadeh and R. Mathar, "Robust multi-user decode-and-forward relaying with full-duplex operation," in *The Eleventh International Symposium on Wireless Communication Systems (ISWCS 2014)*, Barcelona, Spain, Sep. 2014.

[121] ——, "Full-duplex decode-and-forward relaying with limited self-interference cancellation," in *Proceedings of International ITG Workshop on Smart Antennas (WSA), Erlangen, Germany*, March 2014.

[122] O. Taghizadeh, T. Yang, A. C. Cirik, and R. Mathar, "Distortion-loop-aware amplify-and-forward full-duplex relaying with multiple antennas," in *International Symposium on Wireless Communication Systems (ISWCS'2016)*, Poznan, Poland, Sep. 2016, pp. 54–58.

[123] O. Taghizadeh, V. Radhakrishnan, A. C. Cirik, S. Shojaee, R. Mathar, and L. Lampe, "Linear precoder and decoder design for bidirectional Full-Duplex MIMO OFDM systems," in *PIMRC'17*, Montreal, Canada, 2017.

[124] A. Cirik, L. Lampe, A. Liu, R. Mathar, and O. Taghizadeh, "Sum-power minimization under rate constraints in full-duplex MIMO interference-channels," in *WSA 2017; 21th International ITG Workshop on Smart Antennas*, March 2017, pp. 1–5.

[125] J. Zhang, O. Taghizadeh, and M. Haardt, "Transmit strategies for full-duplex point-to-point systems with residual self-interference," *in Proceedings of International ITG Workshop on Smart Antennas (WSA), Stuttgart, Germany*, March 2013.

[126] ——, "Robust transmit beamforming design for full-duplex point-to-point MIMO systems," *Proceedings of the Tenth International Symposium on Wireless Communication Systems (ISWCS)*, Aug. 2013.

[127] O. Taghizadeh, V. Radhakrishnan, A. C. Cirik, R. Mathar, and L. Lampe, "Hardware impairments aware transceiver design for bidirectional full-duplex MIMO OFDM systems," *IEEE Transactions on Vehicular Technology*, 2018.

[128] O. Taghizadeh, P. Sirvi, S. Narasimha, J. Leon Calvo, and R. Mathar, "Minimum-Cost wireless backhaul network planning with Full-Duplex links," in *2018 IEEE Wireless Communications and Networking Conference (WCNC'18) (accepted for publication)*, Barcelona, Spain, Apr. 2018.

[129] ——, "Environment-aware minimum-cost wireless backhaul network planning with Full-Duplex links," in *IEEE Systems Journal (submitted for publication).*

[130] A. C. Cirik, S. Biswas, S. O. T. Motlagh, and T. Ratnarajah, "Robust transceiver design in full-duplex MIMO cognitive radios," *IEEE Transactions on Vehicular Technology*, vol. PP, no. 99, pp. 1–1, 2017.

[131] A. C. Cirik, O. Taghizadeh, L. Lampe, and R. Mathar, "Fronthaul compression and precoding design for full-duplex cloud radio access network," in *IEEE Systems Journal (submitted for publication).*

[132] ——, "Fronthaul compression and precoding design for MIMO full-duplex cognitive radio networks," in *2018 IEEE Wireless Communications and Networking Conference (WCNC'18) (accepted for publication)*, Barcelona, Spain, Apr. 2018.

[133] A. C. Cirik, R. Wang, Y. Rong, and Y. Hua, "MSE based transceiver designs for bi-directional full-duplex MIMO systems," in *2014 IEEE 15th International Workshop on Signal Processing Advances in Wireless Communications (SPAWC)*, June 2014, pp. 384–388.

[134] T. Riihonen and R. Wichman, "Analog and digital self-interference cancellation in full-duplex MIMO-OFDM transceivers with limited resolution in A/D conversion," in *2012 Conference Record of the Forty Sixth Asilomar Conference on Signals, Systems and Computers (ASILOMAR)*, Nov 2012, pp. 45–49.

[135] T. Riihonen, K. Haneda, S. Werner, and R. Wichman, "SINR analysis of full-duplex OFDM repeaters," in *2009 IEEE 20th International Symposium on Personal, Indoor and Mobile Radio Communications*, Sep 2009, pp. 3169–3173.

[136] M. Mokhtar, N. Al-Dhahir, and R. Hamila, "OFDM full-duplex DF relaying under I/Q imbalance and loopback self-interference," *IEEE Transactions on Vehicular Technology*, vol. 65, no. 8, pp. 6737–6741, Aug 2016.

[137] N. Li, Y. Li, M. Peng, and W. Wang, "Resource allocation in multi-carrier full-duplex amplify-and-forward relaying networks," in *2016 IEEE 83rd Vehicular Technology Conference (VTC Spring)*, May 2016, pp. 1–5.

[138] Y. Sun, D. W. K. Ng, Z. Ding, and R. Schober, "Optimal joint power and subcarrier allocation for full-duplex multicarrier non-orthogonal multiple access systems," *IEEE Transactions on Communications*, vol. PP, no. 99, pp. 1–1, 2017.

[139] M. Al-Imari, M. Ghoraishi, and P. Xiao, "Radio resource allocation for full-duplex multicarrier wireless systems," in *2015 International Symposium on Wireless Communication Systems (ISWCS)*, Aug 2015, pp. 571–575.

[140] W. Li, J. Lilleberg, and K. Rikkinen, "On rate region analysis of half- and full-duplex OFDM communication links," *IEEE Journal on Selected Areas in Communications*, vol. 32, no. 9, pp. 1688–1698, Sep 2014.

[141] D. W. K. Ng, E. S. Lo, and R. Schober, "Dynamic resource allocation in MIMO-OFDMA systems with full-duplex and hybrid relaying," *IEEE Transactions on Communications*, vol. 60, no. 5, pp. 1291–1304, 2012.

[142] G. Santella and F. Mazzenga, "A hybrid analytical-simulation procedure for performance evaluation in M-QAM-OFDM schemes in presence of nonlinear distortions," *IEEE Transactions on Vehicular Technology*, vol. 47, no. 1, pp. 142–151, Feb 1998.

[143] W. Namgoong, "Modeling and analysis of nonlinearities and mismatches in AC-coupled direct-conversion receiver," *IEEE Transactions on Wireless Communications*, vol. 4, no. 1, pp. 163–173, Jan 2005.

[144] H. Suzuki, T. V. A. Tran, I. B. Collings, G. Daniels, and M. Hedley, "Transmitter noise effect on the performance of a MIMO-OFDM hardware implementation achieving improved coverage," *IEEE Journal on Selected Areas in Communications*, vol. 26, no. 6, pp. 867–876, Aug 2008.

[145] S. S. Christensen, R. Agarwal, E. D. Carvalho, and J. M. Cioffi, "Weighted sum-rate maximization using weighted MMSE for MIMO-BC beamforming design," *IEEE Transactions on Wireless Communications*, vol. 7, no. 12, pp. 4792–4799, Dec 2008.

[146] M. Duarte, C. Dick, and A. Sabharwal, "Experiment-driven characterization of full-duplex wireless systems," *IEEE Transactions on Wireless Communications*, vol. 11, no. 12, pp. 4296–4307, Dec 2012.

[147] W. Xie, X. Xia, Y. Xu, K. Xu, and Y. Wang, "Massive MIMO full-duplex relaying with hardware impairments," *Journal of Communications and Networks*, vol. 19, no. 4, pp. 351–362, Aug 2017.

[148] S. Jia and B. Aazhang, "Signaling design of two-way MIMO full-duplex channel: Optimality under imperfect transmit front-end chain," *IEEE Transactions on Wireless Communications*, vol. 16, no. 3, pp. 1619–1632, March 2017.

[149] Y. S. Cho, J. Kim, W. Y. Yang, and C. G. Kang, *MIMO-OFDM wireless communications with MATLAB*. John Wiley & Sons, 2010.

[150] U. Siddique, H. Tabassum, E. Hossain, and D. I. Kim, "Wireless backhauling of 5G small cells: challenges and solution approaches," *IEEE Wireless Communications*, vol. 22, no. 5, pp. 22–31, Oct 2015.

[151] D. Bertesekas, "Nonlinear programming. athena scientific," *Belmont, Massachusetts*, 1999.

[152] H. Shen, B. Li, M. Tao, and X. Wang, "MSE-based transceiver designs for the MIMO interference channel," *IEEE Transactions on Wireless Communications*, vol. 9, no. 11, pp. 3480–3489, Nov 2010.

[153] J. Jose, N. Prasad, M. Khojastepour, and S. Rangarajan, "On robust weighted-sum rate maximization in MIMO interference networks," in *2011 IEEE International Conference on Communications (ICC)*, June 2011, pp. 1–6.

[154] J. Wang and D. P. Palomar, "Worst-case robust MIMO transmission with imperfect channel knowledge," *IEEE Transactions on Signal Processing*, vol. 57, no. 8, pp. 3086–3100, 2009.

[155] K. B. Petersen and M. S. Pedersen, *The Matrix Cookbook*. Technical University of Denmark, Nov 2012, version 20121115. [Online]. Available: http://www2.imm.dtu.dk/pubdb/p.php?3274

[156] Y. C. Eldar and N. Merhav, "A competitive minimax approach to robust estimation of random parameters," *IEEE Transactions on Signal Processing*, vol. 52, no. 7, pp. 1931–1946, July 2004.

[157] M. V. Khlebnikov and P. S. Shcherbakov, "Petersens lemma on matrix uncertainty and its generalizations," *Automation and Remote Control*, vol. 69, no. 11, pp. 1932–1945, 2008.

[158] L. Vandenberghe, S. Boyd, and S.-P. Wu, "Determinant maximization with linear matrix inequality constraints," *SIAM Journal on matrix analysis and applications*, vol. 19, no. 2, pp. 499–533, 1998.

[159] A. Mutapcic and S. Boyd, "Cutting-set methods for robust convex optimization with pessimizing oracles," *Optimization Methods & Software*, vol. 24, no. 3, pp. 381–406, 2009.

[160] X. Zheng, X. Sun, D. Li, and Y. Xu, "On zero duality gap in nonconvex quadratic programming problems," *Journal of Global Optimization*, vol. 52, no. 2, pp. 229–242, 2012.

[161] A. Ben-Tal and A. Nemirovski, *Lectures on modern convex optimization: analysis, algorithms, and engineering applications*. Siam, 2001, vol. 2.

[162] C. T. Lin, F. S. Tseng, and W. R. Wu, "MMSE transceiver design for full-duplex MIMO relay systems," *IEEE Transactions on Vehicular Technology*, vol. 66, no. 8, pp. 6849–6861, Aug 2017.

[163] C. T. Lin and W. R. Wu, "Linear transceiver design for full-duplex MIMO relay systems: A non-iterative approach," *IEEE Wireless Communications Letters*, vol. 6, no. 4, pp. 518–521, Aug 2017.

[164] D. P. M. Osorio, E. E. B. Olivo, H. Alves, J. C. S. S. Filho, and M. Latva-aho, "Exploiting the direct link in full-duplex amplify-and-forward relaying networks," *IEEE Signal Processing Letters*, vol. 22, no. 10, pp. 1766–1770, Oct 2015.

[165] G. E. Bottomley, T. Ottosson, and Y. P. E. Wang, "A generalized RAKE receiver for interference suppression," *IEEE Journal on Selected Areas in Communications*, vol. 18, no. 8, pp. 1536–1545, Aug 2000.

[166] T. Riihonen, S. Werner, and R. Wichman, "Hybrid full-duplex/half-duplex relaying with transmit power adaptation," *IEEE Transactions on Wireless Communications*, vol. 10, no. 9, pp. 3074–3085, Sep 2011.

[167] D. Bertsekas, *Nonlinear programming*. Athena Scientific, 1999.

[168] A. Cohen, "Stepsize analysis for descent methods," in *Proceedings of IEEE 12th International Symposium on Adaptive Processes*, Dec. 1973.

[169] S. Ye and R. S. Blum, "Optimized signaling for MIMO interference systems with feedback," *IEEE Transactions on Signal Processing*, vol. 51, no. 11, pp. 2839–2848, Nov 2003.

[170] R.-C. Li, "Rayleigh quotient based optimization methods for eigenvalue problems," *Matrix Functions and Matrix Equations*, vol. 19, pp. 76–108, 2014.

[171] Y. Huang and D. P. Palomar, "Rank-constrained separable semidefinite programming with applications to optimal beamforming," *IEEE Transactions on Signal Processing*, vol. 58, pp. 664–678, Feb. 2010.

[172] C. Kong, C. Zhong, S. Jin, S. Yang, H. Lin, and Z. Zhang, "Full-duplex massive MIMO relaying systems with low-resolution ADCs," *IEEE Transactions on Wireless Communications*, vol. 16, no. 8, pp. 5033–5047, Aug 2017.

[173] A. Mukherjee, S. A. A. Fakoorian, J. Huang, and A. L. Swindlehurst, "Principles of physical layer security in multiuser wireless networks: A survey," *IEEE Communications Surveys Tutorials*, vol. 16, no. 3, pp. 1550–1573, March 2014.

[174] A. D. Wyner, "The wire-tap channel," *The Bell System Technical Journal*, vol. 54, no. 8, pp. 1355–1387, Oct 1975.

[175] Y. Liang, H. V. Poor, and S. Shamai, "Secure communication over fading channels," *IEEE Transactions on Information Theory*, vol. 54, no. 6, pp. 2470–2492, June 2008.

[176] E. Ekrem and S. Ulukus, "The secrecy capacity region of the gaussian MIMO multi-receiver wiretap channel," *IEEE Transactions on Information Theory*, vol. 57, no. 4, pp. 2083–2114, April 2011.

[177] F. Oggier and B. Hassibi, "The secrecy capacity of the MIMO wiretap channel," *IEEE Transactions on Information Theory*, vol. 57, no. 8, pp. 4961–4972, Aug 2011.

[178] C. Ling, L. Luzzi, and J. C. Belfiore, "Lattice codes achieving strong secrecy over the mod-λ gaussian channel," in *2012 IEEE International Symposium on Information Theory Proceedings*, July 2012, pp. 2306–2310.

[179] H. Mahdavifar and A. Vardy, "Achieving the secrecy capacity of wiretap channels using polar codes," *IEEE Transactions on Information Theory*, vol. 57, no. 10, pp. 6428–6443, Oct 2011.

[180] M. Andersson, V. Rathi, R. Thobaben, J. Kliewer, and M. Skoglund, "Nested polar codes for wiretap and relay channels," *IEEE Communications Letters*, vol. 14, no. 8, pp. 752–754, Aug 2010.

[181] A. L. Swindlehurst, "Fixed SINR solutions for the MIMO wiretap channel," in *2009 IEEE International Conference on Acoustics, Speech and Signal Processing*, April 2009, pp. 2437–2440.

[182] S. Goel and R. Negi, "Guaranteeing secrecy using artificial noise," *IEEE Transactions on Wireless Communications*, vol. 7, no. 6, pp. 2180–2189, June 2008.

[183] I. Krikidis, J. S. Thompson, and S. Mclaughlin, "Relay selection for secure cooperative networks with jamming," *IEEE Transactions on Wireless Communications*, vol. 8, no. 10, pp. 5003–5011, Oct 2009.

[184] Z. Ding, M. Peng, and H. H. Chen, "A general relaying transmission protocol for MIMO secrecy communications," *IEEE Transactions on Communications*, vol. 60, no. 11, pp. 3461–3471, Nov 2012.

[185] J. Huang and A. L. Swindlehurst, "Cooperative jamming for secure communications in MIMO relay networks," *IEEE Transactions on Signal Processing*, vol. 59, no. 10, pp. 4871–4884, Oct 2011.

[186] L. Li, Z. Chen, D. Zhang, and J. Fang, "A full-duplex bob in the MIMO gaussian wiretap channel: Scheme and performance," *IEEE Signal Processing Letters*, vol. 23, no. 1, pp. 107–111, Jan 2016.

[187] F. Zhu, F. Gao, M. Yao, and H. Zou, "Joint information- and jamming-beamforming for physical layer security with full duplex base station," *IEEE Transactions on Signal Processing*, vol. 62, Dec 2014.

[188] B. Akgun, O. O. Koyluoglu, and M. Krunz, "Exploiting full-duplex receivers for achieving secret communications in multiuser MISO networks," *IEEE Transactions on Communications*, vol. 65, no. 2, pp. 956–968, Feb 2017.

[189] S. Buzzi, C. L. I, T. E. Klein, H. V. Poor, C. Yang, and A. Zappone, "A survey of energy-efficient techniques for 5G networks and challenges ahead," *IEEE Journal on Selected Areas in Communications*, vol. 34, no. 4, pp. 697–709, April 2016.

[190] A. Fehske, G. Fettweis, J. Malmodin, and G. Biczok, "The global footprint of mobile communications: The ecological and economic perspective," *IEEE Communications Magazine*, vol. 49, no. 8, pp. 55–62, Aug 2011.

[191] P.-H. Lin, S.-H. Lai, S.-C. Lin, and H.-J. Su, "On secrecy rate of the generalized artificial-noise assisted secure beamforming for wiretap channels," *IEEE Journal on Selected Areas in Communications*, vol. 31, no. 9, pp. 1728–1740, 2013.

[192] A. Zappone, P.-H. Lin, and E. Jorswieck, "Energy efficiency of confidential multi-antenna systems with artificial noise and statistical csi," *IEEE Journal of Selected Topics in Signal Processing*, vol. 10, no. 8, pp. 1462–1477, 2016.

[193] S. Kim, R. Pasupathy, and S. G. Henderson, "A guide to sample average approximation," in *Handbook of Simulation Optimization*. Springer, 2015, pp. 207–243.

[194] M. Razaviyayn, M. Hong, and Z.-Q. Luo, "A unified convergence analysis of block successive minimization methods for nonsmooth optimization," *SIAM Journal on Optimization*, vol. 23, no. 2, pp. 1126–1153, 2013.

[195] C. Shuguang, A. Goldsmith, and A. Bahai, "Energy-efficiency of MIMO and cooperative MIMO techniques in sensor networks," *Selected Areas in Communications, IEEE Journal on*, Aug. 2004.

[196] B. R. Marks and G. P. Wright, "Technical note: A general inner approximation algorithm for nonconvex mathematical programs," *Operations Research*, vol. 26, no. 4, pp. 681–683, 1978.

[197] E. Beckenbach *et al.*, "Generalized convex functions," *Bull. Amer. Math. Soc*, vol. 43, no. 6, pp. 363–371, 1937.

[198] W. Dinkelbach, "On nonlinear fractional programming," *Management science*, vol. 13, no. 7, pp. 492–498, 1967.

[199] A. Zappone, E. Jorswieck *et al.*, "Energy efficiency in wireless networks via fractional programming theory," *Foundations and Trends® in Communications and Information Theory*, vol. 11, no. 3-4, pp. 185–396, 2015.

[200] O. Taghizadeh, P. Neuhaus, and R. Mathar, "Secrecy energy efficiency of mimome wiretap channels with full-duplex jamming," *arXiv preprint arXiv:1708.05402*, 2017.

[201] R. Hunger, *Floating point operations in matrix-vector calculus*. Munich University of Technology, Inst. for Circuit Theory and Signal Processing Munich, 2005.

[202] D. W. K. Ng, E. S. Lo, and R. Schober, "Robust beamforming for secure communication in systems with wireless information and power transfer," *IEEE Transactions on Wireless Communications*, vol. 13, no. 8, pp. 4599–4615, Aug 2014.

[203] A. P. Ruszczynski and A. Shapiro, *Stochastic programming*. Elsevier Amsterdam, 2003, vol. 10.

[204] Y. Ye, M. Grant, and S. Boyd, *CVX users' guide*. stanford.edu, 2008.

[205] J. Hoydis, M. Kobayashi, and M. Debbah, "Green small-cell networks," *IEEE Vehicular Technology Magazine*, vol. 6, no. 1, pp. 37–43, March 2011.

[206] X. Ge, H. Cheng, M. Guizani, and T. Han, "5G wireless backhaul networks: challenges and research advances," *IEEE Network*, vol. 28, no. 6, pp. 6–11, Nov 2014.

[207] A. Barradas, N. Correia, J. Coimbra, and G. Schütz, "Load adaptive and fault tolerant framework for energy saving in fiber-wireless access networks," *IEEE/OSA Journal of Optical Communications and Networking*, vol. 5, no. 9, pp. 957–967, Sept 2013.

[208] C. Charnsripinyo and D. Tipper, "Topological design of survivable wireless access networks," in *Design of Reliable Communication Networks, 2003.(DRCN 2003). Proceedings. Fourth International Workshop on*. IEEE, 2003, pp. 371–378.

[209] D. Tipper, T. Dahlberg, H. Shin, and C. Charnsripinyo, "Providing fault tolerance in wireless access networks," *IEEE Communications Magazine*, vol. 40, no. 1, pp. 58–64, Jan 2002.

[210] F. C. Kuo, F. A. Zdarsky, J. Lessmann, and S. Schmid, "Cost-efficient wireless mobile backhaul topologies: An analytical study," in *Global Telecommunications Conference (GLOBECOM 2010), 2010 IEEE*, Dec. 2010, pp. 1–5.

[211] P. Monti, S. Tombaz, L. Wosinska, and J. Zander, "Mobile backhaul in heterogeneous network deployments: Technology options and power consumption," in *Transparent Optical Networks (ICTON), 2012 14th International Conference on*. IEEE, 2012, pp. 1–7.

[212] S. Tombaz, P. Monti, K. Wang, A. Vastberg, M. Forzati, and J. Zander, "Impact of backhauling power consumption on the deployment of heterogeneous mobile networks," in *2011 IEEE Global Telecommunications Conference - GLOBECOM 2011*, Dec 2011, pp. 1–5.

[213] O. Grøndalen, O. Østerbø, G. Millstein, and T. Tjelta, "On planning small cell backhaul networks," in *Networks and Communications (EuCNC), 2015 European Conference on*, June 2015, pp. 397–402.

[214] Y. Li, G. Qiao, A. Cai, L. Shi, H. Zhao, and G. Shen, "Microwave backhaul topology planning for wireless access networks," in *Transparent Optical Networks (ICTON), 2014 16th International Conference on*, July 2014, pp. 1–4.

[215] Y. Li, A. Cai, G. Qiao, L. Shi, S. K. Bose, and G. Shen, "Multi-objective topology planning for microwave-based wireless backhaul networks," *IEEE Access*, vol. 4, pp. 5742–5754, 2016.

[216] R. Nadiv and T. Naveh, "Wireless backhaul topologies: Analyzing backhaul topology strategies," *Ceragon White Paper*, pp. 1–15, 2010.

[217] U. Lauther, T. Winter, and M. Ziegelmann, "Proximity graph based clustering algorithms for optimized planning of UMTS access network topologies," in *10th International Conference on Telecommunications, 2003. ICT 2003.*, vol. 2, Feb 2003, pp. 1329–1334 vol.2.

[218] M. Coldrey, H. Koorapaty, J. Berg, Z. Ghebretensae, J. Hansryd, A. Derneryd, and S. Falahati, "Small-cell wireless backhauling: A non-line-of-sight approach for point-to-point microwave links," in *Vehicular Technology Conference (VTC Fall), 2012 IEEE*. IEEE, 2012, pp. 1–5.

[219] M. Coldrey, J.-E. Berg, L. Manholm, C. Larsson, and J. Hansryd, "Non-line-of-sight small cell backhauling using microwave technology," *IEEE Communications Magazine*, vol. 51, no. 9, pp. 78–84, 2013.

[220] S. Hur, T. Kim, D. J. Love, J. V. Krogmeier, T. A. Thomas, A. Ghosh *et al.*, "Millimeter wave beamforming for wireless backhaul and access in small cell networks," *IEEE Trans. Communications*, vol. 61, no. 10, pp. 4391–4403, 2013.

[221] Y. Li, N. Pappas, V. Angelakis, M. Pióro, and D. Yuan, "Optimization of free space optical wireless network for cellular backhauling," *IEEE Journal on Selected Areas in Communications*, vol. 33, no. 9, pp. 1841–1854, 2015.

[222] I. Atzeni and M. Kountouris, "Full-duplex MIMO small-cell networks: Performance analysis," *CoRR*, vol. abs/1504.04167, 2015.

[223] Y. Wu and S. Pierre, "Optimization of access network design in 3G networks," in *CCECE 2003 - Canadian Conference on Electrical and Computer Engineering. Toward a Caring and Humane Technology (Cat. No.03CH37436)*, vol. 2, May 2003, pp. 781–784 vol.2.

[224] A. Jüttner, A. Orbán, and Z. Fiala, "Two new algorithms for UMTS access network topology design," *European Journal of Operational Research*, vol. 164, no. 2, pp. 456–474, 2005.

[225] Y. Wu and S. Pierre, "Optimization of 3G mobile network design using a hybrid search strategy," *Journal of Communications and Networks*, vol. 7, no. 4, pp. 471–477, 2005.

[226] G. Zhang, T. Q. S. Quek, M. Kountouris, A. Huang, and H. Shan, "Fundamentals of heterogeneous backhaul design — analysis and optimization," *IEEE Transactions on Communications*, vol. 64, no. 2, pp. 876–889, Feb. 2016.

[227] I. Marie, B. Bostjancic, and A. Goldsmith, "Resource allocation for constrained backhaul in picocell networks," in *2011 Information Theory and Applications Workshop*, Feb 2011, pp. 1–6.

[228] S. Yi and M. Lei, "Backhaul resource allocation in LTE-advanced relaying systems," in *Wireless Communications and Networking Conference (WCNC), 2012 IEEE*. IEEE, 2012, pp. 1207–1211.

[229] F. Schröder, M. Reyer, and R. Mathar, "Efficient implementation and evaluation of parallel radio wave propagation," in *EuCAP 2011 - 5th European Conference on Antennas and Propagation*, Apr 2011, pp. 2466–2470.

[230] ——, "Field strength prediction for environment aware MIMO channel models," in *6th European Conference on Antennas and Propagation (EUCAP)*, Prague, Czech, March 2012, pp. 1–4.

[231] S. P. Boyd and L. Vandenberghe, *Convex optimization*. Cambridge University Press, 2004.

[232] J. F. Sturm, "Using SeDuMi 1.02, a MATLAB toolbox for optimization over symmetric cones," *Optimization methods and software*, vol. 11, no. 1-4, pp. 625–653, 1999.

[233] R. Tütüncü, K. Toh, and M. Todd, "SDPT3—a MATLAB software package for semidefinite-quadratic-linear programming, version 3.0," 2001. [Online]. Available: http://www.math.nus.edu.sg/mattohkc/sdpt3.html

[234] J. A. L. Calvo, F. Schröder, X. Xu, and R. Mathar, "A validation using measurement data of a radio channel model with geographical information," in *9th European Conference on Antennas and Propagation (EUCAP 2015)*, Lisabon, Portugal, Apr. 2015, pp. 1–4.

[235] E. ETSI, "302 217-4-1 v1. 2.1:"fixed radio systems; characteristics and requirements for point-to-point equipment and antennas; part 4-1: System-dependent requirements for antennas"," *European Standard, Telecommunications Series*.

[236] M. Mahloo, P. Monti, J. Chen, and L. Wosinska, "Cost modeling of backhaul for mobile networks," in *Communications Workshops (ICC), 2014 IEEE International Conference on*. IEEE, 2014, pp. 397–402.

[237] A. A. W. Ahmed, J. Markendahl, C. Cavdar, and A. Ghanbari, "Study on the effects of backhual solutions on indoor mobile deployment „macrocell vs. femtocell"," in *Personal Indoor and Mobile Radio Communications (PIMRC), 2013 IEEE 24th International Symposium on*. IEEE, 2013, pp. 2444–2448.

Curriculum Vitae

Seyed Omid Taghizadeh Motlagh

Sep. 16, 1983	Born in Tehran, Iran
1989 - 1994	Elementary school “Nezam ma fi Elementary school” Tehran, Iran
1994 - 1997	Middle school “Mofid Middle School”, Tehran, Iran
1997 - 2001	High school and pre-university qualifications in math and physics
	“Alame Helli High School”, Tehran, Iran
Sep. 2001 - Sep. 2007	Undergraduate educations in Electrical Engineering “Shahid Beheshti University”, Tehran, Iran
April. 2008 - March. 2010	Hardware and algorithm developer Iran Industrial Communication Research & Developments Co., Tehran, Iran
April. 2010 - Aug. 2010	Hardware and algorithm developer Rasa Andishan e Shargh Gostar Co., Tehran, Iran
Oct. 2010 - April. 2013	Master of Science educations in Communications and Signal Processing TU Ilmenau, Ilmenau, Germany
Feb. 2012 - Feb. 2013	Student researcher Communications Research Lab TU Ilmenau, Ilmenau, Germany
Since Sept. 2013	Research and Teaching Assistant Institute for Theoretical Information Technology RWTH Aachen University, Aachen, Germany